

FIELD, GEOCHEMICAL, AND EXPERIMENTAL STUDIES OF ALUMINOUS
ARC MAGMAS

by

Thomas Winslow Sisson

B. Sc. Geology, Stanford University
(1978)

M. A. Geology, University of California, Santa Barbara
(1982)

Submitted to the Department of Earth, Atmospheric and
Planetary Sciences in Partial Fulfillment of the
Requirements for the Degree of

DOCTOR OF PHILOSOPHY

in

GEOLOGY

at the

MASSACHUSETTS INSTITUTE OF TECHNOLOGY

February, 1991

c Massachusetts Institute of Technology

Signature of Author

Department of Earth, Atmospheric, &
Planetary Sciences, MIT
February, 1991

Certified by:

Dr. Timothy L. Grove
Thesis Supervisor

Accepted by:

Dr. Thomas H. Jordan
Chairman, Departmental Committee on Graduate Students

MASSACHUSETTS INSTITUTE
WITHDRAWN
FEB 12 1991
FROM
MIT LIBRARIES

FIELD, GEOCHEMICAL, AND EXPERIMENTAL STUDIES OF
ALUMINOUS ARC MAGMAS

by

Thomas Winslow Sisson

Submitted to the Department of
Earth, Atmospheric, and Planetary Sciences
in partial fulfillment of
the requirements for
the degree of

Doctor of Philosophy

February, 1991

ABSTRACT

Field observations, geochemistry, and experimental petrology are used to interpret the origin, evolution, and volatile content of some high alumina basalts and basaltic andesites of modern and ancient magmatic arcs, and their role in the creation of more silicic magmas.

GEOCHEMISTRY OF THE MAFIC SILL COMPLEX AT ONION VALLEY,
SOUTHEASTERN SIERRA NEVADA, CALIFORNIA, AND IMPLICATIONS FOR
THE ORIGIN OF SIERRAN GRANITOIDS

Sheeted mafic sills of the Jurassic intrusive complex at Onion Valley, southeastern Sierra Nevada, preserve evolved high alumina basalts through aluminous andesites that were present during growth of the Sierra Nevada batholith. Mafic magmas were water-rich. Many reached volatile saturation, as evidenced by miarolytic cavities. Onion Valley high alumina basalts differentiated to andesites by crystallization and separation of hornblende, calcic plagioclase, magnetite, and apatite. Associated sequences of layered cumulates were precipitated by magmas slightly more primitive than those preserved as sills. The magmas at Onion Valley probably originated as the derivative liquids of primitive wet high alumina basalts that differentiated at the base of the sub-Sierran crust, leaving ultramafic cumulates and evolved wet high alumina basalt liquids.

Simple mixing calculations show that the major and trace element characteristics of average Sierran granodiorite are readily produced by a mixture of average basaltic sill from Onion Valley and average Sierran low-silica granite. This result supports models deriving Sierran granitoids from mixtures of crustal and mantle magmas. Characteristic chemical differences occur between typical mafic inclusions in Sierran granitoids and Onion Valley high alumina basalts. The

differences are interpreted as resulting from chemical exchange between inclusions and host granitoid magmas.

EXPERIMENTAL EVIDENCE FOR HIGH WATER CONTENTS IN SOME ALUMINOUS ARC MAGMAS

Phase relations of natural aphyric high alumina basalts and their intrusive equivalents were studied through rock-melting experiments at 2kb, water-saturated, with fO_2 buffered at Ni-NiO. Experimental liquids saturated with olivine, calcic plagioclase, and either high calcium pyroxene or hornblende (+/- magnetite) have compositions close to those of many natural high alumina basalts and basaltic andesites with moderate-to-low MgO contents. Experimental solid phases, particularly plagioclase, match the compositions of phenocrysts observed in many natural high alumina basalts. The results lead to the interpretation that many mafic-to-intermediate aluminous arc magmas are very water-rich, commonly with $H_2O > 4$ wt.%, and have temperatures below 1100 °C. The wet magmas reach volatile-saturation in the upper crust. Continued ascent promotes decompression-degassing and the growth of plagioclase phenocrysts. Specific applications are made to the Aleutians, Fuego Volcano, Guatemala, and mafic sills of the Sierra Nevada batholith, California. The study supports models in which arc magmatism results from the introduction of water into the mantle wedge above the subducting slab.

Thesis supervisor: Dr. Timothy L. Grove
Associate Professor of Geology

TABLE OF CONTENTS

Abstract	ii
Table of Contents	iv
List of Figures	v
List of Tables	vii
Acknowledgements	viii
Introductory Note	x
Chapter 1	
Geochemistry of the Mafic Sill Complex at Onion Valley, Southeastern Sierra Nevada, and Implications for the Origin of Sierran Granitoids	1
Introduction	2
Geologic Setting	3
Geology and Petrography of the Sill Swarm	4
Sample Selection and Preparation	8
Analytical Techniques	11
Precision and Accuracy	12
Chemical Variation	13
Discussion	19
Summary and Conclusions	39
References	42
Chapter 2	
Experimental Evidence for High Water Contents in Some Aluminous Arc Magmas	116
Introduction	117
Experimental Methods	125
Results	129
Geothermometry	147
Discussion	153
Geologic Applications	162
Geologic Implications	177
Conclusion	180
References	182
Appendix 2-1	261
Appendix 2-2	262
Appendix A. T2M Run Assembly	263

LIST OF FIGURES

Figure

1-1	Simplified geologic map of the mafic intrusive complex at Onion Valley	52
1-2	Outcrop relations in the sill swarm	54
1-3	A. Geologic map of the north face of pt. 3782m	56
	B. Model of Onion Valley-type magma chamber	57
1-4	Backscatter electron images of plagioclase crystals in thin sills	59
1-5	Major oxide vs silica variation diagrams for sheeted sills and associated cumulates	61-64
1-6	Sills and inter-sill septa plotted on FeO*/MgO vs SiO ₂ variation diagram	66
1-7	Sills, inter-sill septa, and cumulates projected on the AFM diagram	68
1-8	CaO vs Al ₂ O ₃ variation diagram	70
1-9	Trace element vs silica variation diagrams	72-76
1-10	Chondrite-normalized rare earth element abundances in sills and septa	78-79
1-11	Rare earth element abundances in liquid-depleted sills	81
1-12	MORB-normalized elemental abundance patterns of basaltic sills	83
1-13	Chondrite-normalized rare earth element abundances in cumulates	85-86
1-14	Crystal fractionation modeled liquids and cumulates	88
1-15	Rare earth element contents of mineral cores from sample 86S48 normalized to whole rock abundances of sample 86S55	90-91
1-16	Trace element vs SiO ₂ variation diagrams comparing model liquids with observed abundances	93-96
1-17	Calculated rare earth element abundances for magmas parental to olivine hornblendite cumulates	98
1-18	Lead isotopic ratios of hornblende gabbro cumulates	100
1-19	An contents in plagioclase crystal cores	102
1-20	Trace element contents of average and calculated Sierran granodiorites	104
1-21	Trace element contents of mafic inclusions normalized to average abundances in Onion Valley basaltic sills	106
2-1	Experimental high-Ca pyroxenes projected onto the Ca - Mg -Fe ternary	200
2-2	Fe/Mg in pyroxene vs Fe/Mg in glass	202

2-3	Fe/Mg in olivine vs Fe/Mg in glass	204
2-4	A. Ca/Na in plagioclase vs Ca/Na in glass	206
	B. Ca-Na exchange K_D for plagioclase vs pressure	207
2-5	Experimental spinels compared to natural compositions	209
2-6	Al/Si in hornblende vs Al/Si in glass or matrix	211-212
2-7	Fe/Mg in hornblende vs Fe/Mg in glass	214
2-8	Experimental liquids projected on an AFM diagram	216
2-9	Experimental liquids projected on an FeO*/MgO vs SiO ₂ variation diagram	218
2-10	Pseudo-ternary projections of 2 kb water-saturated experimental liquids	221-222
2-11	Pseudo-ternary projections illustrating the hornblende-in reaction	224
2-12	Pseudo-ternary projection illustrating the effect of sodium on hornblende stability	226
2-13	A. Temperature recovery of the multiply-saturated liquid geothermometer	228
	B. Temperature recovery of the olivine-liquid geothermometer	229
2-14	Critical plane of silica undersaturation showing the shift of multiple saturation points with increasing pH ₂ O	231
2-15	Pseudo-ternary projections of multiple saturation boundaries showing change in positions induced by increased pH ₂ O	233
2-16	Aleutian HABs and associated magmas compared to multiple saturation boundaries	235
2-17	Calculated and observed olivine and plagioclase phenocryst cores for Aleutian HABs	237
2-18	Pseudo-ternary projection of Aleutian crystal fractionation models	239
2-19	Crystal fractionation models compared to Aleutian HABs and associated magmas	241
2-20	Fuego, Guatemala magmas compared to multiple saturation boundaries	243
2-21	Mafic sills of the Onion Valley complex compared to multiple saturation boundaries	245
2-22	A. Estimated temperatures and water contents for HABs and BAs	247
	B. Estimated temperatures and water contents of HAB and BA glasses	248

LIST OF TABLES

Table

1-1	Chemical analyses of sheeted sills and magmatic septa	107-109
1-2	Chemical analyses of representative cumulates	110
1-3	Rb, Sr, and Pb isotopic data for cumulates	111
1-4	Accuracy and precision of neutron activation analyses	112
1-5	Crystal fractionation models	113
1-6	Mineral-rock abundance ratios and partition coefficients	114
1-7	Average granitoid compositions and mixing model results	115
2-1	High-alumina basalts and basaltic andesites with low MgO contents	249
2-2	Compositions of starting materials	250
2-3	Experimental conditions and products	251
2-4	Electron microprobe analyses of experimental phases	252-257
2-5	Experimental conditions and products, fO_2 >or< Ni-NiO	258
2-6	Electron microprobe analyses of experimental phases, fO_2 >or< Ni-NiO	259
2-7	Aleutian crystal fractionation models	260
Appendix 2-1	Additional experimental results	261
Appendix 2-2	Compositions of natural hornblende rims and glasses	262

ACKNOWLEDGEMENTS

Many people have contributed their ideas, labor, and support to the evolution and completion of this work. Tim Grove and Jim Moore are foremost among these. Tim has created a facility and an environment at MIT in which I and others have been able to develop, investigate, and most importantly test our ideas about igneous systems through direct experimentation. Tim has also consistently urged me to reach further and apply our ideas and results widely, and thus contribute to resolving the larger issues of igneous petrogenesis. Jim has supported my field work in the Sierra Nevada and provided analyses of rocks through the U.S. Geological Survey. He has also been a good friend and companion in the field in the Sierra Nevada and elsewhere. Much of my appreciation for igneous rocks follows from his example.

Other colleagues at the Geological Survey have helped with this research. Gerry Czamanske has advised me on mineral analysis and interpretation, has provided electron probe standards and polished sections, and has been an enthusiastic partner on climbing excursions in Yosemite. Charlie Bacon has given advice on whole-rock analytical methods and uncertainties, and has been my example of a well-rounded petrologist. Dave Sherrod has always been willing to help, whether in scientific or personal matters, and has been a pleasure to associate with.

Nobu Shimizu and Fred Frey are the other faculty members at MIT who have made large contributions to this work. Nobu has provided original and creative, yet rigorous interpretations of geologic and geochemical observations, and encourages others to do the same. Fred has found and assisted in solving errors of logic or interpretation, particularly in the first chapter, and his advice has substantially improved the interpretation and presentation of results.

Fellow graduate students and colleagues have helped in particular ways, including: Tom Juster, Jon Blundy, and Peter Keleman in the construction and interpretation of phase diagrams; Mary Reid, Vincent Salters, and Levant Gulen in isotopic analyses; Jureck Blusztajn, Graham Layne, and Ken Burrhus in use of the ion microprobe; Steve Recca in use of the electron probe and in computing. Mike Baker, Karen Bartels, Tom Juster, and Ro Kinzler have shared unpublished experimental results and interpretations. Bill Rose donated samples of hornblende HAB and BA from Guatemala, and Mike Carr shared his observations on Central American volcanics. Jim Chen provided unpublished isotopic analyses of Sierran granitoids used to construct figure 1-18. Mac Rutherford traded TZM tricks and secrets, as well as reviewing the manuscripts.

Liz Schermer, Joyce Federuick, and Eric Keto have made recreational contributions to this work. Liz has shown notable courage on certain occasions. I close by thanking Susan Coons for her love, companionship, and support.

INTRODUCTORY NOTE

This thesis consists of two independent and free-standing chapters. They deal with questions of petrogenesis of certain aluminous arc magmas. Chapter 1 presents the geochemistry of hornblende high alumina basalt through aluminous andesite sills of the mafic intrusive complex at Onion Valley in the southeastern Sierra Nevada batholith. This study documents for the first time that typical arc high alumina basalts were present during growth of the Sierra Nevada batholith, shows how those mafic magmas differentiated, and shows that mixing of such mafic magmas with typical Sierran granite magmas can produce typical Sierran granodiorites. The results support models for the origin of Sierran granitoids as mixtures of crustal and mantle melts.

It was readily apparent in the field at Onion Valley that the Sierran high alumina basalt magmas were very water-rich. Sills and cumulates commonly contain miarolytic cavities, hornblende crystallized early in mafic magmas, and hornblende-plagioclase pegmatites are common. Similar features are found at every other mafic intrusive complex in the High Sierra and lead to the conclusion that high magmatic water contents were characteristic of Sierran mafic magmas. This observation prompted an experimental study, presented in chapter 2 investigating the phase relations of high alumina basalts and basaltic andesites under water-saturated conditions.

Chapter 2 presents the experimental phase relations of aphyric high alumina basalts and basaltic andesites, water-

saturated at 2kb pressure. A principle conclusion of this work is that certain high alumina basalts and basaltic andesites from modern magmatic arcs have substantial water contents prior to eruption. This conclusion is at odds with many previously published studies that interpret arc high alumina basalts as nearly dry magmas (some certainly are dry, but many probably are not). The presence of high dissolved water contents allows low-MgO high alumina basalts to exist as liquids at comparatively low temperatures ($<1100^{\circ}\text{C}$). This may be important in allowing such wet basalts to mix with more silicic magmas.

Each chapter is presented as a self-contained article including references. Figures and tables for each chapter are placed at the end of the text. The abstracts have been combined into the thesis abstract presented at the beginning of the document.

CHAPTER 1

Geochemistry of the Mafic Sill Complex at Onion Valley, Southeastern Sierra Nevada, and Implications for the Origin of Sierran Granitoids

INTRODUCTION

Small hornblende-rich mafic intrusions are scattered throughout the Mesozoic Sierra Nevada batholith. Most are made up of hornblende gabbro and diorite but some contain rocks ranging from ultramafic olivine hornblendite through to leucocratic tonalite. Early hornblende crystallization, minute miarolitic cavities, and hornblende-plagioclase pegmatites are evidence of high magmatic water contents. Nevertheless, the hornblende-rich mafic intrusions are the least evolved members of the voluminous Sierra Nevada batholith.

This paper reports and interprets the major and trace element chemistry of sheeted gabbro through quartz diorite sills from the mafic intrusive complex at Onion Valley in the southeastern Sierra Nevada batholith. Data for some associated cumulates are also presented. Our goals in this work have been to identify the compositions of mafic liquids present during growth of the Sierra Nevada batholith, to explore the mechanisms by which those liquids originated and differentiated, and finally to address the question of the role of such wet mafic liquids in the production of the more voluminous granitoid plutons of the batholith.

The sills at Onion Valley provide samples of some mafic-to-intermediate composition magmas that were present at shallow levels during growth of the batholith. As such, they provide evidence of basaltic magmas that may have contributed in

creating the more common granodiorites and granites found throughout the batholith. Mafic rocks like those at Onion Valley do not constitute large plutons in the Sierra Nevada batholith. The large plutons are granites or granodiorites that only rarely and locally zone to dioritic or gabbroic compositions (Bateman and Chappell, 1979). Most of the large granodiorite plutons do, however, contain gabbroic through dioritic mafic inclusions that are exposed in abundances of one to a few per square meter of outcrop area. The inclusions could have originated as mafic magmas (Reid et al., 1983) like those preserved at Onion Valley. If so, their original settings have been destroyed and their compositions are likely adulterated by immersion in host granitoid magmas. Mafic intrusive complexes, including Onion Valley, are the only areas preserving original field relations, mineralogy, textures, and compositions of the mafic magmatic constituents of the Sierra Nevada batholith. Studies of these complexes are essential, therefore, to assess the role of mafic magmas in the formation of the batholith.

GEOLOGIC SETTING

The mafic intrusive complex at Onion Valley straddles the main crest of the Sierra Nevada, lying entirely at elevations above 2300m (7600 ft) in Kings Canyon National Park and the Inyo National Forest (figure 1). The intrusive complex is most probably Jurassic in age, has dimensions of 10 by 2 km,

and lies as a WNW-trending sliver between Cretaceous plutons (Moore, 1963; Chen and Moore, 1982). The field relations, petrography, and mineralogy of the mafic intrusive complex are abstracted below from unpublished work of T.W. Sisson.

The mafic sill swarm and its associated layered cumulate bodies were intruded second out of four sequentially younger pre-Cretaceous mafic units at Onion Valley. The following younger unit cuts rocks of the sill complex, and has an age of 168my (U-Pb sphene; Sisson, unpublished). The older and younger members of the mafic intrusive complex at Onion Valley are considered to be of similar age with the exception of small mafic dikes and plugs that cut Cretaceous granitoid plutons. Field relations and U-Pb zircon dates (Saleeby, unpublished data) establish that the crosscutting dikes were nearly contemporaneous with their host Cretaceous plutons and therefore are unrelated to the main mafic intrusive complex.

Other mafic intrusive complexes similar to that at Onion Valley lie to the north along the crest of the Sierra Nevada. The few that have been dated are Jurassic (Frost, 1988, written communication), comparable to the mafic complex at Onion Valley. Jurassic granitoid plutons are also scattered throughout the region (Chen and Moore, 1982).

GEOLOGY AND PETROGRAPHY OF THE SILL SWARM

Myriad shallowly-dipping hornblende gabbro and diorite sills lie parallel to and chilled against one another forming

a sheeted sill swarm (figure 2). Thin sills, with thicknesses up to 1.5m, predominate at elevations above about 3600m. Meters-thick, multiply injected sills lie at lower elevations. Lens-shaped masses of layered cumulates, on the order of 150-200m thick and at least 700m broad lie concordantly at the transition from chiefly thin to thick sills (figure 3).

Thin sheeted sills

The thin sills are massive fine-grained equigranular rocks with distinctly finer-grained-to-aphanitic margins chilled either against other parallel sills or against inter-sill septa (see below). Euhedral-to-subhedral shapes of hornblende, calcic plagioclase, magnetite, apatite, and rare ilmenite suggests that these were early-crystallizing phases. Interstitial quartz, K-feldspar, biotite, sphene, and rare zircon crystallized late. The presence of skeletal plagioclase with swallowtail terminations as cores of subhedral crystals indicates growth from initially undercooled liquids (figure 4). Some samples also contain scattered plagioclase crystals with homogeneous tabular cores. Such crystals may have been entrained from other magmas. Some uncommon sills are distinguished by the parallel close-packed arrangement of tabular plagioclase laths and subhedral hornblende and a scarcity of interstitial minerals. Such sills are interpreted as having lost liquid, perhaps through filter-pressing.

Inter-sill septa

Many thin sills are separated by septa up to 15cm thick of coarser-grained and lighter-colored rock that ranges in composition from hornblende gabbro through tonalite. Very many localities have been found in which a sill is chilled against an adjacent septum, but the septum is continuous with small dikes that cut the sill (figure 2). This and petrographic features are evidence that the inter-sill septa were partly molten during injection of the sills. Most samples of inter-sill septa show the same minerals and crystallization sequences as the sills. Contact surfaces between sills and septa are decorated by concentrations of hornblende and biotite a few millimeters thick. These dark selvages are crowded with inclusions of apatite and, in some samples, zircon. The selvages have been avoided in selecting samples for geochemical analysis.

Thick sills

The rocks below about 3600m are massive and medium-grained hornblende gabbro through leucotonalite. Outcrop relations are complex. Vertical sections expose distinctly finer-grained chilled contacts spaced every few meters either as shallowly-dipping horizons or outlining meter-sized pillow-shaped masses (figure 2). The shallowly-dipping chilled

contacts lead to the interpretation that the rocks were emplaced one into the next as sills, each on the order of 2-4m thick. The pillow-shaped masses are evidence that thick sills were repeatedly reinjected with new magma. Crystal-liquid segregation has clearly taken place, as evidenced by the local presence of shallow troughs of accumulated mafic minerals and by the widespread occurrence of vuggy pegmatoid patches. Again, the same minerals and crystallization sequences are found as in the thin sills and inter-sill septa.

Layered cumulate bodies

Modally-layered cumulate bodies lie near the transition from thin to thick sills (figure 3). Most rocks are hornblende gabbros that consist of roughly equal proportions of cumulus hornblende and calcic plagioclase with accessory magnetite and occasional ilmenite. Quartz, biotite, and sphene grew late from intercumulus liquid. Apatite can be found as inclusions in cumulus minerals, or as a postcumulus phase, or both. Olivine hornblendites and hornblendites form occasional cumulus layers interspersed with the more common cumulate hornblende gabbros and also form intrusive plugs. The olivine hornblendites contain early-formed olivine (Fo^{72-81}), calcic plagioclase (up to An^{98}), and magnetite, encased in coarse hornblende. The olivine is embayed and was apparently in reaction with liquid to produce hornblende. Biotite, hypersthene, and very rare apatite are postcumulus

phases. Olivine hornblendite layers pass directly to olivine-free hornblende gabbros. No intervening stage of pyroxene crystallization is observed. Clinopyroxene has been found in some plagioclase hornblendite cumulates but is uncommon and may have been produced by a magma distinct in volatile or other chemical characteristics. Olivine hornblendites recur through the cumulate sections and provide graphic evidence for replenishment by relatively primitive magmas.

SAMPLE SELECTION AND PREPARATION

During field mapping we have collected over 200 samples of the diverse rocks that constitute the Onion Valley complex. The suite includes samples of each of the rock units that make up the sill swarm and its associated cumulates. All of the samples have been examined in thin section. The freshest representative samples were selected for chemical analysis. Selection criteria for rocks from the sill complex are outlined below.

Thin sills and septa

A large proportion of the analyzed samples are from the homogeneous interiors of thin sheeted sills that display distinct quenched margins. These thin sill samples are thought to be the most likely candidates for magmatic liquid compositions, based on their homogeneous texture, fine grain-

size, quenched margins and mineral habits, and absence of phenocrysts. Sampling of (thin) sills thicker than 1m not undertaken because of the possibility for crystal-liquid segregation. Sills thinner than 10cm were avoided in the sampling because of the possibility of chemical exchange between sills and septa. Two samples of particularly dark sills were collected. The two dark sills have petrographic features, described above, that suggest that they have lost magmatic liquid, and chemistry reinforces the petrographic conclusions. Two samples were collected of fine-grained dikes, one of which is equigranular and cuts sills and the other of which is porphyritic and cuts cumulates. Four samples were collected of light-colored inter-sill septa. A single sample was collected of a sliver of schistose diorite along a fault cutting the sill complex.

Thick sills

Samples from thick sills were also analyzed. These were collected from the massive medium-grained interiors of sills, avoiding obvious heterogeneities such as internal chills or crystal accumulations.

Cumulates

There was a clear bias in the sampling of cumulates toward those rocks that are modally layered or are particularly

mafic. Unlayered cumulates with laminated hornblende and plagioclase crystals are abundant at Onion Valley but are severely underrepresented in the sample collection. Many of the analyzed cumulates are members of the earliest intrusive group at Onion Valley and are not strictly related to the sheeted sill complex. However, with the exception of certain clinopyroxene-bearing cumulates, the differences between rocks of the first and second intrusive episodes are minor.

Sample preparation

Fresh-appearing hand samples were broken to pieces <1cm on the outcrop. Bleached fractures and areas with epidote, pyrite, or obvious chlorite were discarded. Nevertheless, all rocks at Onion Valley (as with most intrusive rocks) show some alteration in addition to subsolidus re-equilibration. All samples show some reaction of late igneous biotite to chlorite plus sphene, and minor pitting of calcic plagioclase and growth of sericite. Samples collected for geochemistry were subsequently examined in thin section and all but the least altered were rejected. Typically, samples used for geochemistry have no more than 20 % of the biotite replaced by chlorite and no more than 5 % of the plagioclase pitted and replaced by sericite. Rock chips were subsequently powdered in an alumina (USGS) or agate (MIT) grinding vessel in preparation for analysis.

ANALYTICAL TECHNIQUES

Except as noted, all analyses were performed in the laboratories of the U. S. Geological Survey by the staff of the Branch of Analytical Chemistry (analytical credits in table 1). Major elements were determined by wavelength dispersive X-ray fluorescence in Lakewood, Colorado (techniques of Taggart et al., 1987). Na_2O and for some samples K_2O were measured by flame emission spectrometry; FeO , CO_2 , and $\text{H}_2\text{O} \pm$ were determined by wet chemical titration or gravimetry in Menlo Park, California (techniques of Jackson, et al., 1987). Rubidium, Sr, Y, Zr, and Ba were determined by energy-dispersive X-ray fluorescence in Menlo Park (technique of Johnson and King, 1987). Niobium was separated by ion exchange and measured by spectrophotometry in either Menlo Park or Reston, Virginia. ICP emission spectrography was used for Ni and V. The rare earth elements, Cs, Th, U, Hf, Ta, Sc, Cr, Co, and Zn were measured by neutron activation analysis in Lakewood, Colorado (techniques described by Baedeker and McKown, 1987).

Four additional samples of thin sheeted sills were analyzed for major elements at MIT. The samples were fused on Fe-Pt alloy loops in a 1-atm gas mixing furnace and quenched to glasses. The glasses were analyzed by electron microprobe using standard techniques. A previously analyzed sample prepared in the same fashion gives results within error of its XRF major element analysis calculated volatile-free.

A number of hornblende, plagioclase, and apatite crystals have been analyzed for various trace elements using the Cameca IMS-3f ion microprobe at MIT. Analytical techniques are outlined in Shimizu and Le Roex (1986), Jolliff et al. (1989), and Sisson (1991, submitted).

Strontium and Pb isotopic ratios were measured at MIT on a very few cumulate samples using techniques described by Hart and Brooks (1977) and Pegram (1987).

Major and trace element analyses of sills and septa are presented in table 1; table 2 contains analyses of representative cumulates. Isotopic data are presented in table 3.

PRECISION AND ACCURACY

The precision and accuracy of neutron activation analyses were evaluated by repeat analysis of USGS standard rocks AGV-1 and RGM-1 and one sample from Onion Valley. Mean values and standard deviations are presented in table 4. Standard rock analyses agree with "consensus" values and analytical precision is adequate for the purposes of the present study.

Bacon and Druitt (1988) also evaluate major element, ICP, and ED-XRF precision and accuracy for U.S.G.S. laboratories. Samples for the present study were analyzed in the same laboratories using the same equipment and techniques. Precision and accuracy are assumed to be comparable to the values reported by Bacon and Druitt (1988).

CHEMICAL VARIATION

Major elements in sills

Thin and thick sheeted sills and inter-sill septa together form well-defined trends on silica variation diagrams (figure 5). Most thin sheeted sills have silica in the range 48.5-51.5 wt.% and thus would be classified as basalts or basaltic andesites if erupted; they will subsequently be referred to as basaltic sills. Silica reaches as high as 58.5 wt.%. The more siliceous sills will be referred to as andesitic. Two sills interpreted by petrography to have lost magmatic liquid are distinguished by very low silica.

Alumina contents are high. The basaltic sills have alumina near 20 wt.%, and alumina decreases only slightly with increasing silica. Magnesia contents and Mg numbers ($Mg\# = 100 * \text{molar Mg} / (\text{Mg} + \text{total Fe})$) are low. Most basaltic sills have MgO between 4 and 5 wt.% and Mg#s in the range 44-48. Magnesia decreases to near 2 wt.% in the most siliceous sills.

The Na₂O contents of the sills are high, on the order of 3.5-4 wt.% at 50 % silica, and show significant scatter. K₂O, in contrast, shows a more clear trend of increase with increasing silica.

The sills define trends typical of calc-alkaline suites on standard discriminant diagrams (figures 6 and 7). On a diagram of FeO/MgO vs. SiO₂ the sill suite begins in the

tholeiitic field and crosses into the calc-alkaline field (figure 6). This type of trend is found in many calc-alkaline volcanic suites that include mafic rocks (Grove and Kinzler, 1986).

The distinctive characteristics, high Al_2O_3 and Na_2O and low MgO even at low silica contents, are shared by many recent volcanic suites situated on convergent plate boundaries. Noteworthy, the volcanic rocks most similar to the Sierran mafic sills have been erupted atop particularly thick crust and show evidence of high magmatic water contents (eg. Guatemala, Rose et al., 1978; Carr and Rose, 1987; Carr and Stoiber, 1988). The present day crust beneath Onion Valley is also thick (ca. 50 km, Dodge and Bateman, 1988). Chemically similar volcanic rocks can also, however, be found in oceanic settings not noted for thick crust (Atka volcanic center, Aleutians, Marsh, 1982).

Major elements in cumulates

The compositions of the Onion Valley cumulates fall in groups that are distinguished by the dominant cumulus phases. A diagram of CaO vs. Al_2O_3 (figure 8) separates the effects of olivine, hornblende, plagioclase, and clinopyroxene accumulation, and illustrates this correlation between cumulus mineralogy and bulk composition. Of note, few cumulate samples lie on the mafic or low silica extension of the sill trend on many major element variation diagrams. This is

particularly apparent on the AFM diagram (figure 7). The sills have nearly constant FeO/MgO. If magmas crystallized along the sill trend, their cumulates would have close to the same FeO/MgO as the sills. However, virtually all analyzed cumulates have FeO/MgO distinctly lower than the sills. Two exceptions are unlayered hornblende gabbro cumulates. The discrepancy between sill and cumulate FeO/MgO is believed to result from the preferential sampling of the layered and mafic mineral-rich cumulates, as discussed above. The layered and mafic mineral-rich cumulates likely were precipitated from magmas more primitive than those sampled as sills, and the presence of olivine in cumulates and its absence in sills supports this interpretation.

Trace elements in sills

The strongly compatible trace elements Ni, Co, and Cr are present in low abundances, even in the basaltic sills, relative to concentrations found in primitive, potentially primary arc basalts (primary magmas are chemically-unmodified liquids produced by melting of a mantle source region, primitive magmas are characterized by high contents of compatible major and trace elements; Perfit, et al., 1980; Nye and Reid, 1986; Bacon, 1990). This is, however, a common characteristic shared by most arc basaltic magmas including those basalts with major element contents similar to the Onion Valley basaltic sills (Basaltic Volcanism Study Project, 1981;

Carr and Rose, 1987; Crawford, et al., 1987). All of the ferro-magnesian trace elements are less abundant at higher silica contents (figure 9, Ni is omitted because its abundance is generally below the limits of accurate measurement).

Abundances of the incompatible elements Rb, Cs, and Ba increase with silica content (figure 9) from the basaltic to the andesitic sills and septa. In contrast, the plagioclase-compatible elements, Sr and Eu, decrease with silica. Other incompatible elements Th, Ta, and U show increasing variation at higher silica contents. In the most silicic sills and septa Th, Ta, and U range from values higher than, to comparable to those found in basaltic sills. Variations in the abundances of Zr, Hf, and Nb are not strongly correlated with silica content.

Certain samples stand out on the silica variation diagrams and consequently deserve special mention. Two sills interpreted as having lost magmatic liquid lie at the low silica end of the trace element arrays defined by the other sills. Other anomalous samples are a thick sill and a thin sill. The anomalous thick sill (85S47A) has high Rb and Cs contents. This sample has higher than normal sericitic alteration that may account for the unusually high alkali contents. The anomalous thin sill (86S41A) has high Sc, Co, Cr, Ni, and V (see also table 1). 86S41A is distinct from the other sills in having the highest MgO and lowest Al_2O_3 at comparable concentrations of the other major elements. As the sample is quite fresh, its distinctive characteristics are

believed to be igneous. Finally, an inter-sill septum (86S32C) lies off the sill trends with distinctly high Zr, Hf, Th, Sr, and light rare earth elements (see also figure 10) and low Ta.

Sills and septa are light rare earth enriched and display small negative europium anomalies on chondrite-normalized abundance diagrams (figure 10). The chondrite-normalized patterns are uniform and show little variation with silica content. Light rare earth elements (La, Ce) have broadly constant concentrations whereas middle and heavy rare earths decrease slightly with increasing silica. Basaltic sills (<52 wt.% SiO₂) show the greatest diversity in rare earth abundances. The samples that have lost magmatic liquid have gently convex-upward patterns if normalized to average basaltic sills (figure 11) and this is consistent with accumulated hornblende. The rare earth abundances of sills and septa are similar to those of local granodiorites (Sawka, et al., 1990; and unpublished analyses of T.W. Sisson and J.G. Moore).

As with major elements, the trace element abundances in sills and septa are similar to those of many modern subduction-related volcanics. Specifically, basaltic and andesitic sills and septa show depletion of Nb, Ta, Zr, and Hf (high field-strength ions) relative to Rb, Sr, K, Ba, Th, and light rare earth elements (figure 12) that is characteristic of many calc-alkaline magmas.

Trace elements in cumulates

Most cumulates are distinguished from the sills by higher concentrations of Co, Sc, and V, and lower concentrations of light rare earth elements, Ba, Rb, and Ta. Concentrations of the other trace elements are generally distinct from but overlap those of the sills and septa. Notably, the layered cumulates are distinct from those sills that have lost magmatic liquid, and lie off of the trends defined by sills and septa for many trace elements.

Trace element contents accord with cumulus mineralogy. Hornblende-rich cumulates have high Sc contents (table 1). Many have convex-upward chondrite-normalized rare earth element abundance patterns, as would be expected of hornblende equilibrated with light rare earth enriched liquids (figure 13). Plagioclase-rich cumulates have high Sr contents. The plagioclase-rich cumulates are light rare earth enriched and some show positive Eu anomalies. Olivine-hornblendites have the lowest rare earth element abundances with convex-upward chondrite-normalized patterns and high Ni, Co, and Cr.

Isotopic variations

The age corrected $^{87}\text{Sr}/^{86}\text{Sr}$ varies for four cumulate samples from 0.7058 to 0.7078, a range well outside of analytical precision (table 3). Lead isotopes are similarly inhomogeneous. The limited data preclude identification of

isotope-isotope or isotope-element correlations. Significance of the isotopic data is discussed below.

DISCUSSION

Geochemical modeling of compositional variations in the Onion Valley Complex: major elements in sills

The major element trends defined by the sills and intersill septa are readily modeled by the crystallization and extraction of the observed early-formed minerals hornblende, calcic plagioclase, magnetite, and apatite. Experimental studies (Sisson and Grove, 1991; Cawthorn and O'Hara, 1976) establish that these minerals are liquidus or near-liquidus phases in wet, sodic, high alumina, low magnesia basalts.

Crystallization and separation of subequal proportions of calcic plagioclase (42-49 %) and hornblende (50-40 %), and moderate amounts of titanomagnetite (6-10 %) and apatite (1 %) from a basaltic sill match the observed major element trends (figure 14 and table 5; see table 5 for explanation of calculations). The most silicic compositions are reproduced by nearly 50 % crystallization of a low-silica basaltic sill. The sills that show petrographic evidence of having lost magmatic liquid are intermediate between calculated crystalline extracts and liquids (figure 14). More complex models involving assimilation or mixing or crystallization of

minerals other than those found in the rocks are not required by the major element data.

Major elements in cumulates

Cumulates and sills are closely-associated in the Onion Valley Complex. This suggests that the cumulates could be the crystal-rich compliments to the liquids now preserved as sills. Compositions of mafic and strongly-layered Onion Valley cumulates are not, however, predicted by the crystallization model presented above. For example, the sills have nearly constant FeO/MgO, and their cumulates are expected to have close to the same FeO/MgO as the sills (figure 14). Yet, most layered cumulates have FeO/MgO distinctly lower than that predicted by the crystallization model. Petrographic and mineralogic evidence suggests that many layered cumulates were precipitated by magmas more primitive than those that have been preserved as sills. Olivine or clinopyroxene are preserved in reaction to hornblende in some cumulate samples, whereas these early minerals are not found in the sills.

We can use cumulus mineral compositions and recent experimental results to judge if magmas parental to the layered cumulates were greatly or only slightly more primitive than the sills. Sisson and Grove (1991) demonstrate that a typical basaltic sill from Onion Valley, 87S35A, can crystallize olivine, hornblende, and calcic plagioclase on its liquidus under water-rich conditions. The liquidus olivine is

Fo⁷⁶, plagioclase is An⁸⁵, and liquidus hornblende has Mg#=71. The experimental mineral compositions are within the range observed in Onion Valley olivine hornblendites (Fo⁷²⁻⁸¹, An⁸⁴⁻⁹⁸, Mg#_{hbl}⁷¹⁻⁷²). The concordance in mineral compositions suggests only small amounts of crystallization from parental magmas to typical sills.

The low FeO/MgO observed in layered cumulates, compared to modeled values, probably results from variations in the proportion of magnetite that crystallized during differentiation of Onion Valley magmas. Sisson and Grove find that magnetite appears shortly below the liquidus in 87S35A and that olivine is subsequently consumed by reaction with liquid. Thus, we expect the proportion of magnetite in cumulates could increase from as low as zero to as much as ~10 wt.% as magmas crystallized and liquids became evolved. The available major element evidence is consistent with the conclusions that: 1) the layered and mafic cumulates at Onion Valley were produced by magmas related to but slightly more primitive than those preserved as sills, and 2) the more primitive magmas crystallized only small amounts to produce basaltic sill-type magmas.

Trace elements in sills

Abundance variations of selected trace elements have been used to test the sheeted sill crystallization model derived using major element data. Field relations are not consistent

with any model involving the crystallization of a single parent magma. Thin sills of various compositions cross cut one another with no temporal succession from mafic to felsic, thick sills were clearly repeatedly-injected with fresh liquids, and primitive cumulates recur throughout the layered cumulate sequences. Initial isotopic ratios of Sr and Pb for cumulates are diverse, further ruling out simple differentiation of a single parent magma. Rather, the geologic evidence is consistent with the presence of multiple chemically-similar but not identical basaltic sill magmas. These magmas crystallized the same types of minerals in the same proportions. In the following discussion we test models of this process and evaluate whether they account for the observed trace element abundance trends.

Trace element modeling has required a judicious choice of mineral-liquid partition coefficients, as the absolute values of many partition coefficients vary with bulk composition and temperature. Concentrations of rare earth and other trace elements were measured (by ion microprobe) in the cores of hornblende, plagioclase, and apatite crystals from one of the sills (86S48) that has lost magmatic liquid. A liquid-depleted sill was chosen because it contains the most crystals likely to preserve near-liquidus trace element concentrations, and crystal cores were chosen to avoid measuring materials grown from near-solidus liquids. Trace elements were not measured in minerals from typical (non-liquid-depleted) sills because patchy major element zoning in hornblende in many of

these samples indicates that the minerals have variably re-equilibrated with near-solidus interstitial liquids. The measured core concentrations were divided by the concentrations of respective trace elements from sample 86S55, an intermediate silica content sill judged to be representative of a liquid composition. The abundance ratios (table 6 and figure 15) are used as guides for the estimation of hornblende-liquid, plagioclase-liquid, and apatite-liquid partition coefficients. While other sills than 86S55 could have been selected without altering the main conclusions reached below, there are additional reasons for using 86S55. First, plagioclase crystal cores in 86S48 are An⁶⁹⁻⁷² and in 86S55 they reach a high of An⁶⁹, suggesting that crystals accumulated in 86S48 could have grown from a liquid like 86S55. Second, use of 86S55 gives D_{Hbl}^{Sm} approximately equal to D_{Hbl}^{Yb} , as is typical of both natural and experimental hornblende/liquid partition coefficients. The estimated partition coefficients (86S48 crystal cores/86S55 whole rock) resemble partition coefficients determined in phenocryst-matrix and experimental studies (Nicholls and Harris, 1980; Green and Pearson, 1985; Schnetzler and Philpotts, 1970; Philpotts and Schnetzler, 1970; Watson and Green, 1981). Titanomagnetite-liquid partition coefficients have, by necessity, been taken from the literature.

The estimated light and middle rare earth element partition coefficients for apatite (figure 15) are higher than experimental values for basaltic to andesitic liquids (table

6) (Watson and Green, 1981). Several factors could account for the discrepancy between estimated values for Onion Valley rocks and those determined experimentally. 1) Disequilibrium growth of apatite is suggested in the natural sills by diverse apatite crystal shapes, ranging from equant to acicular and hollow, and this process could change trace element partition coefficients. 2) Rare earth substitutions in apatite are complex (Burt, 1989) and other factors could influence equilibrium apatite-liquid partition coefficients than those explored experimentally. In light of this discrepancy, two alternate models were constructed using either estimated (this study) or literature (Watson and Green, 1981) apatite-liquid partition coefficients.

Variations in La, Sm, Yb, Rb, Sr, Sc, and V have been calculated for fractional crystallization of basaltic sill magmas, employing the major element model for phase proportions and the estimated and literature trace element partition coefficients. Calculated variations with increasing silica are in broad agreement with the natural samples (figure 16), and lend support to fractional crystallization as the process that created the range of compositions in Onion Valley magmas. Sills that have lost residual liquid have compositions appropriate for magmas with accumulated early-formed crystals. Moderate and realistic adjustments in estimated partition coefficients for Sr in plagioclase (figure 16a), V in magnetite (fig. 16b), and Sc in hornblende (fig. 16b) further improve the agreement between model and samples.

Rb concentrations have been modeled using two initial values of Rb that bracket the range observed in natural Onion Valley basaltic sills (excluding one altered sample with high Rb). Rb calculated in derivative liquids delimit the field defined by Onion Valley andesitic sills.

Crystal fractionation models are not presented for other trace elements either because of the large variation in concentrations independent of silica content (Ba, Zr, Th, U, Ta), poor analytical data due to low concentrations (Cr, Ni), redundancy (many rare earths), or large scatter in or absence of literature partition coefficients (Eu, Ta, Nb, Zr, Y).

Model and natural La abundance trends (figure 16) diverge above about 55 wt.% silica, with the apatite-liquid partition coefficients based on ion-probe data giving closer consistency than the literature value. A further increase in the apatite-liquid rare earth partition coefficients for liquids with greater than 55 wt.% silica would bring the modeled and natural trends into coincidence; such an increase in partition coefficients is plausible on experimental grounds (Watson and Green, 1981).

The crystal-fractionation model (table 5) succeeds in reproducing the dominant major and many trace element abundance variations in the sheeted sills and inter-sill septa (figures 14 and 16). This result accords with the interpretation, based on field relations and petrography, that most thin sheeted sills are quenched liquids and suggests that the thick sills and some inter-sill septa are also composed

largely of crystallized liquid, with few accumulated or entrained crystals.

The factor of ~4 variations in the concentration of Ta, U, Th, Ba, and Zr (figure 9) in basaltic sills indicates diversity in the trace element contents of magmas that reached the Onion Valley complex. The large incompatible element abundance variations in rocks with similar major element compositions could reflect diverse primary magmas or could result from a number of processes such as assimilation or mixing that acted prior to shallow crystallization differentiation. One sample of rock cut by sills, the schistose diorite 88OV7, has high concentrations of Zr, Ba, and Sr (table 1), and incorporation of small amounts of this or similar materials would modify trace element contents in basaltic sill magmas. Resolving the origin of Ta, U, Th, Ba, and Zr abundance variations in basaltic sills will require a larger sample suite than is currently possessed.

Trace elements in cumulates

The rare earth element abundances in the olivine hornblende cumulates can be used to estimate rare earth element characteristics of the least evolved magmas to have reached the intrusive complex. These estimates provide a further test of the hypothesis that the mafic cumulates were produced by magmas related to and only slightly more primitive than those sampled as sheeted sills. Six of seven olivine

hornblendites have uniform rare earth element contents (figure 13). The average major element contents of these six samples are mass balanced by ~40 % olivine, 45 % hornblende, 10 % calcic plagioclase, and 5 % titanomagnetite (using measured cumulus mineral compositions). All of the olivine hornblendites contain as much as a few percent of the intercumulus minerals biotite, orthopyroxene, intermediate plagioclase, and very rare apatite, reflecting the former presence of small amounts of trapped liquid in addition to the cumulus phases.

Hornblende is the only cumulus mineral expected to host significant amounts of rare earth elements. The content of a rare earth element "a" in the parent liquid can therefore be estimated by:

$$\text{Conc a}_{\text{liq}} = \text{Conc a}_{\text{wr}} / (D_a * X_{\text{hbl}} + X_{\text{tl}})$$

where $\text{Conc a}_{\text{liq}}$, $\text{Conc a}_{\text{wr}}$ are concentrations of element a in liquid and whole rock respectively, X_{hbl} , X_{tl} are weight fractions of hornblende and trapped liquid in the whole rock respectively, and D_a is the hornblende-liquid partition coefficient for element a. Furthermore, it is assumed that the trapped liquid is the same as the parent magma.

Results are presented in figure 17 for 0 and 5 % trapped liquid, using both natural and experimental hornblende-basalt partition coefficients (Irving and Frey, 1984; Nicholls and Harris, 1980) and the average rare earth contents of the 6

olivine hornblendites that have nearly uniform rare earth contents. The chosen partition coefficients are lower than those used to model the differentiation of the sheeted sills. The lower values for partition coefficients were chosen because they are consistent with a hotter, less silicic, more primitive magma. Experiments by Nicholls and Harris (1980) and Green and Pearson (1985) and many studies of natural samples document that D increases in cooler, more differentiated magmas.

The calculated rare earth contents of magma parental to the olivine hornblendites strongly resemble those measured in basaltic sheeted sills at Onion Valley (figure 17). The models that assume small amounts of trapped liquid provide a better fit. This result suggests that the most primitive magmas to reach the intrusive complex did not greatly differ from those sampled as basaltic sheeted sills. Therefore, no exotic magma is required to explain the olivine-bearing cumulates. Rather, the major and trace element modeling reinforce the interpretation that the sill complex and associated cumulates are the products of an integrated magmatic system in which crystal fractionation of wet high alumina basalt was the major differentiation process.

Generation of basaltic sill magmas

A variety of basaltic magmas are found in modern subduction-related magmatic arcs (eg. Kuno, 1960). Most are

thought to originate by fusion of mantle peridotite (+/- subduction-zone components) followed by crystallization differentiation and/or assimilation. The low Mg#s and compatible trace element contents of the basaltic sills at Onion Valley preclude an origin as direct partial melts of mantle peridotite. These basalts could have been produced by deep crystallization of hydrous primary basaltic magmas. Ulmer (1986, 1989) conducted melting experiments on hornblende picrite dikes from the Adamello Massif, Italy. He produced water-undersaturated high alumina basalt liquids coexisting with a mantle-like solid phase assemblage of olivine (Fo^{86-81}), high and low calcium pyroxenes, and aluminous spinel at 10 kb and 1120-1090 °C. Hornblende appeared by 1060 ° and olivine was lost by 1000 °. The major element contents of high pressure liquids coexisting with hornblende are similar to the compositions of basaltic sills at Onion Valley. Normalized to 100 %, the hornblende-bearing experimental glasses contain 51-49 wt.% SiO_2 , 20-23 wt.% Al_2O_3 , 5.0-4.5 wt.% MgO , and 4.1-3.5 wt.% Na_2O (Ulmer, 1986), abundances that are comparable to the basaltic sills at Onion Valley (table 1).

We infer that wet primary high alumina basalts originating in the mantle beneath the Mesozoic Sierra Nevada batholith could have been broadly similar to Ulmers 1120-1090 °C liquids, and that crystallization of this liquid at high pressure (eg. base of the crust) generated ultramafic cumulates and residual evolved basaltic liquids of the type

found as sills at Onion Valley. Contamination with rock or magma derived from the crust is a likely complication that can not be addressed with the available sample suite. Discovery of more primitive sills or dikes would establish the interpretation more firmly and reveal a potential role for crustal contamination.

Dry partial-melting of eclogite has also been proposed for the generation of low-magnesium, high alumina basalts (Brophy and Marsh, 1986) similar in major elements to the basaltic sills at Onion Valley. Eclogite melting models find little support at Onion Valley. First, evidence for abundant magmatic water rules out any dry melting to produce the mafic sills. Second, residual garnet in an eclogite source would be expected to produce liquids notably depleted in heavy rare earth elements, a feature not characteristic of basaltic sills at Onion Valley.

The isotopic data presented in table 3, though limited, aids speculation on the origin of the mafic intrusive complex. The age corrected $^{87}\text{Sr}/^{86}\text{Sr}$ isotopic ratios of cumulate samples range from 0.7058 to 0.7078 and are high compared to values of common basalts derived from the oceanic mantle, including most ocean island basalts. The significance of the high ratios is debatable. High $^{87}\text{Sr}/^{86}\text{Sr}$ could have resulted by contamination of low $^{87}\text{Sr}/^{86}\text{Sr}$ mantle-derived magmas with radiogenic continental crust. Alternately, the high $^{87}\text{Sr}/^{86}\text{Sr}$ could be taken as evidence that the mafic rocks at Onion Valley were generated wholly by fusion in the crust. Finally,

some of the sub-Sierran upper mantle could itself have $^{87}\text{Sr}/^{86}\text{Sr}$ elevated relative to common oceanic mantle, and reflected in the magmas derived from it.

Support for the latter interpretation comes from isotopic measurements of Cenozoic mafic volcanic rocks erupted through the Sierra Nevada batholith. Alkali-olivine basalts and olivine tholeiites with high Mg#s and compatible trace element contents have $^{87}\text{Sr}/^{86}\text{Sr} \sim 0.7060$ (Ormerod, et al., 1988). Likewise, an alkali-olivine and ultra-potassic basalt suite with 1200-2400 ppm Sr has average $^{87}\text{Sr}/^{86}\text{Sr}_i = 0.70631 \pm 25$ (Van Kooten, 1981). Peridotite xenoliths carried up in some of the Cenozoic lavas also have high $^{87}\text{Sr}/^{86}\text{Sr}$. Peridotite $^{87}\text{Sr}/^{86}\text{Sr}$ ranges from 0.7031 to 0.7063, and 4 of 6 measured samples have $^{87}\text{Sr}/^{86}\text{Sr} > 0.7056$ (Domenick, et al., 1983; Dodge, et al., 1986). Thus, it is likely that some of the upper mantle below the Sierra Nevada batholith has $^{87}\text{Sr}/^{86}\text{Sr} \sim 0.7060$. Values of $^{87}\text{Sr}/^{86}\text{Sr}_i$ of 0.7058-0.7066 measured in the Onion Valley cumulates therefore do not require extensive assimilation of or generation in the crust. Interaction with radiogenic rock or melt from the crust is probable, however, and may account for some isotopic heterogeneity, especially the higher $^{87}\text{Sr}/^{86}\text{Sr}_i$ of 0.7078 found in one sample.

Interpretation of Pb isotopic ratios is less equivocal. Figure 18 shows age corrected $^{208}\text{Pb}/^{204}\text{Pb}$ and $^{207}\text{Pb}/^{204}\text{Pb}$ plotted against $^{206}\text{Pb}/^{204}\text{Pb}$ for the two cumulate samples, as well as fields for feldspars from granitoid rocks of the Sierra Nevada batholith (Chen and Tilton, 1978, and

unpublished data). The samples from Onion Valley are isotopically distinct from the granitoids and extend the granitoid array toward less radiogenic compositions. Magmas parental to the cumulates cannot have been produced from the same sources that created the Sierran granitoids (eg. by higher degrees of melting). Conversely, most granitoids could be mixtures of a radiogenic (crustal?) component and unradiogenic mafic melt like the Onion Valley magma that precipitated the cumulates. Lead isotopic ratios of the mafic cumulates overlap those of modern oceanic basalts and approach some mid-ocean ridge basalt values (compilation of Hart and Zindler, 1989), lending credibility the interpretation of an ultimate mantle origin for the mafic rocks at Onion Valley.

*Relation to Sierran granitoids: crystallization
differentiation*

Sills from Onion Valley overlap with compositions of Sierran intrusive rocks and extend the chemical trends to more primitive compositions (for example, figure 7). We assume that the mafic liquids at Onion Valley were comparable to mafic liquids that participated in generating the more voluminous and more evolved granodioritic and granitic rocks that constitute the bulk of the Sierran batholith.

Several lines of evidence suggest that the voluminous granodiorites did not form as derivative liquids through fractional crystallization of basaltic sill-type magmas. Many

low-silica Sierran granitoids (59-63 wt.% SiO_2) contain augite preserved in the cores of hornblende crystals (Bateman and Chappell, 1979; Sawka et al., 1990; Hirt, 1989). Basaltic sills crystallized hornblende as the liquidus Fe-Mg silicate, and do not show evidence of augite crystallization at any point during their solidification history. To be parental, basaltic sill-type liquids would have to have carried or crystallized late clinopyroxene. Simple petrography shows that they did not and this is amply confirmed by experiment (Sisson and Grove, 1991). Early-crystallized clinopyroxene can be found in some mafic rocks at Onion Valley and at other mafic intrusive complexes in the region, but the pyroxene is replaced by hornblende before granodioritic compositions are reached.

The mafic sill magmas at Onion Valley and comparable mafic magmas from elsewhere in the Sierra Nevada also had very high magmatic water contents. They may commonly have reached water-saturation. Evidence includes miarolytic cavities and vugs, very calcic plagioclase, and association with hornblende-plagioclase pegmatites. Granitoid magmas derivative by fractional crystallization of these mafic sills would have had even higher water contents. Evidence for such high water contents in the voluminous granitoids is lacking. Sierran granitoids generally do not contain miarolitic cavities or vugs, pegmatites are present but not abundant, and plagioclase is not notably calcic (figure 19). Together, the evidence suggests that basaltic sill-type magmas were not

parental to Sierran granitoids through crystallization differentiation.

Magma mixing

Common Sierran granodiorites could have formed as hybrids by the mixing of basaltic sill type magmas and crustal melts. Several studies have concluded that Sierran granitoids are mixtures of felsic and mafic components derived from the crust and mantle respectively (Reid, et al., 1983; Frost and Mahood, 1987; Kistler, et al., 1987; Saleeby, et al., 1987). The studies have been limited by the lack of samples of the mafic mixing component(s). They were forced to either use mafic inclusions in granitoids as analogs of the mafic mixing component, or use the chemical variation in granitoids to infer the mafic components composition. The analog or inferred basaltic components in these models have major element compositions similar to the basaltic sills at Onion Valley.

The mixing hypothesis has been explored using the average trace element contents of basaltic sills from Onion Valley, Sierran granites, and Sierran granodiorites (table 7). Average basaltic sill is taken as the mafic mixing component and corresponds to hydrous high alumina basalt. Average low-silica granite is taken as the felsic and dominantly crustal component, and is likely drier than the basalt, having been produced by dehydration melting of continental crust. Average

granodiorite is the hybrid what we seek to produce. Seventy-one per cent average low-silica granite (72 wt.% SiO_2) mixed with 29 % average basaltic sill (50.8 wt.% SiO_2) yields average granodiorite with 65.8 wt.% SiO_2 . Trace element contents for this mixture closely approximate the average trace element contents of Sierran granodiorite (table 7, figure 20). Nine of 17 geochemically-diverse trace elements have predicted abundances that differ from the average granodiorite values by less than 5 % relative. None of the 17 elements deviate by as much as 10 % relative. Including the 9 major elements, concentrations of 26 elements ranging in abundance from tens of weight percents to less than 1 ppm are successfully predicted by a mixing model. The agreement between predicted and average trace element contents support the interpretation that common granodiorite of the Sierra Nevada batholith is a hybrid of evolved wet high alumina basalt and granitic melt. Lead isotopic data discussed above reinforce this conclusion.

The differences in crystallization temperatures of basalts and rhyolites limit the proportions that can mix to produce homogeneous hybrids (Sparks and Marshall, 1986). Frost and Mahood (1987) explored the physical limitations on mixing of basalt with granite in the Sierra Nevada batholith. They concluded that hybrids with greater than 62 wt.% silica were unlikely to have formed since smaller fractions of basalt would have been quenched long before mixing could occur. Experiments on high alumina basalt and basaltic andesite, and

hornblende gabbro and diorite show that Frost and Mahood overestimated the wet liquidii of appropriate basalt compositions by close to 200 °C (Frost and Mahood, 1987; Frost and Lindsay, 1988; Sisson and Grove, 1991). Homogeneous hybrids with silica >62 wt.% could have formed, since the quenching effect on the basalt would have been far less than had been estimated. Higher-silica hybrids accord with the modeling results of Kistler and others (1986) for the Tuolumne Intrusive Suite.

The mixing model falls far short of explaining the detailed differences between specific samples of intrusive rocks of the Sierra Nevada batholith. Hybrid magmas likely underwent subsequent crystallization differentiation and/or additional mixing. Sources for anatectic melts certainly varied in major and trace element contents, and this would have been reflected by diversity in their fusion products. Variable trace element contents are also likely for the basalts and basaltic andesites, as is found at modern convergent margins. Nonetheless, mixing between wet high alumina basalt and granitic melt produced by crustal fusion can reproduce most of the chemical characteristics of typical Sierran granodiorite.

Relation to mafic inclusions

Field evidence for mixing between basalt and granite is rare in the Sierra Nevada batholith. Places can be found where incompletely mixed magmas have frozen, but these areas

are small, of limited extent, and are restricted to the vicinity of mafic intrusions. In contrast, fine-grained and dark-colored mafic inclusions are common, being scattered one or more per m^2 in granodiorite and granite plutons covering hundreds of km^2 (Moore, 1963; Bateman et al., 1963). The abundance and ubiquity of the mafic inclusions is evidence that they are in some way related to the genesis of their host plutons. Field relations and petrography show that a small subset of mafic inclusions originated as quenched masses of basaltic or andesitic magma. For most inclusions, outcrop observations provide little evidence of their origin except to show that they were not derived from adjacent wallrocks (Pabst, 1928; Moore, 1963). Most possess igneous textures, such as zoned tabular plagioclase laths and interstitial late-crystallized quartz, and many contain outsized crystals apparently entrained from their hosts (authors observations, see also Pabst, 1928; Vernon, 1983; and Hirt, 1989).

Mafic inclusions have been hypothesized to be quenched magmas (Reid, et al., 1983; Didier, 1973), early-formed indigenous cumulates of their host magmas (Dodge and Kistler, 1990), or unmelted refractory material (restite) from a postulated crustal source area of their hosts (Bateman, et al. 1963; Presnall and Bateman, 1973). Both quenched magmas and cumulates are present as inclusions in many volcanic rocks (Bacon and Metz, 1984; Grove and Donnelly-Nolan, 1986), whereas erupted restite inclusions are unusual.

We address the question of the origin of mafic inclusions by comparing their compositions with those of the basaltic sills at Onion Valley. Major and trace element analyses of mafic inclusions have been compiled from the literature and average compositions have been calculated for inclusions with less than 52.5 wt.% SiO_2 . As noted previously the major element compositions of mafic inclusions resemble those of the sills at Onion Valley. There are systematic differences between the trace element contents of low-silica mafic inclusions and basaltic sills (figure 21). Relative to basaltic sills, mafic inclusions are enriched in trace elements which are both compatible in biotite, sphene, and hornblende and are abundant in most granitic magmas (Rb, U, Th, Nb, Y, Zr, middle rare earths). The inclusions are depleted in elements compatible in alkali feldspars (Sr, Ba, Eu). Light rare earth contents are variable, and the inclusions are depleted in V relative to the sills.

The textural evidence that the inclusions are igneous is compelling. The cumulate hypothesis provides no ready explanation for the fine grain-size and the entrained coarse host crystals. We consider it likely that the inclusions began as magmas like the basaltic sills and were incorporated either as partly-quenched magma blobs or as partly-solidified mafic rock fragments, and that elements have exchanged between host and inclusions as the host magma slowly solidified. Strontium, Ba, and Eu have been lost to the alkali feldspars in the crystallizing host. Biotite has grown as a product of

reaction between aluminous hornblende and granitic liquid and has fixed Rb in the inclusions. Likewise, U, Th, Nb, Y, Zr, and the middle rare earths have been scavenged from the host magma into the sphene and hornblende in the inclusions. Residual granitic liquids contain little Sc, Co, and V and thus these elements are not enriched in the inclusions and may even have been depleted (eg. V).

Dodge and Kistler (1990) have shown that many Sierran mafic inclusions have the same initial $^{87}\text{Sr}/^{86}\text{Sr}$ as their host rocks. Isotopic equilibrium between host and inclusions is consistent with chemical exchange. Leshner (1990) has demonstrated experimentally that isotopes of Sr exchange rapidly between mafic and felsic melts leading to isotopically homogeneous but chemically inhomogeneous magmas. This process has been demonstrated to occur in volcanic environments (Grove, et al., 1988), and so is expected in slowly cooled plutons as well.

SUMMARY AND CONCLUSIONS

The sheeted sill complex at Onion Valley preserves evolved wet high alumina basalts through aluminous andesites that were present during formation of the Sierra Nevada batholith. The basaltic magmas crystallized hornblende, plagioclase, magnetite, and apatite in a high-level intrusive complex and produced andesite sills and magmatic septa as derivative

liquids. Layered and mafic cumulates were precipitated by less evolved magmas than those sampled as sills.

The Onion Valley high alumina basalts were not primary magmas derived by melting of the mantle. Primitive basalts apparently failed to ascend through the thick crust of the continental margin. Experimental studies show that the Onion Valley high alumina basalts could have evolved from more primitive mantle-derived basalts that lodged near the base of the crust.

Wet mafic magmas similar to the basaltic sills were important for the production of the more common granodiorite magmas of the Sierra Nevada batholith. A mixture of average basaltic sill and average low silica granite reproduces the major and trace element characteristics of average Sierran granodiorite. Low basalt-fraction mixtures are allowed by the low liquidus temperatures of the basaltic sill magmas. The common mafic inclusions in Sierran granitoids could plausibly have originated as inclusions of magmas similar to the basaltic sills at Onion Valley, but have undergone extensive chemical exchange with their hosts.

The present study supports the concept that the Sierra Nevada batholith formed by massive underplating of the crust by wet arc basalts. Most crystallized at depth leaving ultramafic cumulates and liberating heat and water to fuse and flux the crust. Anatectic melts mixed with wet evolved basalts, producing granodioritic hybrids. These ascended with entrained magmatic inclusions to form the common plutons of

the Sierra Nevada batholith. Some evolved wet basalts leaked to shallow depths to create mafic intrusive complexes such as that exposed at Onion Valley.

References

- Bacon, C.R. (1990) Calc-alkaline, shoshonitic, and primitive tholeiitic lavas from monogenetic volcanoes near Crater Lake, Oregon. *Jour. Petrol.* 31, 135-166.
- Bacon, C.R. and Druitt, T.H. (1988) Compositional evolution of zoned calc-alkaline magma chamber of Mount Mazama, Crater Lake, Oregon. *Contr. Miner. Petrol.* 98, 224-256.
- Bacon, C.R. and Metz, J. (1984) Magmatic inclusions in rhyolites, contaminated basalts, and compositional zonation beneath the Coso volcanic field, California. *Contr. Miner. Petrol.* 85, 346-365.
- Baedecker, P.E., and McKown, D.M. (1987) Instrumental neutron activation analysis of geochemical samples. In: P.E. Baedecker, ed., *Methods for geochemical analysis*, U.S. Geol. Survey Bull. 1770, H1-H14.
- Barbarin, B. (1990) Plagioclase xenocrysts and mafic magmatic enclaves in some granitoids of the Sierra Nevada batholith, California. *Jour. Geophys. Res.* 95, 17747-17756.
- Barbarin, B., Dodge, F.C.W., Kistler, R.W., and Bateman, P.C. (1989) Mafic inclusions and associated aggregates and dikes in granitoid rocks, central Sierra Nevada Batholith, analytic data. U.S. Geol. Survey Bull. 1899, 28pp.
- Basaltic Volcanism Study Project (1981) "Basaltic volcanism on the terrestrial planets". Pergamon Press, Inc., 1286pp.
- Bateman, P.C., and Chappell, B.W. (1979) Crystallization, fractionation, and solidification of the Tuolumne Intrusive Series, Yosemite National Park, California. *Geol. Soc. Amer. Bull.*, Part I. 90, 465-482.
- Bateman, P.C., Clark, L.D., Huber, N.K., Moore, J.G., and Reinhart, C.D. (1963) The Sierra Nevada batholith-a synthesis of recent work across the central part. U.S. Geol. Survey Prof. Paper 414D, D1-D46.

- Bateman, P.C., and Nokleberg, W.G. (1978) Solidification of the Mount Givens granodiorite, Sierra Nevada, California. *Jour. Geol.* 86, 563-579.
- Bateman, P.C., Chappell, B.W., Kistler, R.W., Peck, D.L., and Busacca, A (1988) Tuolumne Meadows quadrangle-analytic data. U.S. Geol. Survey Bull. 1819, 43pp.
- Boynton, W.V. (1984) Cosmochemistry of the rare earth elements: meteorite studies. In: P. Henderson, ed., Rare earth element geochemistry, Elsevier, New York.
- Brophy, J.G., and Marsh, B.D. (1986) On the origin of high-alumina arc basalt and the mechanics of melt extraction. *Jour. Petrol.* 27, 763-789.
- Burt, D.M. (1989) Compositional and phase relations in rare earth minerals. In: B.R. Lipkin and G.A. McKay, eds., Geochemistry and mineralogy of rare earth elements. *Reviews in mineralogy.* 21, 259-307.
- Carr, M.J., and Rose, W.I. (1987) Centam-a data base of Central American volcanic rocks. *Jour. Volc. Geotherm. Res.* 33, 239-240.
- Carr, M.J., and Stoiber R.E. (1988) Volcanism. In: G. Dengo and J.E. Case, eds., The geology of North America, vol. H, the Caribbean region. *Geol. Soc. Amer.*
- Cawthorn R.G., and O'Hara, M.J. (1976) Amphibole fractionation in calc-alkaline magma genesis. *Amer. Jour. Sci.* 276, 309-329.
- Chen, J.H., and Moore, J.G. (1982) Uranium-lead isotopic ages from the Sierra Nevada batholith, California. *Jour. Geophys. Res.* 87, 4761-4784.
- Chen, J.H., and Tilton, G.R. (1978) Lead and strontium isotopic studies of the southern Sierra Nevada batholith, California. *Geol. Soc. Amer. Abstr. Programs* 10, 99-100.
- Crawford, A.J., Falloon, T.J., and Eggins, S. (1987) The origin of island arc high-alumina basalts. *Contr. Miner. Petrol.* 97, 417-430.

- Didier, J. (1973) Granites and their enclaves. Developments in petrology, vol. 3, 393pp, Elsevier, New York.
- Dodge, F.C.W., and Bateman, P.C. (1988) Nature and origin of the root of the Sierra Nevada. Amer. Jour. Sci. 288-A, 341-357.
- Dodge, F.C.W., and Calk, L.C. (1987) Lake Eleanor quadrangle, central Sierra Nevada, California-Analytic data. U.S. Geol. Survey Bull. 1585. 19pp.
- Dodge, F.C.W. and Kistler, R.W. (1990) Some additional observations on inclusions in the granitic rocks of the Sierra Nevada. Jour. Geophys. Res. 95, 17,841-17,848.
- Dodge, F.C.W., Calk, L.C. and Kistler, R.W. (1986) Lower crustal xenoliths, Chinese Peak lava flow, central Sierra Nevada. Jour. Petrol. 27, 1277-1304.
- Dodge, F.C.W., Millard, H.T., and Elsheimer, H.N. (1982) Compositional variations and abundances of selected elements in granitoid rocks and constituent minerals, central Sierra Nevada batholith, California. U.S. Geol. Survey Prof. Paper 1248. 24pp.
- Domenick, M.A., Kistler, R.W., Dodge, F.C.W., and Tatsumoto, M. (1983) Nd and Sr isotopic study of crustal and mantle inclusions from the Sierra Nevada and implications for batholith petrogenesis. Geol. Soc. Amer. Bull. 94, 713-719.
- Frost, T.P., and Lindsay J.R. (1988) Magmix: a BASIC program to calculate viscosities of interacting magmas of differing composition, temperature, and water content. Comput. Geosci. 14, 213-228
- Frost, T.P., and Mahood, G.A. (1987) Field, chemical, and physical constraints on mafic-felsic magma interaction in the Lamark Granodiorite, Sierra Nevada, California. Geol. Soc. Amer. Bull. 99, 272-291.
- Frost, T.P. (1988) written communication containing U-Pb ages of mafic intrusive bodies north of the Onion Valley complex.

- Gill, J.B. (1981) Orogenic andesites and plate tectonics. Springer-Verlag, Berlin, 390pp.
- Gladney, E.S., Burns, C.E., and Roelandts, I. (1983) 1982 compilation of elemental concentrations in eleven United States Geological Survey rock standards: Geost. News1. 7, 3-226.
- Gladney, E.S., and Roelandts, I. (1988) Compilation of elemental concentration data for USGS BHVO-1, MAG-1, QLO-1, RGM-1, SCO-1, SDC-1, SGR-1, and STM-1. Geost. News1. 12, 253-362.
- Green, T.H., and Pearson, N.J. (1985) Experimental determination of REE partition coefficients between amphibole and basaltic liquids at high pressure. Geochim. Cosmochim. Acta 49, 1465-1468.
- Grove, T.L., and Donnelly-Nolan, J.M. (1986) The evolution of young silicic lavas at Medicine Lake volcano, California: implications for the origin of compositional gaps in calc-alkaline series lavas. Contr. Miner. Petrol. 92, 281-302.
- Grove, T.L., and Kinzler, R.J. (1986) Petrogenesis of andesites. Ann. Rev. Earth Planet. Sci. 14, 417-454.
- Grove, T.L., Kinzler, R.J., Baker, M.B., Donnelly-Nolan, J.M., and Leshner, C.E. (1988) Assimilation of granite by basaltic magma at Burnt Lava flow, Medicine Lake volcano, northern California: decoupling of heat and mass transfer. Contrib. Miner. Petrol. 99, 320-343.
- Hart, S.R., and Brooks, C. (1977) The geochemistry and evolution of early Precambrian mantle. Contrib. Mineral. Petrol. 61, 109-128.
- Hart, S.R., and Zindler, A. (1989) Constraints on the nature and development of chemical heterogeneities in the mantle. In: D. Peltier, ed., Mantle Convection. Gordon Breach pubs.
- Hirt, W.H. (1989) The petrological and mineralogical zonation of the Mount Whitney Intrusive Suite, eastern

- Sierra Nevada, California. University of Calif, Santa Barbara, PhD thesis. 278p.
- Irvine, T.N., and Baragar, W.R.A. (1971) A guide to the classification of the common volcanic rocks. *Can. Jour. Earth Sci.* 8, 523-548.
- Irving, A.J., and Frey, F.A. (1984) Trace element abundances in megacrysts and their host basalts: constraints on partition coefficients and megacryst genesis. *Geochim. Cosmochim. Acta* 48, 1201-1221.
- Jackson, L.L., Brown, F.W., and Neil, S.T. (1987) Major and minor elements requiring individual determination, classical whole rock analysis, and rapid rock analysis. *In*: P.E. Baedecker, ed., *Methods for geochemical analysis*, U.S. Geol. Survey Bull. 1770, G1-G23.
- Johnson, R.G., and King, B.-S.L. (1987) Energy-dispersive X-ray fluorescence spectrometry. *In*: P.E. Baedecker, ed., *Methods for geochemical analysis*, U.S. Geol. Survey Bull. 1770, F1-F5.
- Jolliff, B.L., Papike, J.J., Shearer, C.K. and Shimizu, N. (1989) Inter-and intra-crystal REE variations in apatite from the Bob Ingersoll pegmatite, Black Hills, South Dakota. *Geochim. Cosmochim. Acta*. 53, 429-441.
- Kistler, R.W., Chappell, B.W., Peck, D.L., and Bateman, P.C. (1987) Isotopic variations in the Tuolumne Intrusive Suite, central Sierra Nevada, California. *Contr. Miner. Petrol.* 94, 205-220.
- Kuno, H. (1960) High-alumina basalt. *Jour. Petrol.* 1, 121-145.
- Leshner, C.E. (1990) Decoupling of chemical and isotopic exchange during magma mixing. *Nature*, 344, 235-237.
- Marsh, B.D. (1982) The Aleutians. *In*: R.S. Thorpe, ed., *Andesites*. Wiley, New York, pp 99-114.
- Miyashiro, A. (1974) Volcanic rock series in island arcs and active continental margins. *Am. Jour. Sci.* 274, 321-355.

- Moore, J.G. (1963) Geology of the Mount Pinchot quadrangle southern Sierra Nevada California. U.S. Geol. Survey Bull. 1130, 152pp.
- Nicholls, I.A., and Harris, K.L. (1980) Experimental rare earth element partition coefficients for garnet, clinopyroxene, and amphibole coexisting with andesitic and basaltic liquids. *Geochim. Cosmochim. Acta*, 44, 287-308.
- Noyes, H.J., Frey, F.A., and Wones, D.R. (1983) A tale of two plutons: geochemical evidence bearing on the origin and differentiation of the Red Lake and Eagle Peak plutons, central Sierra Nevada, California. *Jour. Geol.* 91, 487-509.
- Nye, C.J., and Reid, M.R. (1986) Geochemistry of primary and least-fractionated lavas from Okmok Volcano, central Aleutians: implications for arc magma genesis. *Journ. Geophys. Res.* 91, 271-287.
- Ormerod, D.S., Rogers, N.W. and Hawkesworth, C.J. (1988) Use of the inverse modelling technique in determining the composition of the sub-continental lithospheric mantle. *Chem. Geol.* 70, p154.
- Pabst, A. (1928) Observations on inclusions in the granitic rocks of the Sierra Nevada. *Univ. of Calif. Publ., Bull. of the Dept. of Geol. Sci.* vol 17, no 10, 325-386.
- Pearce, J.A. (1982) Trace element characteristics of lavas from destructive plate boundaries. In: R.S. Thorpe, ed., *Andesites*. John Wiley, New York, 525-548.
- Peck, D.L., and Van Kooten, G.K. (1983) Merced Peak quadrangle, California-analytic data. U.S. Geol. Survey Prof. Paper 1170-D. 11pp.
- Pegram, W.J. (1986) Geochemical processes in the sub-continental mantle and the nature of crust mantle interaction: Evidence from the Mesozoic Appalachian tholeiite province. Mass. Inst. Technology, PhD thesis.

- Perfit, M.R., Gust, D.A., Bence, A.E., Arculus, R.J., and Taylor, S.R. (1980) Chemical characteristics of island arc basalts: implications for mantle sources. *Chem. Geol.* 30, 227-256.
- Philpotts, J.A., and Schnetzler, C.C. (1970) Phenocryst-matrix partition coefficients for K, Rb, Sr, and Ba with applications to anorthosite and basalt genesis. *Geochim. Cosmochim. Acta*, 34, 307-322.
- Piwinskii, A.J. (1968) Studies of batholithic feldspars: Sierra Nevada, California. *Contr. Miner. Petrol.* 17, 204-223.
- Presnall, D.C., and Bateman, P.C. (1973) Fusion relations in the system $\text{NaAlSi}_3\text{O}_8$ - $\text{CaAl}_2\text{Si}_2\text{O}_8$ - KAlSi_3O_8 - SiO_2 - H_2O and generation of granitic magmas in the Sierra Nevada batholith. *Geol. Soc. Amer. Bull.* 84, 3181-3202.
- Reid, J.B., Evans, O.C., and Fates, D.G. (1983) Magma mixing in granitic rocks of the central Sierra Nevada, California. *Earth Planet. Sci. Lett.* 66, 243-261.
- Rose, W.I., Anderson, A.T., Woodruff, L.G. and Bonis, S.B. (1978) The October 1974 basaltic tephra from Fuego Volcano: Description and history of the magma body. *Jour. Volc. Geotherm. Res.* 4, 3-53.
- Saleeby, J.B., Sams, D.B., and Kistler, R.W. (1987) U/Pb zircon, strontium and oxygen isotopic and geochronological study of the southernmost Sierra Nevada batholith, California. *Jour. Geophys. Res.* 92, 10443-10466.
- Sawka, W.N. (1988) REE and trace element variations in accessory minerals and hornblende from the strongly zoned McMurtry Meadows pluton, California. *Trans. Roy. Soc. Edinburgh: Earth Sci.* 79, 157-168.
- Sawka, W.N., Chappell, B.W., and Kistler, R.W., (1990) Granitoid compositional zoning by side-wall boundary layer differentiation: Evidence from the Palisade Crest Intrusive Suite, central Sierra Nevada, California. *Jour. Petrol.* 31, 519-553.

- Schnetzler, C.C., and Philpotts, J.A., (1970) Partition coefficients of rare earth elements between igneous matrix material and rock-forming mineral phenocrysts. *Geochim. Cosmochim. Acta.* 34, 331-340.
- Shimizu, N., and le Roex, A.P., (1986) The chemical zoning of augite phenocrysts in alkaline basalts from Gough Island, South Atlantic. *Jour. Volc. Geotherm. Res.* 29, 159-188.
- Sisson, T.W. (1991) Pyroxene-high silica rhyolite trace element partition coefficients measured by ion microprobe. Submitted to *Geochimica et Cosmochimica Acta*.
- Sisson, T.W., and Grove, T.L., (1991) Experimental evidence for high water contents in some aluminous arc magmas. Chapter 2 of this thesis.
- Sparks, R.S.J., and Marshall, L. (1986) Thermal and mechanical constraints on mixing between mafic and silicic magmas. *Jour. Volc. Geotherm. Res.* 29, 99-124.
- Taggart, J.E., Lindsay, J.R., Scott, B.A., Vivit, D.V., Bartel, A.J., and Stewart, K.C. (1987) Analysis of geologic materials by wavelength-dispersive X-ray fluorescence spectrometry. In: P.E. Baedeker, ed., *Methods for geochemical analysis*, U.S. Geol. Survey Bull. 1770, E1-E19.
- Ulmer, P. (1986) *Basische und ultrabasische Gesteine des Adamello*. ETH, Zurich, PhD dissertation.
- Ulmer, P. (1989) The dependence of the Fe²⁺-Mg cation-partitioning between olivine and basaltic liquid on pressure, temperature, and composition. *Contrib. Miner. Petrol.* 101, 261-273.
- Van Kooten, G.K. (1981) Pb and Sr systematics of ultrapotassic and basaltic rocks of the central Sierra Nevada, California. *Contr. Miner. Petrol.* 76, 378-385.
- Vernon, R.H. (1983) Restite, xenoliths, and microgranitoid enclaves in granites. *Jour. Proc. R. Soc. N. S. W.*, 116, 77-103.

Watson, E.B., and Green, T.H. (1981) Apatite/liquid partition coefficients for the rare earth elements and strontium. *Earth Planet. Sci. Lett.* 56, 405-421.

Figure 1-1. Simplified geologic map of the mafic intrusive complex at Onion Valley.

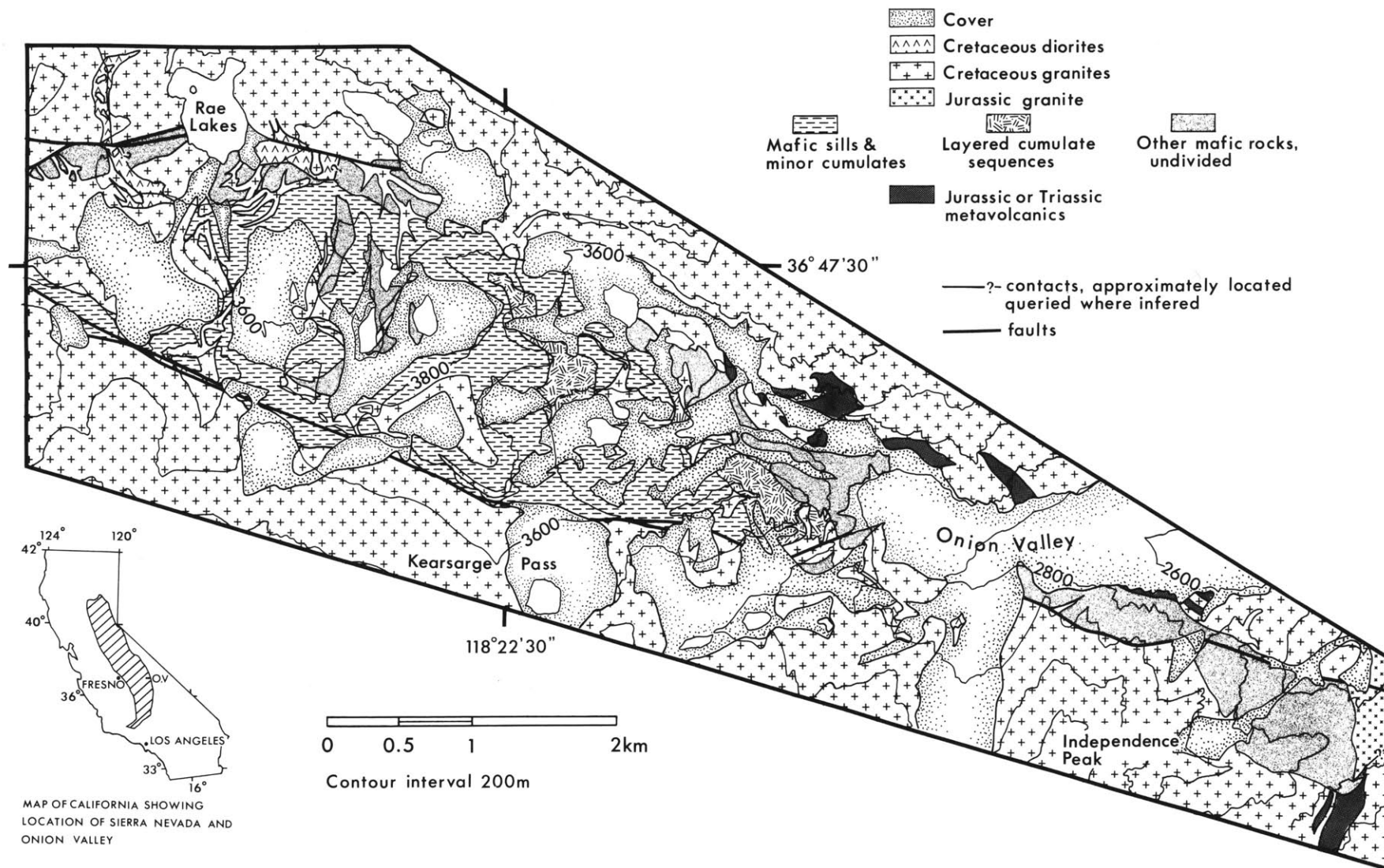


Figure 1-2. Outcrop relations in the sill swarm. A. Three thin sills (stippled) exposed in a talus block have chilled contacts (finely stippled) against light-colored intersill magmatic septa (unpatterned). Hornblende and biotite (black) are concentrated at the tops of apophyses of intersill septa. Handlens for scale. B. Detail of a thin sill (horizontal) with chilled upper and lower contacts cut by a small dike fed from the magmatic septum that underlies the sill. C. Dike of intersill magmatic septum (unpatterned) cuts a thin sill but is itself cut by a younger thin sill. Y, O indicates relative ages across contacts. D. Diorite pillows with chilled contacts in the interior of a thick sill. T-talus, sh-shadow, handlens for scale.

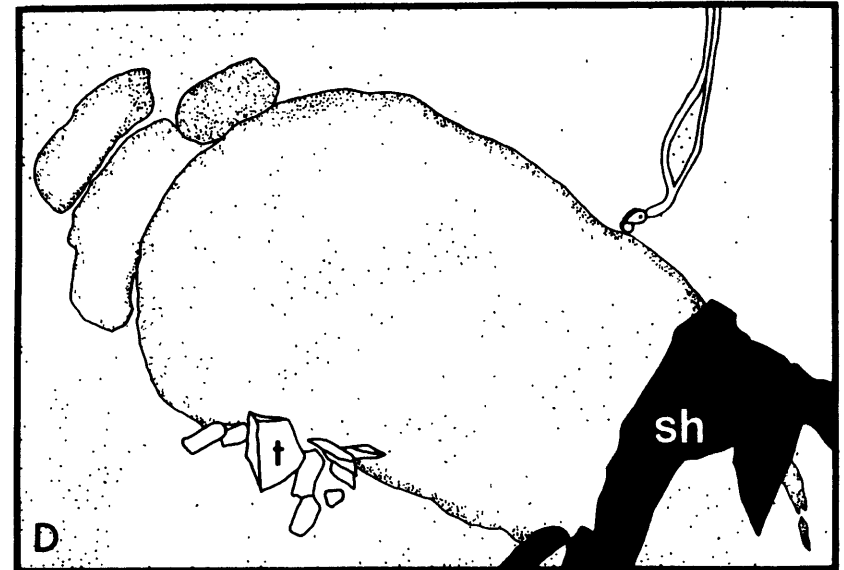
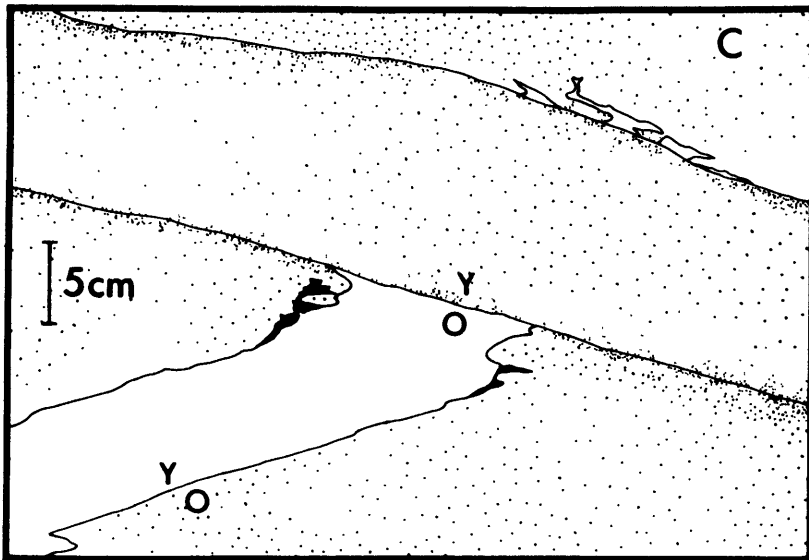
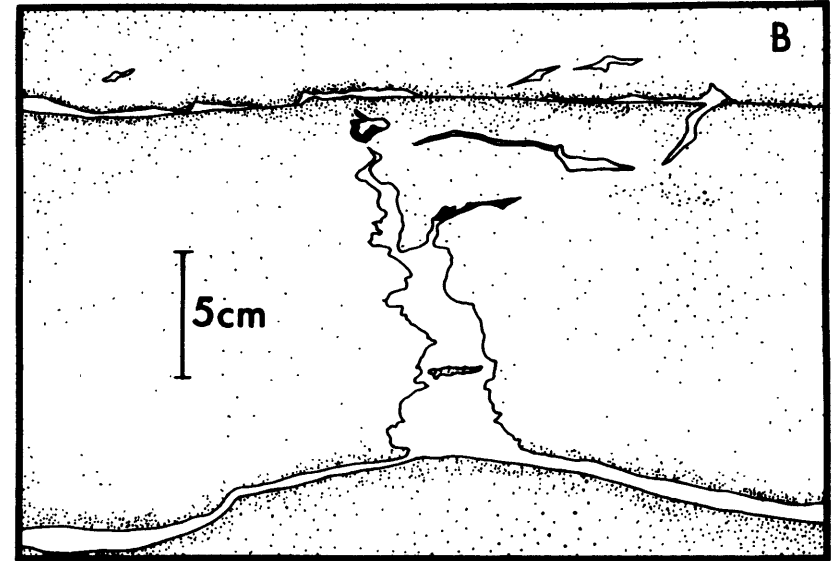
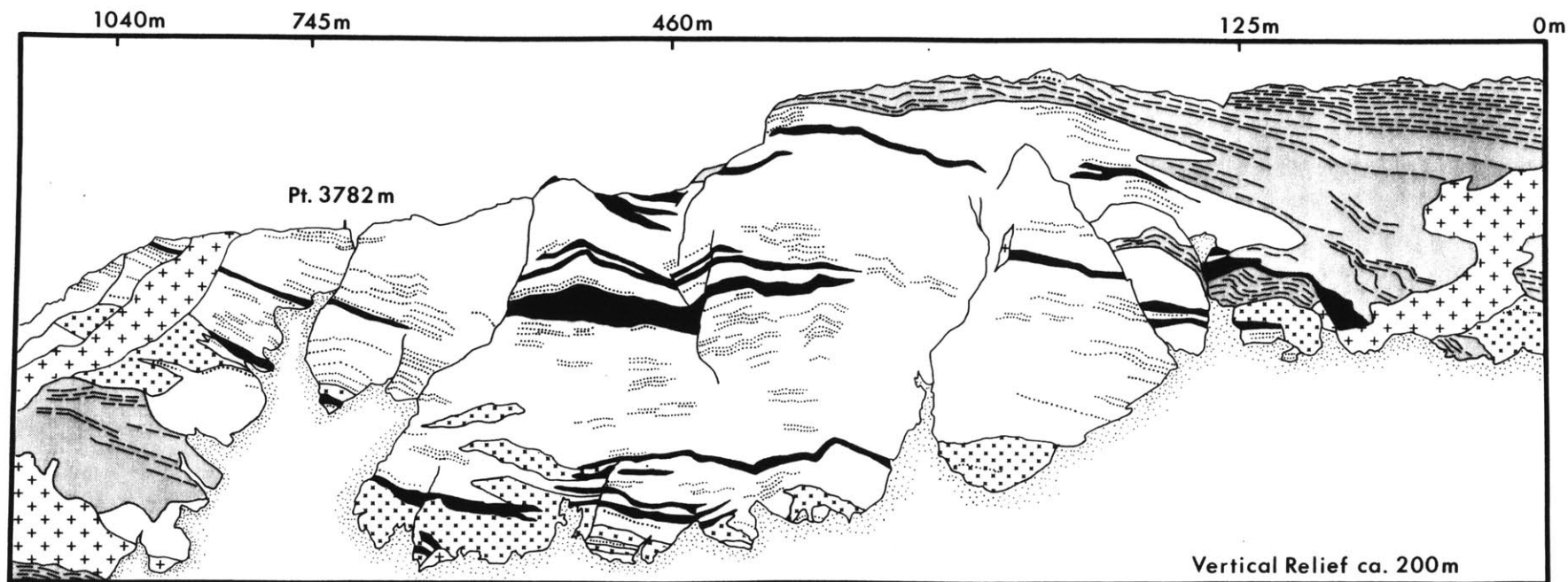
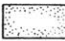
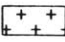
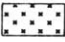
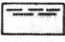
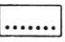



Figure 1-3. A. Geologic map of the north face of the ridge containing Pt. 3782 m, in the mafic intrusive complex at Onion Valley. The cliff face exposes a lens of layered cumulates overlain and underlain by, and passing along strike to sheeted sills. Mafic cumulates recur through the cumulate series, indicating replenishment with new magmas. Hornblende-plagioclase pegmatites were mobile late and may have formed from water-rich residual liquids. Distance along the ridge crest is shown at the top. Vertical relief is ~200 m.

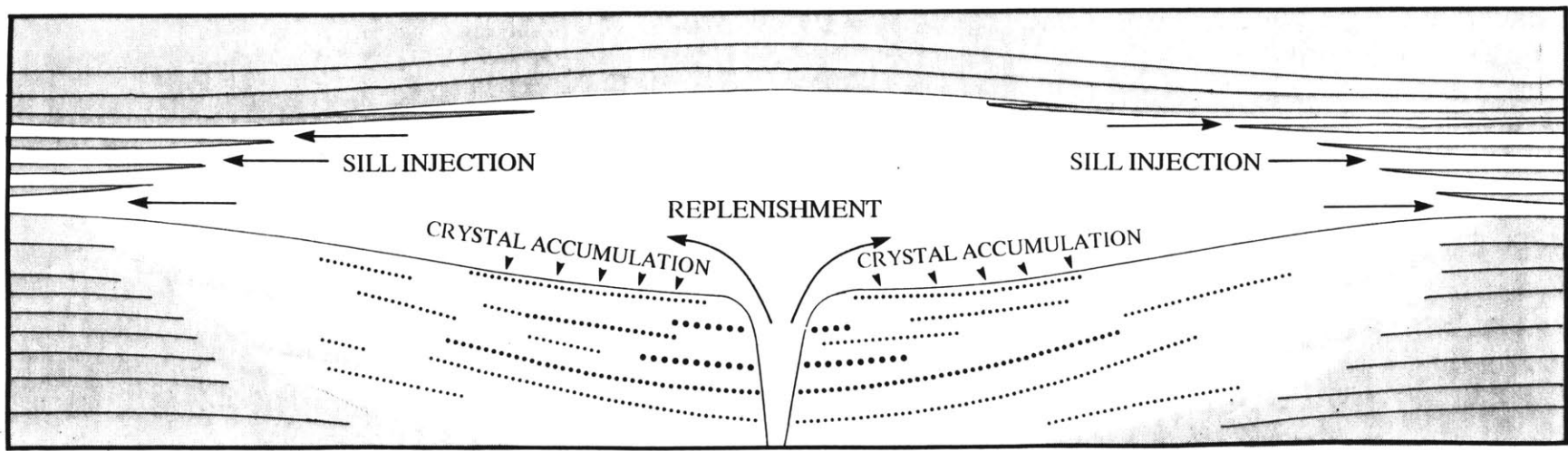
B. Model of an Onion Valley-type lens-shaped magma chamber, based on field observations shown in figure 1-2 A, and exposures of other layered cumulate bodies in the mafic intrusive complex. Breadth is ~700 to 1000 m, thickness is ~150 to 300 m.



-  Talus and snow
-  Cretaceous aplite and composite dikes
-  Coarse hbl gabbro and hbl-plag pegmatite
-  Sheeted sills
-  Layered & massive hbl-gabbro cumulates
-  Hbl mela-gabbro, hblite, oliv-hblite

A.

Dashed lines show trace of sheeting in sills.
Dotted lines show trace of layering in cumulates.



B.

VERTICAL EXAGGERATION ~2X

Figure 1-4. Backscatter electron images of skeletal and swallowtail calcic cores of plagioclase crystals in thin sills. Scale bars are 10 or 100 microns as indicated. H-hornblende, M-magnetite, A-apatite, B-biotite, q-quartz.

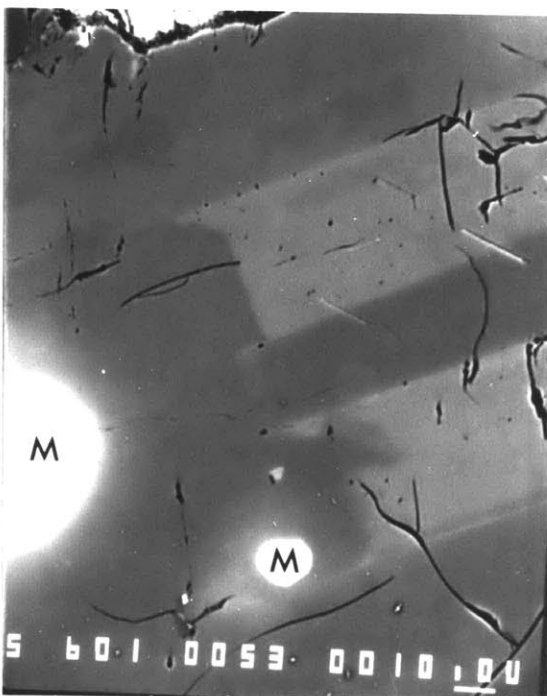
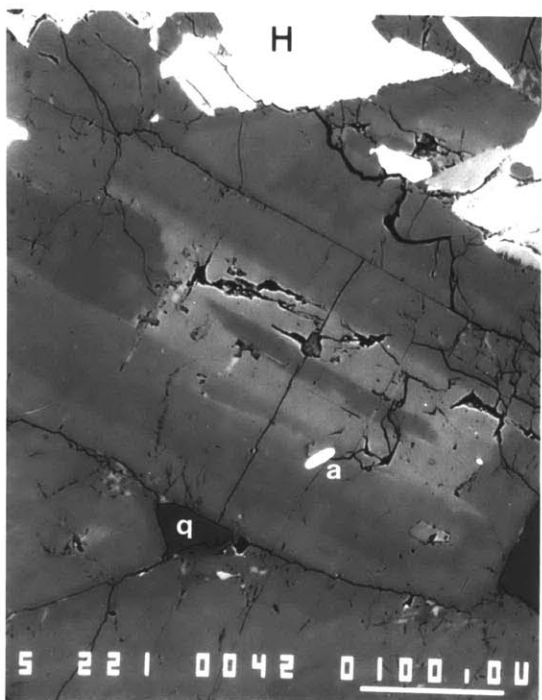
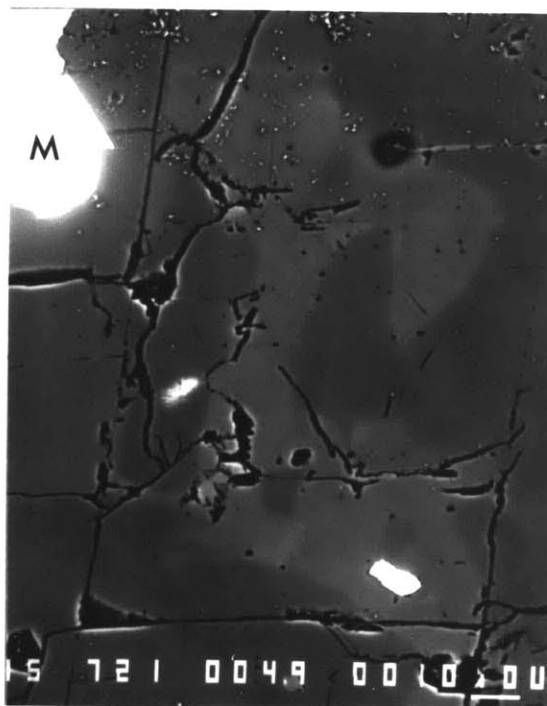
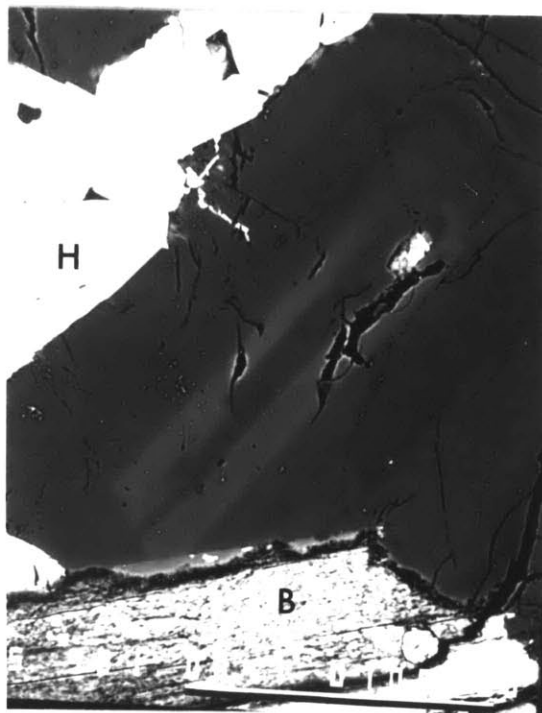
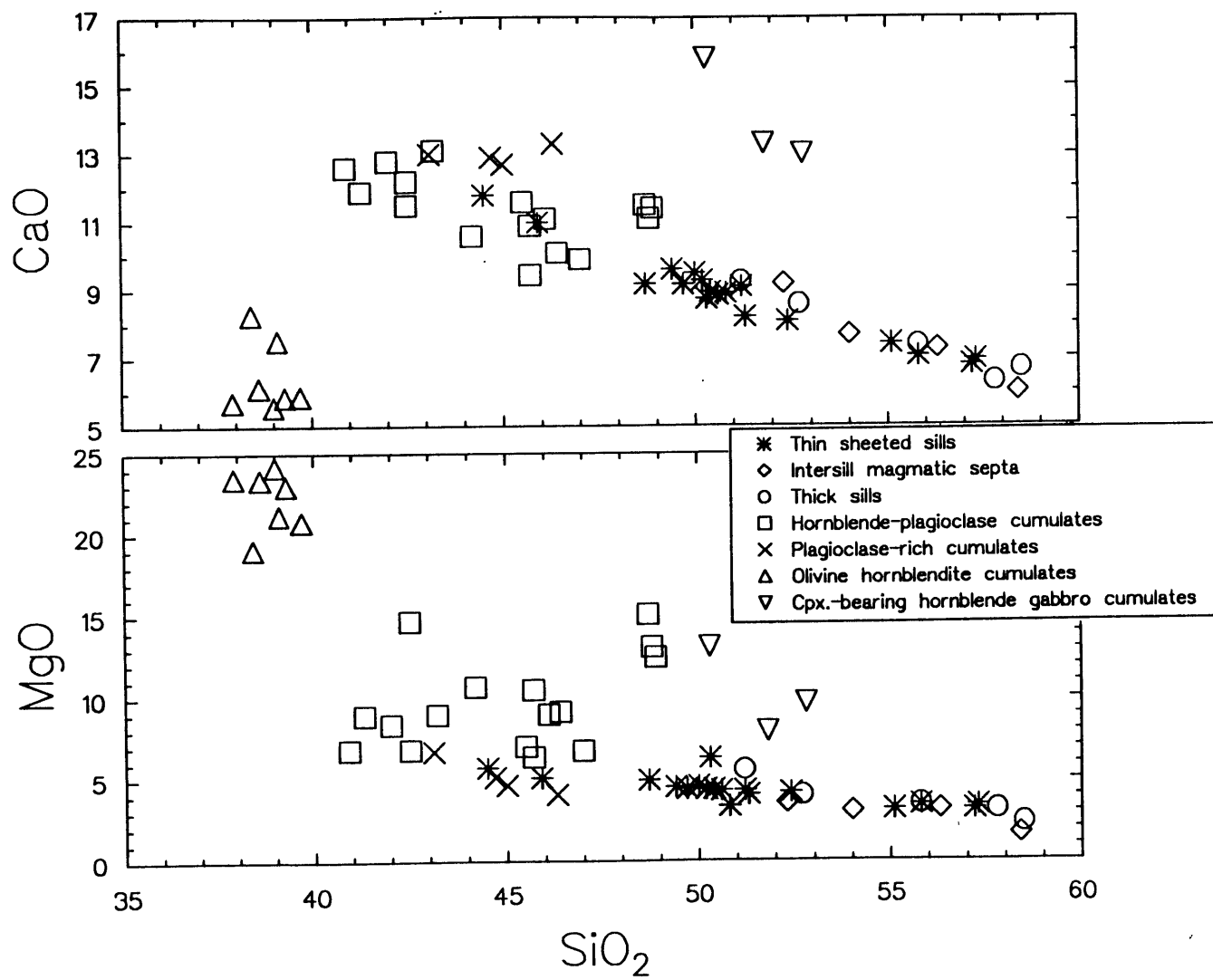
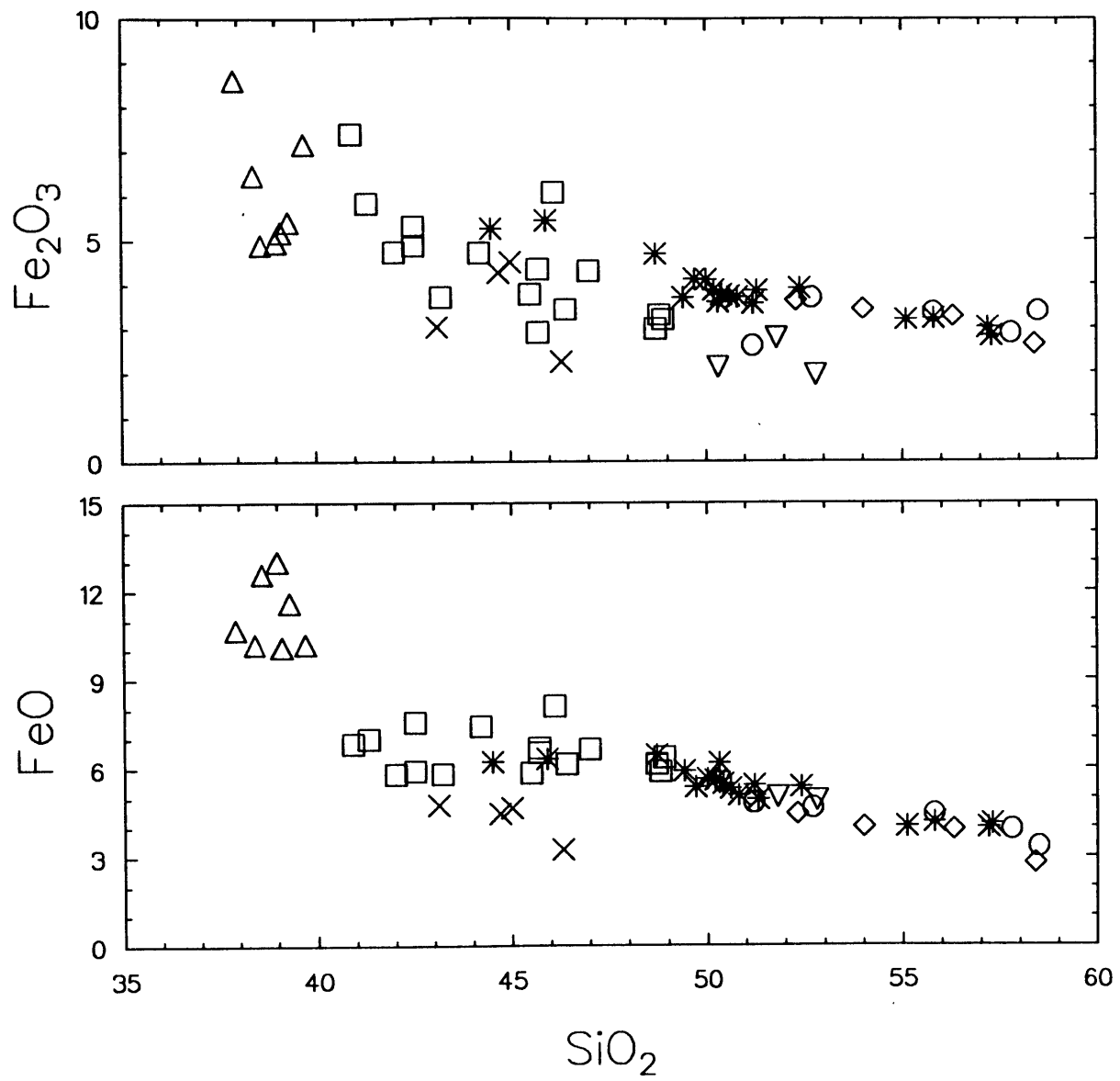
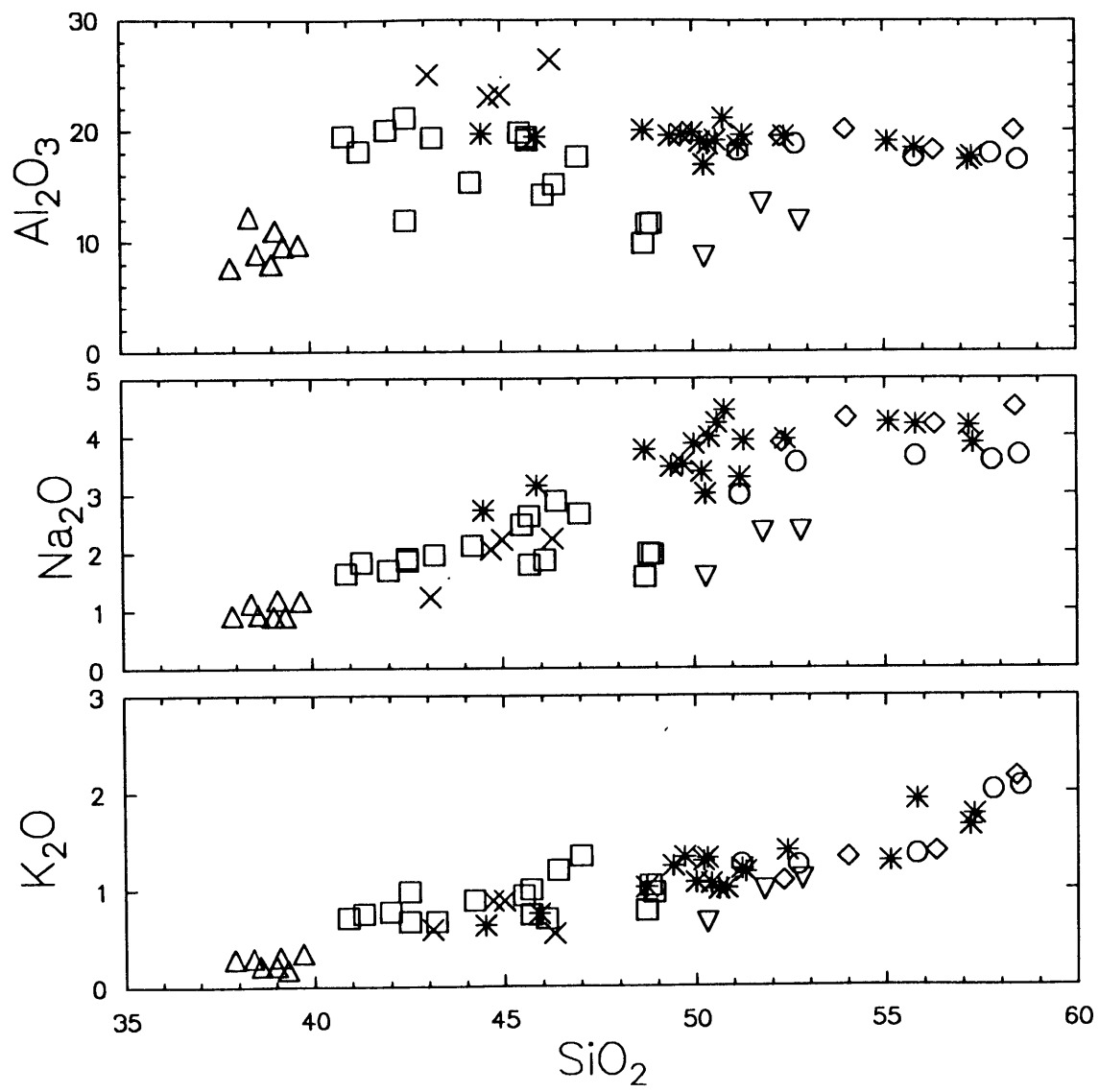


Figure 1-5. Major oxide vs silica variation diagrams for sheeted sills and associated cumulates of the mafic intrusive complex at Onion Valley. STARS-thin sheeted sills, CIRCLES-intersill magmatic septa, DIAMONDS-thick sills, SQUARES-hornblende gabbro and hornblendite cumulates, Xs-plagioclase-rich cumulates, TRIANGLES-olivine hornblendites, INVERTED TRIANGLES-clinopyroxene-bearing porphyritic hornblende gabbros.







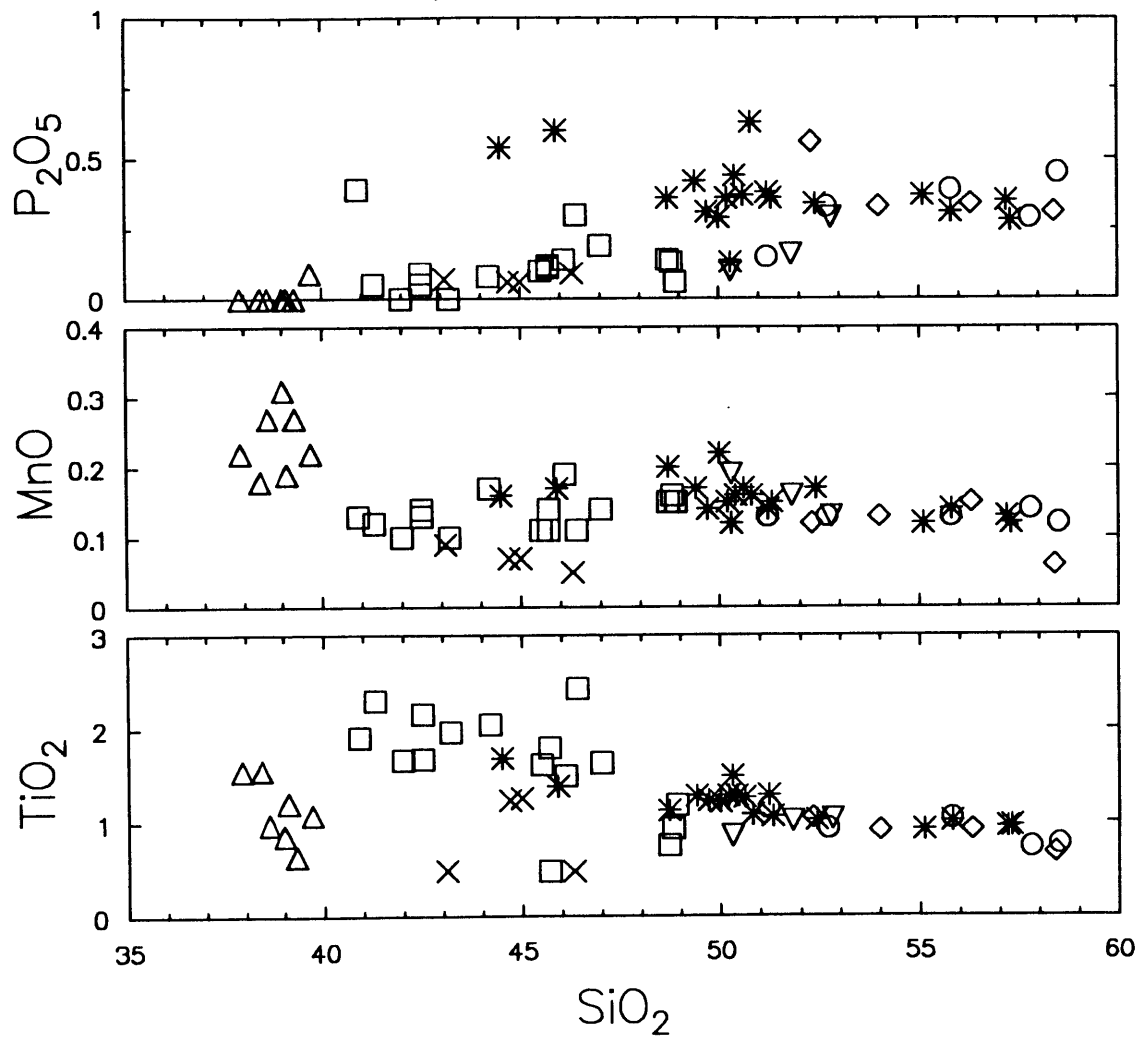


Figure 1-6. Thin and thick sheeted sills and inter-sill magmatic septa plotted on the FeO^*/MgO vs SiO_2 variation diagram ($\text{FeO}^* = \text{FeO} + 0.9 * \text{Fe}_2\text{O}_3$). The tholeiitic (TH) vs calc-alkaline dividing line is from Miyashiro (1974). Arrows show trends defined by common tholeiitic or calc-alkaline volcanic rock series.

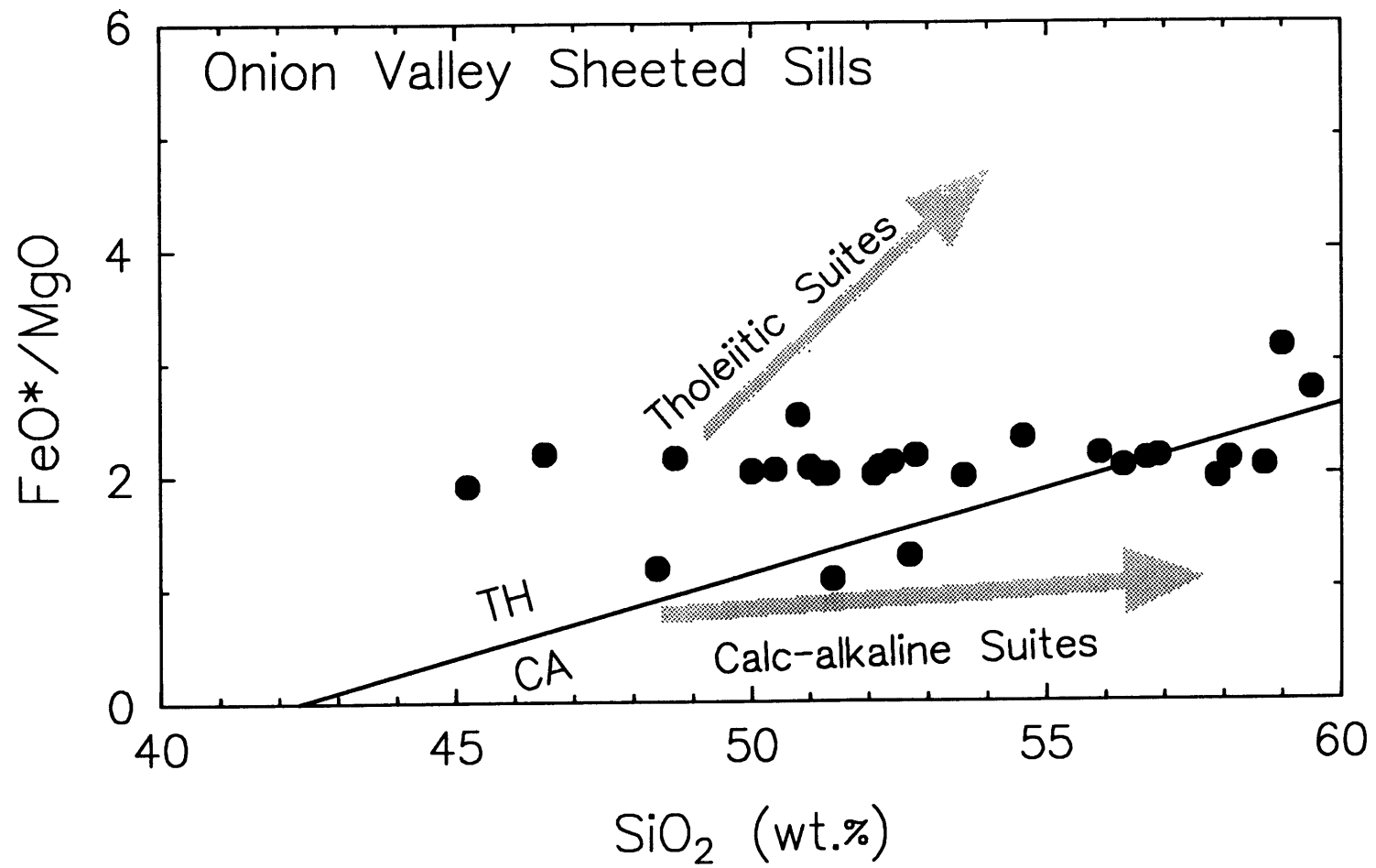


Figure 1-7. Sheeted sills and septa (crosses) and associated cumulates (triangles and squares) projected on the AFM diagram ($A=Na_2O+K_2O$, $F=FeO+0.9*Fe_2O_3$, $M=MgO$). Curve separates fields of tholeiitic (TH) and calc-alkaline (CA) volcanic rock suites, as defined by Irvine and Baragar (1971). Field of Sierran granitoids (SNB) is after Frost and Mahood (1987), Bateman and Chappell (1979), and Bateman and Nokleberg (1978).

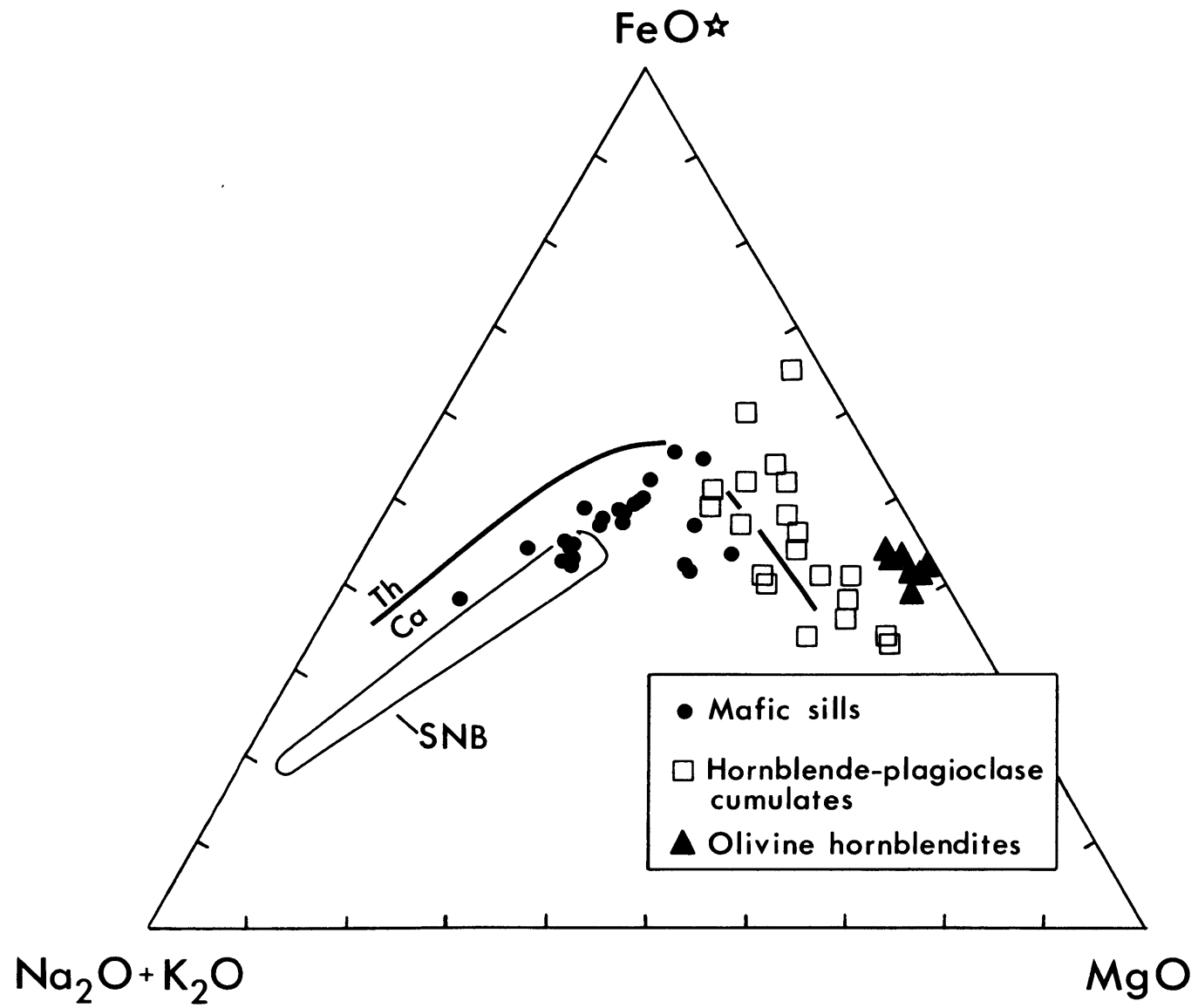


Figure 1-8. Sheeted sills, septa, and associated cumulates plotted on a CaO vs Al₂O₃ variation diagram. Symbols as in figure 1. Cumulate types, defined by modal mineralogy, are displaced toward the plotting position of the dominant cumulus mineral, as indicated.

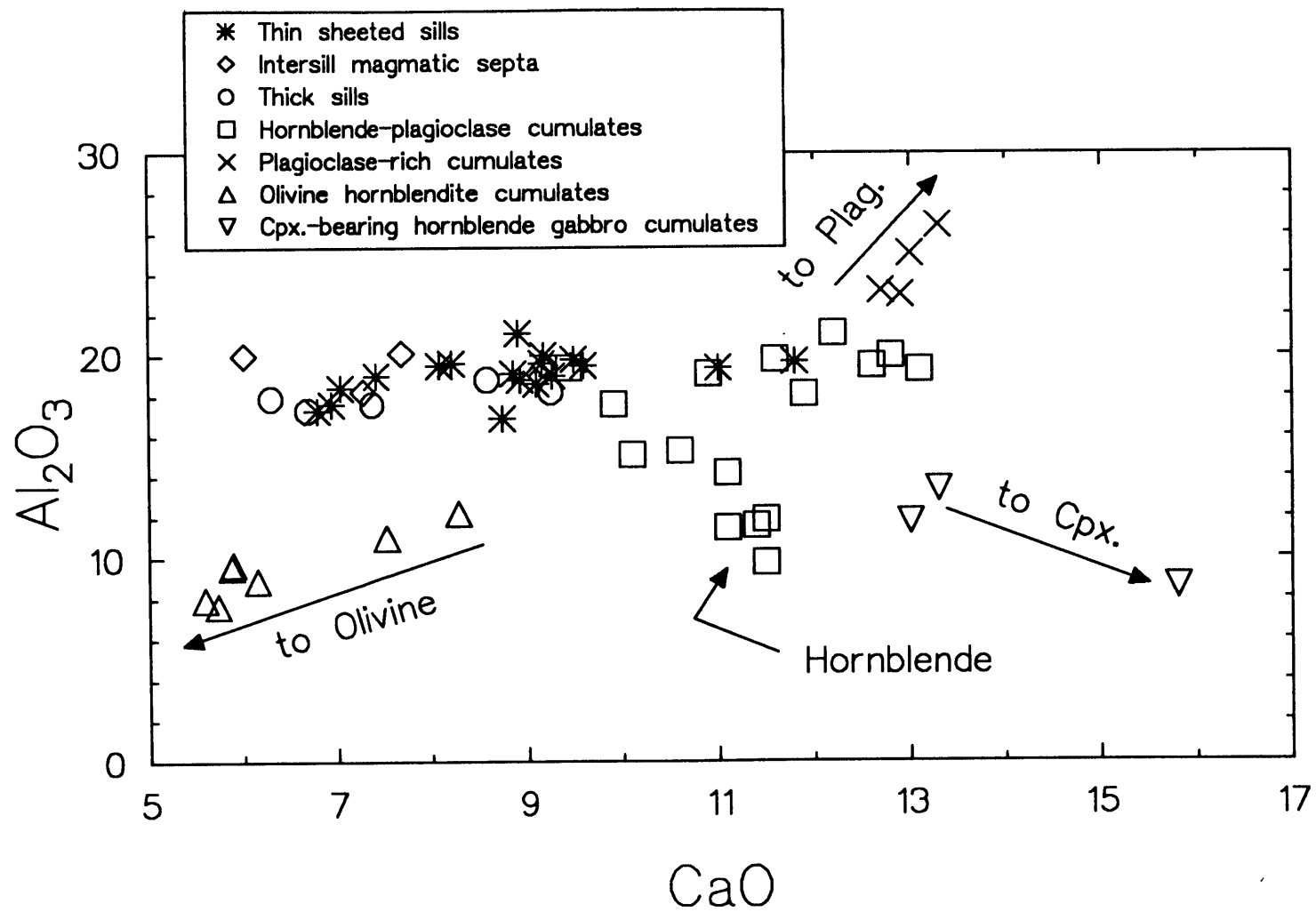
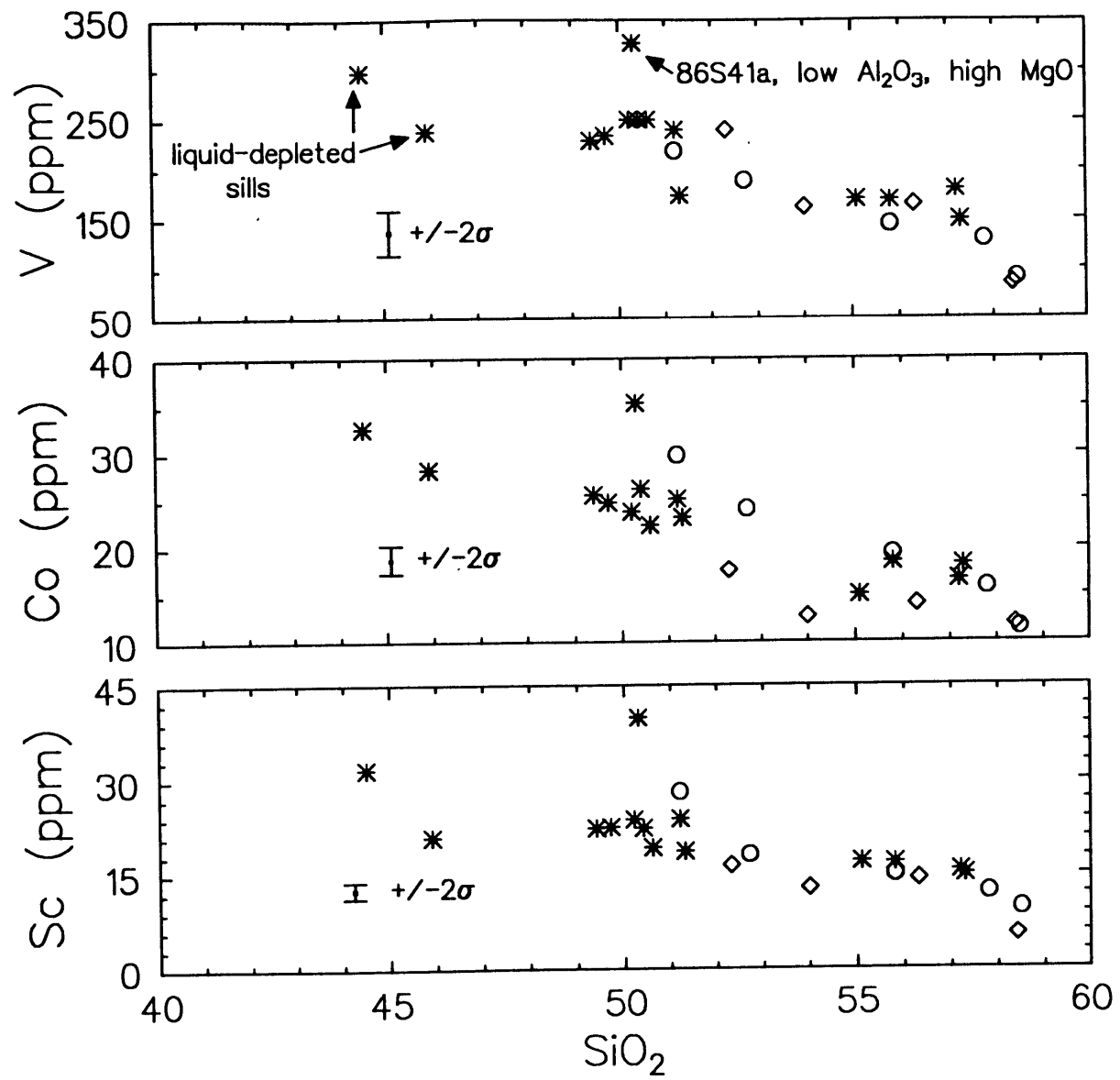
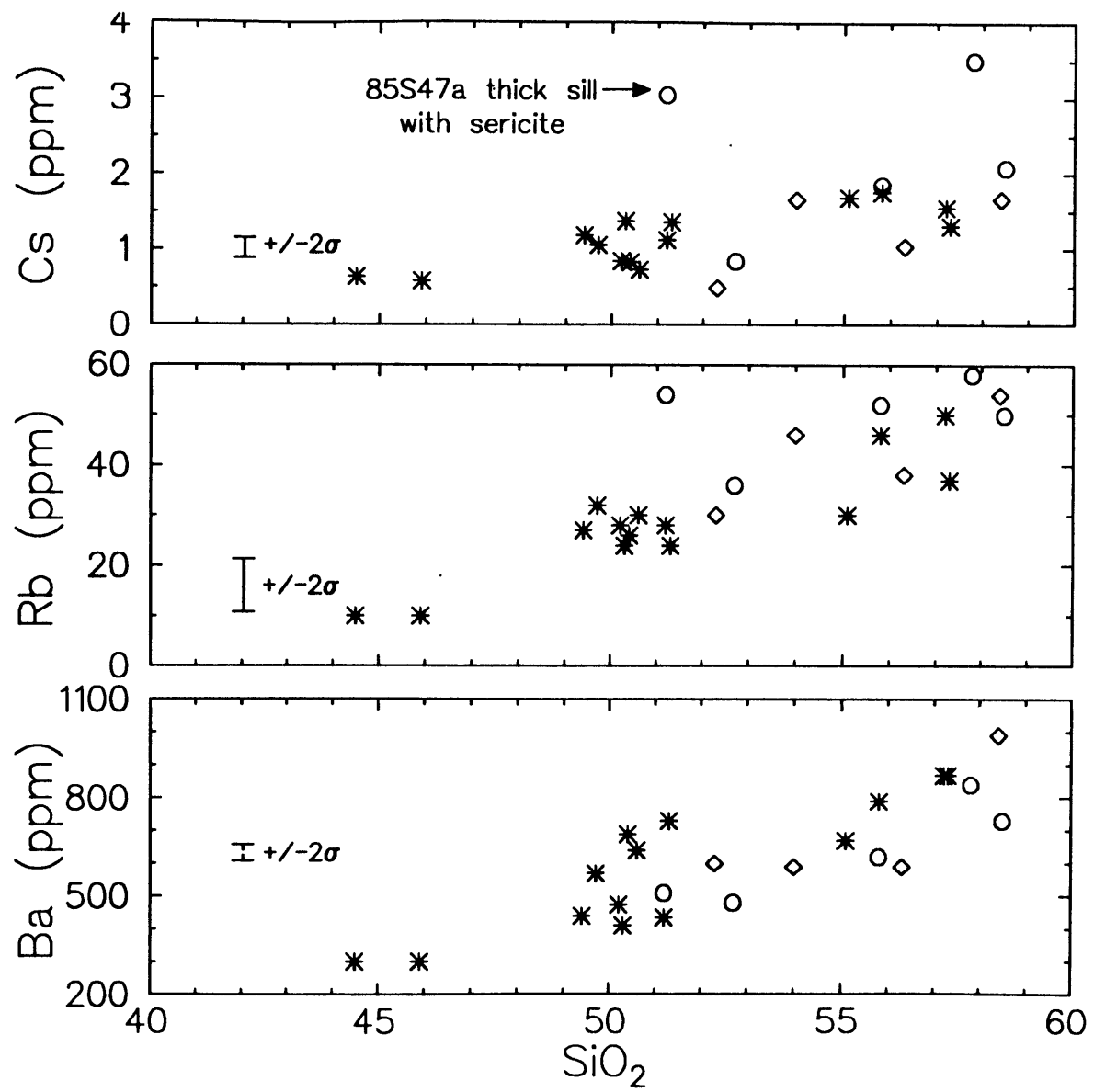
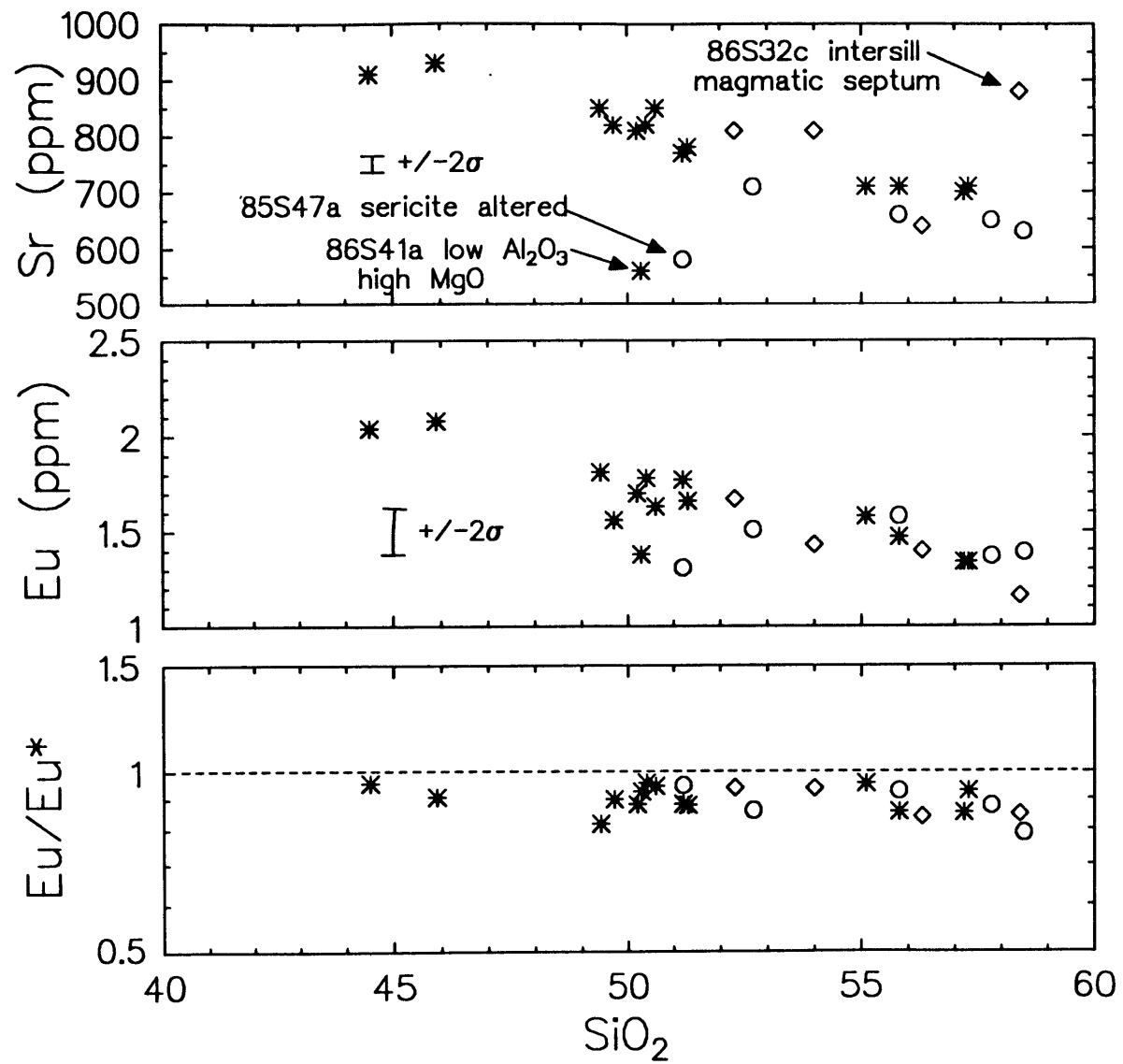
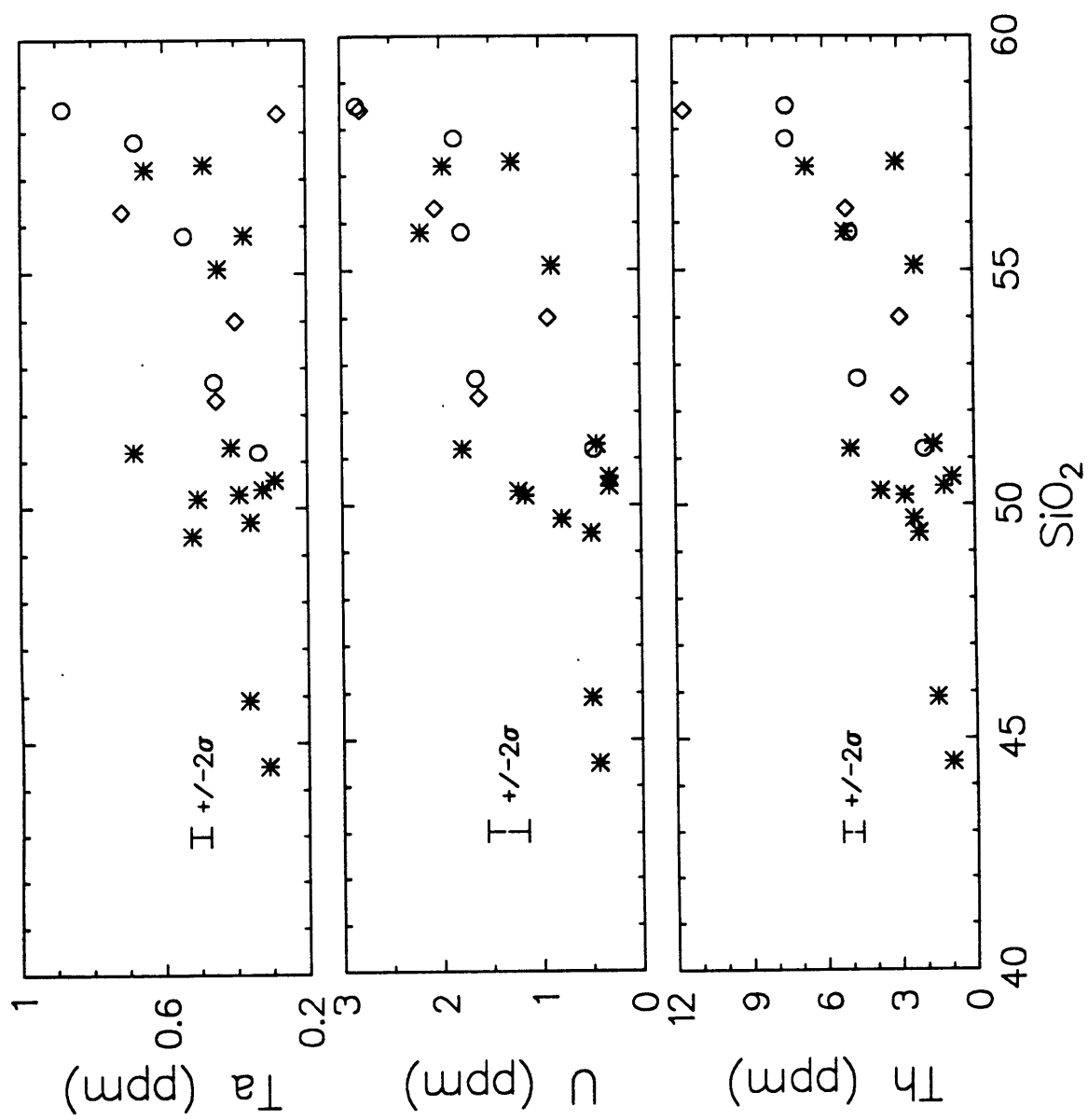


Figure 1-9. Trace element vs silica variation diagrams for thin sheeted sills (STARS), inter-sill magmatic septa (CIRCLES), and thick sills (DIAMONDS). Eu* is the expected Eu interpolated between Sm and Tb on chondrite-normalized abundance diagrams.









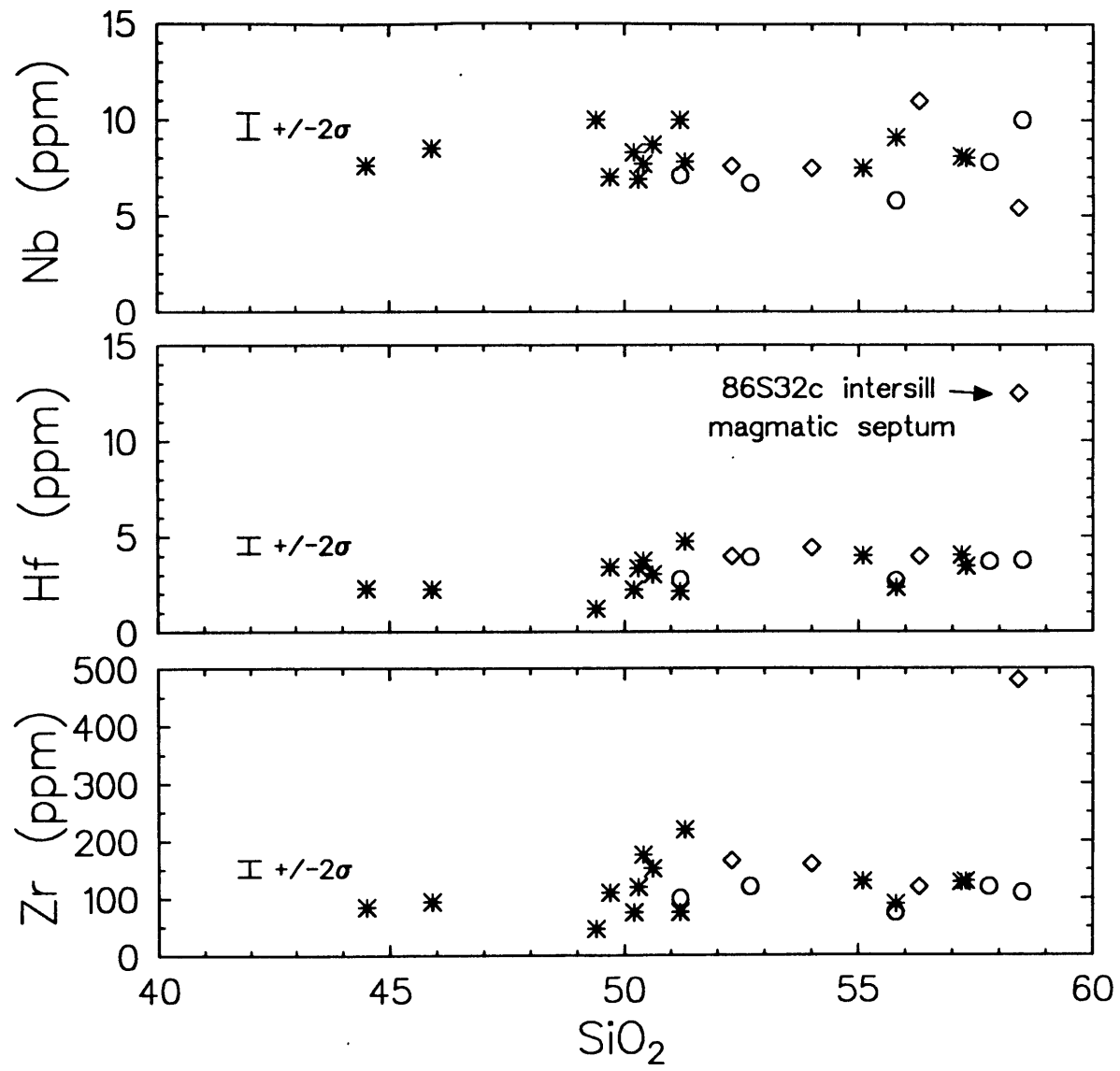
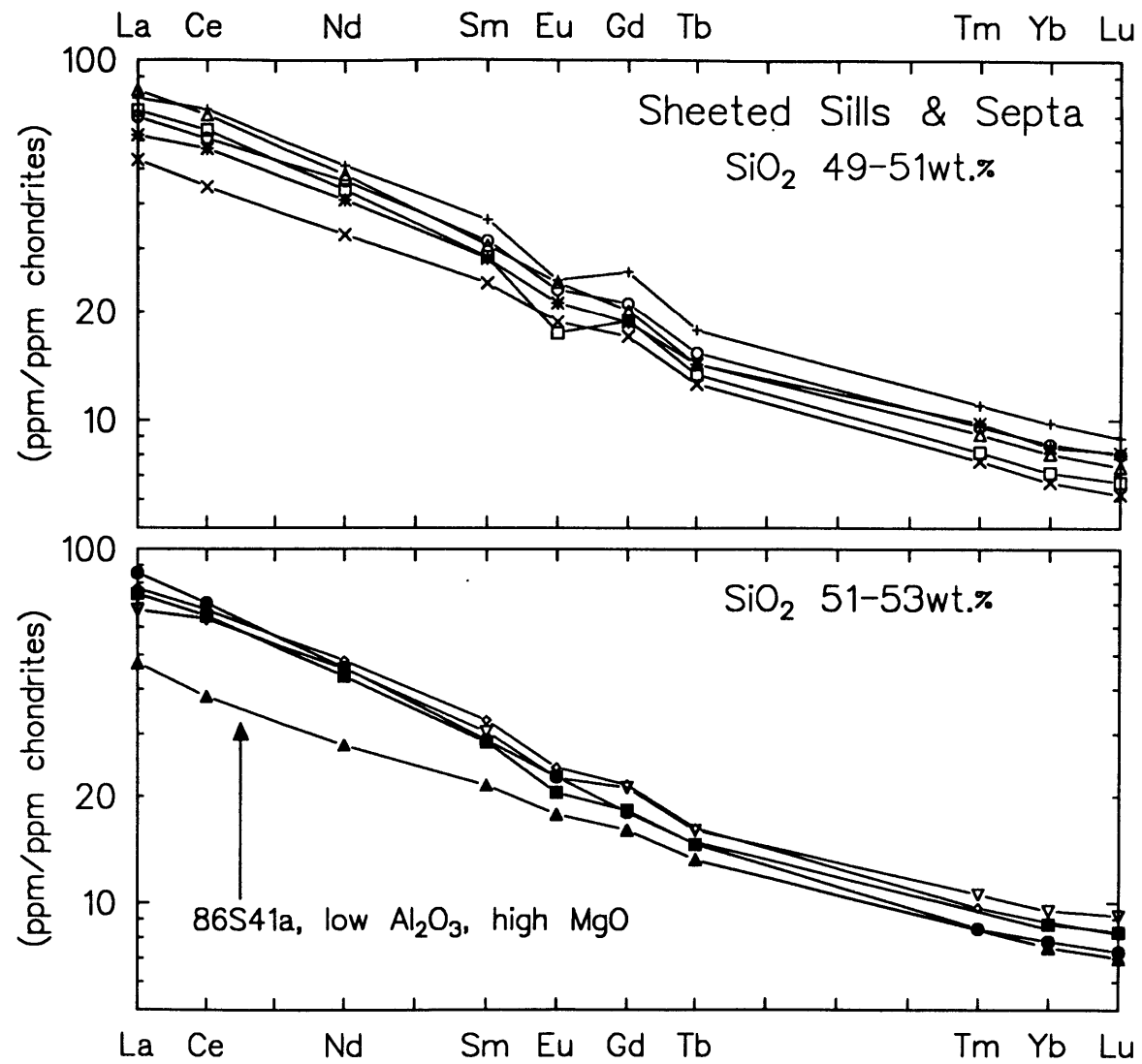


Figure 1-10. Rare earth element abundances in thin and thick sheeted sills and inter-sill septa divided into subgroups based on SiO_2 content. Rare earth element abundances are normalized to the recommended chondritic abundances of Boynton (1984) in this and subsequent diagrams.



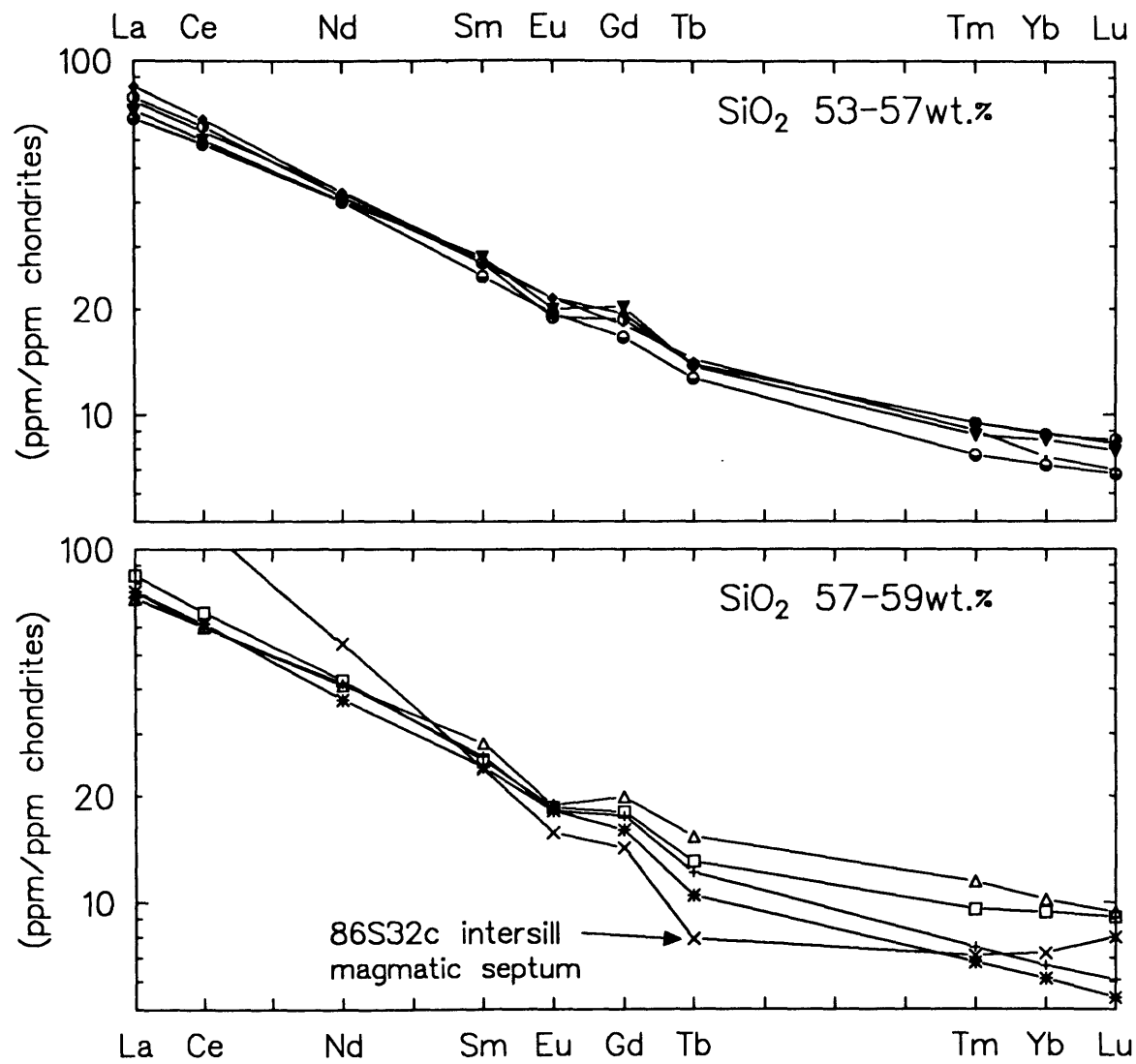


Figure 1-11. Rare earth element abundances in liquid-depleted sills, normalized to the average rare earth content in basaltic sills.

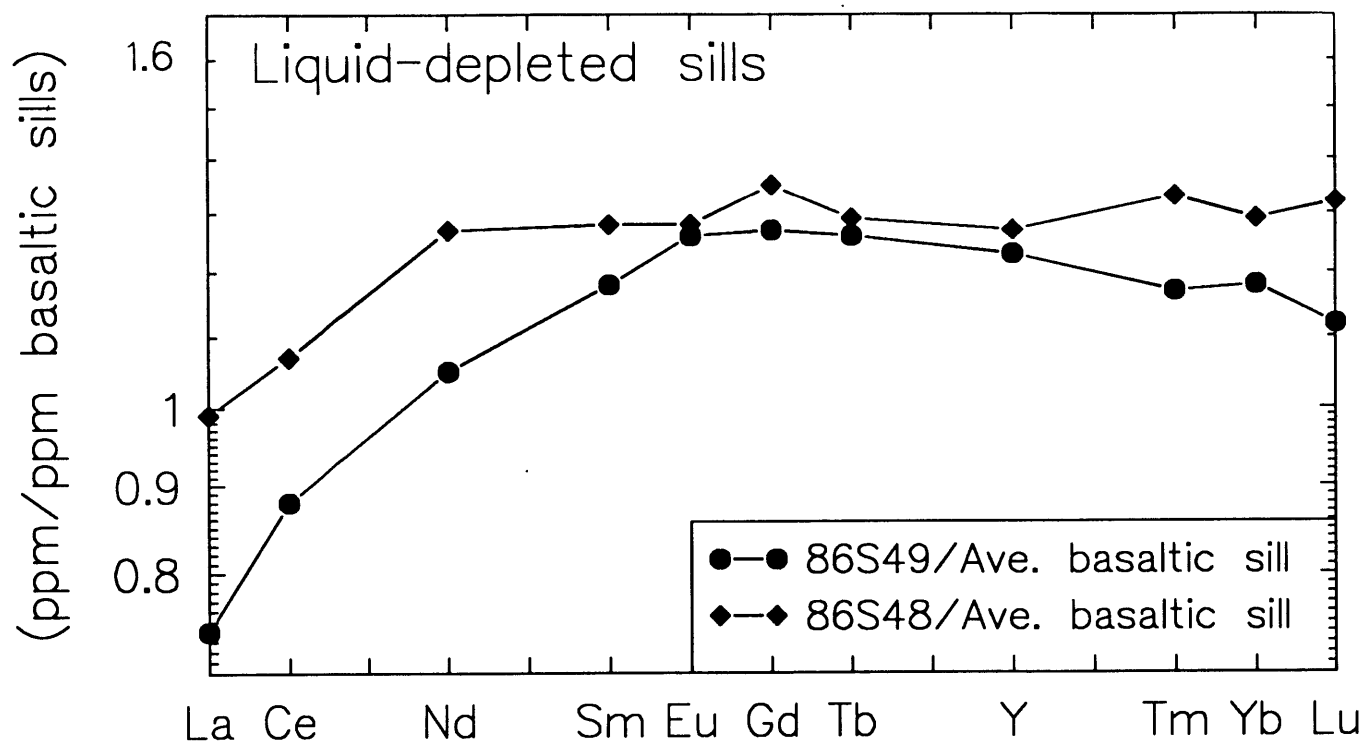


Figure 1-12. Elemental abundance patterns of basaltic sills normalized to MORB composition of Pearce (1982). Analyses are divided as to SiO₂ content.

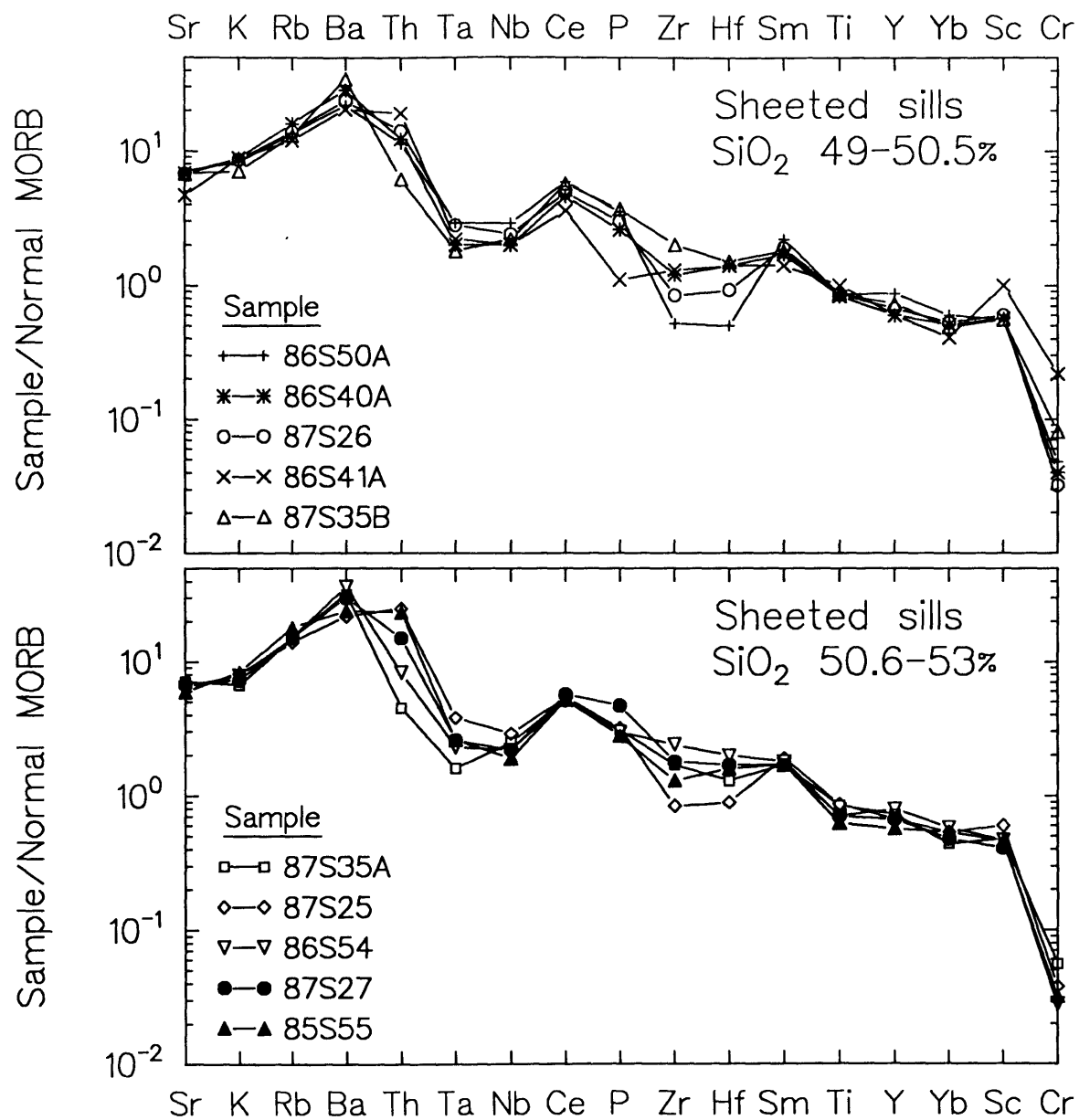
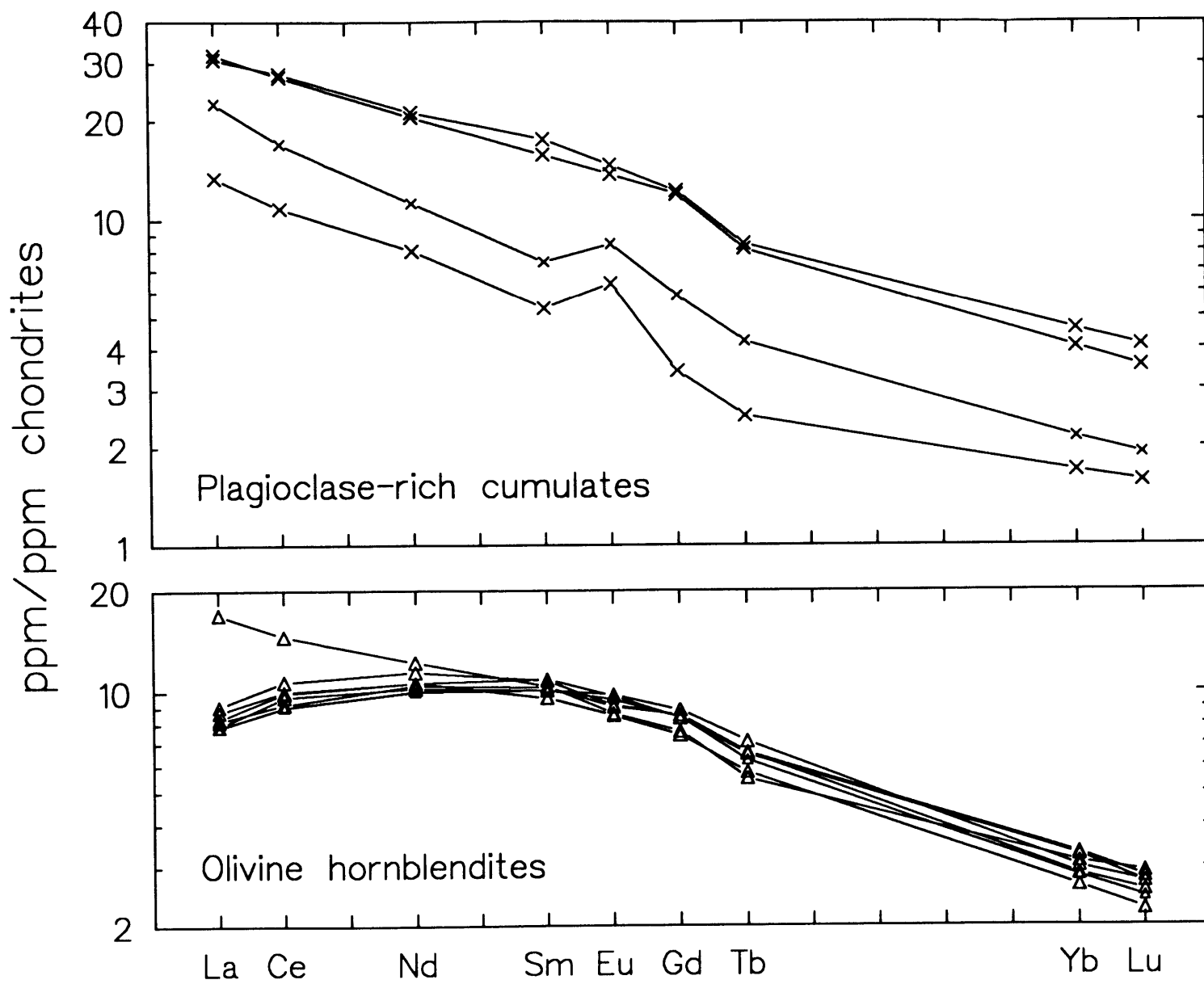


Figure 1-13. Rare earth element abundances in cumulates, divided into subgroups based on rock-type. Convex-upward patterns in olivine hornblendites, hornblende gabbros, and hornblendites result from accumulated hornblende. Greater abundances in hornblende gabbros and hornblendites likely result from higher hornblende-liquid partition coefficients in more evolved magmas.



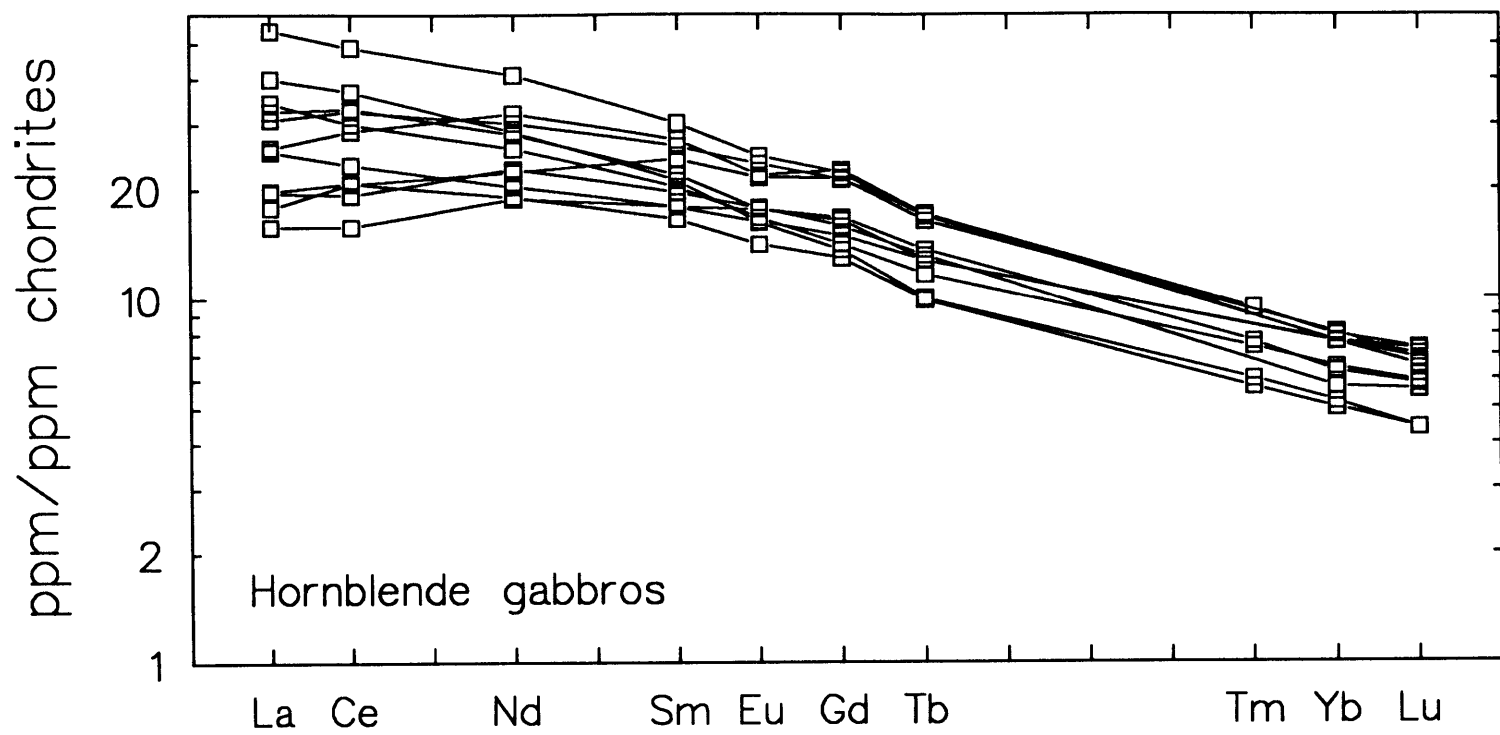


Figure 1-14. Crystal fractionation modeled liquids and cumulates ((CROSSES) table 5, inverse model) compared to observed sill and septa compositions (CIRCLES) plotted on $\text{CaO}/\text{Al}_2\text{O}_3$ vs SiO_2 and FeO/MgO vs SiO_2 variation diagrams. Compositions are normalized to 100 % anhydrous, with all Fe as FeO. H-P-C is field of Onion Valley layered hornblende plagioclase cumulates.

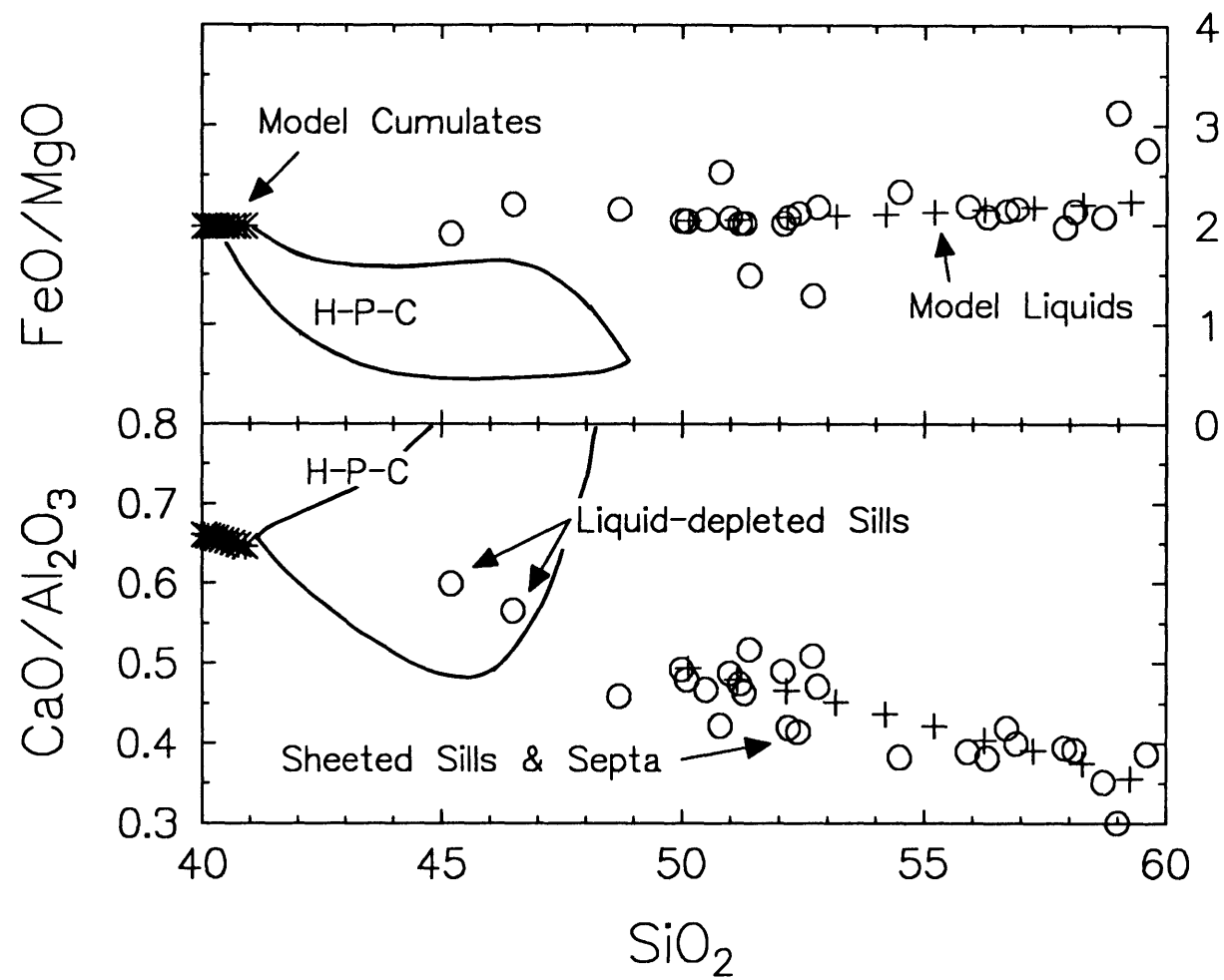
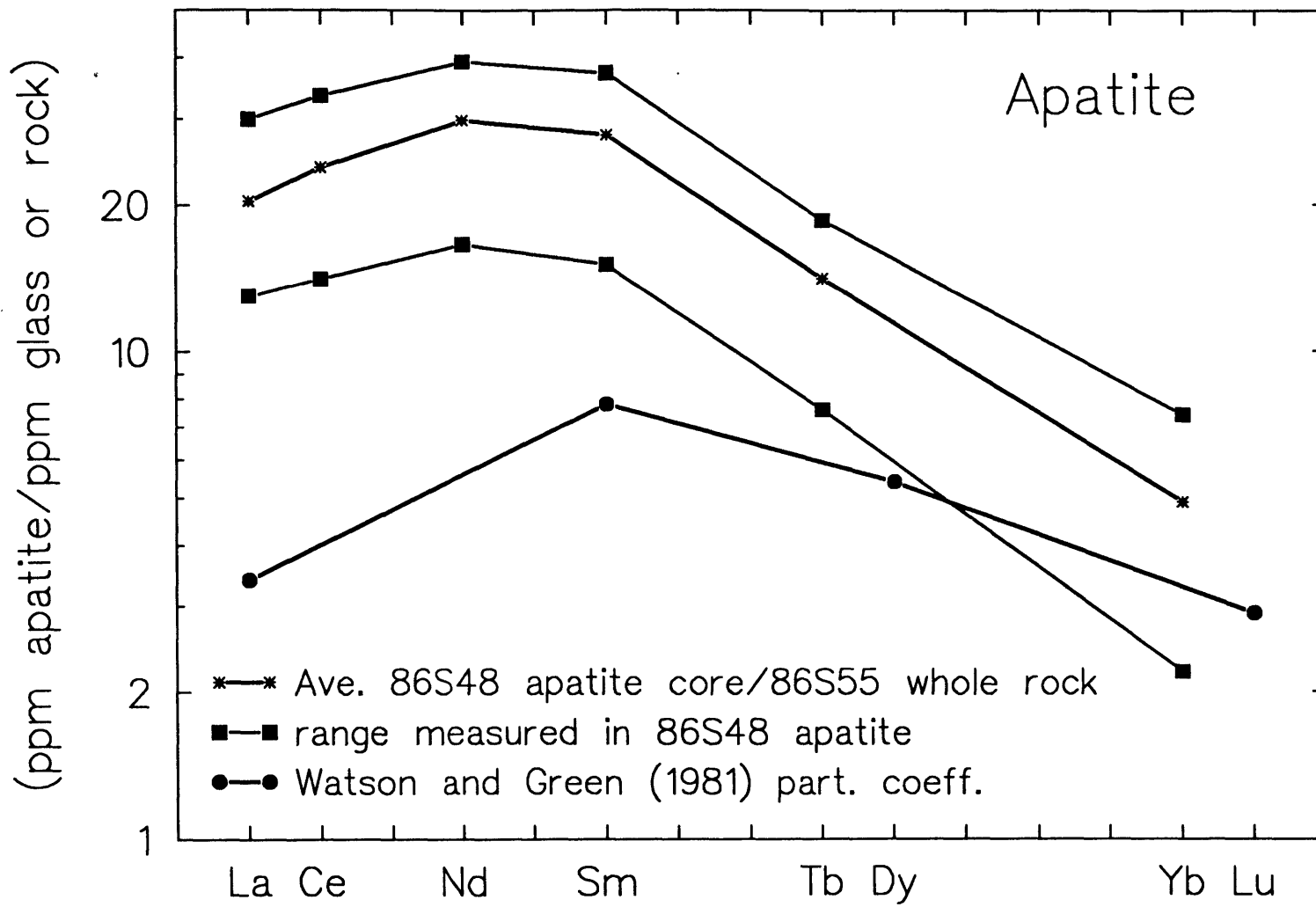


Figure 1-15. Rare earth element contents of mineral cores from sill sample 86S48 normalized to whole rock abundances of sample 86S55. Tb values are interpolated from measured Sm, Dy, and Er in the minerals. Apatite is an average of 6 analyses of equant crystals. Acicular grains show greater variation. Apatite-liquid partition coefficients for tholeiitic andesite (Watson and Green, 1981) are also shown. Plagioclase values are an average of 4 mineral analyses. Hornblende values are a single analysis in the center of a coarse, zoned crystal. Rim analyses give higher abundances. Experimental hornblende-liquid partition coefficients for basalts (lower values) and andesites (higher values) for comparison (Green and Pearson, 1985; Nicholls and Harris, 1980).



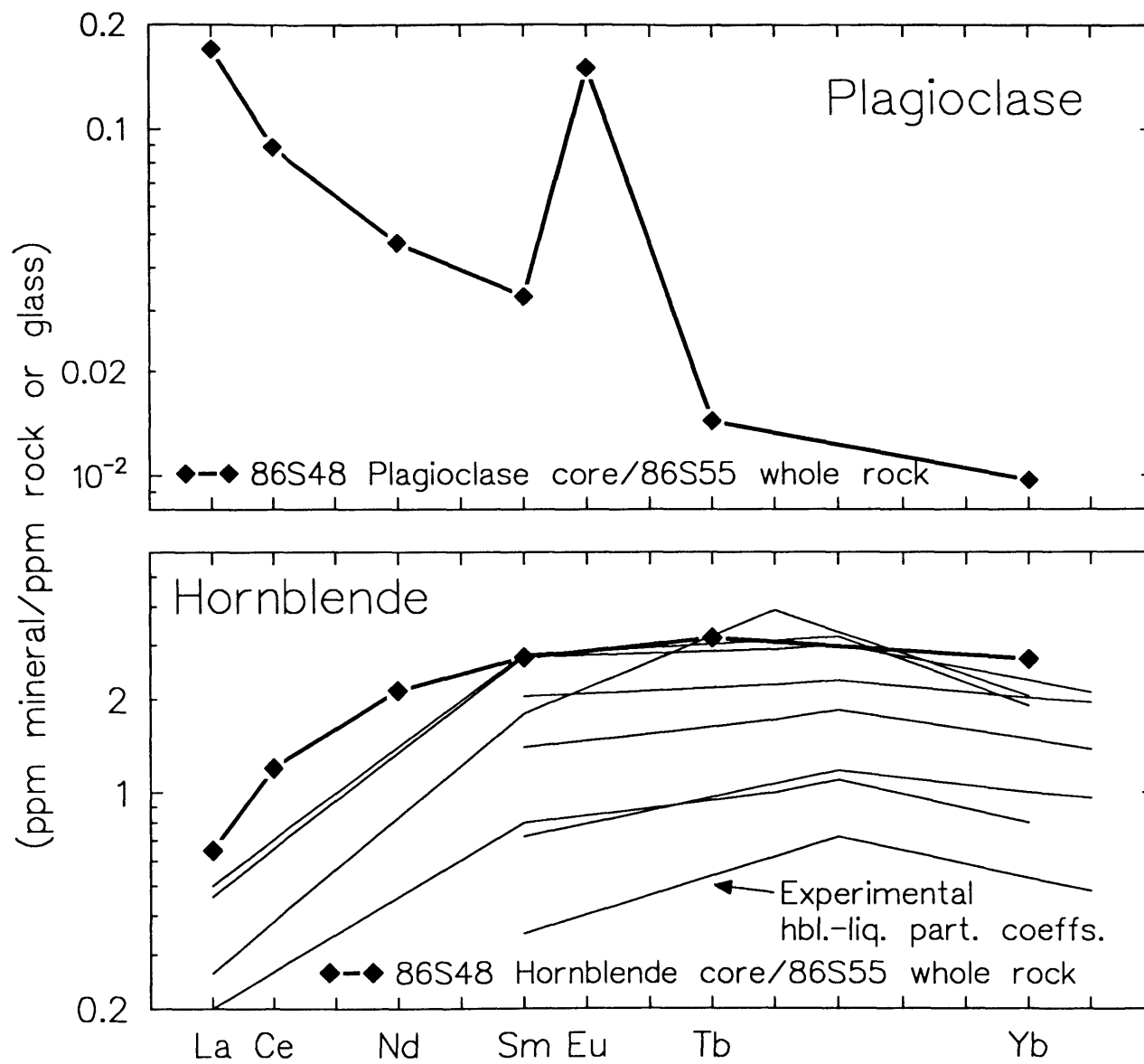


Figure 1-16. Trace element vs SiO₂ variation diagrams comparing crystal fractionation model liquids (Xs) with observed abundances for sills and septa (circles). Model abundances calculated employing SiO₂ and remaining liquid fraction (F) from inverse model of table 5, partition coefficients from table 6, and the Rayleigh fractionation equation: $C_L = C_{int} * F^{Kd-1}$. Initial concentrations (C_{int}) are chosen to match those of sills with SiO₂ near 50 wt.%. Rare earth model 1 uses measured apatite concentrations (table 6, figure 10), rare earth model 2 uses literature apatite-liquid partition coefficients (Watson and Green, 1981).

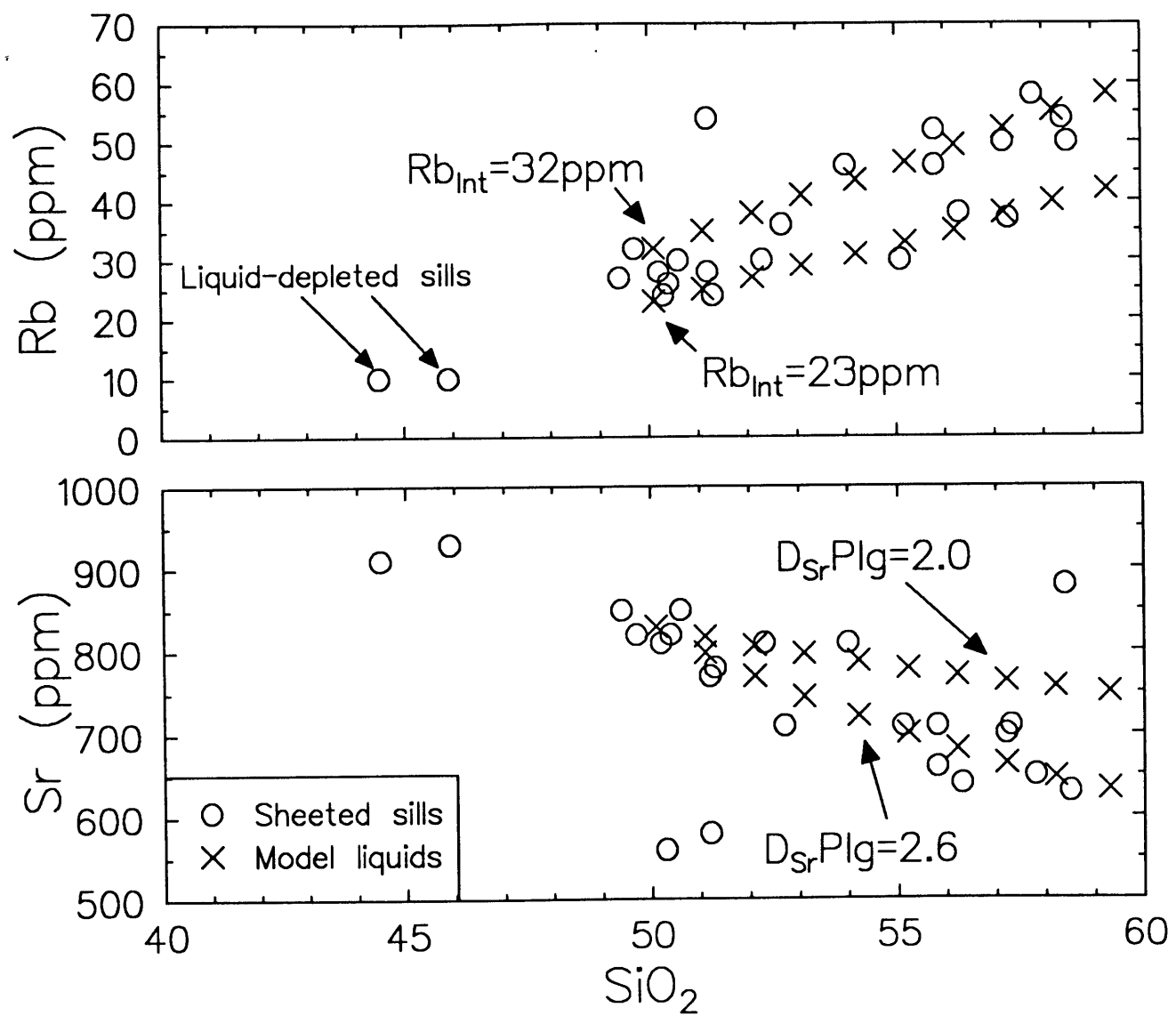


Figure 16a.

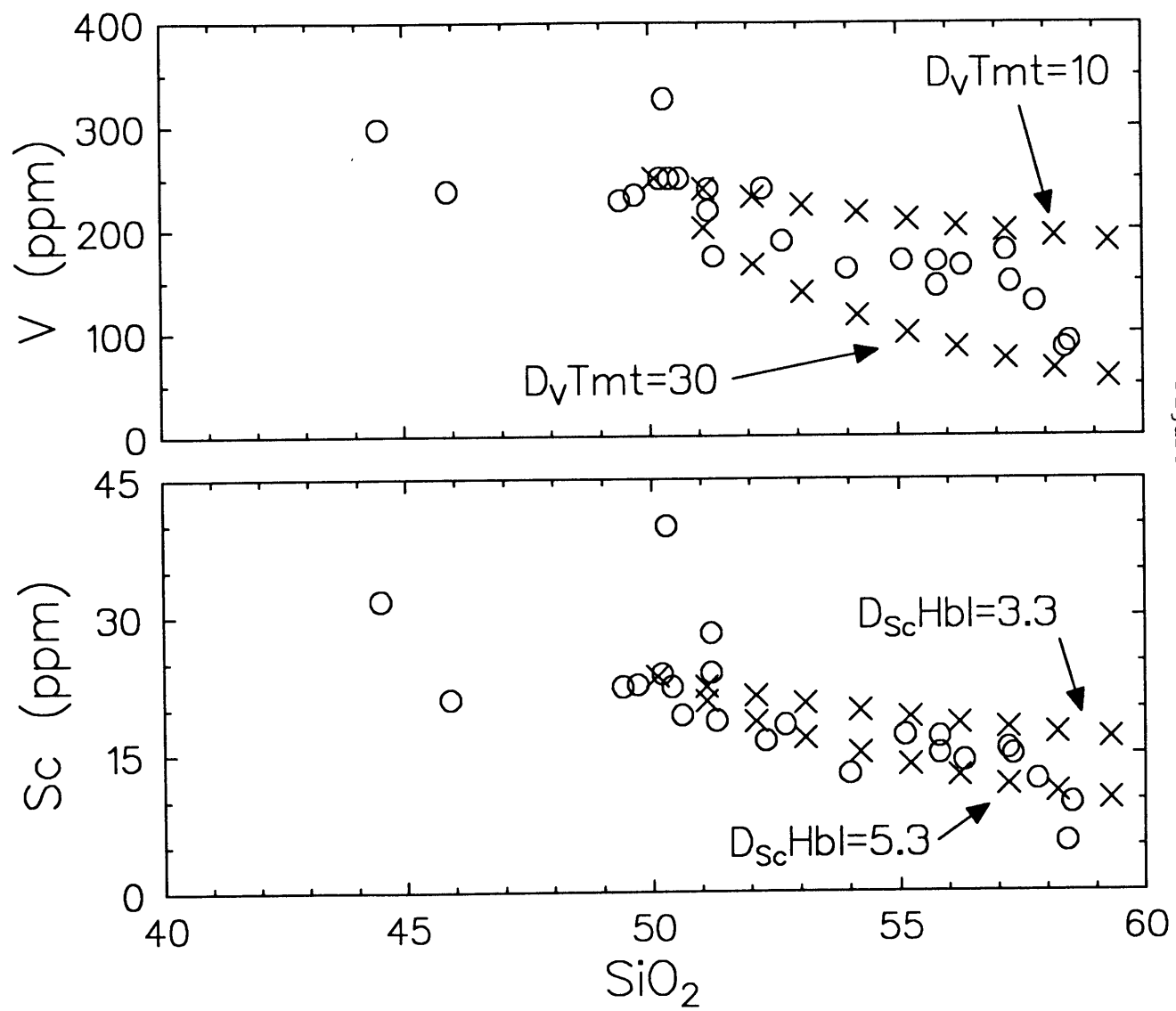


Figure 16b.

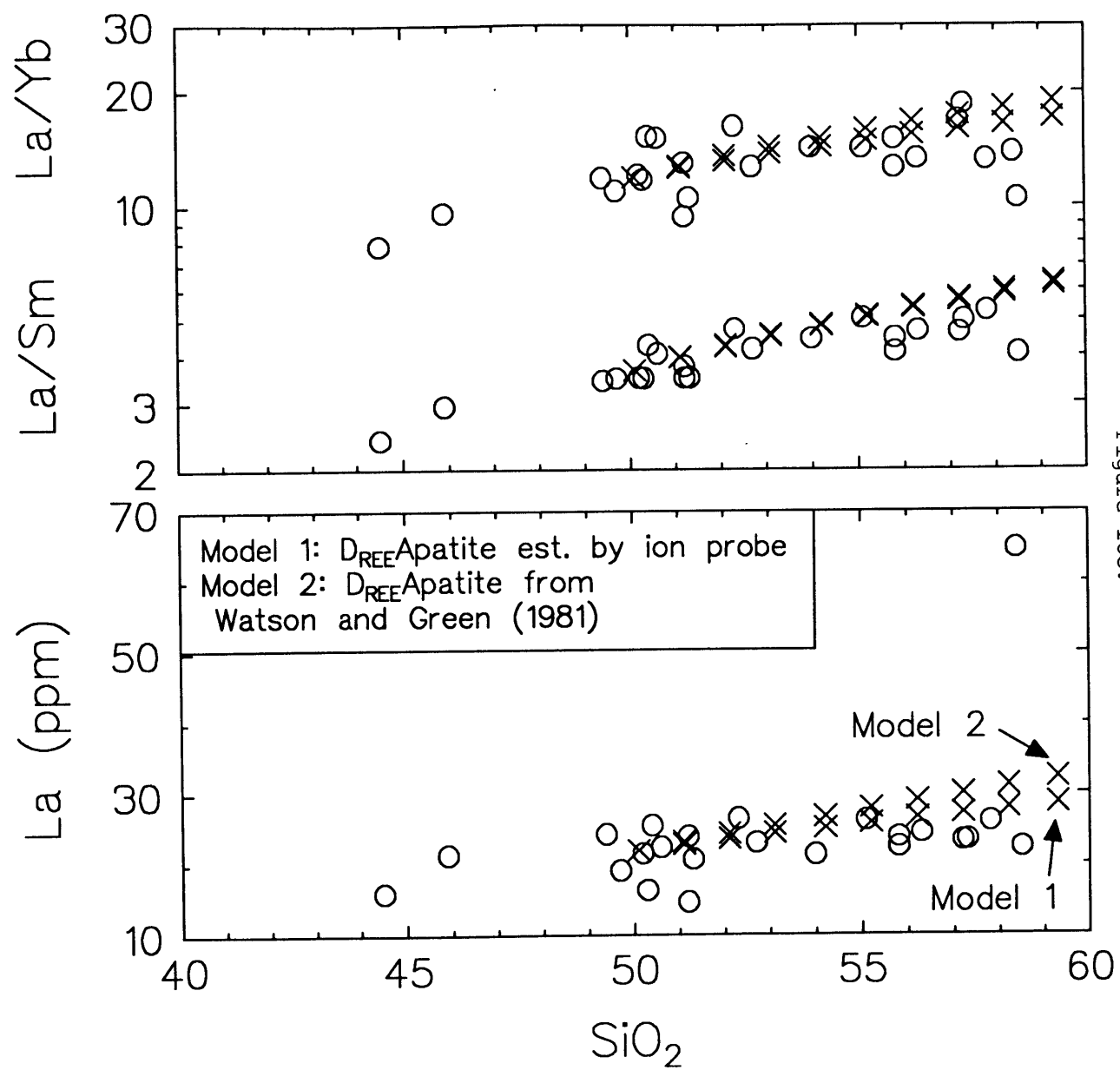


Figure 16c.

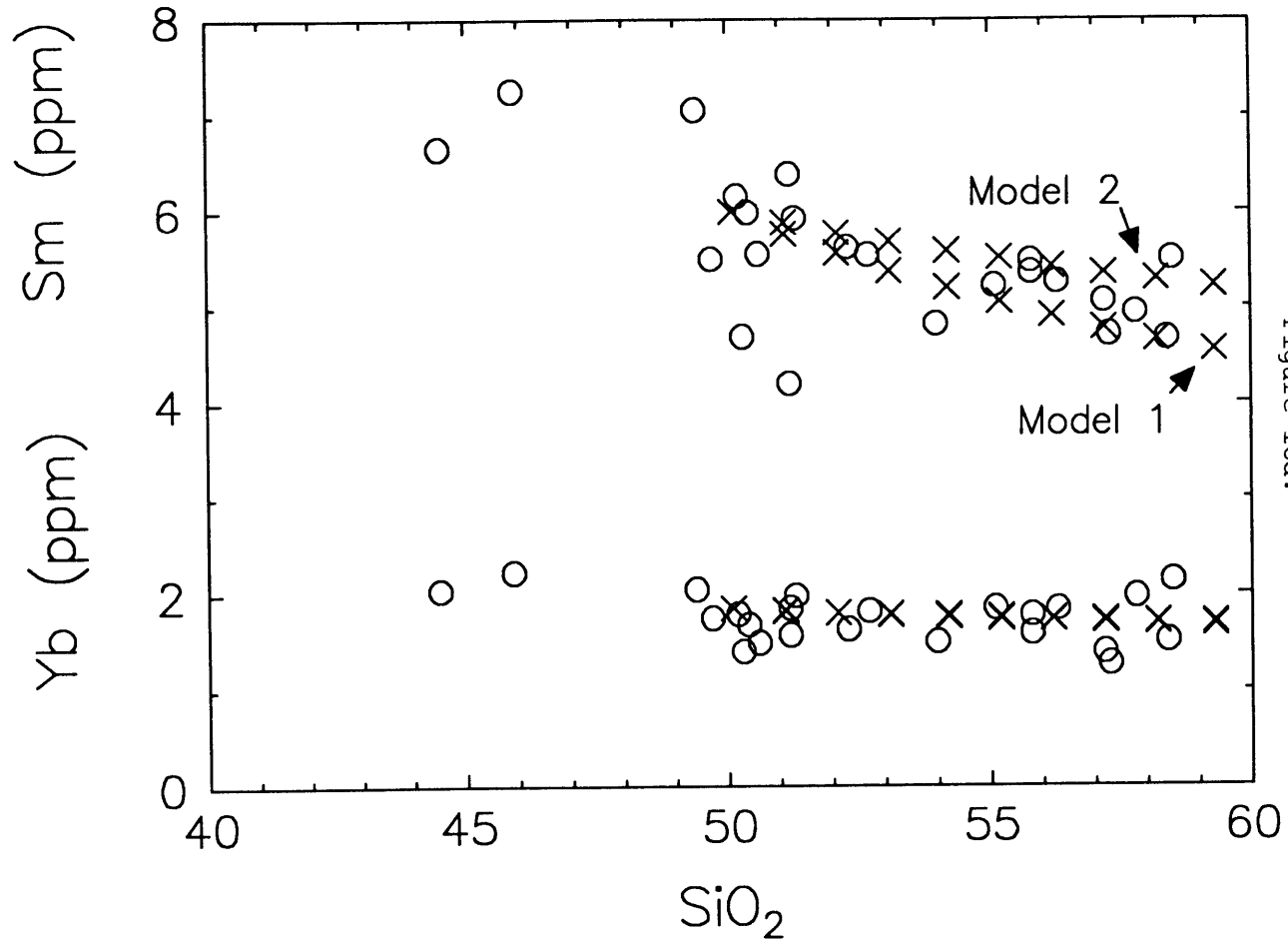


Figure 16d.

Figure 1-17. Calculated rare earth element abundances for magma parental to olivine hornblendite cumulates compared with observed values in basaltic sills. Models assume that the cumulates contain either 0 or 5 wt.% trapped parental liquid.

PREDICTED PARENT MAGMAS

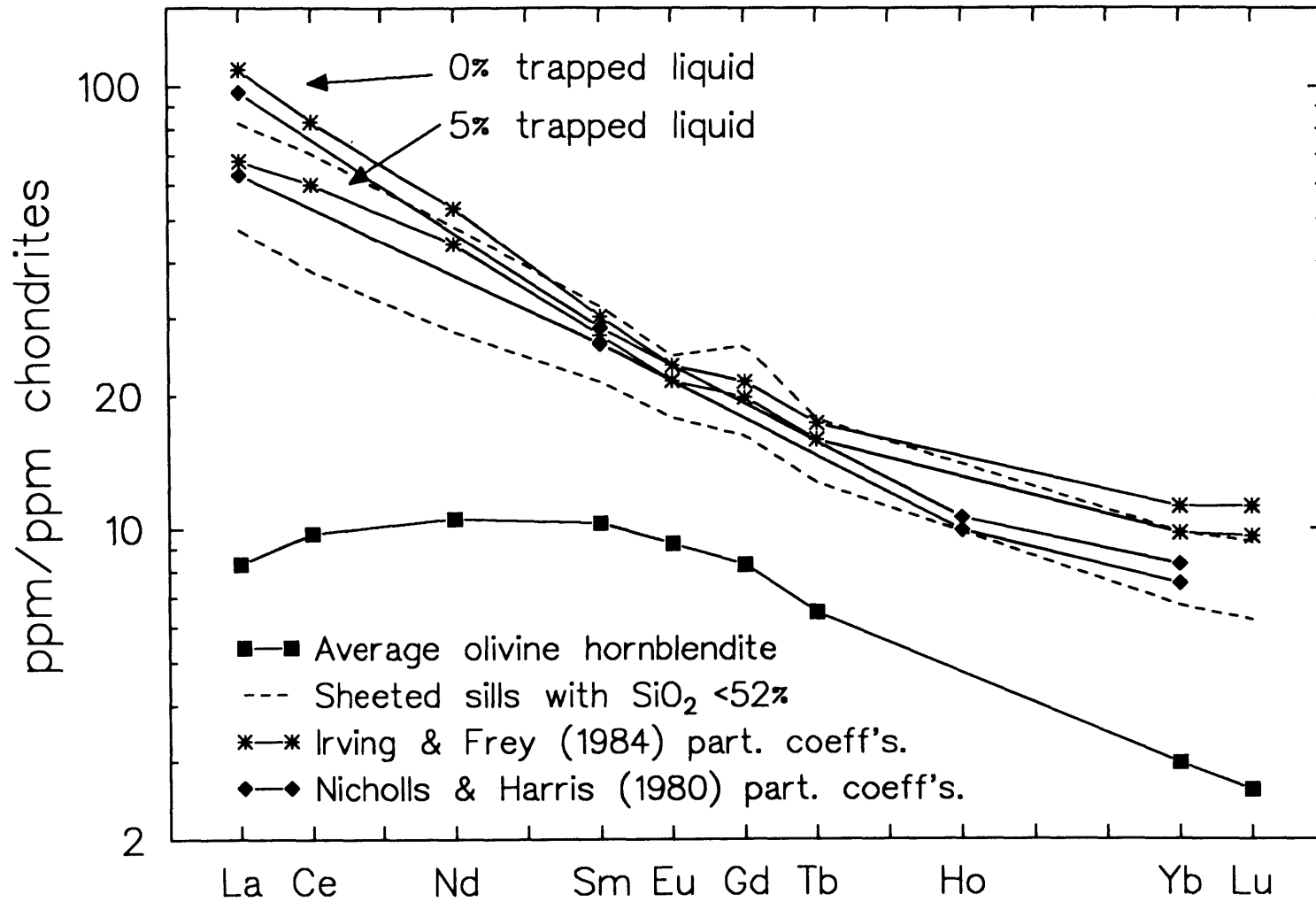


Figure 1-18. Lead isotopic ratios of hornblende gabbro cumulates (solid dots) corrected for 168my of decay (table 3). Patterned field outlines lead isotopic ratios of feldspars of granitoid rocks of the southern Sierra Nevada batholith (Chen and Tilton, 1978, and written communication). Single granitoid outlier is circled. Fields for mid-ocean ridge basalts and northern hemisphere regression lines (NHRL) (Hart and Zindler, 1989) are shown for reference. Analytic error is comparable to symbol size.

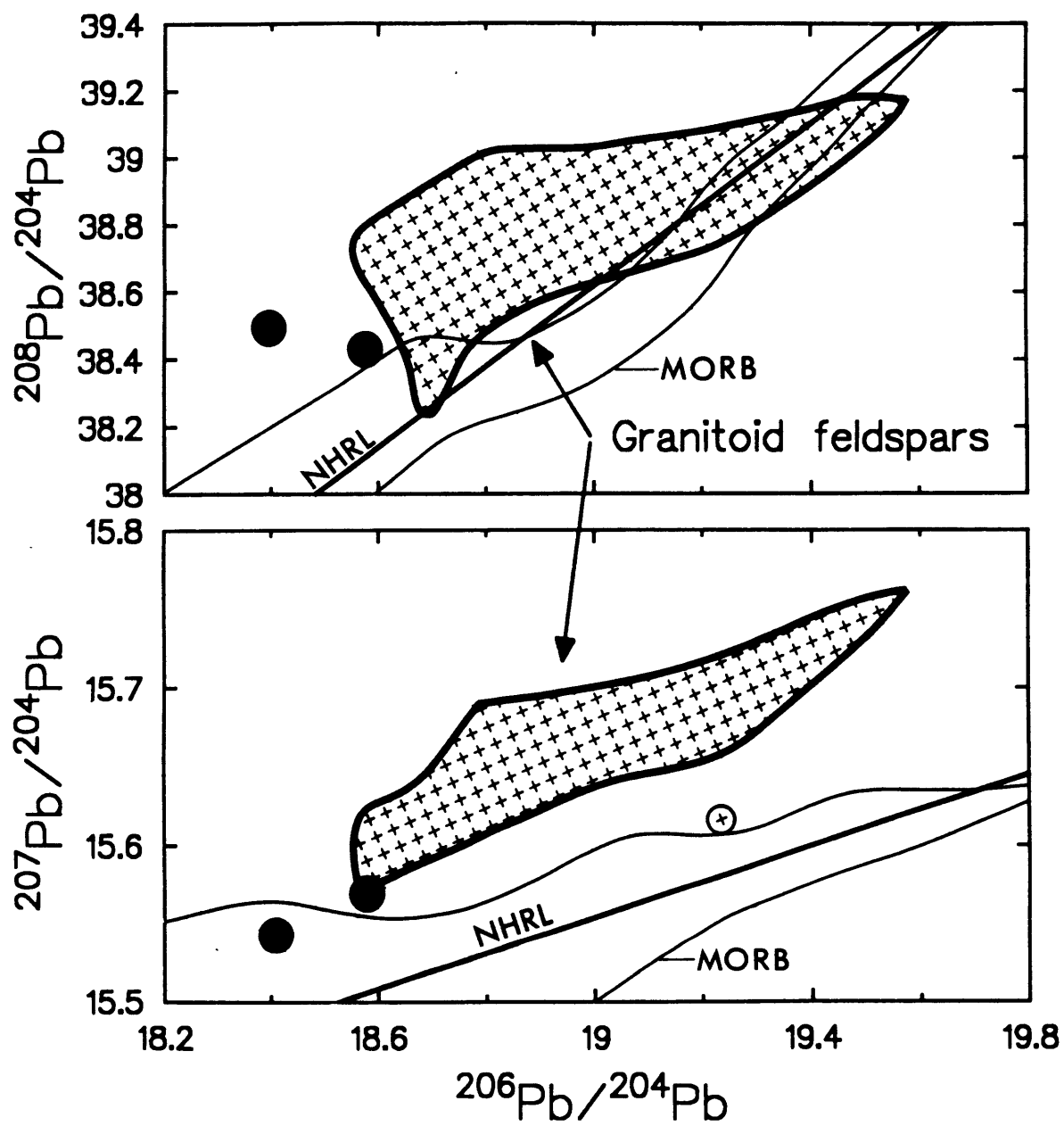


Figure 1-19. Histogram of An contents in plagioclase crystal cores from Sierran granitoids, and Onion Valley sills and layered cumulates. Granitoid data from Barbarin (1990), Piwinski (1968), Bateman and Chappell (1979), Bateman and Nokleberg (1978).

Plagioclase Cores

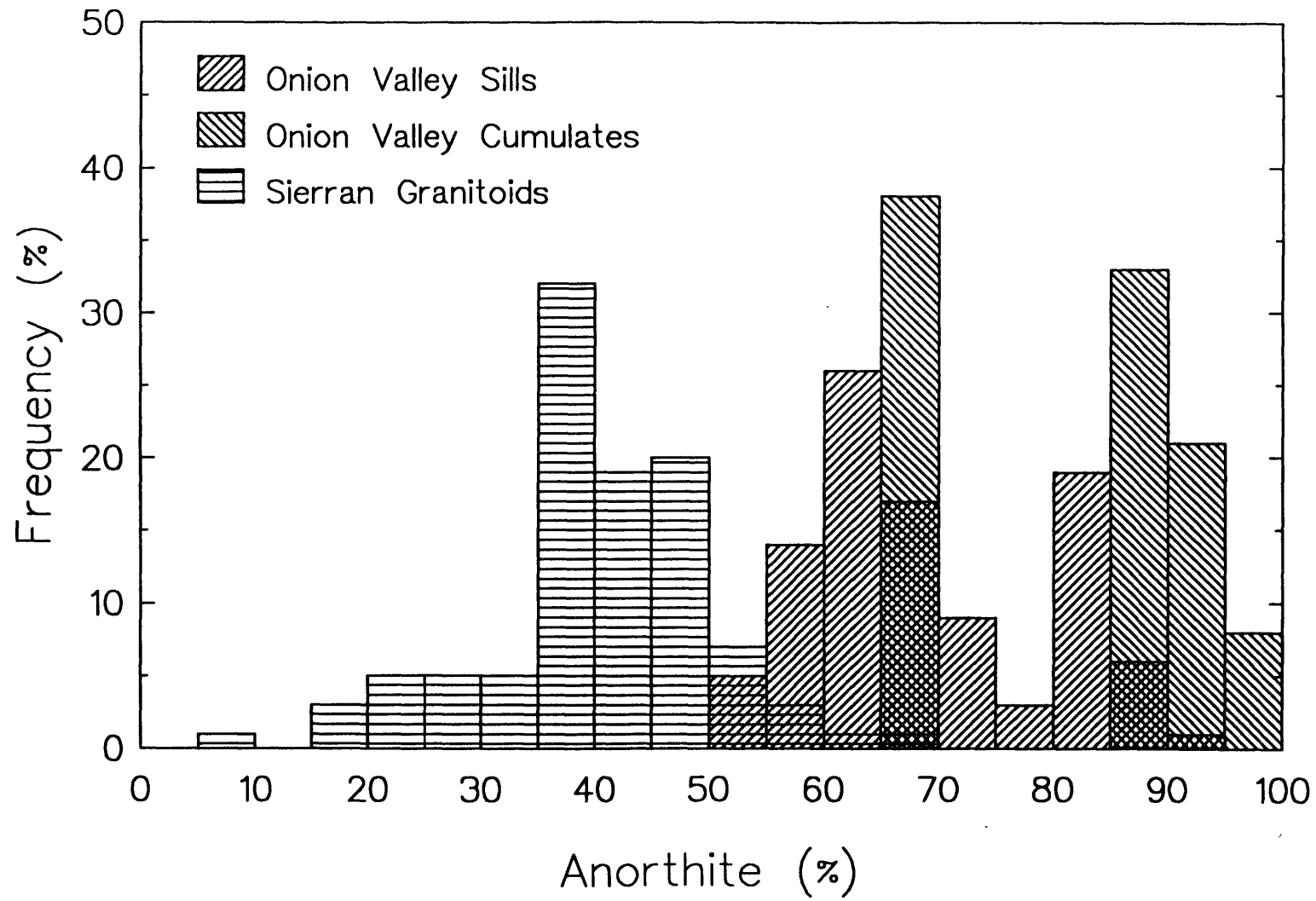


Figure 1-20. Average trace element contents of plutonic rocks of the Sierra Nevada batholith with $60 \leq \text{SiO}_2 < 70$ wt.% compared with calculated trace element contents of a mixture of 71.1 % average Sierran low-silica granite and 28.9 % average basaltic sill from Onion Valley. Line indicates 1:1 correspondence.

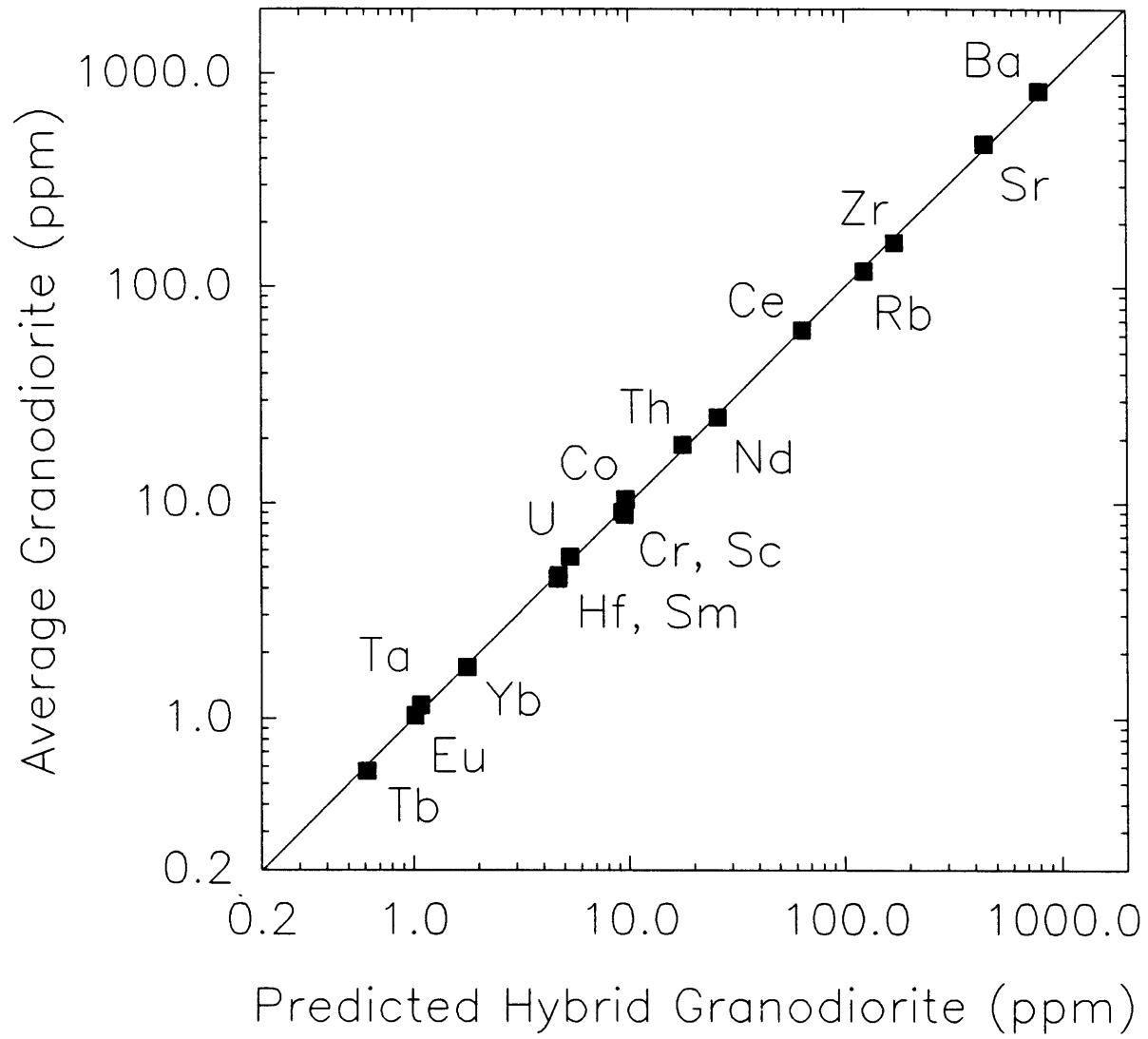


Figure 1-21. Trace element contents of mafic inclusions with $\text{SiO}_2 < 52.5$ wt.% from plutons of the Sierra Nevada batholith (Barbarin, et al., 1989) normalized to average abundances in basaltic sills and dikes at Onion Valley exclusive of the two lowest silica samples. Af, B, S, and Hbl designate elements that are compatible in alkali feldspar, biotite, sphene, and hornblende, respectively.

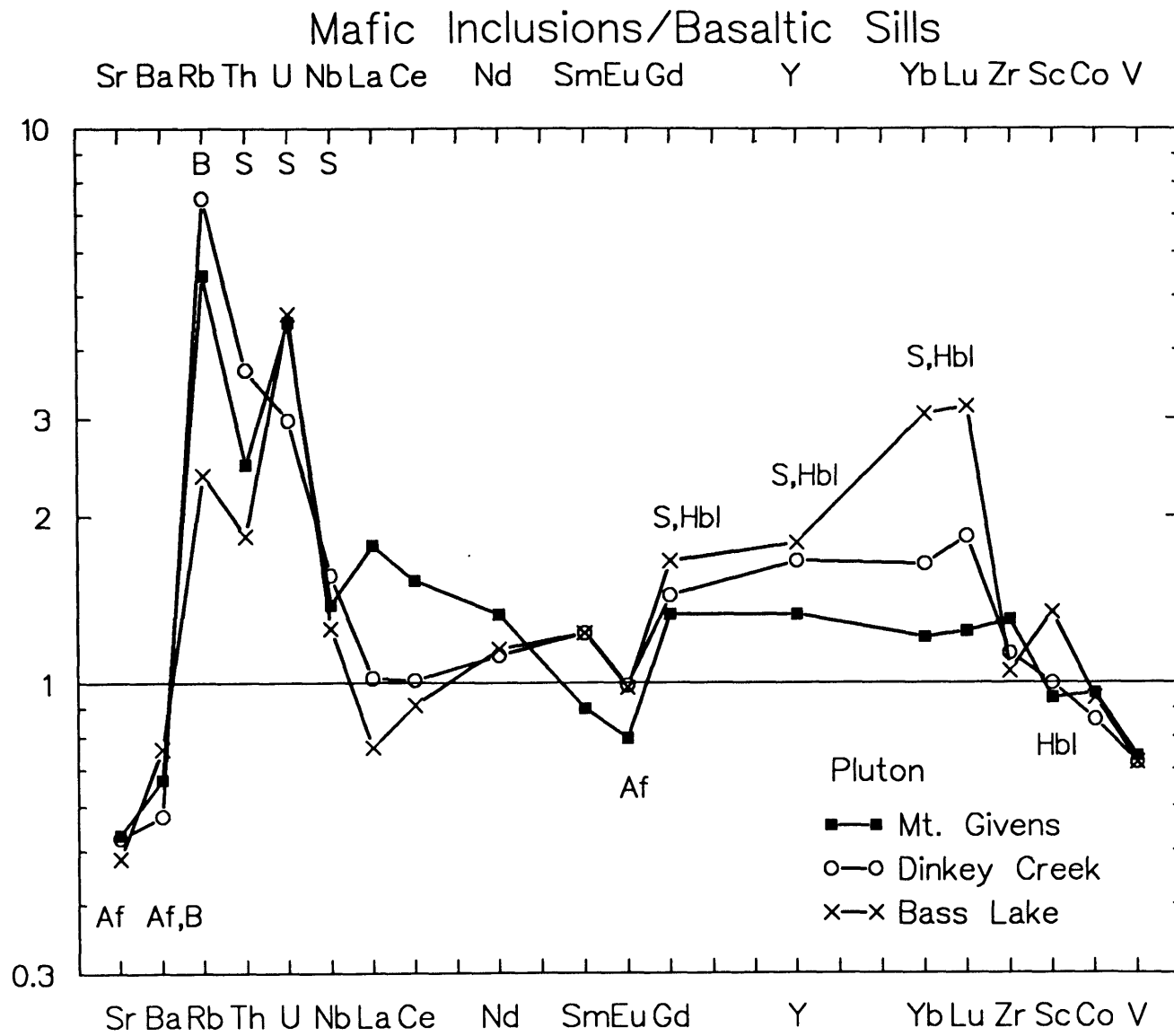


Table 1: Sheeted sills and magmatic septa

Sample Type	86S49 1	86S48 1	86S50A 2	86S40A 2	87S26 2	86S41A 2	87S35B 2	87S35A 2	87S25 2	86S54 2
SiO ₂	44.5	45.9	49.4	49.7	50.2	50.3	50.4	50.6	51.2	51.3
Al ₂ O ₃	19.7	19.4	19.5	19.6	19.0	16.9	18.8	19.1	18.6	19.6
Fe ₂ O ₃	5.27	5.45	3.71	4.12	3.88	3.61	3.77	3.74	3.58	3.86
FeO	6.24	6.34	5.93	5.38	5.60	6.20	5.49	5.33	5.44	4.96
MgO	5.73	5.11	4.54	4.43	4.39	6.34	4.41	4.32	4.31	4.07
CaO	11.8	11.0	9.59	9.15	9.26	8.74	8.92	8.85	9.09	8.21
Na ₂ O	2.73	3.16	3.48	3.52	3.39	3.01	4.10	4.23	3.29	3.93
K ₂ O	0.63	0.75	1.24	1.33	1.29	1.32	1.06	1.00	1.21	1.18
TiO ₂	1.69	1.39	1.29	1.24	1.29	1.50	1.29	1.27	1.30	1.07
P ₂ O ₅	0.54	0.60	0.42	0.31	0.36	0.13	0.44	0.37	0.38	0.36
MnO	0.16	0.17	0.17	0.14	0.15	0.12	0.16	0.17	0.14	0.15
H ₂ O+	1.37	1.05	1.00	1.01	1.20	1.19	1.24	1.13	1.16	1.13
H ₂ O-	0.12	0.15	0.12	0.12	0.12	0.13	0.11	0.15	0.25	0.16
CO ₂	0.03	0.05	0.03	0.04	<0.01	0.05	<0.01	<0.01	0.14	0.05
Total	100.5	100.5	100.4	100.1	100.1	99.5	100.2	100.2	100.1	100.0

Trace-element analyses (parts per million)

Rb	10	10	27	32	28	24	26	30	28	24
Sr	910	930	850	820	810	560	820	850	770	780
Ba	300	300	440	570	475	410	690	640	435	730
Zr	84	94	47	110	76	120	176	152	76	220
Y	25	26	26	18	20	18	22	22	20	24
Nb	7.6	8.5	10	7.0	8.3	6.9	7.7	8.7	10	7.8
V	300	240	230	230	250	330	250	250	240	170
Ni	<15	<15	<15	<15	<10	32	13	10	<10	<15
Co	33	28	26	25	24	35	26	22	25	23
Cr	12	5	12	10	8	54	20	14	10	7
Cs	0.6	0.6	1.2	1.1	0.8	1.4	0.8	0.7	1.1	1.4
Hf	2.3	2.2	1.2	3.4	2.2	3.3	3.7	3.0	2.1	4.7
Ta	0.31	0.37	0.52	0.36	0.51	0.39	0.33	0.29	0.68	0.41
Th	0.97	1.55	2.26	2.45	2.82	3.79	1.23	0.90	4.99	1.65
U	0.4	0.5	0.5	0.8	1.2	1.2	0.3	0.3	1.8	0.4
Zn	123	127	113	115	93	123	118	85	88	112
Sc	31.7	21.0	22.4	22.6	23.8	39.9	22.4	19.3	23.9	18.7
La	16.0	21.4	24.3	19.2	21.6	16.4	25.6	22.5	24.0	20.8
Ce	43.8	52.8	59.0	46.0	49.0	36.0	57.0	51.7	54.3	51.2
Nd	27.2	32.8	30.6	24.6	27.8	19.7	28.9	26.2	28.9	27.4
Sm	6.7	7.3	7.1	5.5	6.2	4.7	6.0	5.6	6.4	5.9
Eu	2.04	2.08	1.81	1.56	1.70	1.38	1.78	1.63	1.77	1.66
Gd	6.5	6.9	6.7	4.9	5.5	4.4	5.2	4.9	5.6	5.5
Tb	0.88	0.90	0.84	0.68	0.73	0.60	0.68	0.64	0.77	0.77
Tm	0.35	0.40	0.36	0.32	0.31	0.25	0.30	0.26	0.31	0.34
Yb	2.04	2.23	2.05	1.75	1.79	1.40	1.68	1.49	1.85	1.98
Lu	0.28	0.33	0.29	0.26	0.26	0.20	0.24	0.22	0.26	0.30

Type: 1-thin sills that lost magmatic liquid, 2-thin sheeted sills, 3-inter-sill magmatic septa, 4-thick sills. *-exceptional analysis by INAA

Table 1 (continued)

Sample Type	86S55 2	86S32B 2	87S39 2	86S45 2	87S27 3	86S40B 3	86S41B 3	86S32C 3	85S47A 4	85S47E 4
SiO ₂	55.1	55.8	57.2	57.3	52.3	54.0	56.3	58.4	51.2	55.8
Al ₂ O ₃	19.0	18.4	17.3	17.6	19.5	20.0	18.2	20.0	18.2	17.6
Fe ₂ O ₃	3.21	3.23	3.02	2.83	3.65	3.45	3.28	2.64	2.62	3.37
FeO	4.05	4.20	4.01	4.13	4.48	4.04	3.95	2.80	4.86	4.48
MgO	3.17	3.42	3.15	3.38	3.57	3.06	3.19	1.65	5.61	3.51
CaO	7.42	7.04	6.79	6.94	9.19	7.69	7.28	6.01	9.25	7.38
Na ₂ O	4.24	4.01	4.18	3.88	3.90	4.32	4.20	4.50	2.99	3.65
K ₂ O	1.29	1.93	1.66	1.77	1.09	1.33	1.39	2.16	1.26	1.36
TiO ₂	0.93	1.02	0.96	0.97	1.06	0.92	0.93	0.68	1.16	1.05
P ₂ O ₅	0.37	0.31	0.35	0.28	0.56	0.33	0.34	0.31	0.15	0.39
MnO	0.12	0.14	0.13	0.12	0.12	0.13	0.15	0.06	0.13	0.13
H ₂ O+	0.69	0.86	0.98	0.79	0.89	0.73	0.69	0.55	1.69	1.09
H ₂ O-	0.10	0.08	0.11	0.11	0.09	0.09	0.13	0.07	0.10	0.12
CO ₂	0.08	0.01	<0.01	0.05	<0.01	0.03	0.07	0.03	0.07	0.05
Total	99.8	100.4	99.8	100.2	100.4	100.1	100.1	99.9	99.3	100.0
Trace-element analyses (parts per million)										
Rb	30	46	50	37	30	46	38	54	54	52
Sr	710	710	700	710	810	810	640	880	580	660
Ba	670	790	870	870	600	590	590	990	510	620
Zr	130	90	128	130	166	160	120	480	100	75
Y	18	20	14	14	20	20	22	20	17	17
Nb	7.5	9.1	8.1	8.0	7.6	7.5	11	5.4	6.2	5.8
V	170	170	190	150	240	160	165	85	219	145
Ni	<15	<15	<10	<15	<10	<15	<15	<15	41	<5
Co	15	19	17	18	18	13	14	12	30	19
Cr	2	4	10	16	1	2	4	4	136	1
Cs	1.7	1.8	1.6	1.3	0.49	1.7	1.0	1.7	3.0	1.9
Hf	4.0	2.3	4.0	3.5	4.0	4.4	4.0	12.5	2.8	2.7
Ta	0.45	0.38	0.65	0.49	0.46	0.40	0.72	0.28	0.34	0.54
Th	2.35	5.18	6.72	3.10	2.99	2.96	5.11	11.6	2.03	4.98
U	0.9	2.2	2.0	1.3	1.6	0.9	2.1	2.8	0.5	1.8
Zn	86	97	72	95	79	91	87	70	76	90
Sc	17.1	16.9	15.6	15.0	16.5	12.9	14.3	5.5	28.2	15.1
La	26.3	22.5	23.4	23.5	26.5	21.4	24.5	64.7	14.7	23.9
Ce	55.5	48.5	48.6	49.5	56.7	47.2	53.0	111	30.9	51.2
Nd	25.6	24.2	24.9	22.4	27.6	24.1	24.9	32.3	16.7	25.8
Sm	5.2	5.5	5.1	4.7	5.6	4.8	5.3	4.7	4.2	5.4
Eu	1.58	1.47	1.34	1.34	1.67	1.43	1.40	1.16	1.31	1.58
Gd	5.0	5.3	4.6	4.2	4.7	4.3	4.9	3.7	4.2	4.7
Tb	0.66	0.65	0.58	0.50	0.70	0.60	0.66	0.37	0.63	0.68
Tm	0.31	0.29	0.24	0.22	0.28	0.25	0.31	0.23	---	0.29
Yb	1.85	1.78	1.39	1.27	1.63	1.50	1.84	1.51	1.57	1.59
Lu	0.27	0.26	0.20	0.17	0.24	0.22	0.27	0.26	0.23	0.23

Table 1 (continued)

Sample	85S48B	85S48A	85S55	86S26	88OV12	88OV10	88OV11	88OV13	88OV7
Type	4	4	Mass. dike	Porph. dike	2	2	2	2	Schistose diorite
SiO ₂	57.8	58.5	52.7	47.3	48.7	50.0	50.8	52.4	54.4
Al ₂ O ₃	17.9	17.3	18.8	18.2	20.0	19.8	21.1	19.5	23.2
Fe ₂ O ₃	2.89	3.39	3.71	3.33	--	--	--	--	--
FeO	3.94	3.34	4.69	5.50	10.7**	9.34**	8.46**	8.91**	5.48**
MgO	3.14	2.32	4.04	7.19	4.96	4.59	3.34	4.21	1.32
CaO	6.30	6.69	8.58	10.6	9.17	9.49	8.90	8.08	6.80
Na ₂ O	3.58	3.67	3.55	2.92	3.77	3.87	4.45	3.95	5.43
K ₂ O	2.02	2.06	1.25	0.93	1.02	1.07	1.01	1.40	1.30
TiO ₂	0.74	0.77	0.94	1.77	1.13	1.22	1.09	1.03	0.83
P ₂ O ₅	0.29	0.45	0.33	0.21	0.36	0.29	0.63	0.34	0.25
MnO	0.14	0.12	0.13	0.12	0.20	0.22	0.16	0.17	0.07
H ₂ O+	0.81	0.75	0.91	1.85	--	--	--	--	--
H ₂ O-	0.24	0.07	0.14	0.08	--	--	--	--	--
CO ₂	0.04	0.07	0.06	0.03	--	--	--	--	--
Total	99.8	99.5	99.8	100.0	100.0	99.9	99.9	100.0	99.1

Trace-element analyses (parts per million)

Rb	58	50	36	22	--	--	--	--	37
Sr	650	630	710	640	--	--	--	--	1050
Ba	840	730	480	400	--	--	--	--	970
Zr	120	110	120	100	--	--	--	--	1070
Y	18	20	17	15	--	--	--	--	--
Nb	7.8	10	6.7	5.2	--	--	--	--	4.1
V	130	91	190	323	--	--	--	--	53
Ni	<15	<5	26	50	--	--	--	--	7
Co	16	12	24	34	--	--	--	--	--
Cr	4	<0.5	8	250	--	--	--	--	1***
Cs	3.5	2.1	0.8	1.0	--	--	--	--	--
Hf	3.7	3.7	3.9	2.4	--	--	--	--	--
Ta	0.68	0.88	0.46	0.24	--	--	--	--	--
Th	7.51	7.50	4.68	1.62	--	--	--	--	--
U	1.9	2.8	1.7	0.4	--	--	--	--	--
Zn	95	73	99	76	--	--	--	--	83***
Sc	12.2	9.7	18.2	51.9	--	--	--	--	--
La	26.1	22.4	23.1	13.0	--	--	--	--	--
Ce	53.3	48.5	52.2	29.9	--	--	--	--	59***
Nd	25.4	24.6	26.1	16.0	--	--	--	--	--
Sm	4.9	5.5	5.5	4.2	--	--	--	--	--
Eu	1.37	1.39	1.51	1.47	--	--	--	--	--
Gd	4.7	5.2	4.8	4.4	--	--	--	--	--
Tb	0.62	0.73	0.70	0.62	--	--	--	--	--
Tm	0.31	0.37	--	0.24	--	--	--	--	--
Yb	1.97	2.14	1.82	1.29	--	--	--	--	--
Lu	0.29	0.30	0.27	0.18	--	--	--	--	--

--all Fe as FeO, *- exceptional analysis by XRF. Major element analyses by J. Taggart, A. J. Bartel, L. Espos, D. Siems, M. Dyslin, S. Neil, and E. Brandt. INAA by J. Budahn, R. Knight, and D. McKown. EDXRF by M. Dyslin, D. Vivit, J. Kent, J. Consul, and B. King. ICPAES by J. Consul, J. Kent, and R. Lerner. Nb by B. Libby, M. Dyslin, and S. Neil.

Table 2: Representative cumulates

Sample Type	87S31 1	87S33A 1	87S17 2	87S49 2	86S16A 3	86S33 3	86S23 4	87S22 4	85S44 4	86S5 5
SiO ₂	39.1	39.3	46.3	43.1	42.5	44.2	40.9	45.7	42.5	51.8
Al ₂ O ₃	11.0	9.56	26.4	25.0	11.9	15.3	19.5	19.1	21.1	13.4
Fe ₂ O ₃	5.18	5.41	2.26	3.04	4.89	4.73	7.40	4.35	5.31	2.79
FeO	10.1	11.6	3.28	4.77	7.57	7.44	6.84	6.70	5.93	5.04
MgO	21.2	23.0	4.09	6.72	14.7	10.7	6.80	6.39	6.85	7.95
CaO	7.53	5.87	13.3	13.0	11.5	10.6	12.6	10.9	12.2	13.3
Na ₂ O	1.19	0.90	2.24	1.13	1.86	2.12	1.64	2.63	1.90	2.34
K ₂ O	0.31	0.18	0.55	0.59	0.67	0.89	0.71	1.00	0.98	0.99
TiO ₂	1.21	0.64	0.48	0.49	2.16	2.05	1.91	1.80	1.68	1.02
P ₂ O ₅	<0.05	<0.05	0.09	0.07	0.05	0.08	0.39	0.12	0.09	0.16
MnO	0.19	0.27	0.05	0.09	0.14	0.17	0.13	0.11	0.13	0.16
H ₂ O+	2.74	3.69	1.36	2.25	2.34	2.18	1.64	1.42	1.63	1.25
H ₂ O-	0.10	0.16	0.11	0.16	0.02	0.05	0.03	0.09	0.14	0.03
CO ₂	0.30	0.18	0.02	0.01	0.09	0.06	0.04	<0.01	0.04	0.03
Total	100.2	100.8	100.5	100.4	100.4	100.6	100.5	100.3	100.5	100.3

Trace-element analyses (parts per million)

Rb	5*	6*	16	28	<1*	12	26	20	26	18
Sr	360	305	940	720	270	480	740	680	760	390
Ba	136	88	250	160	260	320	260	270	220	430
Zr	33	28	54	50	60	86	66	80	60	96
Y	<10	<10	<10	<10	15	17	20	14	<10	18
Nb	3.2	3.0	3.4	3.1	5.0	5.9	5.8	6.2	3	4.4
V	260	140	150	180	432	362	373	420	400	270
Ni	190	240	23	37	208	70	27	22	45	35
Co	110	126	244	32	60	54	44	41	34	26
Cr	610	355	95	115	940	285	3	4	12	187
Cs	0.5	0.7	0.8	2.4	0.4	1.1	0.7	0.6	3.8	0.5
Hf	0.9	0.7	0.9	0.6	2.1	2.6	1.6	2	1.4	2.4
Ta	0.08	0.09	0.14	0.06	0.22	0.25	0.31	0.47	0.16	0.21
Th	0.14	0.11	1.23	0.33	0.53	1.17	0.48	1.25	0.68	2.85
U	0.06	0.08	0.45	0.15	0.16	0.2	0.4	1	0.2	1
Zn	113	146	38	36	110	123	75	90	88	--
Sc	42.1	11.2	8.6	5.1	69.4	58.6	35	42.5	39.1	69.2
La	2.4	2.7	7.0	4.2	5.5	9.6	8.1	10.7	6.1	13.5
Ce	7.3	8.1	13.7	8.7	16.7	26.4	23.3	24.3	16.8	27.7
Nd	6.0	6.4	6.7	4.8	13.3	18.2	19.3	15.5	11.4	14.8
Sm	2.0	1.9	1.5	1.0	4.7	5.1	5.3	4.0	3.2	3.3
Eu	0.70	0.62	0.62	0.47	1.58	1.72	1.60	1.23	1.04	1.13
Gd	2.2	1.9	1.5	0.89	5.5	5.5	5.8	3.6	3.3	3.76
Tb	0.30	0.27	0.20	0.12	0.77	0.81	0.81	0.55	0.47	0.59
Tm	0.10	--	--	--	--	--	0.31	0.24	0.18	0.3
Yb	0.59	0.55	0.45	0.35	1.68	1.59	1.66	1.35	1.05	1.85
Lu	0.08	0.07	0.06	0.05	0.22	0.22	0.23	0.19	0.14	0.27

Type: 1-olivine hornblende, 2-plagioclase-rich hornblende gabbro, 3-hornblende, 4-mafic hornblende gabbro, 5-clinopyroxene-bearing porphyritic hornblende gabbro. *-exceptional analysis by INAA.

Table 3: Rubidium, strontium, and lead isotopic data for cumulates

Sample	Rock type	Rb (ppm)	Sr (ppm)	$^{87}\text{Sr}/^{86}\text{Sr}$ (at 168 Ma)		
85S35	hbl. -plag. cumulate	24.9	715.6	0.70803 (0.7078)		
85S49	hbl. -plag. cumulate	18.3	600.5	0.70683 (0.7066)		
85S39	oliv. -hbl. cumulate	6.1	141.8	0.70678 (0.7065)		
86S5	porph. hbl. gabbro with cpx.	18.1	474.2	0.70610 (0.7058)		
	U (ppm)	Pb (ppm)	Th (ppm)	$^{206}\text{Pb}/^{204}\text{Pb}$ (at 168 Ma)	$^{207}\text{Pb}/^{204}\text{Pb}$ (at 168 Ma)	$^{208}\text{Pb}/^{204}\text{Pb}$ (at 168 Ma)
85S35	0.60	4.67	2.07	18.6153 (18.40)	15.5483 (15.54)	38.5121 (38.50)
85S49	0.16	3.42	0.44	18.6570 (18.58)	15.5741 (15.57)	38.5208 (38.45)

Rubidium, Sr, U, and Pb concentrations by isotope dilution mass spectrometry; Th by INAA. Strontium isotopic ratios precise to 0.0035-0.0030% relative 2 sigma. Lead isotopic ratios precise to 0.012-0.017% relative 2 sigma.

Table 4: Accuracy and precision of neutron activation analyses

	AGV-1			Lit. ¹	RGM-1			Lit. ²	85S56A		
	Mean (n=4)	1 std. dev.	% dev.		Mean (n=3)	1 std. dev.	% dev.		Mean (n=2)	1 std. dev.	% dev.
Rb	67.2	1.5	2.2	67. \pm 1	148.3	2.1	1.4	149. \pm 8	114.5	0.7	0.6
Ba	1243	30	2.4	1221. \pm 16	844.	14.	1.7	807. \pm 46	795	9	1.2
Co	15.1	0.4	2.6	15.1 \pm 1.2	1.94	0.03	1.5	2.0 \pm 0.2	29.3	0.3	1.0
Cr	8.2	0.6	7.3	12. \pm 3	2.3	0.2	8.7	3.7 \pm 1.2	45.2	3.0	6.8
Cs	1.27	0.04	3.1	1.26 \pm 0.12	10.1	0.2	2.0	9.6 \pm 0.6	5.07	0.03	0.6
Hf	5.04	0.08	1.6	5.1 \pm 0.4	6.02	0.05	0.8	6.2 \pm 0.3	3.75	0.01	0.3
Ta	0.961	0.007	0.7	0.92 \pm 0.12	1.06	0.015	1.4	0.95 \pm 0.1	0.461	0.001	0.3
Th	6.31	0.18	2.9	6.50 \pm 0.37	14.8	0.26	1.8	15.1 \pm 1.3	3.62	0.06	1.8
U	1.92	0.09	4.7	1.89 \pm 0.25	5.95	0.20	3.4	5.8 \pm 0.5	1.59	0.15	9.3
Zn	95.7	2.3	2.4	88. \pm 2	35.7	1.8	5.0	32. \pm 6	150.	13.	8.7
Sc	12.0	0.4	3.3	12.1 \pm 0.9	4.55	0.03	0.7	4.4 \pm 0.3	19.0	0.5	2.6
La	38.0	1.1	2.9	38. \pm 3	22.9	0.1	0.4	24. \pm 1.1	23.7	0.8	3.4
Ce	71.0	0.6	0.8	66. \pm 6	46.6	0.6	1.3	47. \pm 4	49.0	1.1	2.2
Nd	32.0	0.6	1.9	34. \pm 5	19.8	0.7	3.5	19. \pm 1	23.8	0.3	1.2
Sm	5.74	0.40	7.0	5.9 \pm 0.5	4.15	0.20	4.8	4.3 \pm 0.3	4.75	0.04	0.9
Eu	1.64	0.05	3.0	1.66 \pm 0.11	0.620	0.015	2.4	0.66 \pm 0.08	1.49	0.06	4.0
Gd	4.66	0.20	4.3	5.2 \pm 0.6	4.12	0.48	11.7	3.7 \pm 0.4	4.53	0.21	4.6
Tb	0.672	0.016	2.4	0.71 \pm 0.10	0.614	0.015	2.4	0.66 \pm 0.06	0.62	0.05	8.1
Tm	0.299	0.016	6.4	0.32 \pm 0.05	0.411	0.009	2.2	0.37 \pm 0.04	---	---	---
Yb	1.71	0.04	2.3	1.67 \pm 0.17	2.61	0.02	0.8	2.6 \pm 0.3	1.36	0.05	3.6
Lu	0.247	0.006	2.4	0.28 \pm 0.03	0.379	<.001	<0.3	0.41 \pm 0.03	0.194	<.001	<0.5

Sample 85S56A is a Cretaceous diorite dike from the Onion Valley area. Consensus values and uncertainties from 1-Gladney, Burns, and Roelandts (1983); 2-Gladney and Roelandts (1988).

Table 5: Crystal fractionation models

Inverse model

SiO ₂	TiO ₂	Al ₂ O ₃	FeO*	MgO	CaO	Na ₂ O	K ₂ O	P ₂ O ₅	XHbl	XPl	XTmt	XAp	F
Parent													
50.1	1.30	19.8	9.26	4.55	9.70	3.71	1.04	0.41	0.408	0.485	0.096	0.011	1.0
Derivative liquids													
51.2	1.25	19.6	8.96	4.36	9.39	3.62	1.15	0.40	0.407	0.486	0.096	0.011	0.913
52.2	1.20	19.4	8.63	4.17	9.02	3.67	1.24	0.39	0.407	0.486	0.096	0.011	0.840
53.2	1.14	19.2	8.31	3.98	8.65	3.72	1.33	0.38	0.407	0.487	0.095	0.011	0.777
54.2	1.09	19.0	7.98	3.79	8.28	3.77	1.42	0.37	0.406	0.488	0.095	0.011	0.723
55.2	1.04	18.8	7.66	3.60	7.91	3.82	1.51	0.36	0.406	0.488	0.095	0.011	0.675
56.2	0.98	18.6	7.34	3.41	7.54	3.87	1.60	0.35	0.405	0.489	0.095	0.011	0.633
57.3	0.93	18.3	7.01	3.22	7.17	3.91	1.69	0.34	0.405	0.489	0.095	0.011	0.596
58.3	0.88	18.1	6.69	3.03	6.80	3.96	1.78	0.33	0.404	0.490	0.095	0.011	0.562
59.3	0.82	18.0	6.35	2.84	6.39	4.08	1.87	0.33					0.532

Forward model I

SiO ₂	TiO ₂	Al ₂ O ₃	FeO*	MgO	CaO	Na ₂ O	K ₂ O	P ₂ O ₅	XHbl	XPl	XTmt	XAp	F
Parent													
50.0	1.31	19.8	9.39	4.60	9.71	3.52	1.26	0.43	0.496	0.418	0.075	0.011	1.0
Derivative liquids													
52.3	1.22	19.3	8.71	4.05	8.74	3.86	1.46	0.42					0.815
54.3	1.14	18.8	8.08	3.58	7.90	4.14	1.63	0.41					0.698
56.6	1.05	18.4	7.30	3.05	6.96	4.45	1.84	0.39					0.599
58.3	0.98	18.0	6.69	2.67	6.28	4.67	2.00	0.38					0.540
59.2	0.95	17.8	6.35	2.47	5.92	4.79	2.08	0.38					0.513

Forward model II

SiO ₂	TiO ₂	Al ₂ O ₃	FeO*	MgO	CaO	Na ₂ O	K ₂ O	P ₂ O ₅	XHbl	XPl	XTmt	XAp	F
Parent													
50.0	1.31	19.8	9.39	4.60	9.71	3.52	1.26	0.43	0.496	0.430	0.063	0.011	1.0
Derivative liquids													
52.2	1.24	19.2	8.90	4.10	8.64	3.88	1.46	0.42					0.815
54.2	1.18	18.6	8.43	3.67	7.71	4.19	1.63	0.40					0.698
56.4	1.11	18.0	7.84	3.20	6.68	4.53	1.84	0.39					0.599
58.1	1.06	17.6	7.37	2.86	5.92	4.77	2.00	0.38					0.540
59.0	1.03	17.4	7.10	2.68	5.52	4.89	2.08	0.37					0.513

Inverse modeling is performed by regressing polynomial equations through oxide-CaO variation diagrams. Equations are then solved for evenly-spaced intervals as a function of CaO. Adjacent end points of intervals are treated as ideal compositions modeling the overall trends in the sill data set. The more CaO-rich of an adjacent pair is treated as a parent, and the matching CaO-poor composition is treated its daughter liquid. The parent composition is then matched by a combination of daughter liquid plus specified minerals with proportions being determined by multiple regression. The process is repeated for each interval. $K_D^{Ca-Na}=6.0$ for plagioclase, $K_D^{Fe-Mg}=0.35$ for hornblende, titanomagnetite is from Sisson and Grove (1991), apatite is stoichiometric $Ca_5P_3O_{12}(OH)$.

Forward modeling follows the procedures of Grove and Donnelly-Nolan (1986). Mineral proportions for model I were determined by multiple regression of representative compositions from the sill data set. $K_D^{Ca-Na}=4.0$ for plagioclase, $K_D^{Fe-Mg}=0.43$ for hornblende, other minerals as above. Crystallizing proportions for model II were determined independently, using 2 kbar phase equilibria experiments on composition 87S35A reported by Sisson and Grove (1991). $K_D^{Ca-Na}=5.0$ for plagioclase, $K_D^{Fe-Mg}=0.44$ for hornblende, other minerals as above. Parent composition for both forward models is 86S50A calculated anhydrous, MnO-free, with all Fe as FeO.

Table 6: Mineral-rock abundance ratios and partition coefficients

	Hornblende	Plagioclase	Apatite ^a	Apatite ^b	Magnetite	Bulk D
La	0.65	0.18	20.4	3.4	0	0.58 ^a , 0.39 ^b
Sm	2.75	0.032	27.8	7.8	0	1.44 ^a , 1.22 ^b
Yb	2.70	0.0096	4.9	2.9	0	1.15 ^a , 1.13 ^b
Sr	0.36	2.04 (2.6)	1.35 ^c	1.35	0	1.16 (1.43)
V	1.2	0	0	0	30 ^c (10)	3.34 (1.44)
Sc	3.3 (5.3)	0	0	0	2 ^c	1.53 (2.34)
Rb	0.045 ^c	0.074 ^c	0	0	0	0.05
Crystallizing proportions						
	0.405	0.489	0.011		0.095	

Hornblende, plagioclase, and apatite^a values are averages of crystal core compositions measured by ion microprobe, in sample 86S48, divided by abundances in sill sample 86S55. Apatite^b values are partition coefficients from Watson and Green (1981) run# 812, tholeiitic andesite. C - literature partition coefficients: Watson and Green (1981)-apatite; Philpotts and Schnetzler (1970)-hornblende (lowest D^{Rb}), plagioclase (ave. D^{Rb}, ≥An 80); Gill (1981)-titanomagnetite. Values in parentheses give better fits to the sill data. Values of zero are interpreted from study of the literature. Crystallizing proportions from inverse modelling, Table 5.

Table 7: Average granitoid compositions and mixing model results

Low-silica Sierran granites (70-74 wt.% SiO₂)

SiO ₂	Ba	Rb	Sr	Zr	Co	Cr	Sc	Hf	Th	U	Ta	Ce	Nd	Sm	Eu	Tb	Yb
Mean																	
71.9	894	161	314	189	3.2	3.1	3.6	5.4	23.9	7.0	1.35	69.3	25.8	4.23	0.78	0.57	1.79
Median																	
72.0	822	160	287	189	2.7	2.4	3.2	4.9	21.8	6.4	1.23	65	23.9	4	0.75	0.51	1.4
N																	
54	38	54	52	33	28	38	34	29	37	37	26	29	29	28	28	22	28

Sierran granodiorites (>60-<70 wt.% SiO₂)

SiO ₂	Ba	Rb	Sr	Zr	Co	Cr	Sc	Hf	Th	U	Ta	Ce	Nd	Sm	Eu	Tb	Yb
Mean																	
65.8	836	119	475	162	10.4	8.8	9.1	4.6	18.8	5.6	1.15	63.3	25.2	4.45	1.03	0.57	1.72
Median																	
65.9	835	120	450	143	9	8.1	8.8	4.3	17.5	5.2	1.09	60	24	4.5	1	0.57	1.79
N																	
96	92	97	91	83	56	70	80	63	80	80	52	75	68	68	68	49	68

Basaltic sills

SiO ₂	Ba	Rb	Sr	Zr	Co	Cr	Sc	Hf	Th	U	Ta	Ce	Nd	Sm	Eu	Tb	Yb
Mean																	
50.8	544	28.5	760	124	25.3	25.4	23.3	3.13	2.71	0.94	0.43	49.5	25.9	5.69	1.62	0.70	1.73
N																	
11	11	10	11	11	11	11	11	11	11	11	11	11	11	11	11	11	11

Mixing model: 0.711 low-silica granite + 0.289 basaltic sill

SiO ₂	Ba	Rb	Sr	Zr	Co	Cr	Sc	Hf	Th	U	Ta	Ce	Nd	Sm	Eu	Tb	Yb
65.8	793	123	443	170	9.6	9.5	9.3	4.7	17.7	5.3	1.08	63.6	25.8	4.65	1.02	0.61	1.77

% difference between model and average granodiorite

set	Ba	Rb	Sr	Zr	Co	Cr	Sc	Hf	Th	U	Ta	Ce	Nd	Sm	Eu	Tb	Yb
	5.1	3.4	6.7	4.9	7.7	8.0	2.2	2.2	5.9	5.4	6.1	0.5	2.4	4.5	1.0	7.0	2.9

Average granitoid data compiled from Bateman et al. (1988), Peck and Van Kooten (1983), Dodge et al. (1982), Dodge and Calk (1987), Barbarin et al. (1989), Noyes et al. (1983), Sawka et al. (1990), and unpublished analyses of T.W. Sisson, J.G. Moore, and F.A. Frey. Rocks of the western foothills, chiefly tonalitic, have been excluded from the compilation. Rocks with SiO₂ > 74 wt.% have been excluded because accessory mineral and alkali feldspar fractionation (Sawka, 1988) has depleted Sr, Ba, and rare earth elements in many samples. Samples 87S25, 87S26, 87S35A, 87S35B, 87S27, 86S40A, 86S41A, 86S50A, 86S54, 85S47A, and 85S55 were utilized for average basaltic sill. Average Rb excludes 85S47A because of sericitic alteration, as discussed in text.

CHAPTER 2

Experimental Evidence for High Water Contents in Some Aluminous Arc Magmas

INTRODUCTION

Subtle and diverse evidence from active or exhumed magmatic arcs suggest that many high-alumina basalt (HAB) and basaltic andesite (BA) magmas contain several or more weight percent of water. In this study we report the results of melting experiments on natural aphyric HABs and their intrusive equivalents. Experiments were carried out at 2 kb pressure under water-saturated conditions, with fO_2 buffered at Ni-NiO. We use the results of these experiments to discuss the effect of water on the crystallization paths followed by hydrous arc magmas as they differentiate in the upper crust and to examine the question of the origin of low-MgO HAB, BA, and their intrusive equivalents. Our experiments show that many low-MgO HABs and BAs were comparatively cool (< 1100 °C) and water-rich (> 4 wt. % H_2O) magmas. We find little evidence to support the hypotheses that low-MgO HABs are hot dry magmas or that they owe their major characteristics to preferential accumulation of plagioclase phenocrysts.

Background

High-alumina basalts and basaltic andesites are common and frequently abundant rocks in magmatic arcs worldwide. Kuno (1960) noted that basalts with high alumina contents are common along the Pacific rim in what are now recognized as magmatic arcs located above subduction zones. Kuno

discriminated between tholeiitic, alkali olivine, and high-alumina basalts on the basis of the petrographic and chemical characteristics of aphyric rocks. To Kuno, HAB contained groundmass olivine with little or no reaction rim of low-calcium pyroxene. High-alumina basalt also contained more than 17 wt.% Al_2O_3 and could contain small amounts of either olivine or quartz in the norm (in addition to plagioclase and augite). Plagioclase porphyritic tholeiites were assumed to be accumulative and were distinguished from similarly porphyritic HABs by groundmass mineralogy and texture and a lower total alkali content. Kuno presented analyses of rocks with silica contents as high as 55 wt.% as representatives of the HAB magma series; these rocks would now be classified as basaltic andesites (Peccherillo and Taylor, 1976). Kuno further observed that HABs are absent from regions that are now recognized as extensional or intraplate environments, even if plagioclase porphyritic rocks are considered.

Subsequent research has confirmed most of Kuno's observations on HABs. Most workers now ignore the subtleties of groundmass mineralogy and use "high-alumina basalt" to refer to any volcanic rock with $\text{SiO}_2 \leq 52$ wt.% (some use 54 %), $\text{Al}_2\text{O}_3 > 17$ wt.%, and an absence of significant normative nepheline. This encompasses a very broad range of rock compositions. Very many HABs and BAs have low-MgO (< 6 wt.% and < 5 wt.% respectively), including some aphyric rocks (Kuno, 1950, 1960; Marsh, 1982; Carr et al., 1982; Brophy, 1986; Myers et al., 1986). More magnesian compositions are not unknown, however,

and have compositions close in some respects to magnesian mid-ocean ridge basalt glasses (Perfit et al., 1980).

Petrogenetic models

Models for the origin of HAB magmas fall into three general categories: (1) direct partial melts of either mantle or subducted slab, (2) derivative liquids produced by fractional crystallization of other primary basalt magma, and (3) derivative liquids that have experienced preferential accumulation of plagioclase. Magnesian HABs have been proposed to be direct partial melts of the mantle wedge above a subducting plate. Magnesian HAB liquid can be produced experimentally under anhydrous conditions close to 10 kb pressure. Liquids are in equilibrium with a spinel or plagioclase lherzolite mineral assemblage (Fujii and Scarfe, 1985; Takahashi, 1986; Falloon and Green, 1987; Bartels et al., 1991).

A primary magma origin has also been proposed for low-MgO HABs and BAs. In this model, HABs are created by dry melting of subducted oceanic crust that has transformed to eclogite (Marsh, 1976, 1982). Trace element abundances require that all garnet is consumed during melting (Brophy and Marsh, 1986). This constraint is difficult to reconcile with the observation that low and moderate-MgO HAB liquids have garnet as a liquidus mineral at appropriate pressures (Johnston, 1986). Other trace element arguments against this model are

summarized by Crawford et al. (1987). In addition, some thermal models of the subducted slab suggest that temperatures generally are too low for dry melting of eclogite to occur (Anderson et al., 1978).

A second model for the origin of low-MgO HABs is by fractional crystallization from a more primitive mantle derived magma. It has proven difficult to produce the more MgO-poor HABs and BAs from MgO-rich HAB liquids by crystallization under dry conditions. The experimental mantle-saturated aluminous and magnesian liquids are close to transitional and crystallization at elevated pressure drives residual liquids to nepheline normative compositions. The resulting liquids are unlike low-MgO HAB and BA. At low pressures magnesian HAB crystallizes plagioclase +/- olivine and yields derivative liquids with low-Al₂O₃, again unlike low-MgO HABs and BAs (Grove et al., 1982; Bartels et al., 1991). The difficulty of producing low-MgO HAB has led to model 3, the interpretation that most such rocks form by accumulation of plagioclase phenocrysts (Crawford et al., 1987). An alternate fractionation model is that low-MgO HABs are derivative liquids from the crystallization of olivine and high calcium pyroxene from magnesian basalts (not high-alumina) found infrequently in some arcs (Kay et al., 1982; Nye and Reid, 1986; Ramsay et al., 1984). The model accounts for the continuous variations in major and some trace elements observed in rock suites (Gust and Perfit, 1987; Brophy, 1986). Experimental studies have failed, however, to produce olivine

on the liquidus of typical HABs with low (Baker and Eggler, 1983, 1987) or moderate-MgO contents (Johnston, 1986) under what have been taken as "reasonable" conditions (eg. anhydrous or nearly anhydrous). Furthermore, crystallization experiments on magnesian compositions (Gust and Perfit, 1987; Baker and Eggler, 1987) have failed to produce derivative liquids with the combined features of high-alumina (≥ 19 wt.%) and low-MgO (< 5 wt.%) so common in arc HABs and BAs.

Water in high-alumina basalt magmas

Most petrologists, geochemists, and volcanologists ascribe an important role to volatile components in the generation of arc magmas. The models that we feel are most plausible for generation of arc magmas involve release of water from subducted slab or hydrated mantle wedge which rises into the overlying hotter mantle and causes melting (Green and Ringwood, 1968; Tatsumi et al., 1983). The question is, how much water is in these melts? Several experimental studies have attempted to estimate the water contents of arc andesites and dacites. These include Eggler (1972), Eggler and Burnham (1973), Ritchey (1980), Rutherford et al. (1985), and Mertzbacher and Eggler (1984). The common conclusion is that andesites have low water contents (2-4 wt.% H₂O). An often repeated argument is that since andesites are known for a variety of reasons to have low water contents, then HABs must contain the same or even less water (Marsh, 1976, 1982; Baker

and Egglar, 1983; Johnston, 1986). The argument assumes, first, that andesites are produced primarily by closed-system crystallization differentiation from HAB. More important, it also assumes that the phenocrysts in both andesites and HABs grew at other than low pressures, and can be used to infer deep petrogenetic processes and conditions. The common disequilibrium textures and compositions of phenocrysts in andesites leads us to question the first assumption. The second assumption is considered near the end of this text.

In the following discussion we will assemble evidence that suggests that many HAB and BA magmas contain several or more weight percent of water. Many may be water-saturated magmas at moderate (1-3 kb) pressures. Evidence includes the presence of surprisingly calcium-rich plagioclase phenocrysts, such as $>An^{90}$ at the Cold Bay center of the Aleutians (Brophy, 1986) and $>An^{95}$ at the Taga volcano, Japan (Kuno, 1950). Hornblende-bearing cumulate inclusions have been reported from the Lesser Antilles (Arculus and Wills, 1980) and the Aleutians (Conrad and Kay, 1984). The inclusions consist of various proportions of olivine, aluminous salite, calcic plagioclase ($> An^{90}$), and both cumulus and intercumulus hornblende. Intercumulus HAB and BA glass survives in some inclusions (Arculus and Wills, 1980). Hornblende has been erupted as rare phenocrysts coexisting with calcic plagioclase, salitic pyroxene +/- olivine in HABs and BAs in Central America (Rose et al., 1978; Peterson and Rose, 1985; Rose, 1987) and the Aleutians (Kay and Kay, 1985), and in the

weakly-alkalic HAB of Bogoslof Island also in the Aleutians (Byers, 1959, 1961; Arculus et al., 1977). Finally, water-bearing HAB and BA glass inclusions are present in phenocrysts from lavas and scoria of the circum-pacific volcanic arcs and the Carribean (Anderson, 1973, 1974, 1979, 1982; Johnston, 1978; Rose et al., 1978; Devine and Sigurdsson, 1983).

Representative analyses of low-MgO HABs and BAs and comparable intercumulus liquids, glass inclusions, and groundmasses are presented in table 1.

Eruptive styles also suggest high volatile contents. Many HABs and BAs are erupted as scoria, and block and ash flows, as well as lavas. The pyroclastic deposits and flows make up mafic to intermediate stratovolcanos such as the familiar Fuji in Japan (Aramaki and Ui, 1978). Volatile effervescence powers the pyroclastic basalt and basaltic andesite eruptions. In light of the evidence above, the likely volatile is water.

The aluminous mafic intrusive rocks of continental margin batholiths show some of the clearest evidence for high magmatic water contents. The evidence includes, again, very calcium-rich plagioclase and early crystallization of hornblende in many HAB dikes and sills. Hornblende-plagioclase pegmatites are common. Tiny miarolytic cavities can be found in almost any handsample of mafic intrusive rock from some intrusive complexes. Examples of hydrous mafic intrusives can be found in the Sierra Nevada, California (Sisson and Grove, 1991), the Adamello Massif, Italy (Ulmer et al., 1983; Blundy and Sparks, 1990-submitted), the Peninsular

Ranges batholith, southern California and Mexico (Walawender, 1976; Walawender and Smith, 1980; Smith et al., 1983), the Tertiary plutons of Washington State (C. A. Hopson, pers. comm.), and the Coastal batholith of Peru (Pitcher et al., 1985).

The evidence, summarized above, for high magmatic water contents has convinced us that water-saturated experiments can provide information useful in understanding the petrogenesis of HAB and BA magmas. Additional justification for water-saturated experiments are: (1) that they provide an absolute limit on the extent water can modify phase relations for a given pressure and bulk composition. (2) Stolper (1982) and coworkers have shown that above ~4 wt.% dissolved H_2O , additional water dissolves in a silicate melt chiefly as undissociated molecular H_2O . We interpret this as evidence that the saturated (~6 wt.% H_2O) phase relations are close to those at intermediate water contents. Mixed volatile experiments support this inference (Eggler and Burnham, 1973; Rutherford et al., 1985). (3) The presence of miarolytic cavities in mafic intrusive rocks establishes that some aluminous arc magmas reach volatile saturation at depth. Finally, (4) for technical reasons saturated experiments, under the conditions of high temperature at the pressure reported here, can be conducted with much greater precision than either vapor-undersaturated or mixed volatile experiments.

EXPERIMENTAL METHODS

Starting materials

Two types of starting materials were most commonly employed. The first consisted of powdered natural igneous rock plus added water. The second consisted of a mixture of natural rock with powdered An⁸⁰ plagioclase from the Stillwater Igneous Complex, Montana, in proportions of 85wt.% rock-15wt.% plagioclase, plus added water. Natural aphyric HABs with high (79-35g) to intermediate MgO contents (82-62, 82-66) were collected from the Giant Crater-Chimney Crater lava flow system at Medicine Lake volcano, CA. The HAB 79-35g has a composition very similar to the Warner basalt used by Yoder and Tilley (1962) in their study of basalt melting. The phase relations of 79-35g at low and high pressures, anhydrous, are reported by Grove et al. (1982) and Bartels et al. (1991). Natural aluminous hornblende gabbro (87S35A) and hornblende diorite (85S52B), with compositions equivalent to low-MgO HAB and BA, were collected from quenched sills and dikes of the mafic intrusive complex at Onion Valley in the Sierra Nevada batholith, CA. The intrusive rock samples have higher alkali and lower magnesia contents relative to the volcanic HAB samples. Experiments addressing hornblende stability used mixtures of basalt sample 82-66 and albite or sodium hydroxide. Experiments were also performed in the simple system Forsterite-Diopside-Anorthite-H₂O and used a finely-

powdered mix of reagent grade oxides and glass prepared from oxides. Rock, plagioclase, and mix compositions are presented in table 2.

Experimental procedures

Synthesis experiments were conducted water-saturated at 2 kb in a TZM (titanium-zirconium-molybdenum) cold-seal pressure vessel using Au inner and outer sample capsules. Fugacity of oxygen was buffered by a solid Ni-NiO assemblage. Most experiments were hotter than the Au-Ni melting point minimum (945-955 °C at 1 atm, Hansen, 1958) and the buffer was isolated from contact with Au by containment in one or more unsealed Pt capsules. The inner capsule holding the sample was twisted and crimped closed, but was not welded, to assure that the oxygen buffer and the sample were in contact with the same aqueous fluid.

Experimental temperatures were measured with Pt-Pt₉₀Rh₁₀ thermocouples positioned in a well on the exterior of the pressure vessel. Thermocouples were calibrated by comparison to a reference thermocouple calibrated to the melting points of NaCl, Au, and Pd on the IPTS (1968) scale. The difference between well temperature and sample temperature was calibrated numerous times, and reported experimental temperatures are precise to ± 7 °C. Pressure was monitored with a Heise gauge and controlled to within 30 bars of the reported pressure. A pressure medium of mixed Ar and methane, in

proportions 2000psi:35psi respectively, reduced diffusive transport of hydrogen through the Au outer capsule.

The pressure vessel was positioned vertically in a Deltech DT31VT resistance furnace, held at pressure and temperature for the experiment, and then quenched. Experiments were begun by heating 10-25 °C above the desired temperature for 1 hour to aid in purging the sample of refractory crystals. Temperature was then reduced over 1-2 hours to the intended level and held for the duration of the experiment. Early experiments (not reported) were quenched by blowing compressed air over the hot vessel. Quench crystallization was common and severe. Timed measurements with an internal thermocouple show that 2-2.25 min are required to cool the sample from 950 to 700 °C with compressed air. Later experiments were quenched by extracting the vessel from the furnace, immediately inverting it, and rapping on the vessel with a heavy object such as a pipe wrench. The sample capsule would fall from the hot end of the vessel to the water-cooled pressure seal and quench immediately with no growth of quench crystals.

Following quenching, the capsules were weighed to measure volatile gain or loss, punctured to verify the presence of water, and buffer capsules were examined for the presence of both Ni (magnetic) and NiO (colored) and to see if the sample had leaked into contact with the Pt buffer capsule.

Experiments which passed these tests and did not grow abundant quench crystals (overall < 30% of all experiments passed) were

considered successful and were mounted for electron probe analysis.

Experimental duration

Duration of experiments was limited by diffusive loss of hydrogen through the Au capsule wall (0.010" thick) to the pressure medium and from the pressure medium out of the vessel to the atmosphere. Loss of hydrogen leads to decreased capsule weight, oxidation of the buffer and, if severe, dessication of the sample. Loss from the Au capsule is through grain boundary diffusion. For unknown reasons, some lengths of Au tubing readily recrystallized and volatile exchange took place rapidly. Other "good" lengths of tubing took much longer to recrystallize and could be used for much longer experiments. Experiments at 1050 °C could be continued for between 8 and 24 hrs. Experiments at 950 °C could be continued for between 72 and 96 hrs.

Analytical techniques

Glass and minerals were analyzed with the MIT four spectrometer JEOL-733 electron microprobe. This instrument uses automatic data reduction with Bence and Albee (1968) matrix corrections with modifications of Albee and Ray (1970). Analytical conditions were varied to avoid Na migration during glass analysis. We settled on a 15 kV accelerating voltage,

10 nA beam current, a 30 micron beam diameter, and measured Na first for 5 seconds. Other elements were subsequently measured for up to 40 seconds depending on abundance. We find that these conditions are too harsh to prevent sodium migration in wet rhyolite glasses, but are adequate for the basalt and andesite glasses produced in this study. Analyses of crystal margins were as above, but the beam was focused to a diameter of 2 microns.

Analytical precision is estimated by replicate measurements of andesite glass from a 1-atm anhydrous experiment (38b-129) of Juster et al. (1989). One standard deviation of replicate glass analyses expressed as relative percent of oxides are SiO₂:0.4%, Al₂O₃:0.9%, CaO:1.5%, MgO:1.5%, FeO:1.4%, MnO:8.1%, P₂O₅:5.6%, Na₂O:1.9%, K₂O:1.1%, based on 121 individual measurements over 13 analytical sessions. The mean sum of analyses of the anhydrous glass is 99.5%.

RESULTS

Preliminary considerations

The experimental conditions and resulting phases and phase proportions are summarized in table 3. Average phase compositions with standard deviations are reported in table 4. Phase proportions are calculated by mass balancing bulk compositions (table 2) with the experimental phase compositions using a least squares technique (Juster et al.,

1989, equation 1). Iron-loss from the samples to Au capsules can be estimated from the mass balance calculations. Results show apparent deficits and excesses ranging from -6.1 to +3.4 % (relative) of the total iron (as FeO) originally present. The similar and small magnitude of apparent deficits and excesses suggests that the amount of Fe lost to the Au capsules is low; certainly less than 10% of the total FeO present has been lost to the Au capsule. This is confirmed by electron probe analysis of the inner walls of used Au sample capsules. Iron concentrations in used Au capsules are below the detection limit of the electron probe even at high beam currents (200 nanoamps, detection limit = 500ppm Fe).

Examples of experiments in which oxygen buffers failed either by oxidation or reduction are presented in tables 5 and 6. The results are included as illustrations of the influence of oxygen fugacity on liquid lines of descent of wet magmas.

Results of additional experiments on a granodiorite from the Sierra Nevada batholith are presented in appendix 1. Phase compositions are used in the interpretation of mineral-liquid exchange reactions reported below.

Equilibrium

Equilibrium can be assessed with respect to phase appearance, composition, and morphology. All of the experiments in this study are direct syntheses. Phase appearance sequences and temperatures have not been reversed. However, we conclude

that the experiments approached equilibrium sufficiently that they can be used to understand aspects of the petrogenesis of HABs and BAs. First, we have succeeded in maintaining constant sample bulk composition with little or no loss of iron to metal capsules (see above). This contrasts with previous hydrous basalt melting experiments that have been performed in AgPd or Pt capsules. Baker and Eggler (1987) have documented that 14-83% (ave.=44%) of the iron was lost from samples that they melted in wustite-treated Ag₅₀Pd₅₀ or Pt, Helz (1973) calculates up to 37% iron-loss from basalt to Ag₄₀Pd₆₀, and Stern and Wyllie (1975) demonstrate that 85% of the iron was lost in 3 hours from samples melted in Pt capsules. In the absence of documentation we must assume comparable iron-loss in the experiments of Spulber and Rutherford (1983) performed in untreated Ag₇₀Pd₃₀, and the classic experiments of Yoder and Tilley (1962) run in Pt. None of the preceding experiments can have reached equilibrium unless and until loss of iron ceased and the bulk composition of the sample stabilized. The large iron-losses in previous hydrous basalt melting studies contrasts with minimal iron-losses in the present study. Low or minimal iron-losses provide a greater opportunity for a close approach to equilibrium. The cost of performing experiments in Au, and preventing iron-loss, has been that we are restricted to temperatures below the melting point of Au (1064 °C at 1 atm). As will be shown below, this is not a serious limitation under water-rich conditions.

Replicate glass analyses show that experimental liquids were homogeneous, a prerequisite for equilibrium. Experimental minerals are euhedral and equant or tabular and individual crystals commonly reach sizes of several hundred microns across. Experiments were of sufficient duration that skeletal crystals were not produced. The crystals are largely newly-grown material and, unlike 1-atm experiments (Juster et al., 1989), the quantities of unreacted starting materials are minimal to completely absent. The average compositions of crystal margins, discussed below, show regular and consistent partitioning of certain elements between minerals and liquids independent of whether the mineral in question was present in the starting material. Mineral-liquid exchange K_D s for olivine, plagioclase, hornblende, and high-Ca pyroxene, discussed below, are as expected from other phase equilibrium studies and natural samples, additional evidence for a close approach to equilibrium.

Nevertheless, individual mineral-rim analyses vary outside of the practical reproducibility established above from glass analyses. Back-scattered electron imaging, in which brightness corresponds to average atomic number, shows that most crystals are weakly zoned, even along their rims. Sector zoning is common in the experimental clinopyroxenes, and has been found in some of the experimental hornblendes. The presence of sector zoning and the albeit small heterogeneities in compositions of crystal rims are inconsistent with the complete attainment of equilibrium. Experiments of far

greater duration than are presently feasible would be required to produce true equilibrium phase compositions. The shortcomings of slightly heterogeneous solid phases are likely to have been present in all previous studies of the wet melting of basalts and andesites, and were compounded in those studies by the additional problem of severe iron-loss. Heterogeneous solid phases may have gone unrecognized in those studies due to less precise analytical and imaging equipment than is currently available, or heterogeneous minerals may simply have been ignored. In the present study, the consistent and reproducible phase appearances and mineral-liquid exchange K_D s suggest that the deviations from equilibrium are not large, and we conclude that the experiments are sufficiently close to equilibrium that they can be used in the interpretation of natural HAB and BA magmas.

Phase appearances in high-alumina basalts

In the following sections we first describe the phase appearance sequences in the samples investigated and the general compositions of the liquids. This is followed by descriptions of the experimental mineral phases and mineral-liquid exchange reactions, expressed as exchange K_D s, referred to above.

The primitive HAB, 79-35g, consists of >90 wt.% liquid plus small amounts of olivine ($\text{Fo}^{86.5}$) and a Cr-Al-Mg spinel at

1050 °C (all temperatures +/-7 °C). A repeat experiment at 1050 °C produced ~85% liquid, plus olivine (oliv), high calcium pyroxene (high-Ca pyx), calcic plagioclase (An^{93}) (Ca-plag), and a Cr-Al-Mg spinel. The liquid corresponds to HAB with an intermediate MgO content (49.4% SiO₂, 19.2% Al₂O₃, 6.58% MgO, normalized to 100% anhydrous). At lower temperatures 79-35g continues to crystallize oliv, high-Ca pyx, Ca-plag, and an increasingly Fe-Ti rich spinel. By 1000 °C, the lowest temperature investigated, the sample is 50% crystalline and the liquid composition resembles a low-MgO high-alumina BA (52.5% SiO₂, 19.2% Al₂O₃, 4.99% MgO).

The two lower-MgO HABs, 82-66 and 82-62, also crystallize oliv, high-Ca pyx, and Ca-plag but a spinel mineral does not form until temperatures below 1000 °C. Hornblende (hbl) appears by 965 °C in sample 82-66 coexisting with oliv, Ca-plag, high-Ca pyx, and an Fe-Ti spinel. Liquid ranges from low-MgO HAB (51.5% SiO₂, 19.2% Al₂O₃, 4.98% MgO) to aluminous andesite (59.1% SiO₂, 19.1% Al₂O₃, 3.25% MgO).

Phase appearances in hornblende gabbro and diorite

Crystallization of the hornblende gabbro and diorite differ from the HABs in several respects. First, liquids with comparable silica contents exist at lower temperatures in the gabbro and diorite. Second, neither the hornblende gabbro nor the diorite crystallize pyroxene. Third, the gabbro and

diorite produce hornblende from liquids with low silica contents, equivalent to low-MgO HAB or BA.

Hornblende gabbro 87S35A saturates nearly simultaneously with oliv, hbl, and Ca-plag between 985 and 970 °C. The liquid at 970 °C is low-MgO high-alumina BA (52.1% SiO₂, 19.3% Al₂O₃, and 4.14% MgO). Magnetite appears at 965 °C, and oliv is lost by 950 °C. Apatite appears between 965 and 950 °C and persists to lower temperatures. By 925 °C, the lowest temperature investigated, the sample is 47% crystalline and the liquid corresponds to corundum-normative aluminous andesite (60.0% SiO₂, 18.9% Al₂O₃, 1.76% MgO). This is the only corundum-normative liquid produced in this study.

Hornblende diorite 85S52B crystallizes oliv from a temperature higher than 1024 °C down to 968 °C. Hornblende joins oliv between 998 and 968 °C. Plagioclase did not crystallize over the temperature range investigated in this composition under water-saturated conditions. Plagioclase (An⁸⁰) was mixed with 85S52B in proportions 85 wt.% rock, 15 wt.% plag to force plag saturation. The plag-added composition grows plag between 965 and 975 °C. Olivine and hbl appear near 965 °C and coexist with Ca-plag and low-MgO high-alumina BA liquid (53.7% SiO₂, 20.0% Al₂O₃, 3.75% MgO). Olivine, hbl and plag coexist through 943 °C, the lowest temperature investigated. By 943 °C the sample is 28% crystalline, and the liquid corresponds to aluminous andesite (57.1% SiO₂, 19.1% Al₂O₃, 2.80% MgO).

Mineralogy and mineral-liquid exchange reactions: pyroxene

The experimental pyroxenes are high calcium with moderate to high alumina contents (2.9-7.9 wt.%). The pyroxenes project as diopsides and salites in a Ca-Mg-Fe discriminant diagram (figure 1). Pyroxenes do not trend toward augite with decreasing temperature, consistent with the absence of a coexisting low-calcium pyroxene.

Pyroxene rim compositions (table 4) are somewhat heterogeneous and sector zoned grains are common. Chemical differences between growth sectors are mimicked by irregularly zoned crystals and small nearly homogeneous grains. Aluminous sectors and grains are more iron and titanium-rich. Low-alumina sectors and grains are more magnesian. Crystals are elongated prisms and the magnesian low-alumina sectors extend in the directions of elongation. Shimizu (1981) describes the same correspondence of growth sectors, crystal habit, and composition in natural igneous clinopyroxene with sector zoning.

Iron and magnesium are systematically partitioned between high-Ca pyx and liquid (figure 2). Moderate alumina crystals and sectors have an exchange K_D , defined as $(Fe/Mg)_{pyx}/(Fe/Mg)_{liq}$, of 0.23. Grove and Bryan (1983) determined the same K_D value (0.23) in 1 atm pressure anhydrous experiments on mid-ocean ridge basalts. Partitioning is more irregular between liquid and higher alumina crystals and sectors, and the crystals are more iron-

rich. The exchange K_D for the more aluminous sectors and grains is ~ 0.27 , though poorly defined.

Olivine

Iron and magnesium also show regular partitioning between oliv and liquid (figure 3). Most oliv-liquid pairs have an exchange K_D , defined as $(\text{Fe/Mg})_{\text{oliv}}/(\text{Fe/Mg})_{\text{liq}}$, near 0.29. This is within error of the K_D value of 0.30 reported by Roedder and Emslie (1970) and confirmed by numerous subsequent studies. Some of the higher temperature experiments produced oliv-liquid pairs with apparent exchange K_D s near 0.25. Liquid compositions have not been adjusted for ferric iron. Apportioning some of the iron as ferric would raise the apparent K_D s. Analytical error likely also contributes to the low K_D values in the high temperature experiments. Olivine is present in those experiments as tiny equant grains that polish with positive relief relative to glass. The relief makes crystal rims difficult to analyze, and analyses are biased toward core compositions. The cores are slightly more magnesian than the rims and this leads to anomalously low apparent K_D s.

Plagioclase

The relation between compositions of plag and coexisting liquid is illustrated in figure 4a. The ratio Ca/Na in plag

varies linearly with the ratio Ca/Na in liquid. We express the relation between plag and liquid by an exchange K_D defined as $(Ca/Na)_{\text{plag}}/(Ca/Na)_{\text{liq}}$. The exchange K_D has a value of ~5.5 for water-saturated liquids at 2 kb pressure. We include two plag-liquid pairs produced in experiments on a granodiorite (appendix 1), and find the exchange K_D to hold for liquids ranging from HAB to low-silica rhyolite. Figure 4a also shows results for experiments on HABs with 2 wt.% H_2O at 2 and 5 kb pressure (Baker and Eggler, 1987). Exchange K_D s with 2 wt.% water are far lower than those at water saturation, and no distinction is found between 2 and 5-kb results.

The water-saturated exchange K_D is also higher than is found in dry experiments at low or high pressures (figure 4b). Only one of fifty exchange K_D s determined from 8 to 12 kb pressure has a value above 2.0. Data at higher pressures are scarce, but all values lie below 2.5 at pressures as high as 20 kb.

Spinel minerals

Experimental spinel ranges from Mg-Al-Cr rich to magnetite. Compositions of spinel crystal rims are illustrated in figure 5. There is an apparent gap in the experimental spinel compositions. No spinels lie with $0.20 < Fe^{3+}/(Fe^{3+}+Al+Cr) < 50$. This is likely an artifact of the spacing of experimental temperatures. Continuous zonation from Mg-Al-Cr cores to aluminous magnetite rims is found in the 1035 and 1025 °C

experiments on sample 79-35g. Experiments between 1050 and 1035 °C would yield spinels with rim compositions within the apparent gap.

Amphibole

Experimental amphiboles are calcic and aluminous with near fully occupied A-sites. They can be classified as pargasites or pargasitic hornblendes (or ferroan varieties) (Hawthorne (1981) figure 2). In the absence of ferric iron determinations such classifications are suspect and the amphiboles are best described simply as hornblende.

Helz (1981) has emphasized that the tetrahedral Al content of hbl correlates with temperature. Higher temperature igneous hbl has a higher ratio of aluminum to silicon (Al/Si) than lower temperature hbl, all else being equal. This feature has been used by Blundy and Holland (1990) to formulate a geothermometer for hbl coexisting with plag and quartz.

Al/Si in hbl is linearly correlated with Al/Si in liquid (figure 6a). An exchange K_D , defined as $(Al/Si)_{hbl}/(Al/Si)_{liq}$, of ~0.94 holds for liquids ranging from high-alumina BA to high-silica rhyolite. Figure 6a includes the two granodiorite experiments (appendix 1) as well as three natural hbl-liquid pairs (appendix 2). Two are natural HAB and BA with hbl phenocrysts provided by W. Rose. The third is a crystal-rich rhyodacite with phenocrysts of hbl in high-

silica rhyolite glass from Inyo Craters, Ca. Hornblende-glass pairs have also been measured for samples from Mount Saint Helens, Crater Lake, and the Fish Canyon Tuff. Al/Si partitioning is close to that shown in figure 6a, but is not utilized because hbl phenocrysts from these localities have heterogeneous rim compositions.

Experimental hbl-glass pairs compiled from the literature are presented in figure 6b. The pairs show a strong positive correlation between Al/Si in hbl and Al/Si in glass, albeit with substantial scatter. An average K_D for the literature data is ~ 1 , close to that determined in this study.

Exchange of iron and magnesium between hbl and liquid is illustrated in figure 7. An exchange K_D ($\text{Fe/Mg}_{\text{hbl}}/\text{Fe/Mg}_{\text{liq}}$) between 0.30 and 0.38 (most are 0.35-0.38) holds for liquids ranging from high-alumina BA to aluminous andesite. Apparent K_D drops markedly for more siliceous liquids. The drop in K_D probably results from high ferric/ferrous iron in the siliceous liquids.

Liquid lines of descent, multiple saturation boundaries, and crystallizing phase proportions

Experimental liquids produced in HABs and the hornblende gabbro define crystallization paths similar to those found in many calc-alkaline suites. This is illustrated with the AFM diagram of Wager and Deer (1939) and the Miyashiro (1974) discriminant diagram of FeO^*/MgO vs SiO_2 (figures 8 and 9).

Crystallization of ferromagnesian silicates and calcic plagioclase enriches the liquids in silica and alkalis. Ferromagnesian silicates crystallize in high proportions relative to plagioclase, thus preventing absolute iron enrichment. Magnetite crystallization further moderates the abundance of iron, preventing strong increases in FeO^*/MgO . Exceptions are the hornblende diorite and diorite + plag mix which do not crystallize magnetite. Their successive plagioclase-saturated liquids show continuously increasing FeO^*/MgO . Otherwise, the liquids evolve similar to the other samples.

Experiments in which oxygen buffers failed illustrate the influence of $f\text{O}_2$ on liquid composition (figure 8). An experiment with $f\text{O}_2 < \text{Ni-NiO}$ has higher FeO^* relative to MgO compared to trends defined by appropriately buffered experiments. Likewise, an experiment with $f\text{O}_2 > \text{Ni-NiO}$ lies at lower FeO^* relative to MgO . Variations in $f\text{O}_2$ control the amount of magnetite that crystallizes, thus modifying the relative abundances of FeO^* and MgO in the liquid.

Liquid lines of descent are simplified by recasting liquid compositions into mineral components and projecting into psuedo-ternary diagrams. Figures 10a and 10b show the recast compositions of liquids produced in experiments on the HABS projected into OLIV (forsterite + fayalite) - CPX (diopside + hedenbergite) - QTZ and CPX - PLAG (anorthite + albite) - QTZ psuedo-ternarys using the projection scheme of Tormey et al. (1987). The ternary diagrams are projections through PLAG and

end-member magnetite, and OLIV and end-member magnetite respectively.

Liquids saturated with oliv, Ca-plag, and high-Ca pyx (+/- a spinel mineral or hbl) define a multiple saturation boundary extending from the OLIV - CPX - PLAG plane toward the QTZ - PLAG join. The multiple saturation boundary is straight in projection from PLAG. Crystallizing proportions of oliv, high-Ca pyx, and Ca-plag are nearly constant in the three bulk compositions. High-Ca pyx, Ca-plag, oliv, and magnetite crystallize in weight proportions 0.26:0.57:0.125:0.045 (all +/-0.005) from 1035-1000 °C in sample 79-35g. Sample 82-66 crystallizes these phases in weight proportions 0.25:0.58:0.138:0.032 from 1012-975 °C. Cotectic cumulates would contain cumulus minerals in these weight proportions.

With the appearance of hbl, contents of other silicates (solid and liquid) decrease (table 3). This suggests that hbl forms through reaction with liquid and the other solid phases. The chemography of the hbl-in reaction is best illustrated by modifying the normal projection scheme so as to calculate a plagioclase component with composition close to that of the saturating mineral. This is illustrated in figure 11b, in which multiple saturation boundaries and phase compositions have been projected from An⁹⁰. Residual albite has been added to the QTZ apex. Hornblende lies within the chemographic volume defined by the projected coexisting phases, and therefore the hbl-in reaction boundary is distributary. Note that while the diagram approximates the coexistence of liquid,

hbl, Ca-plag, high-Ca pyx, oliv, magnetite, and vapor (seven phases) as a psuedo-invariant point, it is more properly represented as a volume.

Two hbl-saturated boundaries should exit the distributary reaction boundary (figure 11a,b). The oliv + hbl + plag boundary has been drawn to be consistent with results presented below. The high-Ca pyx + plag + hbl boundary is schematic.

Experiments on hornblende gabbro and hornblende diorite plus An⁸⁰ produce liquids saturated with oliv, hbl, and Ca-plag (+/- magnetite). These liquids define a different multiple saturation boundary in the psuedo-ternary diagrams (figure 10c,d). The hbl liquidus volume is expanded relative to that found in the HAB experiments, and spans the entire psuedo-quaternary space limited by OLIV, CPX, PLAG, and QTZ. The trajectory of the oliv - hbl - Ca-plag multiple saturation boundary shows that it is a reaction boundary along which liquid and oliv are consumed and hbl is precipitated (figure 10c). Natural oliv-bearing hornblendite cumulates from the source area of samples 87S35A and 85S52B contain embayed olivine encased in coarse hornblende: graphic evidence of the experimentally determined reaction. Liquids that have passed beyond the reaction boundary crystallize hbl, Ca-plag, and magnetite (+/- apatite). Sample 87S35A crystallizes plag and hbl in a mass ratio of 0.8-0.9 (plag/hbl), as shown by mass balance calculations.

Experiments addressing hornblende stability

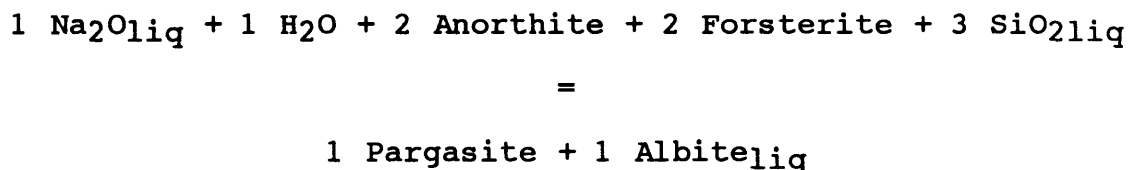
Exploratory experiments have been performed to investigate some controls on hbl stability in water-saturated liquids. Hornblende gabbro sample 87S35A has high-alumina and a basaltic silica content (table 2). It crystallizes hbl as a liquidus mineral. Volcanic sample 82-66 also has high-alumina and a basaltic silica content but has lower Na₂O and higher MgO than 87S35A. It does not crystallize hbl until well below the liquidus, once the liquid has reached an andesitic composition.

We examined the influence of bulk sodium content on hbl stability by artificially raising the sodium content of 82-66 to equal that of 87S35A (as analyzed by electron probe of wholly-fused samples). Sodium was first added by mixing powdered Amelia albite to 82-66. The mix was run at 965 °C, the same temperature at which pure 82-66 (+H₂O) produced 26 wt.% hbl. The albite-added mix produced liquid plus oliv, high-Ca pyx, Ca-plag, and titanomagnetite. No hbl grew from the albite-added mix. Another mix was prepared, this time by adding sodium to 82-66 as NaOH so that the bulk sodium content equaled that of 87S35A. This composition run at 965 °C produced liquid plus high-Ca pyx, titanomagnetite, and abundant hbl. Neither oliv nor plag grew from the NaOH-added composition, and the liquid was nepheline-normative. The NaOH-added composition was also run at 985 °C and produced liquid, hbl, titanomagnetite, high-Ca pyx, and oliv. The

liquid has 54.8% SiO₂ (calculated anhydrous) and is nepheline-normative. One final mix was made by blending equal parts of the NaOH-added mix with pure 82-66. This composition at 965 °C produced the same solid phases as pure 82-66, but the liquid had a lower silica content (55.4 vs 59.1 wt.%)

The NaOH-added experiments establish that, all other factors being equal, higher sodium stabilizes hbl to higher temperatures and allows hbl to grow from liquids of lower silica contents. Increased sodium expands the hbl liquidus volume toward and through the critical plane of silica undersaturation (figure 12). Thus, wet high-sodium sub-alkaline or alkaline basalt liquids can grow hbl whereas equally wet low-sodium basalt liquids do not. These results are in complete agreement with the simple system experiments of Cawthorn (1976).

Differences between the albite-added and NaOH-added experiments can be reconciled by the model reaction:



Addition of Na₂O drives the reaction to the right, producing hbl at the expense of oliv, Ca-plag, and silica. Addition of albite has the opposite effect, consuming hbl.

Simple system experiments

Most of the experiments on HABs produced liquid coexisting with vapor, high-Ca pyx, Ca-plag, and oliv (+/-a spinel). Experiments were performed in the psuedo-quaternary simple system Forsterite-Diopside-Anorthite-H₂O to locate the water-saturated piercing point at which liquid coexists with vapor, diopside solid solution, forsterite, and anorthite. At 2 kb, natural liquids saturated with oliv, high-Ca pyx, plag, and aqueous vapor will lie at lower temperatures than that of the piercing point.

Piercing composition was estimated from the crystallizing proportions of oliv, high-Ca pyx, and Ca-plag in the HAB experiments. A mix was prepared by combining synthetic forsterite, anorthite, and diopside in the observed proportions. A piercing point temperature was estimated from a simple algorithm relating liquid composition to temperature, discussed below. Experiments were run at 2 kb in Pt capsules with excess water and quenched by the rapid technique developed for the natural samples.

An initial experiment at 1132 °C produced liquid, forsterite solid solution (ss), anorthite, and vapor. A second experiment 12 ° cooler (1120 °C) was largely crystalline, but contained small pools of liquid located next to diopside_{ss}, forsterite_{ss}, anorthite, and vapor. The liquid is very slightly enriched in silica relative to the forsterite-diopside-anorthite plane while the pyroxene is enriched in Ca-

tschermak's component. The true piercing point should lie a few degrees hotter than 1120 °C, a difference below our ability to control. The temperature and composition of the near-piercing point liquid are used below to improve the algorithm relating liquid composition to temperature.

GEOOTHERMOMETRY

A principle difference between a water-rich and a dry silicate liquid saturated with the same solid phases is that the wet magma exists at a far lower temperature. A dry HAB liquid in equilibrium with oliv, high-Ca pyx, and plag might exist at ~1170 °C at low to moderate pressures (Grove et al., 1982; Bartels et al., 1991; Gust and Perfit, 1987). Basaltic liquid saturated with water and the same solid phases is cooler by as much as 150 °C at 2 kb. In the following discussion, we want to apply the results of our experiments to the interpretation of HAB and BA magmas. Therefore, we have derived two empirical geothermometers that can be used to estimate the temperatures of HABs and BAs. Successful development of both geothermometers has required estimates of the water content of experimental liquids. Most of our experimental basaltic and andesitic glasses have summation deficits of ~6 %, rounded to the nearest per cent, and we take this as their water content estimated to the nearest per cent. Baker and Eggler (1983) also estimate a 2-kb saturated water content of 6 wt.% in low-MgO HAB liquid. Hydrous rhyolite glasses reported in appendix

1 have summation deficits of 8-8.7 %, higher than the expected solubility of water in rhyolite melt at 2 kb (~7 wt.%, Burnham and Jahns, 1962; Burnham, 1979). We use 7 wt.% as the water content of the hydrous rhyolite glasses.

Multiply-saturated liquids

Helz and Thornber (1987) and Grove and Juster (1990) have shown that liquid composition can be used as a purely empirical geothermometer, so long as appropriate restrictions are made on bulk composition and saturating phases. We have calibrated a geothermometer for liquids containing plagioclase and at least one calcium-rich ferromagnesian silicate, but no low-calcium pyroxene, at low to moderate pressures.

Calibration points are 24 hydrous and 27 dry experiments.

Data include experiments on natural or near natural compositions reported in tables 4, 6, and appendix 1. Wet simple system constraints are the forsterite-diopside-anorthite-H₂O (near) piercing point at 2 kb (table 4) and the diopside-anorthite-H₂O piercing point at 5 kb (Yoder, 1965), assumed to contain 8.5 wt.% H₂O and corrected to the IPTS68 temperature scale.

Dry 1-atm liquids have been restricted to non-alkalic compositions that coexist with plag, oliv, and a high-Ca pyx but no low-Ca pyx (in keeping with the wet experiments). This restriction has the effect of excluding most liquids with SiO₂ > 55 wt.%; we recommend that the geothermometer not be used

for more silica-rich compositions. Data sources are Grove et al. (1982), Grove and Bryan (1983), Grove et al. (1990), Tormey et al. (1987), Walker et al. (1979), and Baker and Eggler (1987). Two experiments of Tormey et al. (1987) had large differences between observed and predicted temperatures, for unknown reasons, and were discarded. Dry simple system constraints are provided by the 1-atm forsterite-diopside-anorthite and forsterite-diopside-albite piercing points as reported by Presnall et al. (1978) and Schairer and Morimoto (1959) (corrected to IPTS68).

A simple empirical model relating liquid composition and temperature uses four liquid compositional parameters: molar $\text{Mg}/(\text{Mg}+\text{Fe})$ referred to as $\text{Mg}^\#$, $\text{wt.}\% (\text{Na}_2\text{O}+\text{K}_2\text{O})/(\text{Na}_2\text{O}+\text{K}_2\text{O}+\text{CaO})$ referred to as $\text{NaK}^\#$, $\text{wt.}\% \text{Al}_2\text{O}_3/\text{SiO}_2$, and $\text{wt.}\% \text{H}_2\text{O}$. Figure 13a shows the temperature recovery of the model:

$$T\text{ }^\circ\text{C} = 1023 - 31.6 * \text{H}_2\text{O} + 378 * (\text{Al}_2\text{O}_3/\text{SiO}_2) - 136.5 * \text{NaK}^\# + 130.8 * \text{Mg}^\#.$$

The adjusted r^2 for this fit is 0.994, and the expression recovers temperature with an average error of 7.0 $^\circ\text{C}$ for the wet data and 6.7 $^\circ\text{C}$ for the dry data.

It is desirable to assess the generality of the regression coefficients before applying the expression to samples other than those from which it was derived. This can be done, qualitatively, for the H_2O and $\text{NaK}^\#$ regression coefficients by comparison with simple systems. The forsterite-diopside-anorthite piercing point lies within a few degrees of 1120 $^\circ\text{C}$

at 2 kb pH_2O and the liquid contains ~6 wt.% H_2O . The dry 1-atm piercing point lies at 1274 °C. Results of Bartels et al. (1991) for high-MgO, low-alkali, high alumina basalt show that the onset of crystallization of olivine plus pyroxene plus plagioclase increases at ~11 °C/kb. Using this result, the dry forsterite-diopside-anorthite piercing point would lie near 1296 °C at 2 kb. The difference between the wet and estimated dry piercing points is -176 °C or -29 °C/(wt.% H_2O). This is close to the regressed value of -31.6 °C/(wt.% H_2O).

Burnham (1979, his figure 6) shows that the melting point depression of albite is close to linear with respect to dissolved H_2O at pressures ≤ 2 kb. Silver and Stolper (1984) present calculated isobaric T- H_2O sections for the system albite- H_2O . Their results also show near-linear melting point depression of albite with added H_2O . From this, we conclude that the functional form of the H_2O term (linear) is a good first order approximation for the melting point depression of natural magmas with added water up to moderate pressures. A more sophisticated and thermodynamically structured model of melting point depression for natural melts is desirable. However, the number of hydrous melting experiments on natural compositions in which iron-loss was minimal, the volatile phase was buffered, the experiment was rapidly-quenched, and all phases were characterized is so small that a more sophisticated treatment is not warranted.

Liquids show little variation in $\text{Al}_2\text{O}_3/\text{SiO}_2$ along the diopside-plagioclase cotectic in the system diopside-

anorthite-albite (Bowen, 1915; Kushiro, 1972). $\text{NaK}^\#$, however, ranges from 0 to 0.82. Linear regression of $\text{NaK}^\#$ against temperature (uncorrected to IPTS68) along the cotectic gives: $T\text{ }^\circ\text{C} = 1268 - 162 * \text{NaK}^\#$ ($r = -0.997$). The $\text{NaK}^\#$ coefficient derived for the largely natural compositions differs from the diopside-albite-anorthite value by $< 20\%$ relative. We take the agreement as encouraging considering the large differences between the natural and simple systems. There are no simple system results that can be used to independently evaluate the coefficients for the remaining terms.

Olivine-liquid

The distribution of magnesium between oliv and liquid can be used to calculate temperature (Roeder and Emslie, 1970; Roeder, 1974; Longhi et al., 1978; Ford et al., 1983). We follow the formulation of Longhi et al. (1978) and express the oliv-liquid distribution coefficient K^{Mg} as:

$$K^{\text{Mg}} = (X^{\text{Mg}}_{\text{ol}}) / ((X^{\text{Mg}}_{\text{L}})(X^{\text{Si}}_{\text{L}})^{0.5}),$$

where $X^{\text{Mg}}_{\text{ol}}$ is the cation mol fraction of Mg in the oliv, and X^{Mg}_{L} and X^{Si}_{L} are the mol fractions of MgO and SiO₂ in the liquid. A thermodynamically valid expression relating temperature to K^{Mg} should be of the form:

$$\text{Log}(K^{\text{Mg}}) = a * (1/T\text{ }^\circ\text{K}) + b.$$

The coefficient a and constant b are calibrated by linear regression of experimental data.

We use the experimental compositions reported in tables 4 and 6, plus coexisting plag-oliv-liquid dry 1-atm experiments reported in the literature, with preference for compositions also containing a high-Ca pyx, but no low-Ca pyx. Data sources are as above but did not include the forsterite-diopside-albite piercing point. The data were supplemented with 1-atm oliv + plag-saturated liquids from Bartels et al. (1991).

The choice of liquid components directly influences K^{Mg} . The most successful simple formulation for the data considered used single cation oxide components (ie. MgO , $PO_{2.5}$, $HO_{0.5}$, etc.) with the exception of the alkalis. Alkali components were calculated as alkali aluminates $NaAlO_2$ and $KAlO_2$. This choice of components was found to remove much of the effect of variable alkali content on K^{Mg} .

The coefficient and constant terms a and b were determined by linear regression of $\text{Log}(K^{Mg})$ against $1/(T \text{ } ^\circ K)$. Data lying outside of the 2sigma uncertainties of the regression were excluded and the regression was repeated. The final data set consists of 24 wet and 32 dry experiments giving:

$$\text{Log}(K^{Mg}) = 3886 * (1/T \text{ } ^\circ K) - 1.80.$$

The correlation coefficient (r) for the regression is 0.989 and the expression recovers temperature for wet and dry experiments used for calibration with an average error of 8.2 °C and 14.6 °C respectively (figure 13b). Residuals (observed-expected) show statistically significant correlations with liquid FeO and TiO₂ contents ($r = -.72, -0.67$ respectively). Predicted temperatures for FeO and TiO₂-rich liquids (eg. evolved tholeiites) are high relative to their true temperatures. We recommend that use of the oliv-liquid geothermometer calibrated herein be restricted to magmas with SiO₂ \leq 55 wt.% and TiO₂ $<$ 2 wt.%.

DISCUSSION

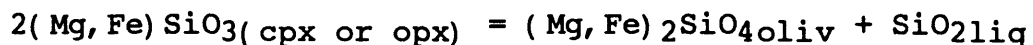
Effect of water on the position of multiple saturation boundaries

Yoder (1965) showed that addition of water to the system diopside-anorthite sharply expands the liquidus volume of diopside_{ss} and shrinks the liquidus volume of anorthite. Positions of the forsterite_{ss} + diopside_{ss} + anorthite piercing point with and without water are shown in the OLIV - CPX - PLAG ternary in figure 14. The shift in position of the piercing point with increased pH₂O reflects the effect discovered by Yoder (1965). The piercing point moves nearly parallel to the CPX - PLAG join, a result of expansion of the high-Ca pyx liquidus volume and contraction of the Ca-plag

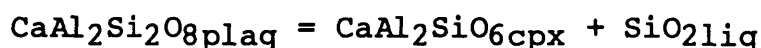
liquidus volume with increased pH_2O . A comparable shift away from CPX and toward PLAG (expansion of the high-Ca pyroxene liquidus volume vs the Ca-plag liquidus volume) with increased pH_2O is seen in natural compositions (figure 14).

Kushiro (1969) studied melting in the system forsterite-diopside-silica in the presence and absence of water. A major result of his research was to show that high pH_2O expands the liquidus volume of oliv at the expense of low-Ca pyx and to a lesser extent at the expense of high-Ca pyx. Some aspects of our experiments accord with Kushiro's findings but others do not. We find that the forsterite_{ss} + diopside_{ss} + anorthite piercing point shows little or no shift away from OLIV with increased pH_2O up to 2 kb (figure 14). We interpret this as evidence either that pH_2O must be greater than 2 kb to stabilize forsterite_{ss} at the expense of diopside_{ss}, or that the high-alumina in wet, plag-saturated liquids stabilizes high-Ca pyroxene by formation of Ca-tschermak's molecule. Natural compositions show a modest expansion of the oliv liquidus volume relative to that of high-Ca pyx with increased pH_2O . The more prominent result of Kushiro (1969), that H_2O destabilizes low-Ca pyx, is seen in the 2-kb water-saturated experiments on natural HABs. Such HABs crystallize low-Ca pyx in 1-atm anhydrous experiments (Grove et al., 1982, and unpublished data), whereas low-Ca pyx does not crystallize from these compositions at 2 kb water-saturated over the temperature interval investigated in this study.

Relative shifts in primary liquidus volumes suggest the model reactions:



and



Water lowers the activity of silica in the liquid driving both reactions to the right. Low-Ca pyx or the enstatite-ferrosilite component of high-Ca pyx are destabilized relative to oliv. Likewise, high-Ca pyx is stabilized relative to Ca-plag and is enriched in Ca-tschermak's component. Fundamental conclusions to be drawn from the results summarized above are that (1) HAB or BA liquids do not crystallize low-Ca pyx if the liquids have high dissolved water contents, and (2) high-Ca pyx in hydrous HAB or BA liquids are low in enstatite-ferrosilite component and high in Ca-tschermak's component.

Figure 15 summarizes how the position of the oliv + pyx + plag (+/- hbl, spinel) multiple saturation boundary moves with increasing pH_2O . In projection from PLAG (figure 15a) the multiple saturation boundary shifts toward the OLIV apex and the low-Ca pyx stability field disappears as pH_2O increases. In projection from QTZ (figure 15b) increased pH_2O shifts the boundary away from the CPX apex and to a lesser extent away from the OLIV apex. Finally, in projection from OLIV high

pH₂O moves the boundary up toward the PLAG apex. The shifts observed with increased pH₂O are in the same general sense as are observed between tholeiitic and calc-alkaline magma series (Grove and Baker, 1984). Projected from PLAG, calc-alkaline magmas are displaced toward the OLIV apex compared to tholeiitic magmas. Likewise, calc-alkaline magmas are displaced toward PLAG in projections from QTZ and QTZ compared to their tholeiitic counterparts, a reflection of the generally higher Al₂O₃ in calc-alkaline magmas. This result supports the inference that magmatic water influences crystallization differentiation paths in many arc magmas, and is discussed at length below. Specific examples of calc-alkaline magma suites that project along or near high-pH₂O oliv + pyx + plag and oliv + hbl + plag multiple saturation boundaries are presented and interpreted in the *Geologic Applications* sections.

Role of water in producing calc-alkaline liquid lines of descent, and crystallization of magnetite from basalt and andesite liquids

An important result of these experiments is the demonstration that liquids formed by fractional crystallization of basalt under water-saturated conditions and geologically reasonable *f*O₂ can follow a calc-alkaline differentiation trend. The calc-alkaline differentiation trend (Miyashiro, 1974) is one that is characterized by early iron depletion and silica

enrichment. Iron depletion has been defined in two ways, and both occur in subduction zone-related differentiation series. One form of iron depletion is an overall decrease in FeO in the liquid. This type of FeO depletion is exhibited in the AFM diagram (figure 8) as an enrichment of Na₂O and K₂O relative to FeO. The second is the trend of a differentiation series in FeO/MgO vs SiO₂ diagrams. The characteristic trend displayed in subduction zone magma series is one of enrichment of SiO₂ with only modest increase in FeO/MgO. Figures 8 and 9 show that water-saturated crustal level crystallization of basalt can cause both types of iron depletion. Furthermore, the paths defined by the experiments are similar to those displayed in the magma series found in many subduction zone environments (Grove and Kinzler, 1986).

Water changes the near-liquidus mineral phase appearance in two ways. First, water destabilizes plagioclase as an early crystallizing phase, thus increasing the proportion of Fe-Mg silicates on the liquidus. When plagioclase appears as a crystallizing mineral, it is Ca-rich, SiO₂-poor, and Na₂O-poor. Crystallization of high proportions of Fe-Mg silicates and lesser Ca-rich plagioclase depletes the residual liquid in FeO and MgO and increases alumina and silica and alkalis, producing the high-alumina basalts and andesites characteristic of arc environments and the trend of increasing alkalis on the AFM diagram. Second, water destabilizes silicate minerals relative to hydrous silicate liquid, but water does not have as great an influence on the stability of

oxide phases. The effect of water-saturation at 2 kb is to lower the appearance temperature of silicates by over 150 °C relative to their appearance at 1-atm anhydrous conditions. Oxides become stable at 1-atm at this low temperature in basaltic bulk compositions, but silicates have crystallized at much higher temperatures and liquids are no longer basaltic. At 2 kb water-saturated conditions oxides and silicate minerals stabilize at close to the same temperature in basaltic or near-basaltic compositions. By stabilizing oxides as near-liquidus phases, FeO is efficiently removed from liquid, and the resulting change in FeO/MgO is that characteristic of the calc-alkaline differentiation series. In contrast, the FeO/MgO path followed when oxide is not part of the crystallization assemblage is much steeper on the FeO/MgO vs SiO₂ diagram and on the AFM diagrams and more closely resembles that of the tholeiitic series (figure 8).

The first of these two influences of water on the path followed during differentiation was anticipated by Grove and Baker (1984) from a comparison of the differentiation paths followed during crystallization of basalt magma at 1 atm with the rock series trends defined by calc-alkaline lavas from subduction-related volcanoes. At 1-atm the differentiation trend followed by basalt is the tholeiitic trend. The tholeiitic trend is characterized by early FeO/MgO enrichment and a lack of alkali enrichment. The crystal-liquid controls on the tholeiitic trend are crystallization of dominantly plagioclase, reduced proportions of Fe-Mg silicates, and

appearance of oxides only at late stages and low temperatures. The 1-atm plagioclase is enriched in Na_2O and SiO_2 , and alkali enrichment is suppressed. Fe-Mg silicates crystallize in diminished proportions, and the residual liquid becomes FeO-enriched.

The second effect of water on crystallization had not been previously anticipated. Kennedy (1955) suggested that the calc-alkaline trend might be produced by the oxidizing effect of continental crust on differentiating magma. Osborn (1959), Roeder and Osborn (1966), Eggler and Osborn (1982) and others carried out experimental investigations at 1-atm in simple systems ($\text{MgO-FeO-Fe}_2\text{O}_3\text{-SiO}_2$ or haplobasalt), exploring the effect of variations $f\text{O}_2$ on the FeO contents of liquids produced by fractional crystallization. From these experiments Osborn and co-workers concluded that any haplobasalt system that undergoes closed system crystallization shows a trend of iron-enrichment at nearly constant SiO_2 content. Osborn and coworkers found that FeO-depletion trends could be achieved during fractional crystallization, if differentiation was carried out at elevated $f\text{O}_2$ that was externally controlled. The problem encountered by these investigators was that the $f\text{O}_2$ required to cause the FeO-depletion trends in haplobasalt are near the hematite-magnetite buffer and are more oxidizing than the crystallization conditions inferred for calc-alkaline magmas. The $f\text{O}_2$ conditions commonly estimated for subduction-related magmas range from one or two log units around the Ni-NiO

buffer (Gill, 1981). Experiments carried out at 1-atm and variable fO_2 conditions using natural compositions have also shown that very high fO_2 s are required to stabilize an oxide phase near the liquidus of basaltic and andesitic liquids. At fO_2 conditions comparable to those inferred arc environments, oxides were not stable near the liquidus at 1-atm.

The results of our water-saturated Ni-NiO experiments provide a mechanism for stabilizing an oxide phases nearer the liquidus in calc-alkaline series, thus promoting early FeO-depletion. Water destabilizes silicate minerals relative to liquid, but has lesser effect on oxides. Other experimental evidence supports this conclusion. Experiments in the system pyrope-diopside-H₂O and pyrope-grossular-H₂O at 10 and 30 kb (Yoder, 1969; Sekine and Wyllie, 1983) show that one effect of adding water to these silicate systems is to expand the liquidus volume of spinel relative to silicates. Similarly, experiments on a lunar high-alumina basalt (Ford et al., 1972) show that the addition of water stabilizes spinel on the liquidus at low pressures (2 kb), whereas at anhydrous conditions spinel does not appear on the liquidus except at pressures in excess of 10 kb. In the case of calc-alkaline magmas, the addition of water depresses the appearance temperature of silicates, but has little effect on the oxide saturation temperature. As a result spinel or titanomagnetite grow as liquidus or near liquidus minerals and can exert the important control on FeO depletion that is

characteristic of some magma series found in subduction environments.

Previous experimental studies under water-bearing or saturated conditions failed, however, to produce liquidus or near liquidus magnetite in terrestrial basalt or andesite, apparently in conflict with the argument presented above (Eggler, 1972; Eggler and Burnham, 1973; Helz 1973, 1976). There are two probable reasons for the discrepancy. First, the experiments were conducted at the QFM or hematite-magnetite oxygen buffers and these may have been sufficiently reducing or oxidizing to inhibit growth of magnetite. More important, the early experiments were conducted in AgPd or Pt capsules. Several studies, previously summarized, have documented losses of ~40 % of the iron from samples contained in AgPd and even higher losses to Pt. Such substantial iron loss would inhibit growth of magnetite. Conclusions regarding magnetite stability based on experiments in AgPd or Pt capsules should be regarded with caution.

Arguments presented above for enhanced magnetite crystallization in hydrous magmas can be extended to chrome-rich spinels. Chrome spinel passes to magnetite as high-Ca pyx increases in abundance in sample 79-35g. This suggests that the chrome is taken up by the pyx. Irvine (1975) interpreted the phase relations in the simple system $\text{MgO-SiO}_2\text{-Cr}_2\text{O}_3$ (Keith, 1954) similarly: chrome spinel crystallization is terminated by reaction with liquid to produce pyx. Water or any other component that depresses the temperature of pyx

crystallization to below that of spinel can promote the growth of chrome-rich spinel.

GEOLOGIC APPLICATIONS

Volcanics: *Aleutians*

Low-MgO HABs and BAs are the most common magmas erupted from Aleutian volcanos (Marsh, 1982). Most lavas or scoria contain abundant phenocrysts of Ca-plag and lesser oliv, magnetite, and high-Ca pyx. Hornblende or low-Ca pyx phenocrysts are present in BAs at some volcanic centers (Kay and Kay, 1985), but are comparatively rare.

Aleutian HAB and BA whole rock compositions closely resemble the compositions of experimental liquids saturated with water, oliv, Ca-plag, magnetite, and either high-Ca pyx or hbl (tables 1, 4). Accordingly, the Aleutian HABs and BAs coincide with the oliv + Ca-plag + vapor + hbl or pyx (+/- spinel)-saturated liquids in psuedo-ternary projections (figure 16). The similarity in the compositions of wet experimental liquids and natural lavas, and the presence of the same saturating minerals, suggests that most Aleutian magmas were once multiply-saturated liquids with several or more wt.% of dissolved water. The experimental results of Baker and Eggler (1983) support this interpretation. Baker and Eggler (1983) show that at 2 kb and dissolved H₂O contents of > 4 wt.% and < 6 wt.% a typical Aleutian HAB has plag,

oliv, opaques, and either hbl or high-Ca pyx simultaneously on its liquidus (Baker and Eggler, 1983, their figure 3). In other words, the typical Aleutian HAB composition is that of a multiply-saturated liquid with a high dissolved water content.

Phenocryst compositions support the interpretation that Aleutian HABs and BAs were multiply-saturated water-rich liquids prior to eruption. Brophy (1986) presents whole rock and phenocryst core compositions for seven HABs from the Cold Bay volcanic center of the Aleutian arc. Observed plag and oliv phenocryst core compositions can be reproduced using experimentally determined water-saturated Ca-Na and Fe-Mg exchange K_D s if the whole rock compositions are used as the liquids from which the phenocryst cores grew (figure 17). Plagioclase compositions cannot be reproduced using Ca-Na exchange K_D s for dry conditions, presented in figure 4b, at any pressure using either whole rock or matrix compositions (Crawford et al., 1987) as liquids. Exchange K_D s determined for low water contents (~2 wt.%), presented in figure 4a, also fail to produce the observed plag phenocrysts.

The observed clinopyroxene phenocryst cores are moderate alumina (ave. 3.6 wt.% Al_2O_3) calcic augite, close in composition to the experimental salites. The natural pyx are more aluminous than pyx grown at 1 atm from HABs (Grove et al. 1982; Baker and Eggler, 1987) and are more calcic than pyx grown from HABs at high pressures, anhydrous (Johnston, 1986; Baker and Eggler, 1987; Bartels et al., 1991). The agreement of whole rocks with multiply-saturated wet liquid compositions

and of phenocryst cores with predicted or experimentally produced compositions assuming that whole rocks were wet liquids are strong evidence that Aleutian low-MgO HABs and BAs were once water-rich multiply-saturated liquids.

If the magmas were liquids, why then are they so typically porphyritic? The abundant plag phenocrysts and common (but not complete) absence of hbl phenocrysts in Aleutian HABs and BAs may result from volatile exsolution upon ascent to shallow depths, prior to eruption. Water-rich magmas will reach vapor saturation as they ascend. Aleutian liquids with ~4-6 wt.% H₂O would saturate with water vapor at ~2-6 km depth (assuming water solubility at 2 kb estimated in this study and Baker and Eggler (1983), and that for Mt. Hood andesite (Hamilton et al., 1964) at lower pressures). If the magmas continue to ascend, water will exsolve into vapor, and the liquids will become drier. Crystals will grow from the liquids as multiple saturation boundaries shift toward 1-atm positions. Any hydrous phenocrysts can be resorbed if the magma equilibrates at a sufficiently low pressure prior to eruption. Furthermore, many basaltic liquids in these arcs will never grow hornblende due to insufficient sodium or excessive temperature, regardless of water content. The presence of abundant phenocrysts in Aleutian HABs and BAs is evidence of shallow degassing and reequilibration prior to eruption.

Aleutian HABs are associated with less abundant basalts with higher MgO and lower Al₂O₃. Kay et al. (1982), Nye and Reid (1986), and Gust and Perfit (1987) have each proposed that the

more magnesian basalts are parental to the HAB and BA suite. Gust and Perfit (1987) conducted anhydrous experiments at 8 kb on a magnesian Aleutian basalt and showed that the composition crystallizes oliv followed by oliv plus high-Ca pyx, and that prior to plag saturation the liquid is progressively enriched in Al_2O_3 and depleted in MgO. Their starting composition and 8-kb experimental liquids are shown in figure 18, projected from QTZ onto the OLIV - CPX - PLAG psuedo-ternary. Also shown is the field defined by Aleutian HABs, BAs, and associated more magnesian lavas, including the starting composition of Gust and Perfit (1987). The fundamental conclusion of Gust and Perfit (1987) is clearly correct: extensive crystallization of oliv and high-Ca pyx (+/- a spinel) is required to produce HAB from low-alumina magnesian basalt. The dry experimental liquids do not, however, follow the field defined by the Aleutian magma series. The Aleutian magmas crystallized under conditions in which the olivine primary phase volume was expanded relative to that in the dry experiments, and as would be expected if the parental Aleutian magmas were water-bearing.

The water content of parental arc basalts has implications for melting processes and for volatile fluxes through subduction zones. Establishing the water content of potentially parental and near-primary magnesian Aleutian basalts awaits direct experimentation on these compositions in the presence of water. The water content can be estimated, however, by crystal fractionation calculations that reproduce

the trends defined by the Aleutian magma series. Results of forward models relating magnesian Aleutian basalts to low-MgO HABs are presented in table 7 and are illustrated in figures 18 and 19. To summarize, magnesian basalt crystallizes ~10 % oliv (+/-minor spinel) yielding moderate-MgO HAB. Moderate-MgO HAB crystallizes oliv + high-Ca pyx (+/-minor spinel) in proportions of ~0.15:0.85 either directly yielding low-MgO HAB or giving way to cotectic oliv + high-Ca pyx + plag crystallization. Typical low-MgO HABs of the Aleutians are the residual liquids left after 30-40 % solidification of typical Aleutian high-MgO basalts (table 7). If low-MgO HABs contained 4-6 wt.% H₂O, as indicated by the experiments of Baker and Eggler (1983) and this study, the parental Aleutian high-MgO basalts contained ~2¹/₂-4¹/₃ wt.% H₂O. Apparently, certain regions of the sub-Aleutian mantle wedge melt because they are fluxed with water, either during amphibole dehydration-melting or by the introduction of a free volatile phase.

Guatemala

Low-MgO HABs and BAs are erupted throughout the length of the active volcanic arc in Central America (Carr and Stoiber, 1988). The compositions of these lavas and scoria are similar to those erupted in the Aleutians (table 1). Carr et al. (1982) show that the average Na₂O content of mafic Central American lavas reaches a maximum at volcanic centers in

Guatemala (~3.7 wt.% Na_2O at 52 wt.% SiO_2). Carr and Stoiber (1988) show that average Na_2O in Central American mafic lavas correlates with regional elevation and interpret this as evidence that crustal thickness influences the alkali content of the mafic magmas.

Geologic evidence of high water contents in Guatemalan HABs and BAs is unequivocal. Hornblende has been recognized in HABs or BAs at the Fuego, Santa Maria, Atitlan, and Ayarza volcanic centers (Rose et al., 1978; Rose, 1987; Rose et al., 1987; Peterson and Rose, 1985). Hornblende phenocrysts are best preserved in mafic scoria erupted in association with more silicic pumice. Hornblende in lavas is resorbed or is preserved as inclusions in other phenocrysts (Rose et al., 1978). Hornblende is absent in low-MgO HAB and BA from volcanos in El Salvador, Costa Rica, and Nicaragua (M. Carr, written communication, 1989), regions where average Na_2O is lower than in Guatemala.

Fuego, in Guatemala, is one of the most active stratovolcanos on earth (Martin and Rose, 1981). Eruptive products range from magnesian HAB (very rare) to silicic andesite, but are overwhelmingly dominated by low-MgO HAB and BA (Chesner and Rose, 1984; CENTAM data base-Carr and Rose, 1987). Rose et al. (1978) provide a comprehensive description of the October 1974 eruption and eruptive products of Fuego. The weighted average October 1974 Fuego magma was low-MgO plag-porphyritic HAB (50.5 % SiO_2 , 19.4% Al_2O_3 , 5.0% MgO). Phenocryst-free groundmass separates of October 1974 scoria

are low-MgO high-alumina BA (53.0% SiO₂, 19.0% Al₂O₃, 3.4% MgO), close to the average composition of glass inclusions in phenocrysts from the 1974 eruption. Rose et al. (1978) interpret low totals of glass inclusion analyses as evidence of ~4 wt.% H₂O in the parent magma.

Eruptive products of Fuego are plotted in figure 20a, b, c. Like Aleutian HABs, the Guatemalan rocks plot coincident with the experimental liquids saturated with water, oliv, Ca-plag, magnetite, and hbl or high-Ca pyx. Agreement is best with hbl-saturated experimental liquids, consistent with the presence of hbl in some rock samples. The agreement between experimental wet, multiply-saturated liquids and natural low-MgO HABs and BAs is taken, as with the Aleutians, as evidence that most of the natural magmas were once multiply-saturated hydrous liquids. The magmas have partly degassed and have grown phenocrysts prior to eruption (Rose et al., 1978). High-sodium and rapid eruption are believed to be responsible for the presence and preservation of hbl in some Guatemalan HABs and BAs. Hornblende-free eruptives could have been somewhat drier or just as wet but either degassed before erupting and consumed their hbl or never grew it because of insufficient Na₂O.

Plutonics: Alaskan-type ultramafic complexes and Aleutian cumulate xenoliths

The crystal fractionation model developed for Aleutian magmas also predicts a cumulate rock series. The predicted cumulate rock series is that observed in both Alaskan-type ultramafic complexes (Irvine, 1974) and in hydrous mineral-bearing xenoliths erupted in lavas of the Aleutians (Conrad and Kay, 1984; Conrad et al., 1983; Debari et al., 1987). Cumulates produced by crystal fractionation of parental Aleutian high-MgO basalt to low-MgO HAB can be inferred from figure 18 and table 7. Parental magmas will first precipitate oliv (+spinel?) leaving dunites. The following high-Ca pyx plus oliv fractionation interval leaves olivine clinopyroxenite or wherlite (again possibly spinel-bearing). Eventually the liquids will reach a sufficiently high alumina content and will crystallize plag, oliv, and high-Ca pyx or hbl, leaving olivine gabbro cumulates. Gabbros would be characterized by very calcium-rich plagioclase. Cumulus olivine and pyroxene would in many cases be partly consumed by reaction with intercumulus liquid to produce hornblende. The Alaskan-type ultramafic complexes have spinel-bearing dunites, olivine clinopyroxenites (in some instances magnetite-rich), gabbros characterized by anorthitic plagioclase, and hornblende-bearing facies. Undeformed erupted cumulate xenoliths from the Aleutians include olivine clinopyroxenites (+/- abundant cumulus hornblende), hornblende gabbros, and anhydrous

orthopyroxene gabbros. Deformed cumulate xenoliths extend the rock types to dunites and wherlites. Pyroxenes in Alaskan-type ultramafic complexes and in Aleutian hydrous cumulate xenoliths are aluminous diopsides and salites, similar to the experimental pyroxenes produced at 2 kb water-saturated (figure 1) and experimental spinels overlap those of Alaskan-type complexes (figure 5) (Irvine, 1974; Conrad and Kay, 1984). The agreement between modeled and observed cumulates and similar experimental and cumulus mineral compositions support the crystal fractionation model relating Aleutian high-MgO basalts to low-MgO HABs, is further evidence for high magmatic water contents in many Aleutian basaltic magmas, and suggests a common crystallization sequence and high magmatic water content in other older arcs.

Sierra Nevada batholith, California

The Sierra Nevada batholith, California, is a link in the great chain of circum-Pacific batholiths formed during Mesozoic subduction. Granodiorites and granites are the most common intrusive rocks of the Sierra Nevada, but small intrusions of hornblende gabbro and diorite are widespread. Some mafic intrusions are composed of myriad aphyric sills and dikes each with very fine-grained chilled margins. Skeletal and swallowtail crystal habits indicate rapid growth from quenched liquids. The sills and dikes have compositions of low-MgO HAB, BA, and aluminous andesite (Sisson and Grove

1991). Na_2O contents are high, commonly 3.5–4.2 wt.%, and comparable to the Guatemalan magmas discussed above. Early crystallization of hbl and common miarolitic cavities are clear evidence of high magmatic water contents. Sills from the Jurassic mafic intrusive complex at Onion Valley in the southeastern Sierra Nevada are plotted in figure 21 a, b, c (Sisson and Grove, 1991). The sills lie along or near to the hbl-oliv reaction curve. Mafic sills are oliv-free but are associated with olivine hornblendite cumulates, in which olivine is resorbed and embayed against hornblende. The olivine hornblendites are cumulates formed by magmas solidifying along the hbl-oliv reaction curve, while the mafic sills preserve compositions of liquids on or near to the reaction curve.

Estimating temperatures and water contents of high-alumina basalts and basaltic andesites

Temperatures and water contents at which HABs and BAs would exist as multiply-saturated liquids can be estimated using the two geothermometers developed from experimental results. For a given composition of rock or glass, assumed to be that of a multiply-saturated liquid, one temperature is given by each geothermometer for an assumed water content. Since there are two equations (geothermometers) and two unknowns (T °C and wt.% H_2O) a unique solution can be derived in which temperature and dissolved H_2O agree for the two

geothermometers. The popular Fe-Ti oxide thermometer-oxygen barometer yields unique solutions by the same principle of solving two simultaneous equations. The bulk liquid geothermometer yields a temperature directly. The oliv-liquid geothermometer requires the equilibrium oliv composition, but this can be estimated using the oliv-liquid Fe-Mg exchange K_D (taken as 0.29).

Two tests are made of the temperature and H₂O estimation technique. Muenow et al. (1990) provide high precision analyses of volatiles (including H₂O) and major elements in three fresh basalt and basaltic andesite glasses quenched at seafloor pressures in the Troodos ophiolite. One glass is known to contain micro-phenocrysts of oliv, high-Ca pyx, and plag (Rautenschlein et al., 1985), and thus is a multiply-saturated liquid. Petrographic descriptions are not available for the other samples. The measured water contents are 2.11, 2.30, and 2.12 wt.%. Water contents calculated with the two geothermometers are 2.1, 2.5, and 2.3 wt.% respectively, in good agreement with the measured values.

The second test is provided by the experimental results of Baker and Eggler (1983) on a HAB from the volcanic center at Atka in the Aleutians. They show that Akta rock AT-1 exists as a multiply-saturated liquid near 1000 °C with dissolved H₂O higher than 4 but less than 6 wt.%. Simultaneous solution of the two geothermometers predicts AT-1 would exist as a multiply-saturated liquid at 1017 °C with dissolved H₂O of 5.6 wt.%, again supporting the accuracy of the estimation

technique. We have also applied the geothermometer-hydrometer to submarine basalt glasses from Hawaii that have had water contents measured by Garcia et al. (1989). The geothermometer-hydrometer yields apparent water contents less than zero for many Hawaiian samples. The high TiO_2 (commonly >2.5 wt.%) in Hawaiian basalt glasses leads to anomalously high oliv-liquid temperatures using our calibration and this results in impossibly low water contents. As we discussed previously, the geothermometers were developed for a limited range of compositions (eg. arc basalts and basaltic andesites). Use of the geothermometer-hydrometer should be restricted to compositions with $\text{TiO}_2 < 2.0$ wt.% and $\text{SiO}_2 < 55$ wt.%.

Figure 22a shows calculated temperatures and water contents for representative HABs and BAs. These are temperatures and water contents at which the rocks would exist as multiply-saturated liquids. Samples range from aphyric MgO-rich HAB from the southern Cascades, to strongly plagioclase-porphyritic low-MgO HAB and BA from the Cold Bay volcanic center in the Aleutians. Including the groundmass composition for the 1974 eruption of Fuego, aphyric material has temperatures ranging from ~ 1200 down to 975°C and water contents from < 1 to 6 wt.%. Porphyritic samples have lower calculated temperatures and higher water contents, on the whole, compared with the aphyric rocks. Most of the porphyritic samples are, technically, basalts in that they have $\text{SiO}_2 < 52$ wt.%. Figure 22a shows that the porphyritic

HABs would exist as multiply-saturated liquids at temperatures far lower than are commonly proposed for basaltic magma.

Figure 22a also shows that to exist as multiply-saturated liquids, the porphyritic samples would require water contents generally in excess of 4 wt.%, consistent with the phase equilibrium arguments presented above.

Figure 22b shows calculated temperatures and water contents for natural HAB and BA liquids. The samples are both inclusions of glass in oliv phenocrysts and interstitial glass and scoria from erupted cumulate nodules. Most compositions are near the transition between basalt and basaltic andesite ($\text{SiO}_2=52\pm 1$ wt.%), have Al_2O_3 in the range 18-20 wt.%, and $\text{MgO}=4\pm 1$ wt.%, and thus are similar to porphyritic HABs and BAs. MgO ranges as high as 7.6 and as low as 1.8 wt.%. The calculated temperatures and water contents for the natural liquids cover much the same range as the erupted HAB and BA lavas and scoria. MgO in glasses does not reach as high as in the rocks and the upper temperature is accordingly lower than for the rocks. The significant conclusion to be drawn from figure 22b is that greater than 90% of the natural HAB and BA liquids preserved as glass and intercumulus groundmass had water contents higher than 3 wt.% and were cooler than 1100 °C.

The plagioclase accumulation hypothesis

Crawford, Falloon, and Eggins (1987) propose that porphyritic, low-MgO HABs form by the accumulation of plag phenocrysts in liquids with lower alumina. Modest accumulation of phenocrysts certainly occurs and has been carefully documented in some instances (Rose et al., 1978). We question, however, whether accumulation of plag is responsible for the major characteristics of low-MgO HABs and BAs. First, the magmas are common in magmatic arcs globally. They are nearly absent from any other tectono-magmatic province. Abundant experimental, field, and petrographic evidence establishes that most basalts are saturated with and contain plag crystals at crustal pressures regardless of tectonic province. If plag accumulation is an efficacious process and nearly all basalts are plag-saturated, then porphyritic low-MgO HABs should be neither more nor less common in magmatic arcs vs other magmatic provinces. Their abundance in arcs suggests that other processes than phenocryst accumulation are responsible for their low-MgO and high alumina contents.

Second, there is a well defined upper limit to the alumina content of porphyritic HABs. Volcanic rocks with $\text{Al}_2\text{O}_3 \geq 20$ wt.% are rare and volcanic rocks with > 21 wt.% Al_2O_3 are very uncommon. Aphyric HABs with $\text{Al}_2\text{O}_3 \sim 18$ wt.% are present at some arc volcanic centers (Kuno, 1960; Gerlach and Grove, 1982). Accumulation of 30 wt.% An^{90} plag (typical of the amount and type of phenocrysts found) into liquid with 18 wt.%

Al_2O_3 would yield magma with 23 wt.% Al_2O_3 , considerably in excess of the observed Al_2O_3 contents. Accumulation would be expected to produce a gradation of alumina contents to very high values. In contrast, the upper limit to alumina contents finds ready explanation as the maximum solubility of Al_2O_3 in hydrous basaltic liquid saturated in plag, oliv, and either high-Ca pyx or hbl at crustal pressures.

Third, low-MgO HABs and BAs form glass inclusions in phenocrysts and interstitial glass and microcrystalline groundmass in erupted cumulate nodules (Anderson, 1973, 1974, 1979, 1982; Rose et al., 1978; Arculus and Wills, 1980; Devine and Sigurdsson, 1983). These quenched materials establish the existence of natural low-MgO HAB and BA liquids. Post-entrapment crystallization has likely modified the compositions of some melt inclusions and it might be argued that the glasses preserve disequilibrium nonrepresentative liquid compositions. This criticism does not hold for the interstitial liquids in erupted cumulates. The low-MgO HAB liquids probably only rarely erupt without degassing and growth of phenocrysts, as discussed above.

GEOLOGIC IMPLICATIONS

Melting in the mantle wedge

Several experimental studies have shown that HABs with high-MgO (≥ 8.5 wt.%) can be produced by anhydrous melting of plagioclase or spinel lherzolite near 10 kb pressure (Fujii and Scarfe, 1985; Takahashi, 1986; Falloon and Green, 1987; Bartels et al. 1990). The dry liquids do not crystallize to low-MgO HABs and cannot produce the mineral compositions found in low-MgO HABs. We have argued that low-MgO HABs are fractionated hydrous liquids that have partly degassed and crystallized prior to eruption. Apparently, some parental arc magmas are (nearly) dry whereas others contain as much as several wt.% H_2O . Water could be inhomogeneously distributed in the mantle wedge. Some parts of the mantle wedge are nearly dry and can melt to high-MgO HABs. Other areas either contain hydrous minerals or a free volatile in sufficient abundance that they can melt to liquids containing as much as a few wt.% H_2O . Significantly, submarine back arc basin basalt glasses have been shown to have magmatic water contents ranging from nil to 2 wt.% (Muenow et al., 1990). There are no comparable data for arc basalts. Nevertheless, the variable and appreciable water contents of basalts erupted near arcs supports a model of comparable or greater variation and abundance of water in arc basalts.

Crystallization to arc andesites and dacites

Crawford, Falloon, and Eggins (1987) and Rose et al. (1978) measured the groundmass compositions of 6 porphyritic HABs and BAs. Measured groundmass compositions encompass typical magmatic arc andesites and dacites. We have interpreted porphyritic HABs as having been liquids, with several or more wt.% of dissolved water, that subsequently crystallized phenocrysts. If this is correct, the groundmass compositions are evidence that some HABs produce typical andesitic or dacitic derivative liquids by crystallization. Two new groundmass analyses are presented in appendix 2 for hbl-phyric samples. Groundmasses of the hbl-phyric samples are andesitic and have Al_2O_3 18.4-18.9 wt.%. The groundmass Al_2O_3 concentrations of the hbl-phyric samples are higher than is typical of magmatic arc andesite (~17.3 wt.%, Gill, 1981), but comparable concentrations are found in andesites in some regions (eg. in the Aleutians, (Marsh 1976) and Guatemala (CENTAM data base, Carr and Rose, 1987)) and are close to the lower temperature liquids produced at 2 kb, water-saturated. The groundmasses analyzed by Crawford, Falloon, and Eggins (1987), with lower Al_2O_3 contents, were either water-undersaturated or formed at pressures less than 2 kb. The groundmass compositions confirm that HABs can be related to various andesites through simple crystallization differentiation.

Magma mixing

Arc volcanics commonly possess features indicative of magma mixing. Crystallization temperatures limit the proportions of mafic and felsic magmas that can mix (Sparks and Marshall, 1986). Small fractions of dry basalt liquid injected into more silicic magma quench to a rigid mesh of crystals and residual liquid, inhibiting mixing. Our experiments and calculations show, however, that many HABs or BAs exist as liquids at comparatively low temperatures. Fe-Ti oxide equilibration temperatures of andesites and low-silica dacites erupted in magmatic arcs are generally in the range 900-1050 °C (Gill 1981, table 4.1; Melson, 1983; Hildreth, 1983; Druitt and Bacon 1989). Results of this study suggest that moderate to low-MgO HABs exist as multiply-saturated liquids at temperatures on the order of 950-1100 °C (figure 22), on average only slightly hotter than the liquidus temperatures of drier, more silicic magmas. If true, prohibitions on mixing between HAB and many more silicic magmas would be minor. The presence of hydrous HABs with low liquidus temperatures facilitates magma mixing in magmatic arcs to an extent not seen in other tectonic environments lacking wet mafic magmas.

CONCLUSION

Moderate to low-MgO HABs and BAs exist as water-rich liquids at moderate pressures. The liquid compositions are controlled by saturation with plag, oliv, and either high-Ca pyx or hbl. Experimentally-produced solid phases match the compositions of phenocrysts observed in lavas, scoria, and intrusions. Solids and liquids produced in dry or low water content experiments do not match natural compositions. The inference that all or most HABs or BAs are nearly anhydrous is incorrect. Many, particularly those with very high- Al_2O_3 and low-MgO, probably contained at least 4 wt.% H_2O at depth. Such wet basalts cannot normally erupt as liquids. The abundant phenocrysts in many HABs probably crystallize at shallow depths as the magma ascends and decompresses and the liquid degasses.

The lack of iron enrichment in calc-alkaline rock series can originate through simple crystallization differentiation processes if liquids contain sufficient dissolved water and oxygen fugacity is otherwise appropriate. Water depresses the crystallization temperatures of silicates, but apparently has less effect on spinels. Magnetite can grow as a near liquidus mineral in hydrous basaltic liquids.

Further experimentation is required to establish the relation of evolved wet HABs to potential primary magmas. Nevertheless, our results supports models in which water carried and released by the subducting slab fluxes the mantle and initiates melting (Nicholls and Ringwood, 1973; Ringwood,

1975; Tatsumi, 1983). The distribution of this water may, however, be inhomogeneous, and the degree to which subducted and recycled water is essential for the creation of many arc magmas remains to be determined.

REFERENCES

- Albee A. L. and Ray L. (1970) Correction factors for electron microprobe microanalysis of silicates, oxides, carbonates, phosphates and sulfates. *Anal. Chem.*, 42, 1408-1414.
- Allen J.C. and Boettcher A.L. (1983) The stability of amphibole in andesite and basalt at high pressure. *Am. Min.*, 68, 307-314.
- Anderson A.T. (1973) The before-eruption water content of some high-alumina magmas. *Bull. Volcanol.*, 37, 530-552.
- Anderson A.T. (1974a) Evidence for a picritic, volatile-rich magma beneath Mt. Shasta, California. *J. Petrol.*, 15, 243-267.
- Anderson A.T. (1974b) Chlorine, sulfur, and water in magmas and oceans. *Geol. Soc. Am. Bull.*, 85, 1485-1492.
- Anderson A.T. (1979) Water in some hypersthenic magmas. *J. Geol.*, 87, 509-531.
- Anderson A.T. (1982) Parental basalts in subduction zones: Implications for continental evolution. *J. Geophys. Res.*, 87, 7047-7060.
- Anderson R.N., DeLong S.E., and Schwarz W.M. (1978) Thermal model for subduction with dehydration in the downgoing slab. *J. Geol.*, 86, 731-739.
- Aramaki S. and Ui T. (1978) Major element frequency distribution of the Japanese Quaternary volcanic rocks. *Bull. Volc.*, 41, 390-407.

- Arculus R.J. and Wills K.J. (1980) The petrology of igneous blocks and inclusions from the Lesser Antilles island arc. *J. Petrol.*, 21, 143-168.
- Arculus R.J., Delong S.E., Kay R.W., Brooks C., and Sun S.-S. (1977) The alkalic rock suite of Bogoslof Island, eastern Aleutian arc, Alaska. *J. Geol.*, 85, 177-186.
- Baker D.R. and Eggler D.H. (1983) Fractionation paths of Atka (Aleutians) high-alumina basalts: constraints from phase relations. *J. Volc. Geotherm. Res.*, 18, 387-404.
- Baker D.R. and Eggler D.H. (1987) Compositions of anhydrous and hydrous melts coexisting with plagioclase, augite, and olivine or low-Ca pyroxene from 1 atm to 8 kbar: Application to the Aleutian volcanic center of Atka. *Am. Mineral.*, 72, 12-28.
- Bartels K.S., Kinlzer R.J., and Grove T.L. (1991) High pressure phase relations of primitive high-alumina basalt from Medicine Lake volcano, northern California. submitted to *Contrib. Miner. Petrol.*
- Beard J.S. and Borgia A. (1989) Temporal variation of mineralogy and petrology in cognate enclaves at Arenal volcano, Costa Rica. *Contrib. Mineral. Petrol.*, 103, 110-122.
- Bence A. E. and Albee A. L. (1968) Empirical correction factors for the electron microanalysis of silicates and oxides. *J. Geol.*, 76, 382-403.
- Blundy J.D. and Holland T.J.B. (1990) Calcic amphibole equilibria and a new amphibole-plagioclase

- geothermometer. *Contrib. Mineral. Petrol.*, 104, 208-224.
- Blundy J.D. and Sparks R.S.J. (1991) Petrogenesis of mafic inclusions in granitoids of the Adamello Massif, Italy. submitted to *J. Petrol.*
- Bowen N.L. (1915) The crystallization of haplobasaltic, haplodioritic, and related magmas. *Am. J. Sci.*, 40, 161-185.
- Brophy J.G. (1986) The Cold Bay volcanic center, Aleutian volcanic arc I. Implications for the origin of high-alumina arc basalt. *Contrib. Mineral. Petrol.*, 93, 368-380.
- Brophy J.G. and Marsh B.D. (1986) On the origin of high-alumina arc basalt and the mechanics of melt extraction. *J. Petrol.*, 27, 763-789.
- Burnham C.W. (1979) The importance of volatile constituents. In: Yoder H.S. Jr. (ed.), *The evolution of the igneous rocks*. Princeton, Princeton Univ. Press, 439-482.
- Burnham C.W. and Jahns R.H. (1962) A method for determining the solubility of water in silicate melts. *Am. J. Sci.*, 260, 721-745.
- Byers F.M. (1959) *Geology of Umnak and Bogoslof Islands Aleutian Islands, Alaska*, U.S. Geol. Surv. Bull. 1028-L, 267-369.
- Byers F.M. (1961) Petrology of three volcanic suites, Umnak and Bogoslof Islands, Aleutian Islands. *Geol. Soc. Am. Bull.*, 79, 93-128.

- Carr M. J. and Rose W. I. (1987) CENTAM—a data base of Central American volcanic rocks. *J. Volc. Geotherm. Res.*, 33, 239–240.
- Carr M. J. and Stoiber R. E. (1988) Volcanism. In: Dengo G. and Case J. E. (eds.), *The geology of North America*, vol H, the Caribbean region. Boulder, Geological Society of America.
- Carr M. J., Rose W. I., and Stoiber R. E. (1982) Central America. In: Thorpe R. S. (ed.), *Andesites*. Wiley, New York, 149–166.
- Cawthorn R. G. (1976) Melting relations in part of the system $\text{CaO-MgO-Al}_2\text{O}_3\text{-SiO}_2\text{-Na}_2\text{O-H}_2\text{O}$ under 5kb pressure. *J. Petrol.* 17, 44–72.
- Cawthorn R. G., Curran E. B., and Arculus R. J. (1973) A petrogenetic model for the origin of the calc-alkaline suite of Grenada, Lesser Antilles. *J. Petrol.*, 14, 327–337.
- Chesner C. A. and Rose W. I. (1984) Geochemistry and evolution of the Fuego volcanic complex, Guatemala. *J. Volc. Geotherm. Res.*, 21, 25–44.
- Conrad W. K. and Kay R. W. (1984) Ultramafic and mafic inclusions from Adak island: crystallization history and implications for the nature of primary magmas and crustal evolution in the Aleutian arc. *J. Petrol.*, 25, 88–125.
- Conrad W. K., Kay S. M., and Kay R. W. (1983) Magma mixing in the Aleutian arc: Evidence from cognate inclusions and

- composite xenoliths: J. Volc. Geotherm. Res., 18, 279-295.
- Crawford A.J., Falloon T.J. and Eggins S. (1987) The origin of island arc high-alumina basalts. Contrib. Mineral. Petrol., 97, 417-430.
- Debari S., Kay S.M., and Kay R.W. (1987) Ultramafic xenoliths from Adagdak volcano, Adak, Aleutian islands, Alaska: Deformed igneous cumulates from the MOHO of an island arc. J. Geol., 95, 329-341.
- Devine J.D. and Sigurdsson H. (1983) The liquid composition and crystallization history of the 1979 Soufriere magma, St. Vincent, W.I. J. Volc. Geotherm. Res., 16, 1-31.
- Druitt T.H. and Bacon C.R. (1989) Petrology of the zoned calcalkaline magma chamber of Mount Mazama, Crater Lake, Oregon. Contrib. Mineral. Petrol., 101, 245-259.
- Eggler D.H. (1972) Water-saturated and undersaturated melting relations in a Paricutin andesite and an estimate of water content in the natural magma. Contrib. Mineral. Petrol., 34, 261-271.
- Eggler D.H. and Burnham C.W. (1973) Crystallization and fractionation trends in the system andesite-H₂O-CO₂-O₂ at pressures to 10 Kb. Geol. Soc. Am. Bull., 84, 2517-2532.
- Eggler D.H. and Osborn E.F. (1982) Experimental studies of the system MgO-FeO-Fe₂O₃-NaAlSi₃O₈-CaAl₂Si₂O₈ - A model for subalkaline magmas. Am. J. Sci., 282, 1012-1041.

- Falloon T.J. and Green D.H. (1987) Anhydrous partial melting of MORB pyrolite and other peridotite compositions at 10 kbar: Implications for the origin of primitive MORB glasses. *Mineral. Petrol.*, 37, 181-219.
- Ford C.E., Biggar G.M., Humphries D.J., Wilson G., Dixon D., and O'Hara M.J. (1972) Role of water in the evolution of the lunar crust; an experimental study of sample 14310; an indication of lunar calc-alkaline volcanism. *Proc. Third. Lunar Sci. Conf.*, 1, 207-229.
- Ford C.E., Russell D.G., Craven J.A. and Fisk M.R. (1983) Olivine-liquid equilibria: temperature, pressure and composition dependence of the crystal/liquid cation partition coefficients for Mg, Fe^{2+} , Ca and Mn. *J. Petrol.*, 24, 256-265.
- Fujii T. and Scarfe C.M. (1985) Compositions of liquids coexisting with spinel lherzolite at 10 kbar and the genesis of MORBs. *Contrib. Mineral. Petrol.*, 90, 18-28.
- Garcia M.O., Muenow D.W., Aggrey K.E., and O'Neil J.R. (1989) Major element, volatile, and stable isotope geochemistry of Hawaiian submarine tholeiitic glasses. *J. Geophys. Res.*, 94, 10525-10538.
- Gerlach D.C. and Grove T.L. (1982) Petrology of Medicine Lake Highlands volcanics: characterization of end-members of magma mixing. *Contrib. Mineral. Petrol.*, 80, 147-159.
- Gill J.B. (1981) *Orogenic andesites and plate tectonics.* Springer, Berlin Heidelberg New York.

- Green T.H. and Pearson N.J. (1985) Experimental determination of REE partition coefficients between amphibole and basaltic to andesitic liquids at high pressure. *Geochim. Cosmochim. Acta.*, 49, 1465-1468.
- Green T.H. and Ringwood A.E. (1968) The genesis of the calc-alkaline rock suite. *Contrib. Mineral. Petrol.*, 18, 105-162.
- Grove T.L. and Baker M.B. (1984) Phase equilibrium controls on the tholeiitic versus calc-alkaline differentiation trends. *J. Geophys. Res.*, 89, 3253-3274.
- Grove T.L. and Bryan W.B. (1983) Fractionation of pyroxene-phyric MORB at low pressure: An experimental study. *Contrib. Mineral. Petrol.*, 84, 293-309.
- Grove T.L. and Juster T.C. (1990) Experimental investigations of low-Ca pyroxene stability and olivine - pyroxene - liquid equilibria at 1-atm in natural basaltic and andesitic liquids. *Contrib. Mineral. Petrol.*, 103, 287-305.
- Grove T.L. and Kinzler R.J. (1986) Petrogenesis of andesites. *Ann. Rev. Earth Planet. Sci.*, 14, 417-454.
- Grove T.L., Gerlach D.C., and Sando T.W. (1982) Origin of calc-alkaline series lavas at Medicine Lake volcano by fractionation, assimilation and mixing. *Contrib. Mineral. Petrol.*, 80, 160-182.
- Grove T.L., Kinzler R.J., and Bryan W.B. (1990) Natural and experimental phase relations of lavas from Seroki

- volcano. Proc. ODP, Sci. Results, 106/109, College Station TX, 9-17.
- Gust D. A. and Perfit M. R. (1987) Phase relations of a high-Mg basalt from the Aleutian Island Arc: Implications for primary island arc basalts and high-Al basalts. Contrib Mineral Petrol 97:7-18.
- Hamilton D. L., Burnham C. W., and Osborn E. F. (1964) The solubility of water and effects of oxygen fugacity and water content on crystallization in mafic magmas. J. Petrol., 5, 21-39.
- Hansen M. (1958) Constitution of binary alloys. McGraw-Hill, New York, 1305pp.
- Harris D. M. and Anderson A. T. (1984) Volatiles H_2O , CO_2 , and Cl in a subduction related basalts. Contrib. Mineral. Petrol., 87, 120-128.
- Hawthorne F. C. (1981) Crystal chemistry of the amphiboles. In: Veblen D. R. (ed.) Amphiboles and other hydrous pyriboles - mineralogy. Reviews in Mineralogy, 9A, Miner. Soc. Am.
- Helz R. T. (1973) Phase relations of basalts in their melting range at $p_{H_2O}=5$ kb as a function of oxygen fugacity. I. Mafic phases. J. Petrol., 14, 249-302.
- Helz R. T. (1976) Phase relations of basalts in their melting ranges at $p_{H_2O}=5$ kb. II. Melt compositions. J. Petrol., 17, 139-193.
- Helz R. T. (1981) Phase relations and compositions of amphiboles produced in studies of the melting behavior

- of rocks. In: Veblen D.R. and Ribbe P.H. (eds.),
Amphiboles: petrology and experimental phase relations.
Reviews in Mineralogy, 9B, Miner. Soc. Am.
- Helz R.T. and Thornber C.R. (1987) Geothermometry of Kilauea
Iki lava lake, Hawaii, Bull. Volc., 49, 651-668.
- Hildreth W. (1983) The compositionally zoned eruption of
1912 in the Valley of Ten Thousand Smokes, Katmai
National Park, Alaska. J. Volc. Geotherm. Res., 18, 1-
56.
- Irvine T.N. (1974) Petrology of the Duke Island Ultramafic
Complex, southeastern Alaska. Mem. Geol. Soc. Am., 138.
- Irvine T.N. (1975) Crystallization sequences in the Muskox
intrusion and other layered intrusions. II. Origin of
chromitite layers and similar deposits of other
magmatic ores. Geochim. Cosmochim. Acta., 39.
- Irvine T.N. and Baragar W.R.A. (1971) A guide to the
chemical classification of the common volcanic rocks.
Can. J. Earth Sci., 8, 523-548.
- Johnston D. (1978) Volcanic gas studies at Alaskan
volcanoes. Accomplishments in Alaska 1978. U.S. Geol.
Surv. Circular 804.
- Johnston A.D. (1986) Anhydrous P-T phase relations of near
-primary high-alumina basalt from the South Sandwich
Islands. Contrib Mineral Petrol 92, 368-382.
- Johnson M.C. and Rutherford M.L. (1989) Experimentally
determined conditions in the Fish Canyon tuff,
Colorado, magma chamber. J. Petrol., 30, 711-737.

- Juster T.C., Grove T.L., and Perfit M.R. (1989) Experimental constraints on the generation of Fe-Ti basalts, andesites, and rhyodacites at the Galapagos Spreading Center, 85°W and 95°W. *J. Geophys. Res.*, 94, 9251-9274.
- Kay S.M. and Kay R.W. (1985) Aleutian tholeiitic and calc-alkaline magma series: I. The mafic phenocrysts. *Contrib. Mineral. Petrol.*, 90, 276-290.
- Kay S.M., Kay R.W., and Citron G.P. (1982) Tectonic controls on tholeiitic and calc-alkaline magmatism in the Aleutian arc. *J. Geophys. Res.*, 87, 4051-4072.
- Keith M.L. (1954) The system $\text{MgO-Cr}_2\text{O}_3\text{-SiO}_2$. *Am. Ceramic Soc. J.*, 37, 490-496.
- Kennedy G.C. (1955) Some aspects of the role of water in rock melts. In: *Crust of the earth - a symposium*. *Geol. Soc. Am. Spec. Paper* 62, 489-503.
- Kinzler R.J. and Grove T.L. (1991) Primary magmas of mid-ocean ridge basalts. submitted to *J. Geophys. Res.*
- Kuno H (1950) Petrology of Hakone volcano and the adjacent areas, Japan. *Geol. Soc. Am. Bull.*, 61, 957-1020.
- Kuno H (1960) High-alumina basalt. *J. Petrol.*, 1, 12-145.
- Kushiro I. (1969) The system forsterite-diopside-silica with and without water at high pressures. *Am. J. Sci.*, 267A, 269-294.
- Kushiro I. (1972) Determination of liquidus relations in synthetic silicate systems with electron probe analysis: The system forsterite-diopside-silica at 1 atmosphere. *Am. Miner.*, 57, 1260-1271.

- Longhi J., Walker D., and Hays J.F. (1978) The distribution of Fe and Mg between olivine and lunar basaltic liquids. *Geochim. Cosmochim. Acta* 42, 1545-1558.
- Marsh B.D. (1976) Some Aleutian andesites: their nature and source. *J. Geol.*, 84, 27-45.
- Marsh B.D. (1982) The Aleutians. In: Thorpe R.S. (ed) *Andesites*. Wiley, New York, 99-114.
- Martin D.P. and Rose W.I. (1981) Behavioral patterns of Fuego volcano, Guatemala. *J. Volc. Geotherm. Res.*, 10, 67-81.
- Meen J.K. (1987) Formation of shoshonites from calcalkaline basalt magmas: geochemical and experimental constraints from the type locality. *Contrib. Mineral. Petrol.*, 97, 333-351.
- Melson W.G. (1983) Monitoring the 1980-1982 eruptions of Mount St. Helens: Compositions and abundances of glass. *Science*, 221, 1387-1391.
- Mertzbacher C. and Eggler D.H. (1984) A magmatic geohydrometer: Applications to Mount St. Helens and other dacitic magmas. *Geology*, 12, 587-590.
- Miyashiro A. (1974) Volcanic rock series in island arcs and active continental margins. *Am. J. Sci.*, 274, 321-355.
- Moore J.G. and Sisson T.W. (1987) Geologic map of the Triple Divide Peak quadrangle, Tulare County, California. U.S. Geol. Surv. Geologic Quad. Map GQ-1636.
- Muenow D.W., Garcia M.O., Aggrey K.E., Bednarz U., Schmincke H.U. (1990) Volatile in submarine glasses as a

- discriminant of tectonic origin: application to the Troodos ophiolite. *Nature*, 343, 159-161.
- Myers J.D., Marsh B.D. and Sinha A.K. (1986) Geochemical and strontium isotopic characteristics of parental Aleutian arc magmas: evidence from the basaltic lavas of Atka. *Contrib. Mineral. Petrol.*, 94, 1-11.
- Naney M.T. (1983) Phase equilibria of rock-forming ferromagnesian silicates in granitic systems. *Am. J. Sci.*, 283, 993-1033.
- Nicholls I.A. and Harris K.L. (1980) Experimental rare earth element partition coefficients for garnet, clinopyroxene, and amphibole coexisting with andesitic and basaltic liquids. *Geochim. Cosmochim. Acta.*, 44, 287-308.
- Nicholls I.A. and Ringwood A.E. (1973) Effect of water on olivine stability in tholeiites and production of SiO₂-saturated magmas in the island-arc environment. *J. Geol.*, 81, 285-300.
- Nye C.J. and Reid M.R. (1986) Geochemistry of primary and least fractionated lavas from Okmok volcano, central Aleutians: implications for arc magma genesis. *J. Geophys. Res.*, 91, 271-287.
- Osborn E.F. (1959) Role of oxygen pressure in the crystallization and differentiation of basaltic magma. *Am. J. Sci.*, 257, 609-647.
- Peccherillo A. and Taylor S.R. (1976) Geochemistry of Eocene calc-alkaline volcanic rocks from the Kastamonu area,

- northern Turkey. *Contrib. Mineral. Petrol.*, 58, 63-81.
- Perfit M. R., Gust D. A., Bence A. E., Arculus R. J. and Taylor S. R. (1980) Chemical characteristics of island arc basalts: Implications for mantle sources. *Chemical Geology*, 30, 227-256.
- Peterson P. S. and Rose W. I. (1985) Explosive eruptions of the Ayarza calderas, southeastern Guatemala. *J. Volc. Geotherm. Res.*, 25, 289-307.
- Pitcher W. S., Atherton M. P., Cobbing E. J., and Beckinsale R. D. (eds.) (1985) *Magmatism at a plate edge: the Peruvian Andes*. Wiley, New York, 287pp.
- Presnall D. C., Dixon S. A., Dixon J. R., O'Donnell T. H., Brenner N. L., Schrock R. L. and Dyeus D. W. (1978) Liquidus phase relations on the join diopside-forsterite-anorthite from 1 atm to 20 kbar: Their bearing on the generation and crystallization of basaltic magma. *Contrib. Mineral. Petrol.*, 66, 203-220.
- Ramsay W. R. H., Crawford A. J., and Foden J. D. (1984) Field setting, mineralogy, chemistry, and genesis of arc picrites, New Georgia, Solomon Islands. *Contrib. Mineral. Petrol.*, 88, 386-402.
- Rautenschlein M., Jenner G. A., Hertogen J., Hoffman R., Schmincke H.-U., and White W. M. (1985) Isotopic and trace element composition of volcanic glasses from the Akaki canyon, Cyprus: implications for the origin of the Troodos ophiolite. *Earth Planet. Sci. Lett.*, 75, 369-383.

- Ringwood A. E. (1975) Composition and petrology of the earth's mantle. McGraw-Hill, New York.
- Ritchey J. L. (1980) Divergent magmas at Crater Lake, Oregon: products of fractional crystallization and vertical zoning in a shallow, water-undersaturated chamber. J. Volc. Geotherm. Res., 7, 373-386.
- Roeder P. L. (1974) Activity of iron and olivine solubility in basaltic liquids. Earth Planet. Sci. Lett., 23, 397-410.
- Roeder P. L. and Emslie R. F. (1970) Olivine-liquid equilibrium. Contrib. Mineral. Petrol., 29, 275-289.
- Roeder P. L. and Osborn E. F. (1966) Experimental data for the system $\text{MgO-FeO-Fe}_2\text{O}_3\text{-CaAl}_2\text{Si}_2\text{O}_8\text{-SiO}_2$ and their petrological implications. Am. J. Sci., 264, 428-480.
- Rose W. I. (1987) Santa Maria, Guatemala: bimodal soda-rich calc-alkalic stratovolcano. J. Volc. Geotherm. Res., 33, 109-129.
- Rose W. I., Anderson A. T., Woodruff L. G., and Bonis S. B. (1978) The October 1974 basaltic tephra from Fuego volcano: Description and history of the magma body. J. Volc. Geotherm. Res., 4, 3-53.
- Rose W. I., Newhall C. G., Bornhorst T. J., and Self S. (1987) Quaternary silicic pyroclastic deposits of Atitlan caldera, Guatemala. J. Volc. Geotherm. Res., 33, 57-80.
- Rutherford M. J., Sigurdsson H., Carey S., and Davis A. (1985) The May 18, 1980, eruption of Mount St. Helens 1. Melt composition and experimental phase equilibria.

- J. Geophys. Res., 90, 2929-2947.
- Sack R. O., Carmichael I. S. E., Rivers M., and Ghiorso M. S.
(1980) Ferric-ferrous equilibria in natural silicate liquids at 1 bar. Contrib. Mineral. Petrol., 75, 369-376.
- Sampson D. E. and Cameron K. L. (1987) The geochemistry of the Inyo volcanic chain: Multiple magma systems in the Long Valley region, eastern California. J. Geophys. Res., 92, 10403-10421.
- Schairer J. F. and Morimoto N. (1959) The system forsterite-diopside-silica-albite. Yb. Carnegie Inst. Wash., 58, 113-118.
- Sekine T. and Wyllie P. J. (1983) Phase relations in the join grossularite-pyrope-7.5 percent H₂O at 30 Kb. Am. J. Sci., 283, 435-453.
- Shimizu N. (1981) Trace element incorporation into a growing augite phenocryst. Nature, 289, 575-577.
- Silver L. and Stolper E. (1984) A thermodynamic model for hydrous silicate melts. J. Geol., 93, 161-178.
- Sisson T. W. and Grove T. L. (1991) Geochemistry of the mafic sill complex at Onion Valley, southeastern Sierra Nevada, and implications for the origin of Sierran granitoids. Chapter 1 of this thesis.
- Smith T. E., Huang C. H., Walawender M. J., Cheung P., and Wheeler C. (1983) The gabbroic rocks of the Peninsular Ranges batholith, southern California: cumulate rocks

- associated with calc-alkalic basalts and andesites. *J. Volc. Geotherm. Res.*, 18, 249-278.
- Sparks R.S.J. and Marshall L.A. (1986) Thermal and mechanical constraints on mixing between mafic and silicic magmas. *J. Volc. Geotherm. Res.*, 29, 99-124.
- Spulber S.D. and Rutherford M.J. (1983) The origin of rhyolite and plagiogranite in oceanic crust: an experimental study. *J. Petrol.*, 24, 1-25.
- Stern C.R. and Wyllie P.J. (1975) Effect of iron absorption by noble-metal capsules on phase boundaries in rock-melting experiments at 30 kilobars. *Am. Min.*, 60, 681-689.
- Stolper E.M. (1982) The speciation of water in silicate melts. *Geochim. Cosmochim. Acta.*, 46, 2609-2620.
- Takahashi E. (1986) Melting of a dry peridotite KLB-1 up to 20 GPa: implications on the origin of peridotite upper mantle. *J. Geophys. Res.*, 91, 9367-9382.
- Tatsumi Y., Sakuyama M., Fukuyama H. and Kushiro I. (1983) Generation of arc basalt magmas and thermal structure of the mantle wedge in subduction zones. *J. Geophys. Res.*, 88-B7, 5815-5825.
- Tormey D.R., Grove T.L. and Bryan W.B. (1987) Experimental petrology of normal MORB near the Kane Fracture Zone: 22°-25°N, mid-Atlantic ridge. *Contrib. Mineral. Petrol.*, 96, 121-139.
- Ulmer P., Callegari E., and Soderregger U.C. (1983) Genesis of the mafic and ultramafic rocks and their genetical

- relations to the tonalitic-trondhjemitic granitoids of the southern part of the Adamello batholith (Northern Italy). *Mem. Soc. Geol. Ital.*, 26, 171-222.
- Wager L.R. and Deer W.A. (1939) The petrology of the Skaergaard intrusion, Kangerlassuaq, East Greenland. *Medd. Groenl.*, 105(4), 1-352.
- Walawender M.J. (1976) Petrology and emplacement of the Los Pinos pluton, southern California. *Can. J. Earth Sci.*, 13, 1288-1300.
- Walawender M.J. and Smith T.E. (1980) Geochemical and petrologic evolution of the basic plutons on the Peninsular Ranges batholith, southern California. *J. Geol.*, 88, 233-242.
- Walker D., Shibata T., DeLong S.E. (1979) Abyssal tholeiite from Oceanographer Fracture Zone, II: phase equilibria and mixing. *Contrib. Mineral. Petrol.*, 70, 111-125.
- Yoder H.S. Jr. (1965) Diopside-anorthite-water at five and ten kilobars and its bearing on explosive volcanism. *Yb. Carnegie Inst. Wash.*, 64, 82-89.
- Yoder H.S. Jr. (1969) The join diopside-pyroxene-H₂O at 10 Kb: Its bearing on the melting of peridotite, the ACF metamorphic facies, and the gedrite-hornblende miscibility gap. *Yb. Carnegie Inst. Wash.*, 69, 176-181.
- Yoder H.S., Jr. and Tilley C.E. (1962) Origin of basalt magmas: An experimental study of natural and synthetic rock systems. *J. Petrol.*, 3, 342-532.

Figure 2-1. Experimental high-Ca pyx (dots) projected onto the Ca - Mg - Fe ternary (molar units). Experimental pyx are diopside or salite. Comparable minerals are found in Alaskan-type ultramafic complexes (shaded area) and in hornblende-bearing cumulates erupted as xenoliths in the Aleutians (horizontal ruled area) (fields after Conrad and Kay, 1983).

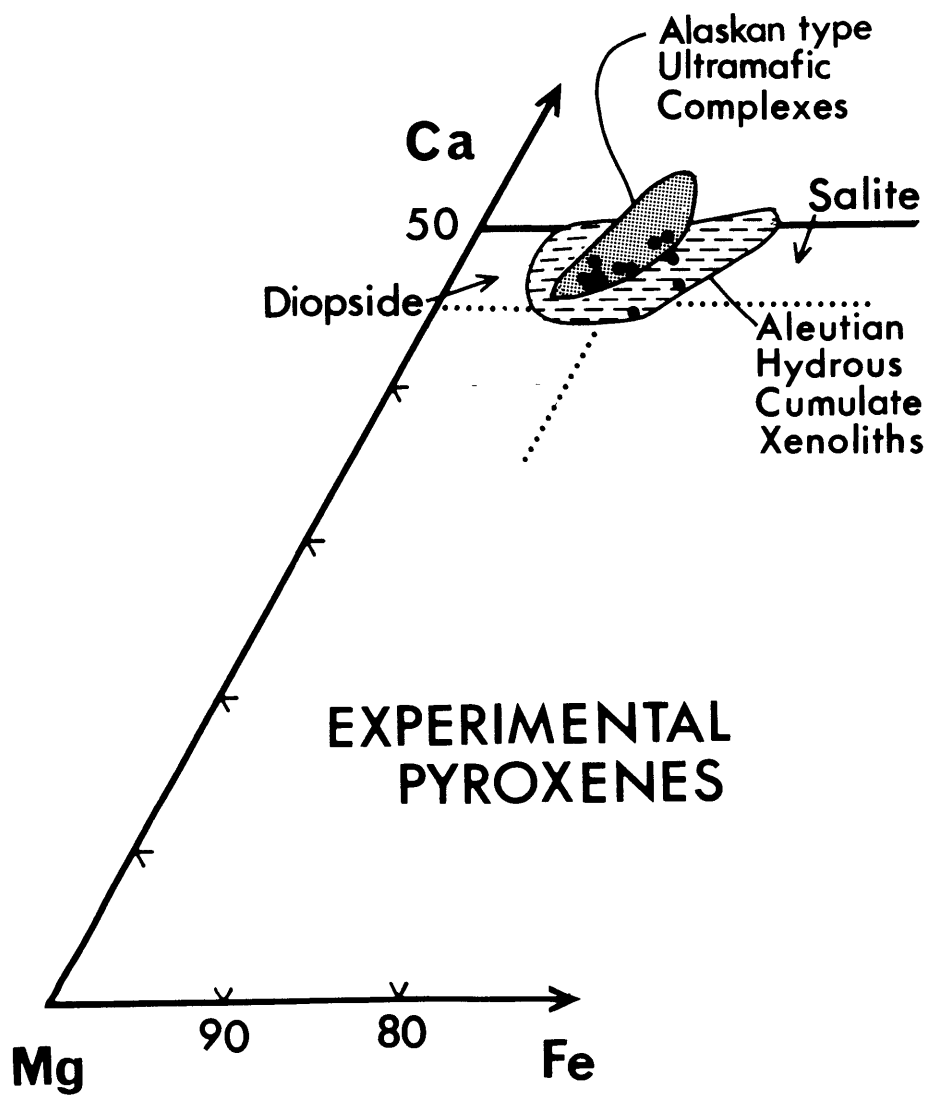


Figure 2-2. Comparison of (total) Fe/Mg (molar) in experimental high-Ca pyx and coexisting liquid (glass). Common high-Ca pyx with moderate to low-Al₂O₃ is more Mg-rich than coexisting high-Ca pyx with high-Al₂O₃. The (common) high-Ca pyx-liquid pairs have an exchange K_D of 0.23, equal to that found in 1 atm pressure experiments (Grove and Bryan, 1983).

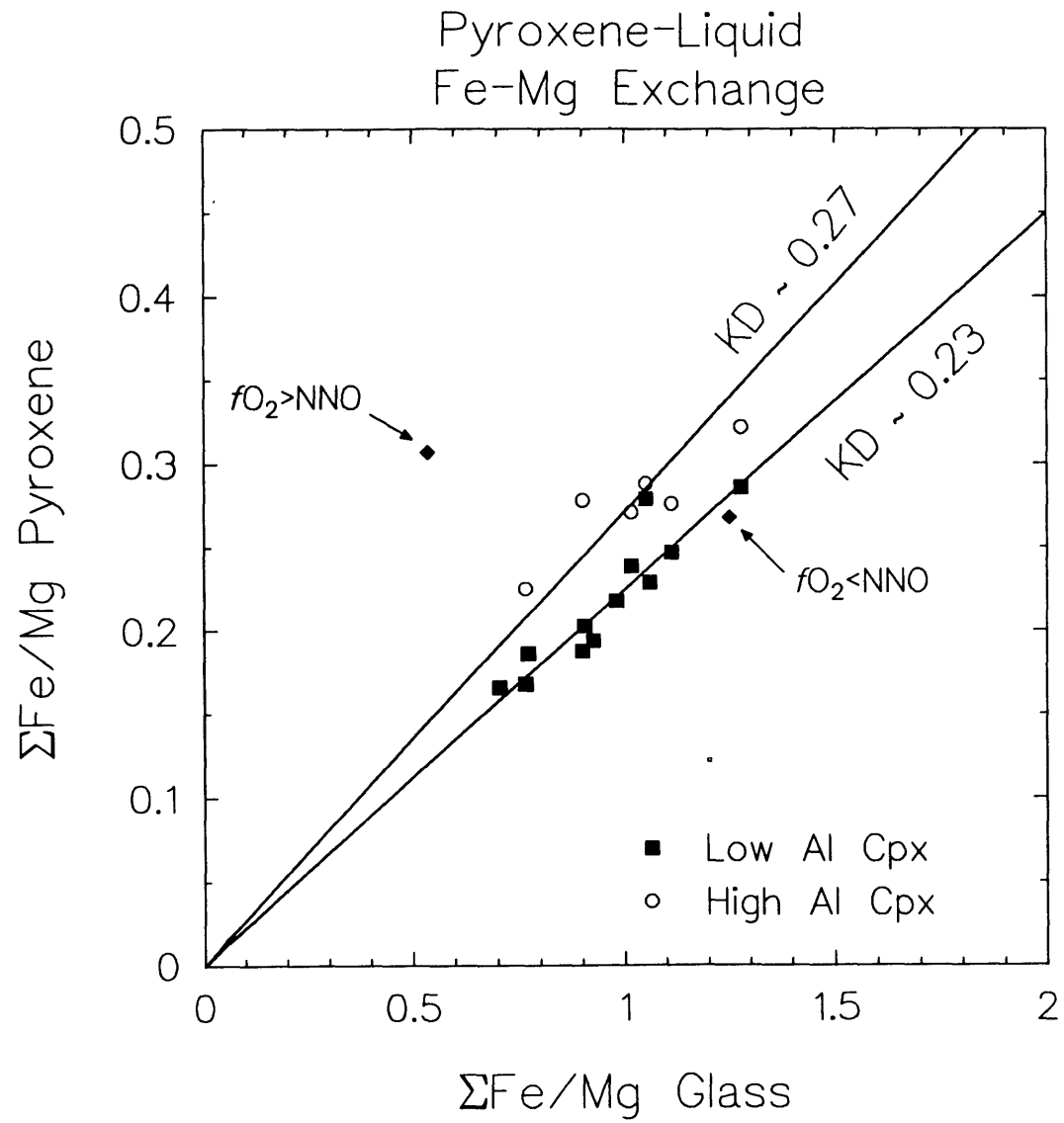


Figure 2-3. Comparison of (total) Fe/Mg (molar) in experimental oliv and coexisting liquid (glass). Most oliv-liquid pairs have an exchange K_D near 0.29, close to that observed in 1 atm pressure experiments (Roeder and Emslie, 1970).

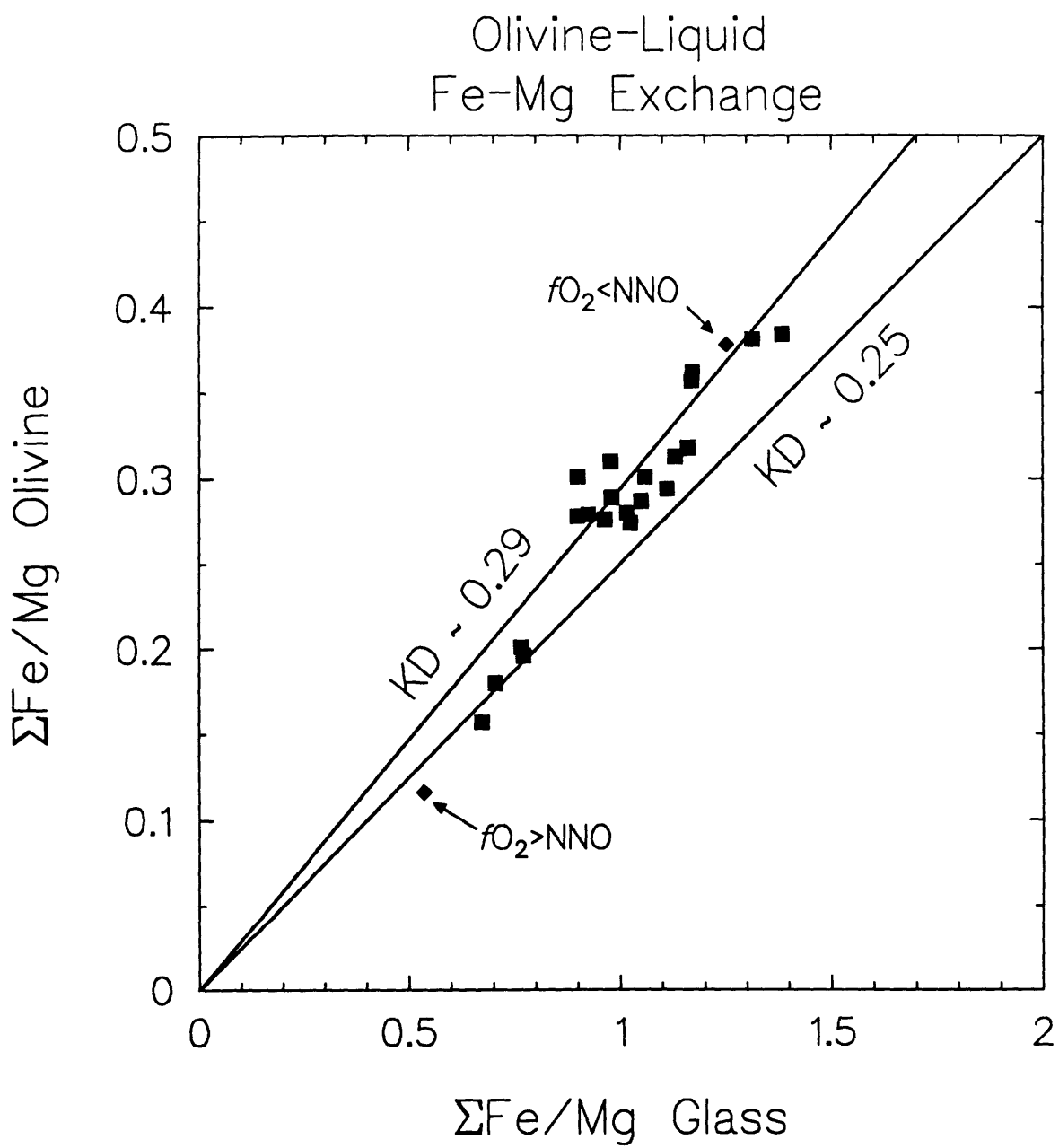


Figure 2-4. A. Comparison of Ca/Na (molar) in experimental plag and coexisting glass. 2 kb water-saturated experiments (this study, table 4 and appendix 1) are represented as squares. The exchange K_D $(Ca/Na)_{plag}/(Ca/Na)_{liq}$ is ~5.5. Comparable results for experiments on HABs with ~2 wt.% H₂O at 2 and 5 kb (Baker and Eggler, 1987) are represented as solid circles. Only liquids with SiO₂ < 62 wt.% (analyses normalized to total 100 %) are shown for the low water content experiments. The 2 wt.% H₂O experiments have a Ca-Na exchange K_D between plag and liquid of 1.3-2.0.

B. Experimental Ca-Na exchange K_D between plag and liquid for anhydrous experiments, compiled from the literature, and plotted against experimental pressure. The 1 atm Ca-Na exchange K_D between plag and basalt liquid (not shown) is near 1.0 (Grove et al., 1990). Data from Meen (1987), Baker and Eggler (1987), Johnston (1986), Bartels et al. (1991), and Kinzler and Grove (1991).

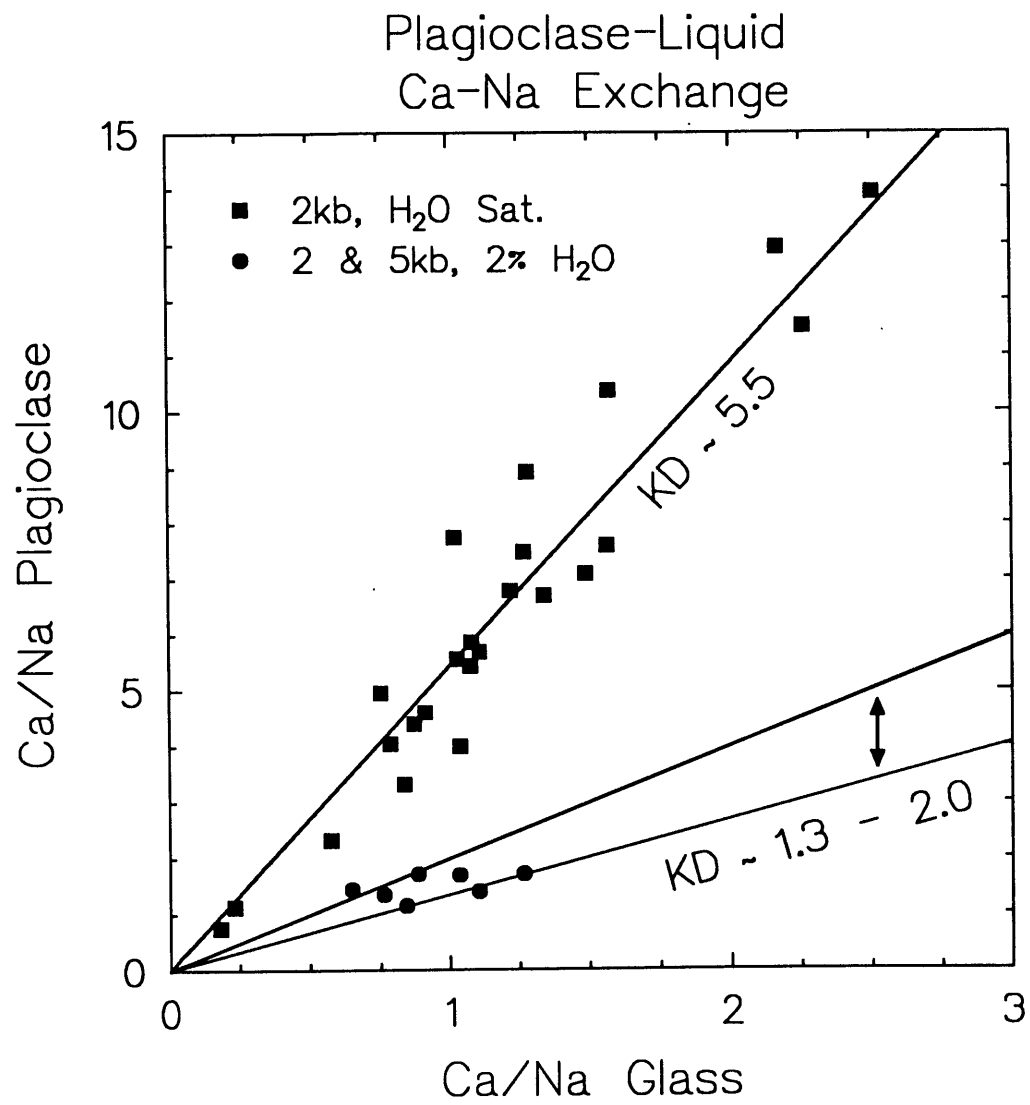


Figure 2-4a.

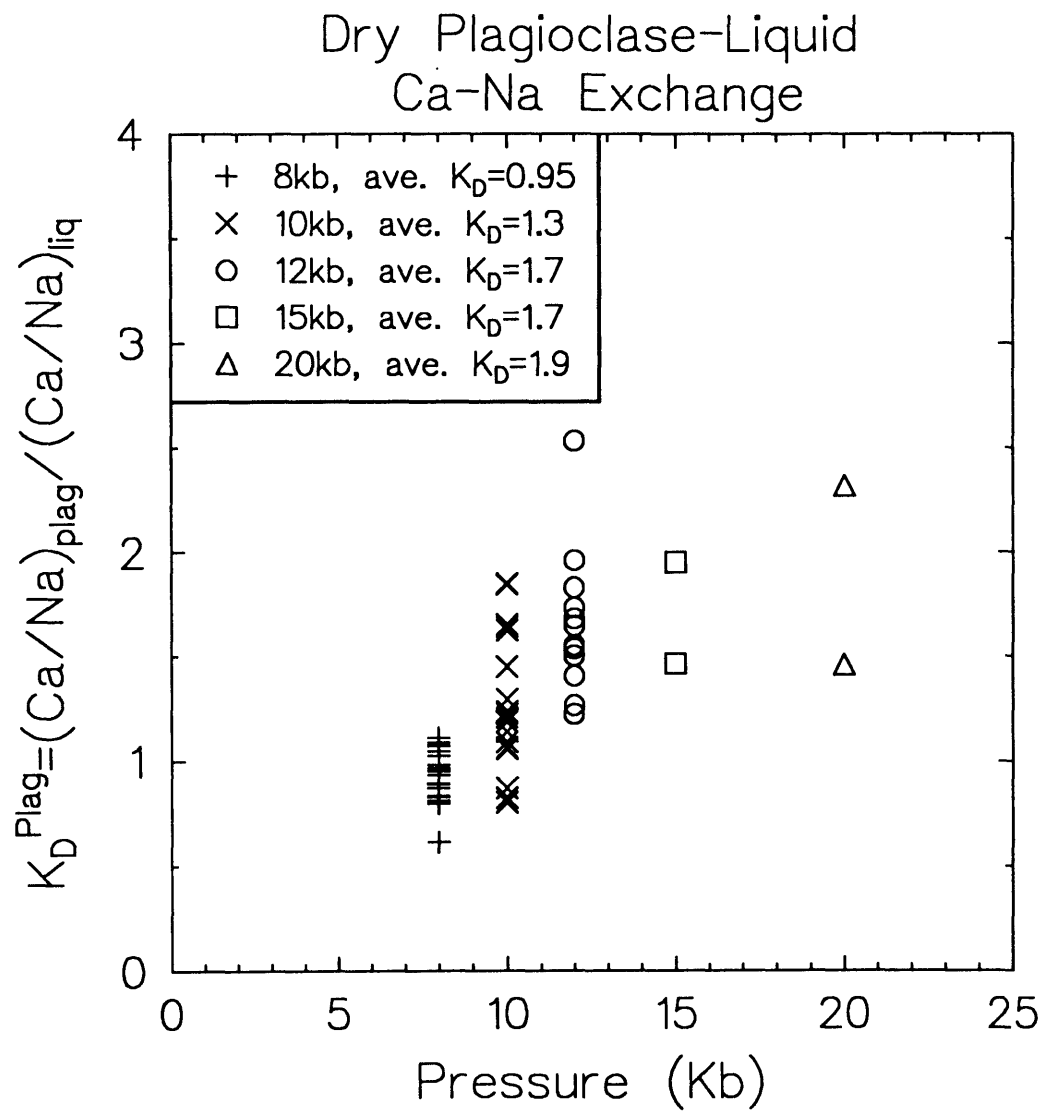


Figure 2-4b.

Figure 2-5. Comparison of trivalent and divalent cation ratios in experimental spinel minerals and natural rocks. Cr-Al-Mg spinels produced at 1050 °C, Ni-NiO in composition 79-35g are represented as inverted triangles. Mg-Al rich magnetites produced at lower temperatures are represented as open diamonds. Magnetite from experiments not buffered at Ni-NiO are represented as filled circles. Hatchured area encompasses spinels found as microphenocrysts in arc volcanic rocks. Shaded area represents compositions of spinels from Alaskan-type ultramafic complexes, and dashed line is the upper limit of spinel compositions from large layered, massif, and xenolithic ultramafics (fields after Conrad and Kay (1983) and Beard and Borgia (1989)).

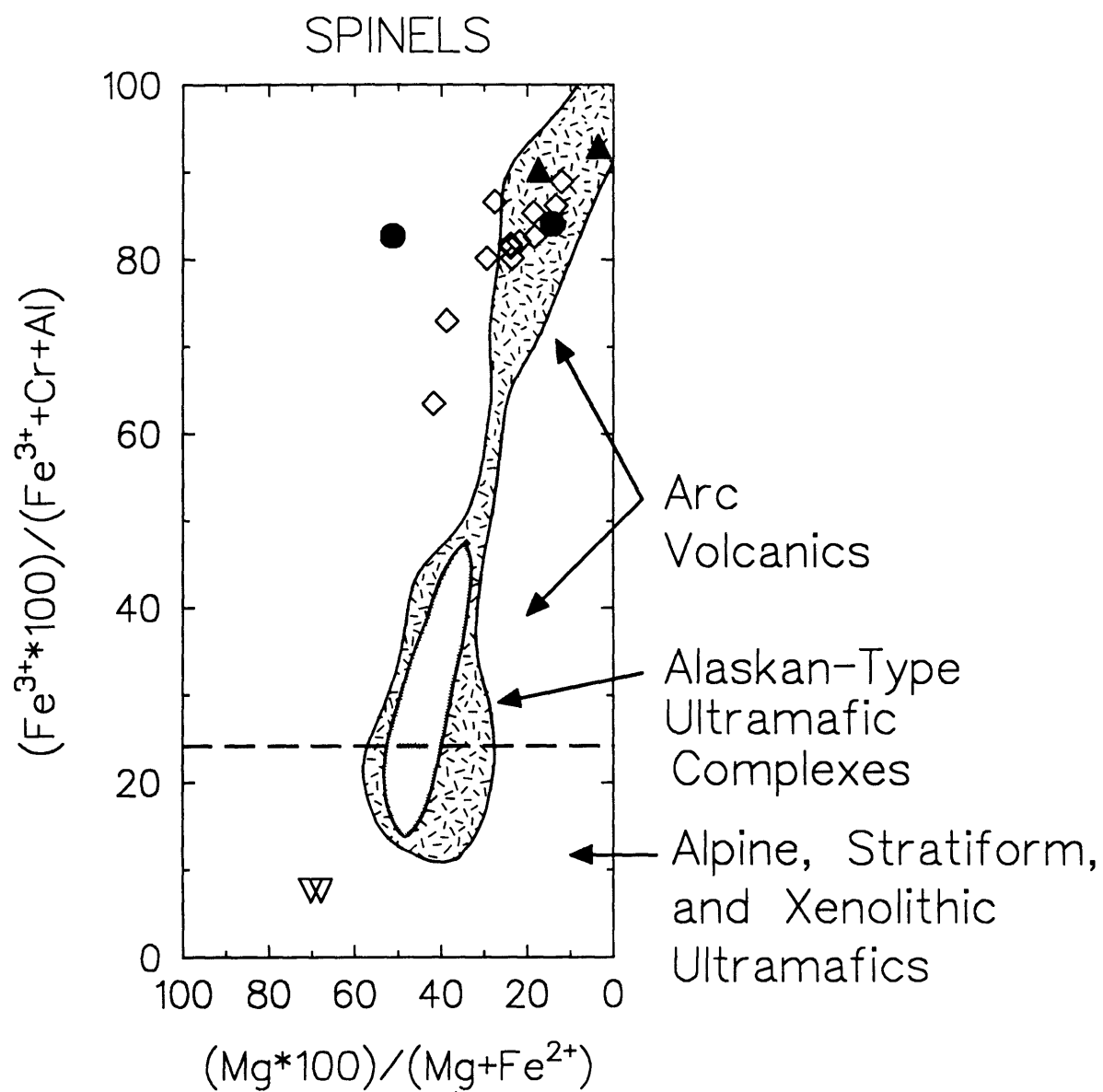


Figure 2-6 A. Comparison of Al/Si (molar) in hbl and coexisting liquid (glass or matrix). Results for experiments at 2 kb water-saturated on extrusive and intrusive mafic rocks and modified compositions are represented as filled diamonds, on a granodiorite as inverted triangles (appendix 1), and for naturally-formed phenocrysts and liquid as split circles (appendix 2). Al and Si show consistent exchange partitioning with an exchange K_D $(\text{Al/Si})_{\text{hbl}}/(\text{Al/Si})_{\text{liq}}$ of 0.94.

B. $\text{Al/Si}_{\text{hbl}}$ vs. $\text{Al/Si}_{\text{liq}}$ for other experimental studies at a variety of pressures, water contents, and oxygen buffers (Helz 1973, 1976; Cawthorn et al. 1973; Nicholls and Harris 1980; Allen and Boettcher 1983; Green and Pearson 1985; Rutherford et al. 1985; Naney 1988; Johnson and Rutherford 1989).

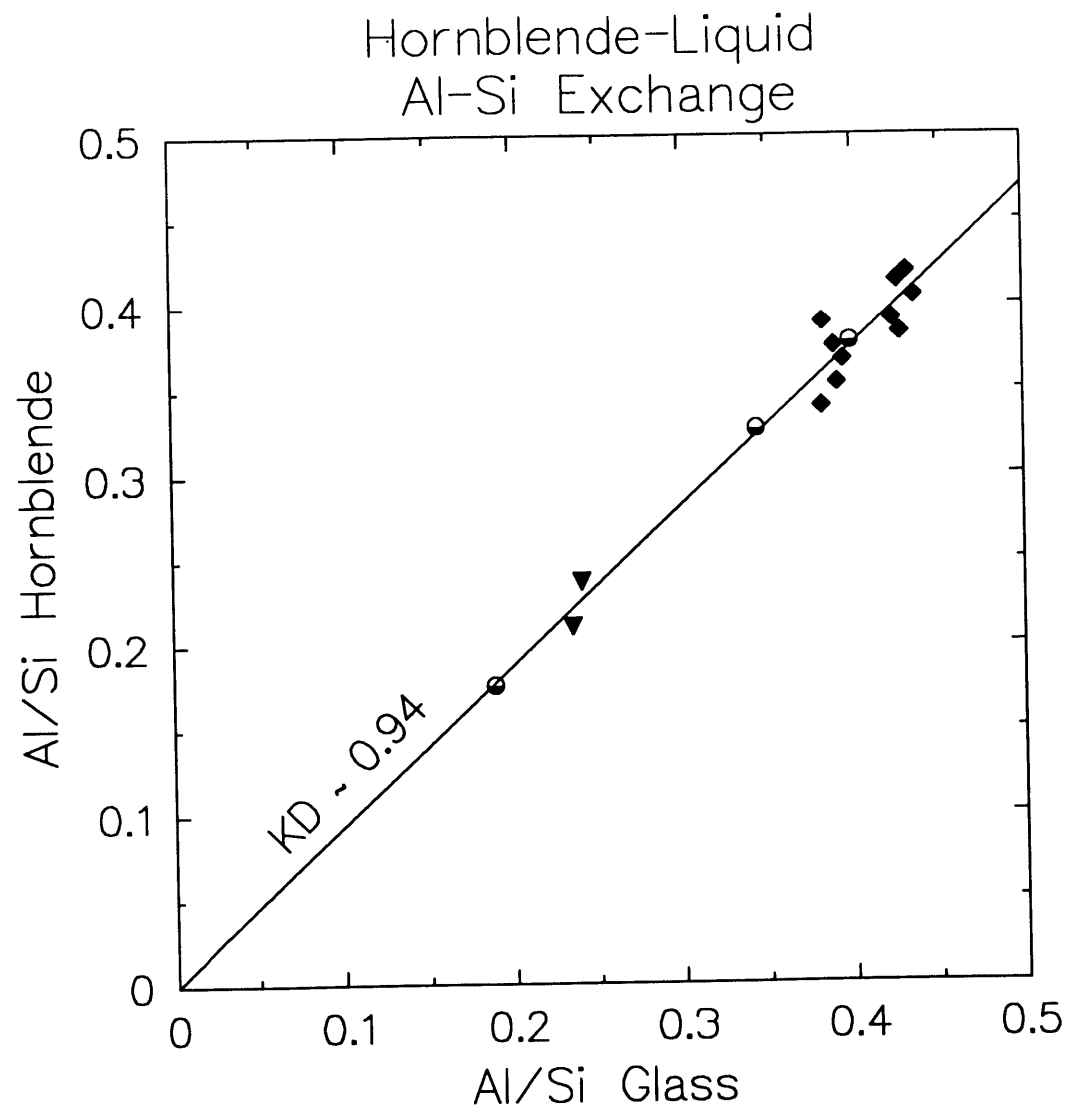


Figure 2-6a.

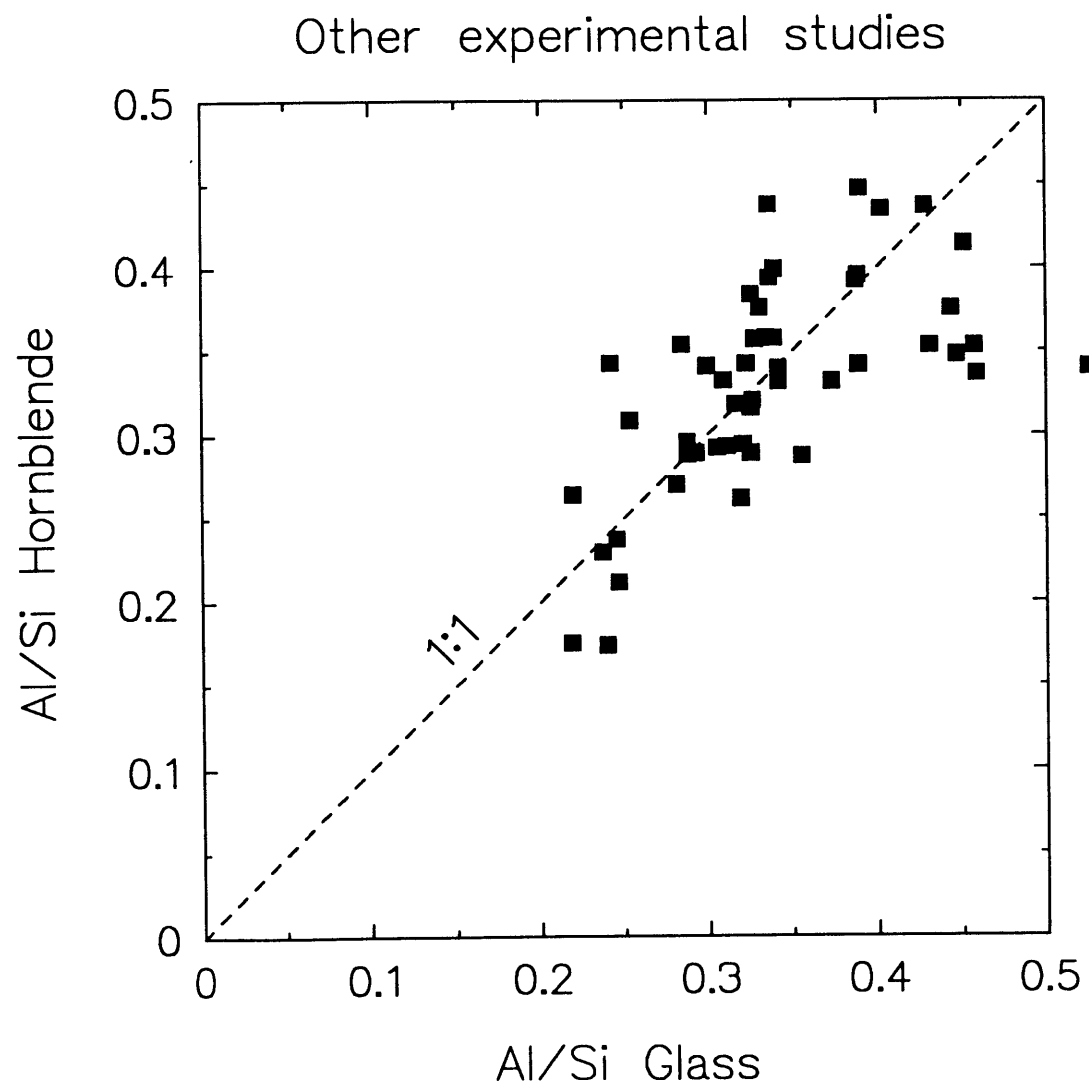


Figure 2-6b.

Figure 2-7. Comparison of Fe/Mg (molar) in hbl and coexisting liquid (glass or matrix). Symbols as in figure 11. Fe and Mg are exchanged with a K_D of ~ 0.38 - 0.30 in basalt and andesite liquids, but the exchange K_D drops to low values in more silica-rich liquids (inset).

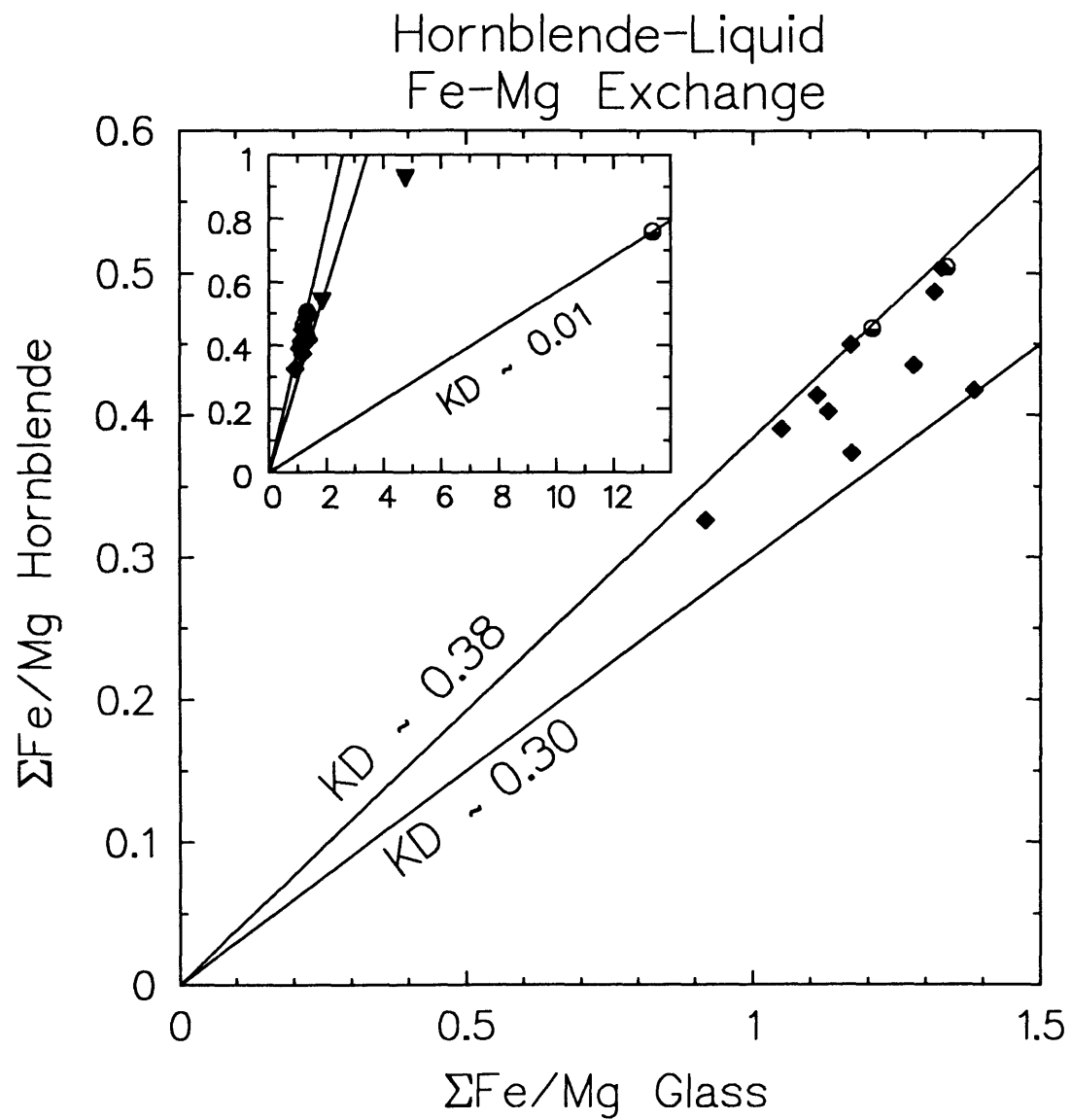


Figure 2-8. 2 kb water-saturated experimental liquids projected on a total alkalis - total iron (FeO*) - MgO ternary (weight units). Curve separates the fields of tholeiitic (TH) and calc-alkaline (CA) suites as defined by Irvine and Baragar (1971). Liquids produced in experiments at Ni-NiO on HAB 79-35g are represented as solid circles, on HAB 82-62 as inverted triangles, on high alumina basalt 82-66 as open diamonds, on hornblende gabbro 87S35a as solid triangles, and on diorite 85S52b + An⁸⁰ as open squares. A single experiment at $fO_2 >$ Ni-NiO on 79-35g is represented by an open circle, and an experiment at $fO_2 <$ Ni-NiO on 82-66 is represented by a filled diamond.

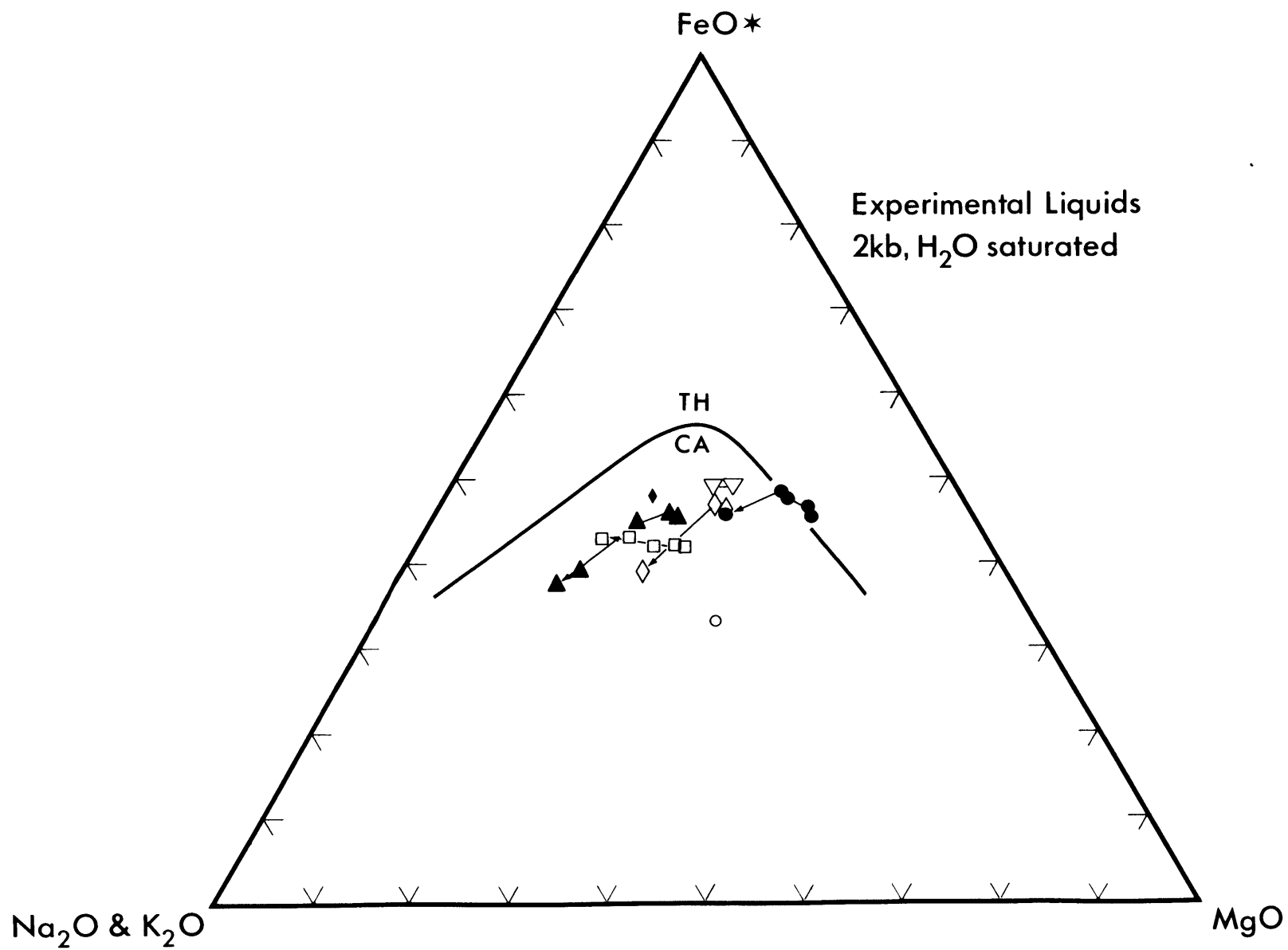


Figure 2-9. 2 kb water-saturated experimental liquids projected on the FeO^*/MgO vs. SiO_2 variation diagram ($\text{FeO}^* = \text{total Fe as FeO}$). The tholeiitic (TH) vs. calc-alkaline (CA) dividing line is from Miyashiro (1974). Liquids produced at Ni-NiO on 79-35g are represented as solid circles, on 82-62 as inverted triangles, on 82-66 as open diamonds, on hornblende gabbro 87S35a as filled triangles, and on diorite 85S52b + An^{80} as filled squares.

General trends followed by tholeiitic or calc-alkaline rock suites are depicted as shaded arrows and are after Grove and Kinzler (1986).

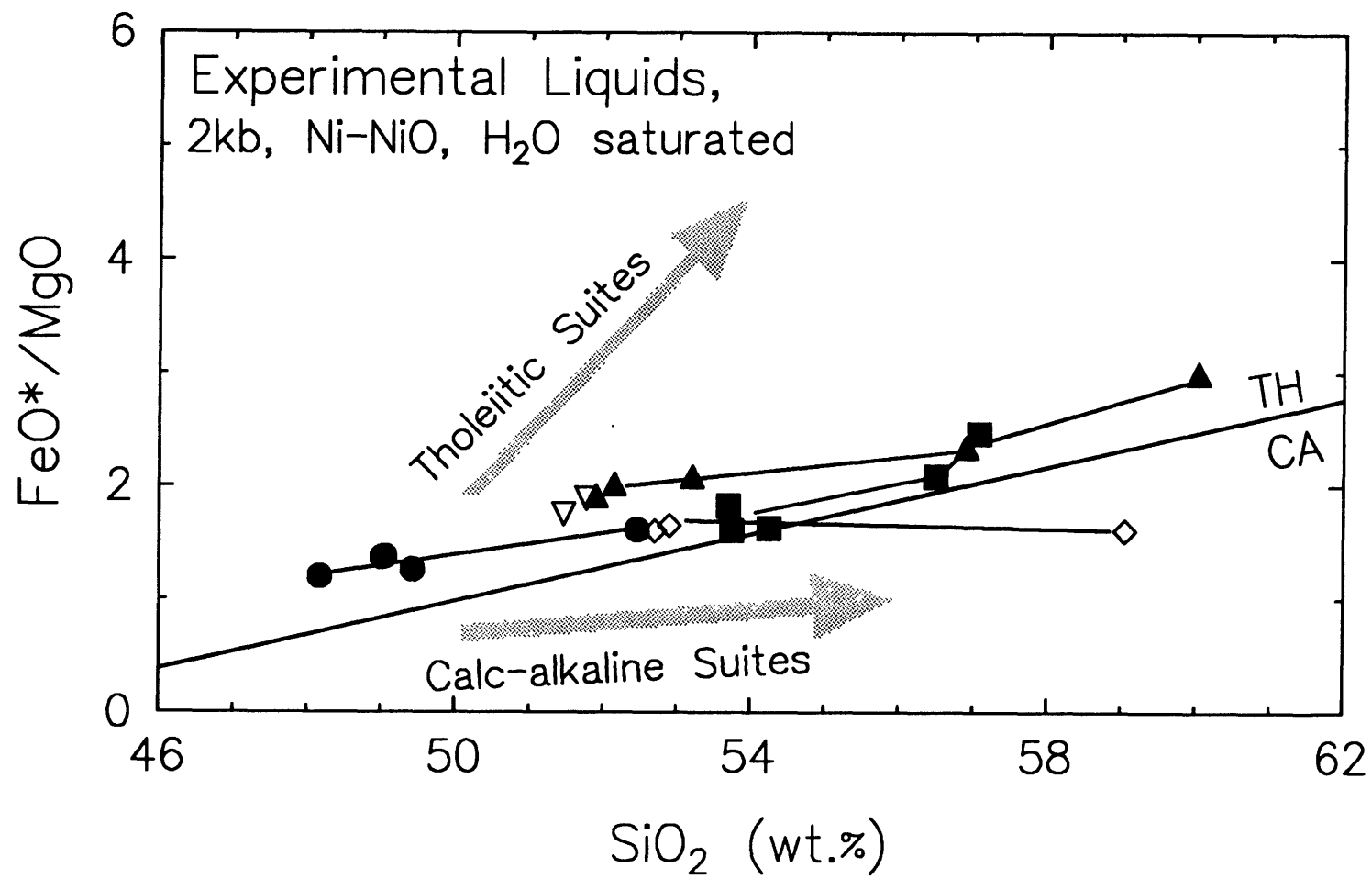


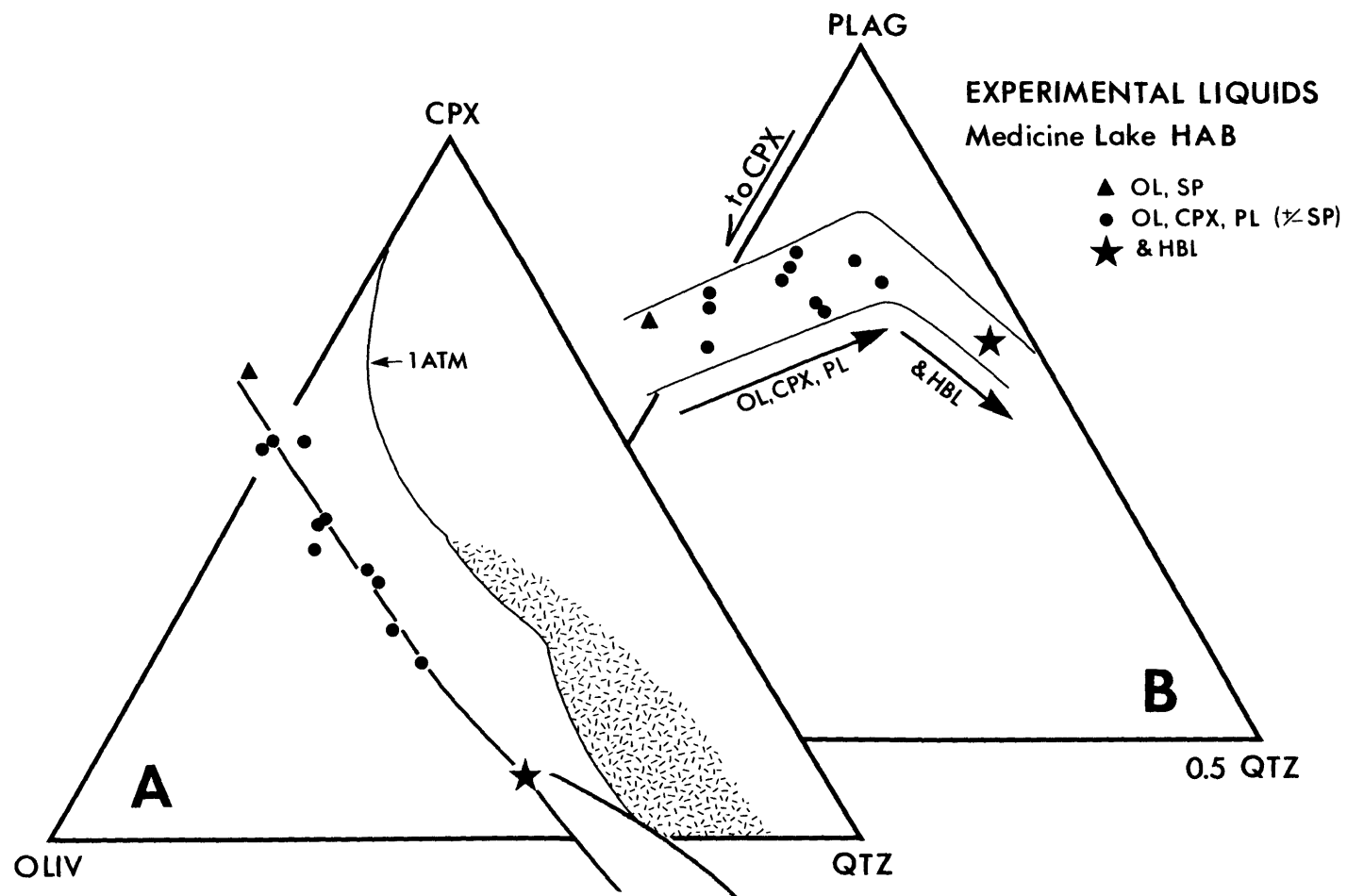
Figure 2-10. Pseudo-ternary projections of experimental liquids produced at 2 kb water-saturated, Ni-NiO buffered. The projection scheme of this and following diagrams is that of Tormey et al. (1987) and uses mineral components normalized to constant oxygen units. This and following diagrams are projections from apatite, orthoclase, and an oxide component (magnetite+ilmenite+chromite). Fe_2O_3 in liquids has been estimated using the expression of Sack et al. (1980).

A. Subprojection from plagioclase (PLAG) of liquids produced in experiments on HABs onto the olivine (OLIV), high-calcium pyroxene (CPX), quartz (QTZ) plane. Liquids saturated with oliv, high-Ca pyx, and plag (+/- a spinel) define a multiple saturation boundary leading from transitional to silica-rich compositions. Shaded area represents the estimated stability field of hbl + plag. 1 atm pressure olivine + pyx + plag multiple saturation boundary is provided for reference (after Walker et al., 1979; Grove et al., 1982). Hatchured area represents the stability field of low-Ca pyx.

B. Subprojection from OLIV onto the CPX, PLAG, QTZ plane, of experimental liquids as in A. Only the area near the PLAG apex is shown.

C. Subprojection from PLAG of liquids produced in experiments on hornblende gabbro and diorite + An⁸⁰. Liquids saturated with oliv, hbl, and plag (+/- a spinel) define a reaction boundary along which oliv and liquid are consumed and hbl is produced. An area inclosing the projected position of experimental hbl is shown and an arrow indicates the direction followed by hbl in successively lower temperature experiments. A corundum-normative liquid lies off of the diagram in the direction indicated by an arrow. Experiment 85S52B-#9 is not plotted because of heterogeneous glass. The positions of 1 atm oliv + pyx + plagioclase and 2 kb oliv + pyx + plag + H₂O multiple saturation boundaries are shown for reference as dotted lines.

D. Subprojection from OLIV onto the CPX, PLAG, QTZ plane, of experimental liquids as in C. Only the area near the PLAG apex is shown. Outline of the area occupied by liquids saturated with oliv + high-Ca pyx + Ca-plag + H₂O and oliv + high-Ca pyx + Ca-plag + hbl + H₂O (both +/- spinel) is provided for reference.



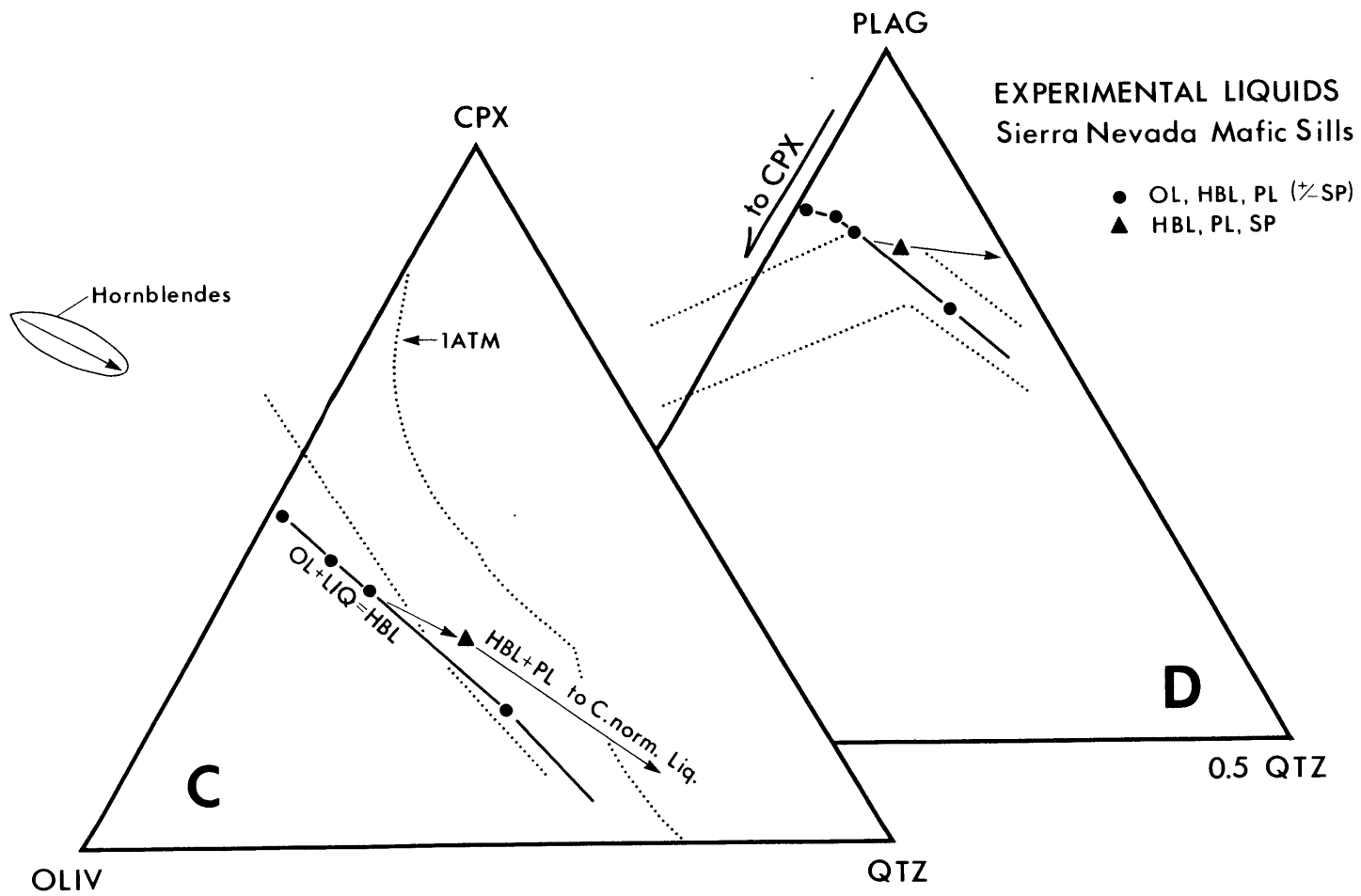


Figure 2-11. Pseudo-ternary projections of liquid and minerals produced at 965 °C in basalt 82-66 illustrating the hbl-in reaction. Multiple saturation boundaries defined by experiments on this and other HABs are also shown.

A. Projection from PLAG (Anorthite+Albite).

B. Projection from An⁹⁰, excess albite has been added to the QTZ apex.

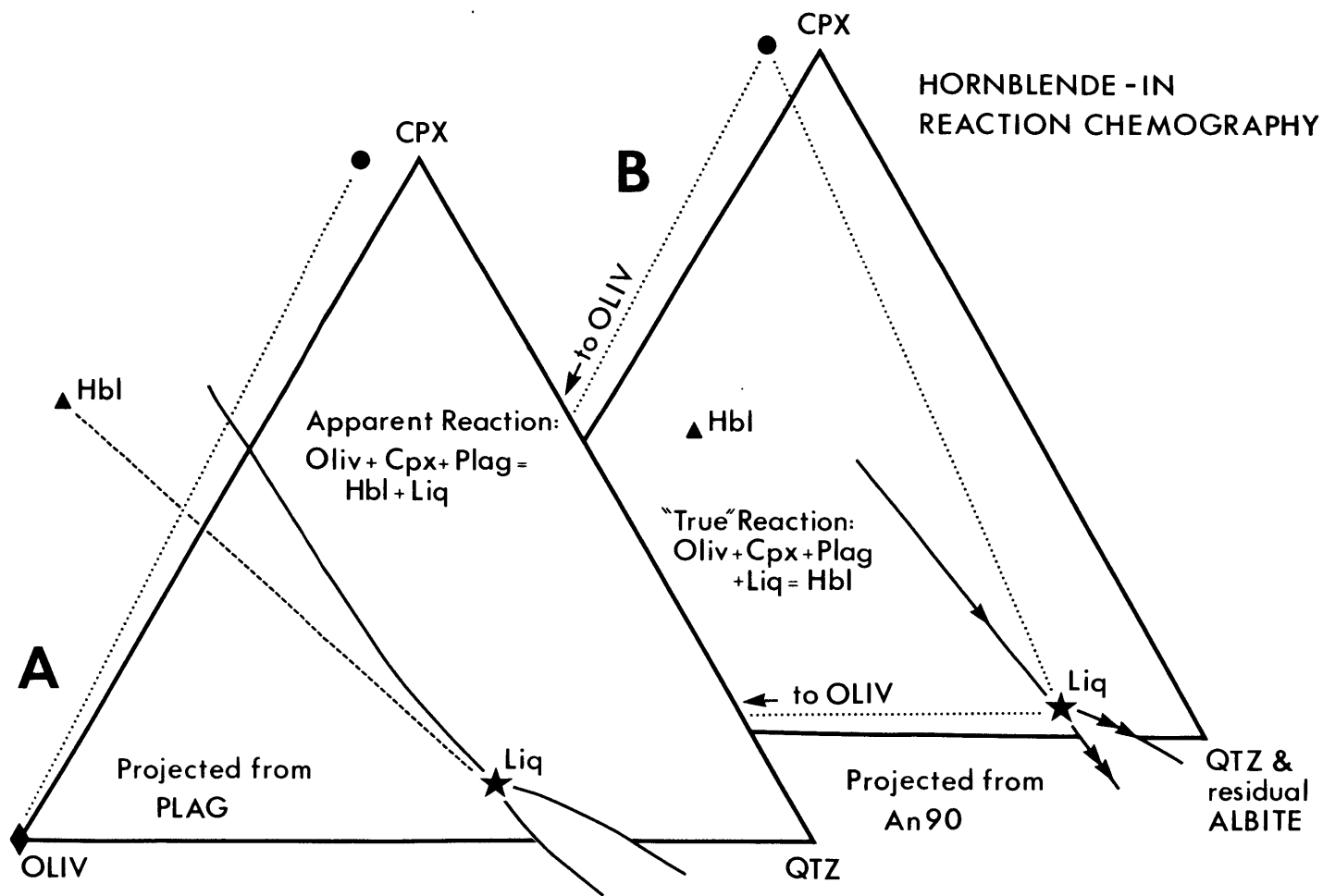


Figure 2-12. Pseudo-ternary projection from PLAG (schematic) illustrating the effect of sodium on hbl stability. Magmas with low- Na_2O do not saturate with hbl (if at all) until liquids reach QTZ-rich compositions. Magmas with high- Na_2O can crystallize hbl before liquids reach QTZ-rich compositions.

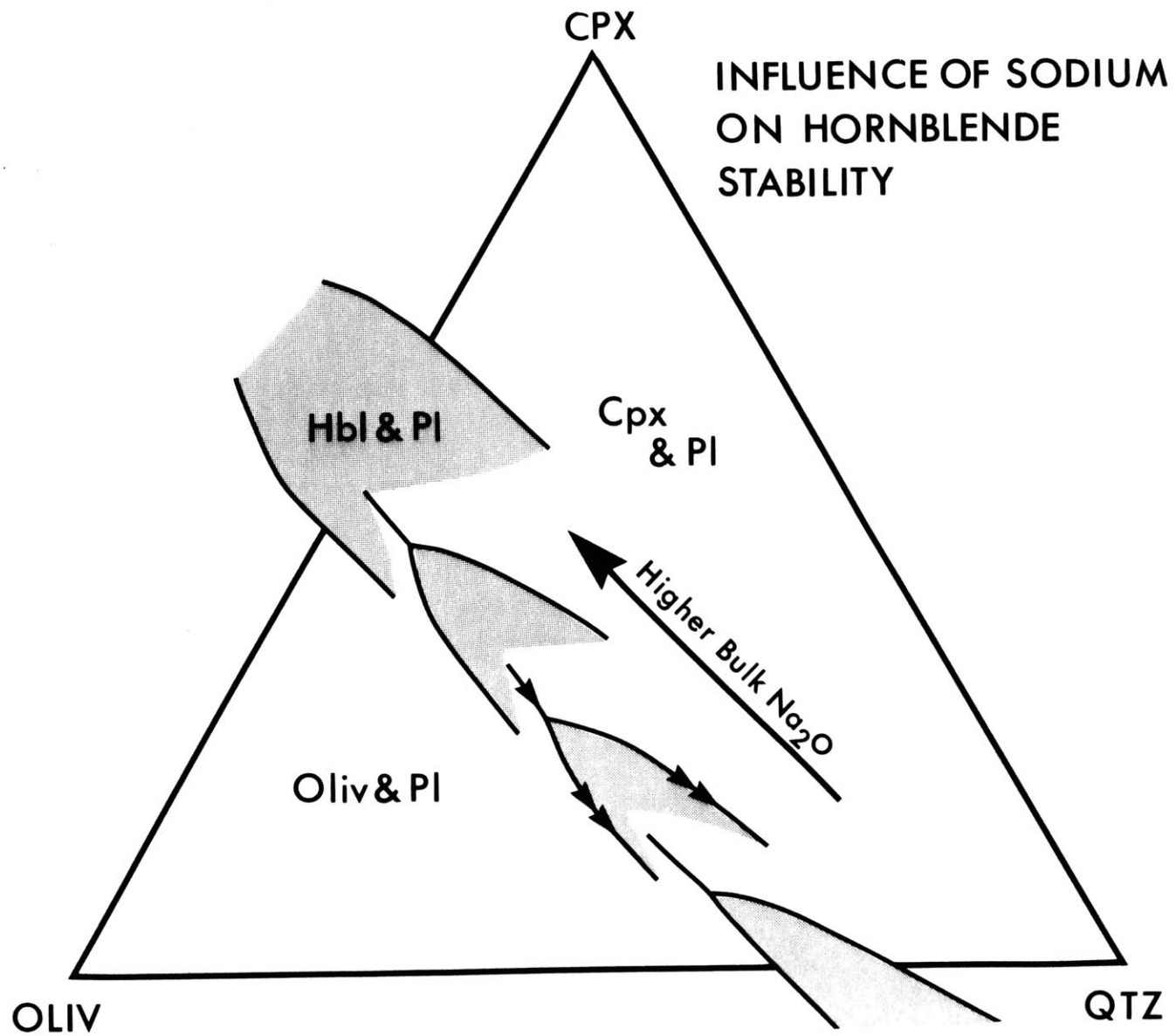


Figure 2-13 A. Experimental (observed) vs. calculated (expected) temperatures for the experiments used to calibrate the multiply-saturated liquid geothermometer. Line represents a 1:1 correspondence.

B. Experimental vs. calculated temperatures for the experiments used to calibrate the olivine-liquid geothermometer. Line represents a 1:1 correspondence. Arrow indicates that high TiO_2 leads to calculated temperatures that are higher than the experimental temperatures.

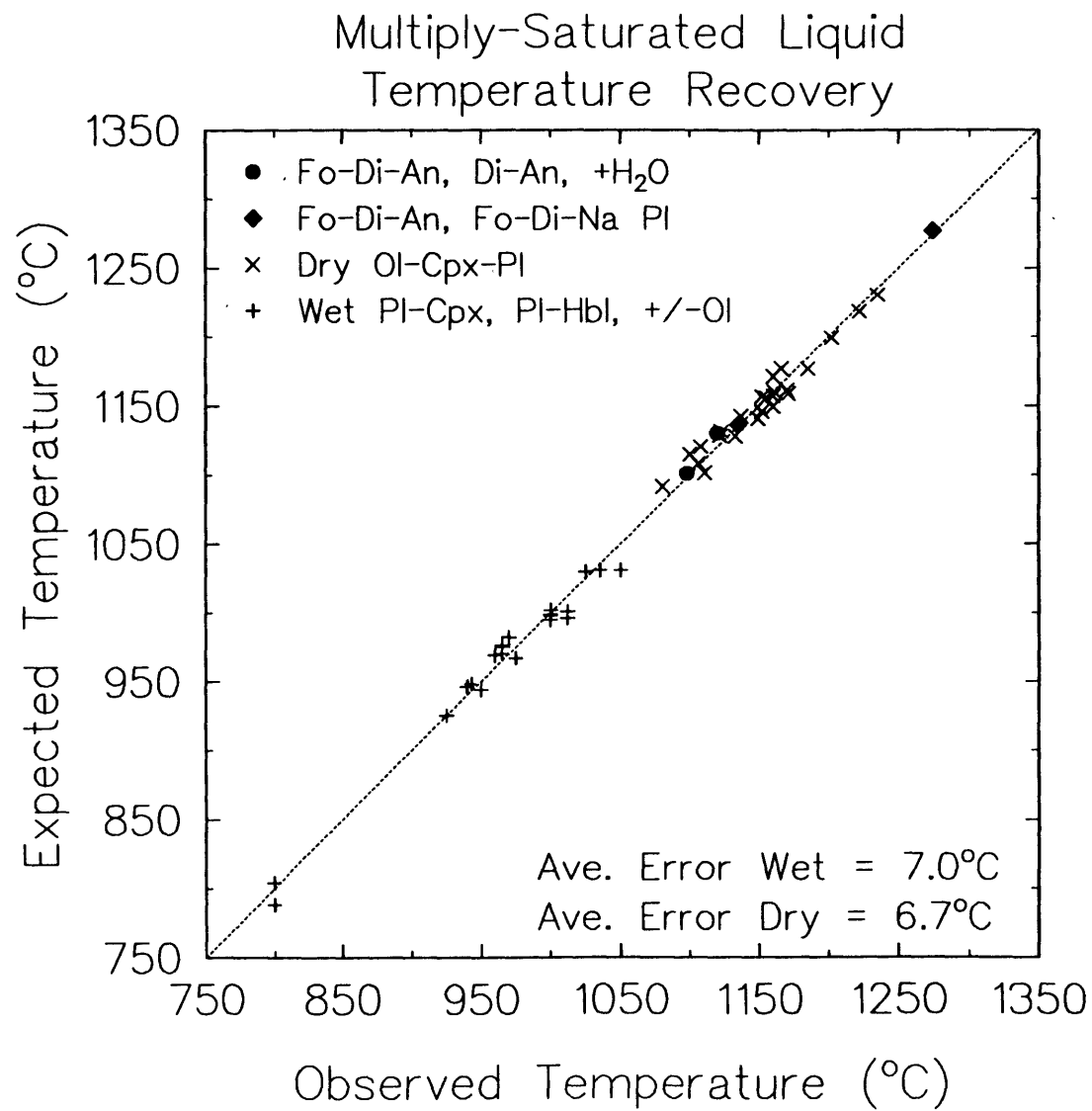


Figure 2-13a.

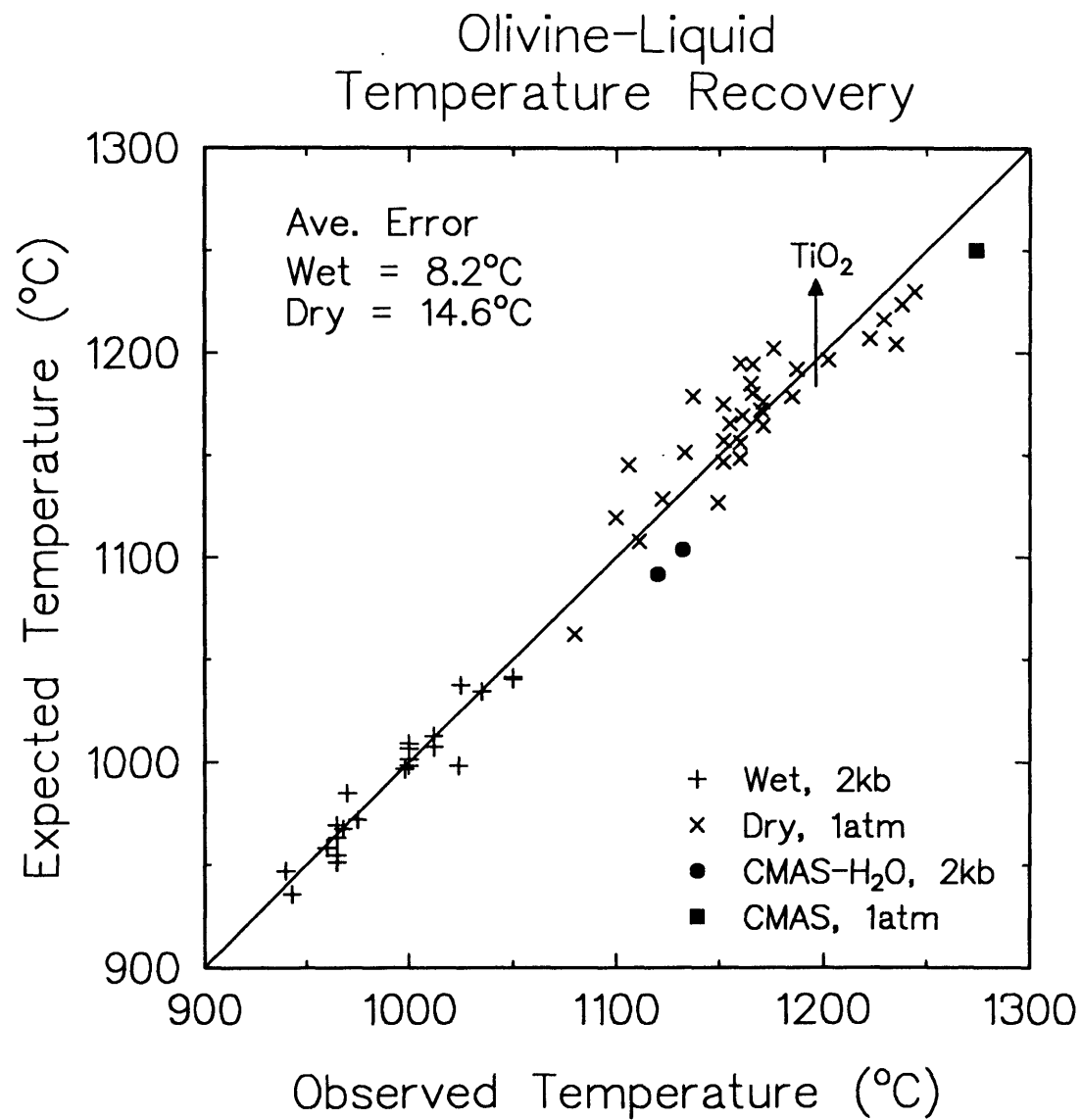


Figure 2-13b.

Figure 2-14. Portion of the critical plane of silica undersaturation showing projected positions of the forsterite - diopside - anorthite piercing point at 1 atm and at 2 kb p_{H_2O} (open and filled diamonds), and projected positions (from QTZ and magnetite) of the highest temperature liquids saturated with oliv + high-Ca pyx + plag (+/- spinel) in HAB 79-35g at 1 atm and 2 kb p_{H_2O} (open and filled circles; Grove et al. 1982, and this study). Dotted lines (schematic) delimit primary liquidus volumes of the phases indicated. Highest temperature multiply-saturated liquids produced in 79-35g lie on or close to the critical plane of silica undersaturation. Lower temperature 2-kb liquids from 79-35g and other HABs saturated with H_2O + oliv + high-Ca pyx + Ca-plag (+/-spinel, hbl) lie within the OLIV-CPX-PLAG-QTZ tetrahedron, and project along the dashed line. Lower temperature 1-atm oliv + high-Ca pyx + plag-saturated experimental liquids from HABs also lie within the tetrahedron but are near-radial to the QTZ apex and thus do not show a comparable shift with decreasing temperature.

INFLUENCE OF pH_2O ON LIQUIDUS VOLUMES

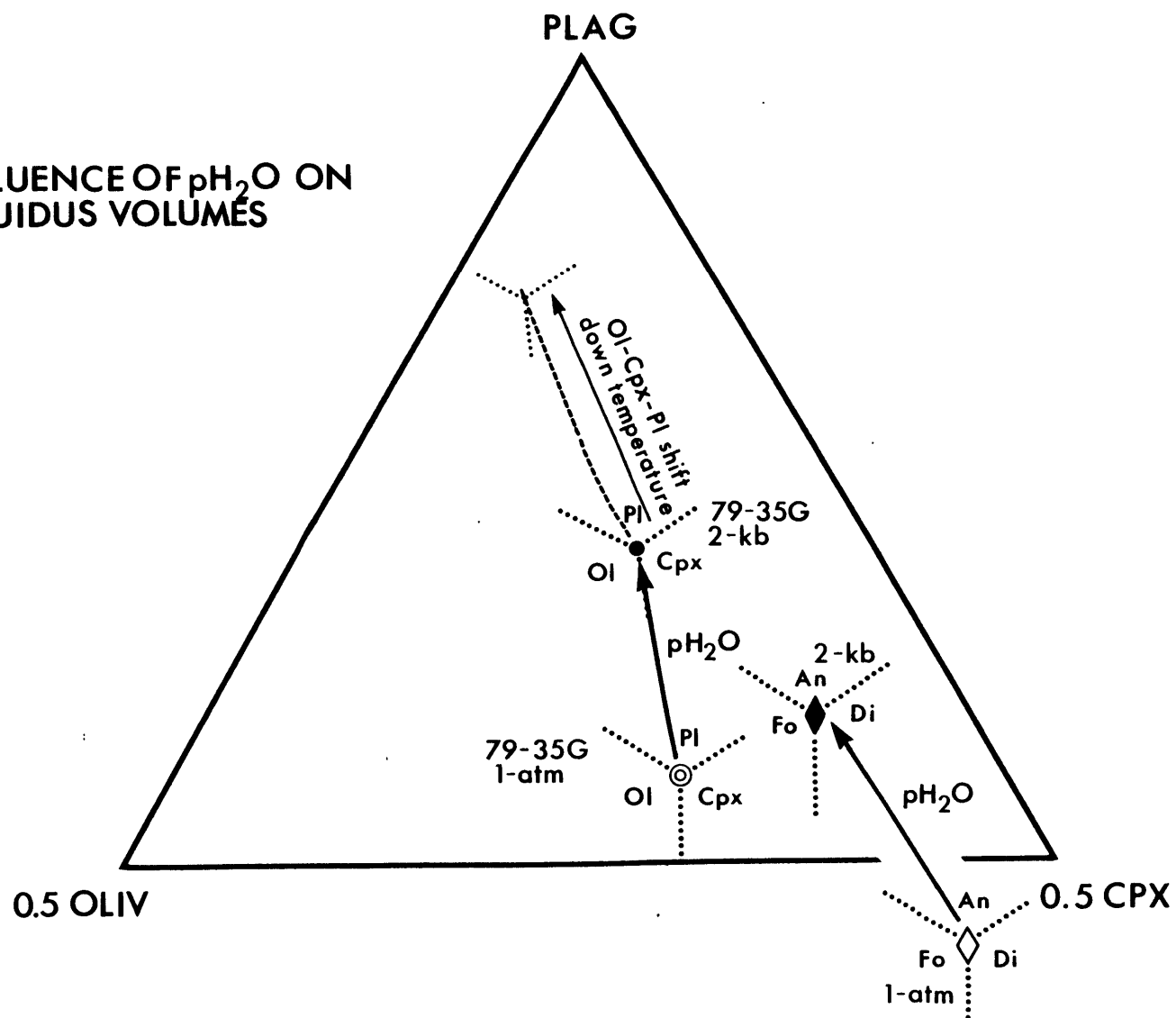


Figure 2-15. Pseudo-ternary projections of multiple saturation boundaries or fields along which oliv, pyx, and plag coexist, and showing the change in projected positions induced by increased pH_2O . 1 atm boundaries after Walker et al. (1979), Grove et al. (1982), and Tormey et al. (1987). 2 kb, $pH_2O=0.7p_{total}$ boundary constructed from experimental data on DO-8 basalt presented by Spulber and Rutherford (1983).

A. In subprojection from PLAG, increased pH_2O moves the oliv + high-Ca pyx + plag (+/- spinel) boundary toward the OLIV apex, and eliminates the stability field of low-Ca pyx (L-Px).

B. In subprojection from QTZ, increased pH_2O shifts the boundaries or fields toward the OLIV-PLAG-QTZ plane and to a lesser extent toward the PLAG apex.

C. In subprojection from OLIV, increased pH_2O moves the fields toward the PLAG apex (kink in water-saturated field results from the onset of hbl crystallization).

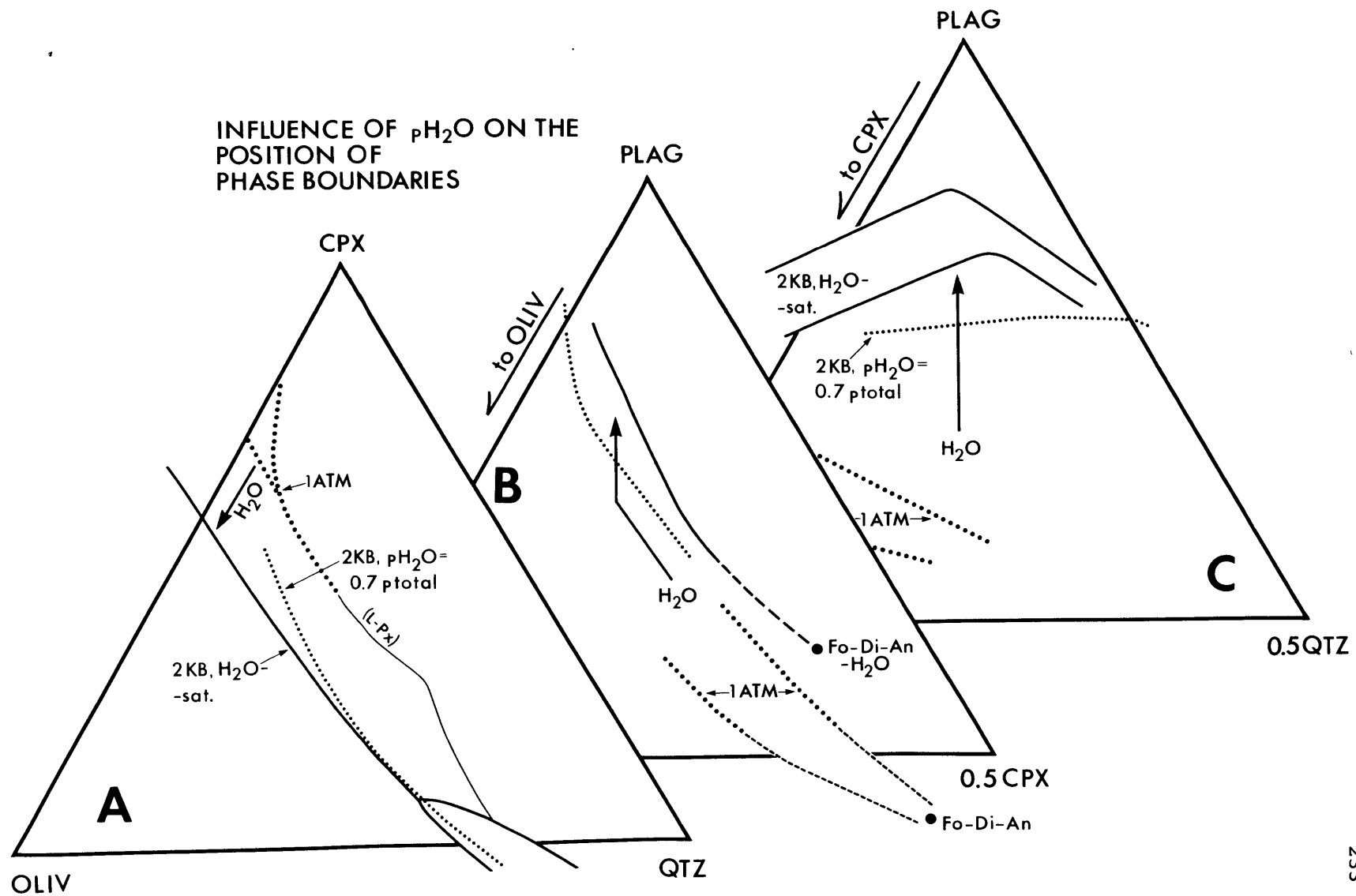


Figure 2-16. Comparison of HABs, BAs, and associated MgO-rich basalts from the Aleutian magmatic arc with multiple saturation boundaries at moderate and high water contents. Aleutian rocks have been divided into compositions with greater or less than 19 wt.% Al_2O_3 for clarity of presentation. Highest alumina volcanics lie along or near to oliv + hbl + Ca-plag + H_2O or oliv + high-Ca pyx + Ca-plag + H_2O (both +/-spinel) multiple saturation boundaries. A. Subprojection from PLAG. B. Subprojection from QTZ. C. Subprojection from OLIV.

ALEUTIAN HAB & BA ($\text{SiO}_2 < 56$, $\text{Al}_2\text{O}_3 > 17$)
and associated Mg-Basalts

○ $\text{Al}_2\text{O}_3 < 19$; × $\text{Al}_2\text{O}_3 > 19$

— 2KB OL, HBL, PL, H_2O

- - - 2KB OL, CPX, PL, H_2O

..... 2KB OL, CPX, PL,
 $\text{pH}_2\text{O} = 0.7 \text{ ptotal}$

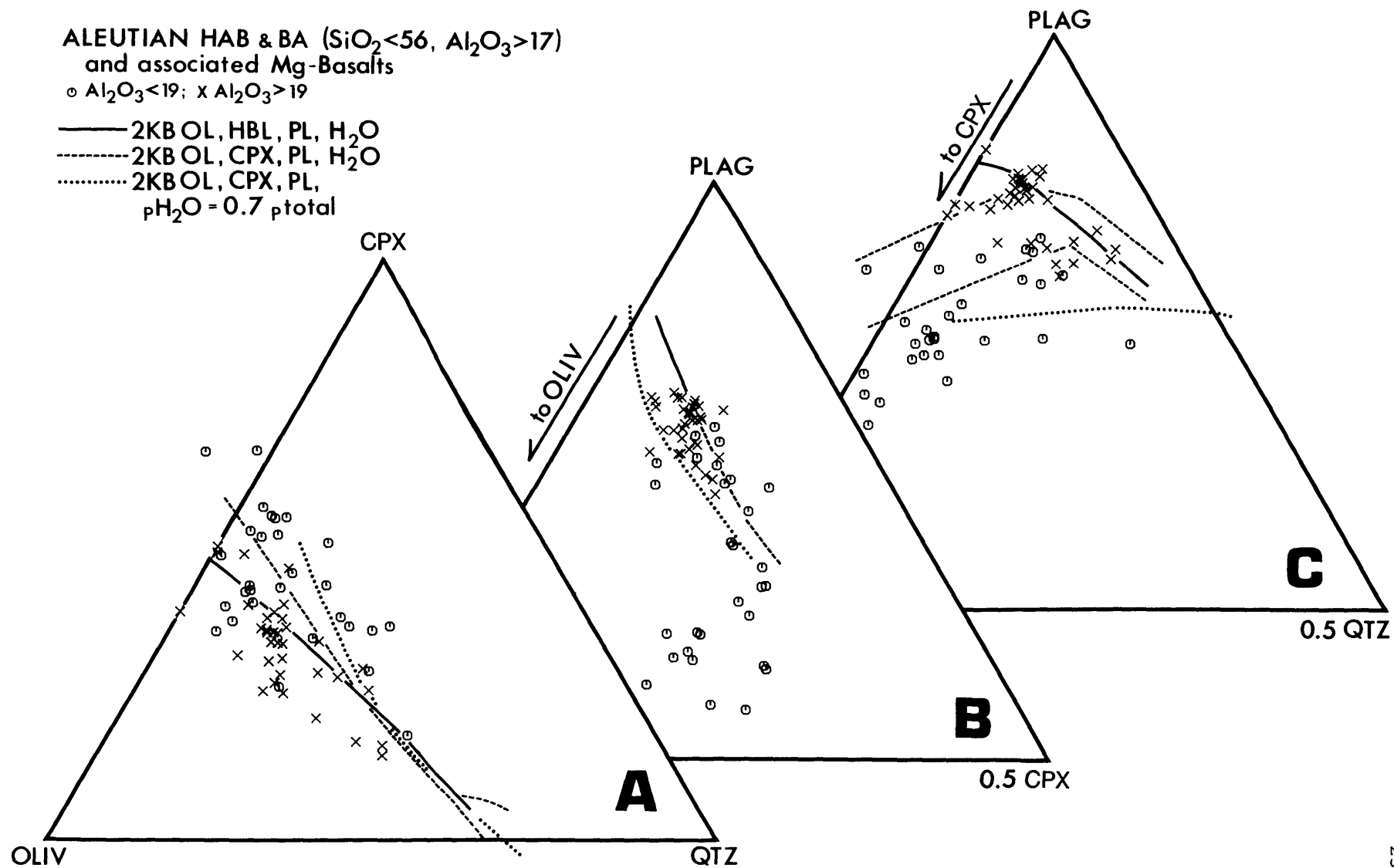


Figure 2-17. Calculated and observed compositions of oliv and plag phenocryst cores for HABs from the Cold Bay volcanic center, Aleutians (Brophy, 1986). Calculations assume that the whole-rocks represent the liquids from which the phenocryst cores grew and use Ca-Na exchange for plag and Fe-Mg exchange for oliv. Results are shown for Ca-Na exchange K_D s appropriate for dry ($K_D \sim 1$), low H_2O ($K_D \sim 1.7$, figure 9A), and water-saturated conditions ($K_D \sim 5.5$). Note that since matrix compositions have lower Ca/Na than whole-rocks (Crawford, Falloon, and Eggins, 1987), calculated plag An content using matrix as liquid will always be lower than that calculated using whole-rock compositions. Fields for minerals from arc intrusives, cumulate inclusions, and volcanics (ARCS) and continental layered intrusions are after Arculus and Wills (1980) and Beard and Borgia (1989).

Olivine and Plagioclase
Cold Bay, Aleutians

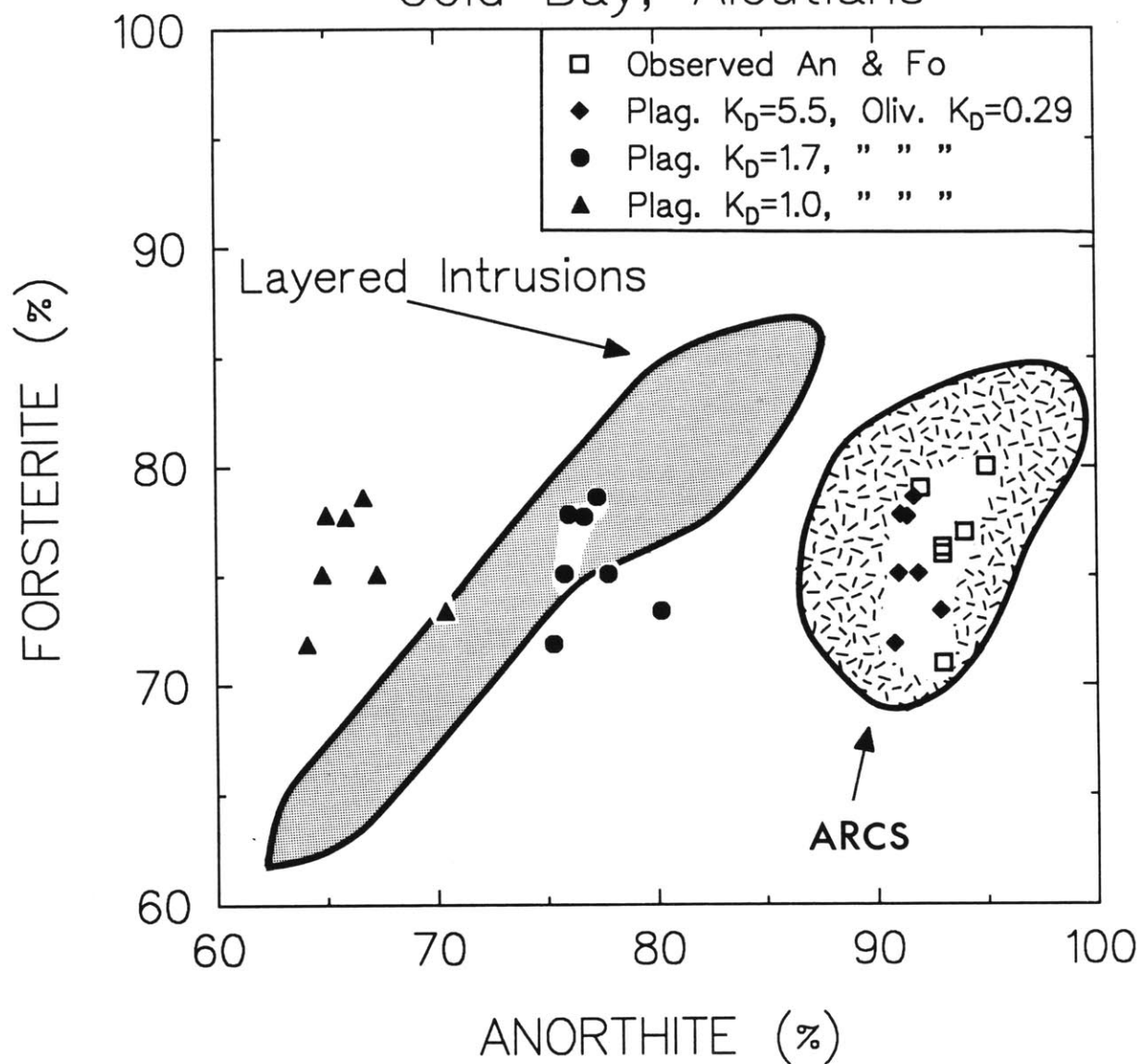


Figure 2-18. Pseudo-ternary subprojection from QTZ of the results of crystal fractionation models (table 7) constructed to match the observed Aleutian magma series (outlined, see also figure 15). Solid dots represent successively lower temperature liquids produced at 8 kb, anhydrous from an MgO-rich Aleutian basalt (starting composition is triangle) by Gust and Perfit (1987).

Models: 1a oliv fractionation from Mg-basalt host for ultramafic xenoliths (square) to $Mg\#_{liq}=62.5$ (diamond), followed by 1b, crystallization of oliv + high-Ca pyx to reach target HAB OK2 (square, model is coincident diamond).

2. Crystallization of oliv from Mg-basalt ID16 (square) to reach target HAB OK2 (square, model is adjacent diamond).

3. Crystallization of oliv + high-Ca pyx from HAB OK2 to reach average Atka HAB (square closest to PLAG apex, model is overlapping diamond).

4a. Crystallization oliv + high-Ca pyx + magnetite from HAB OK2 to $Al_2O_3_{liq}=20\%$ (diamond), followed by 4b, cotectic crystallization of oliv + high-Ca pyx + plag + magnetite to reach average Cold Bay HAB (square, model is adjacent diamond).

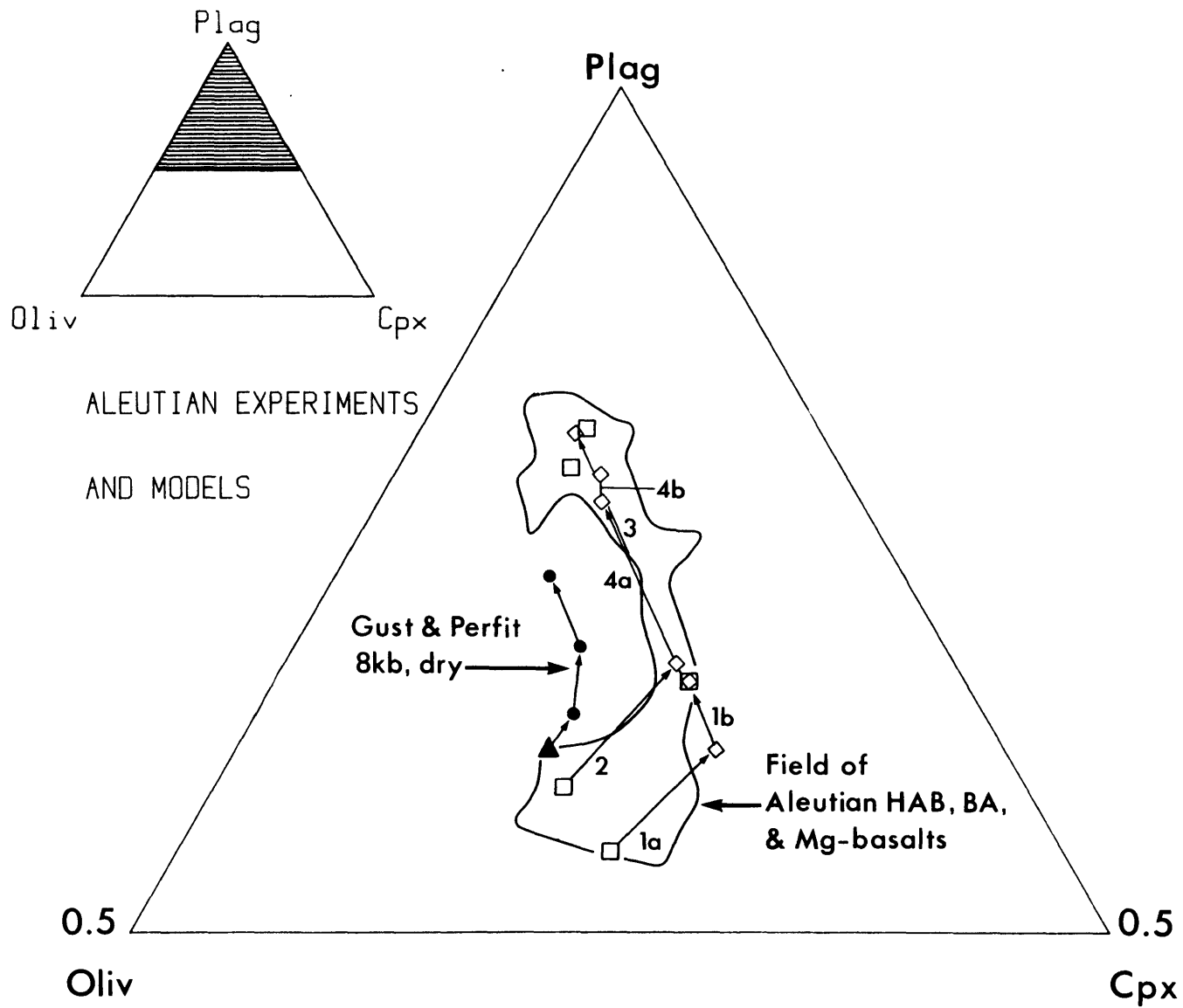


Figure 2-19. Aleutian HABs, BAs, and MgO-rich basalts (stars) and crystal fractionation models (table 7). Model designations as in figure 17.

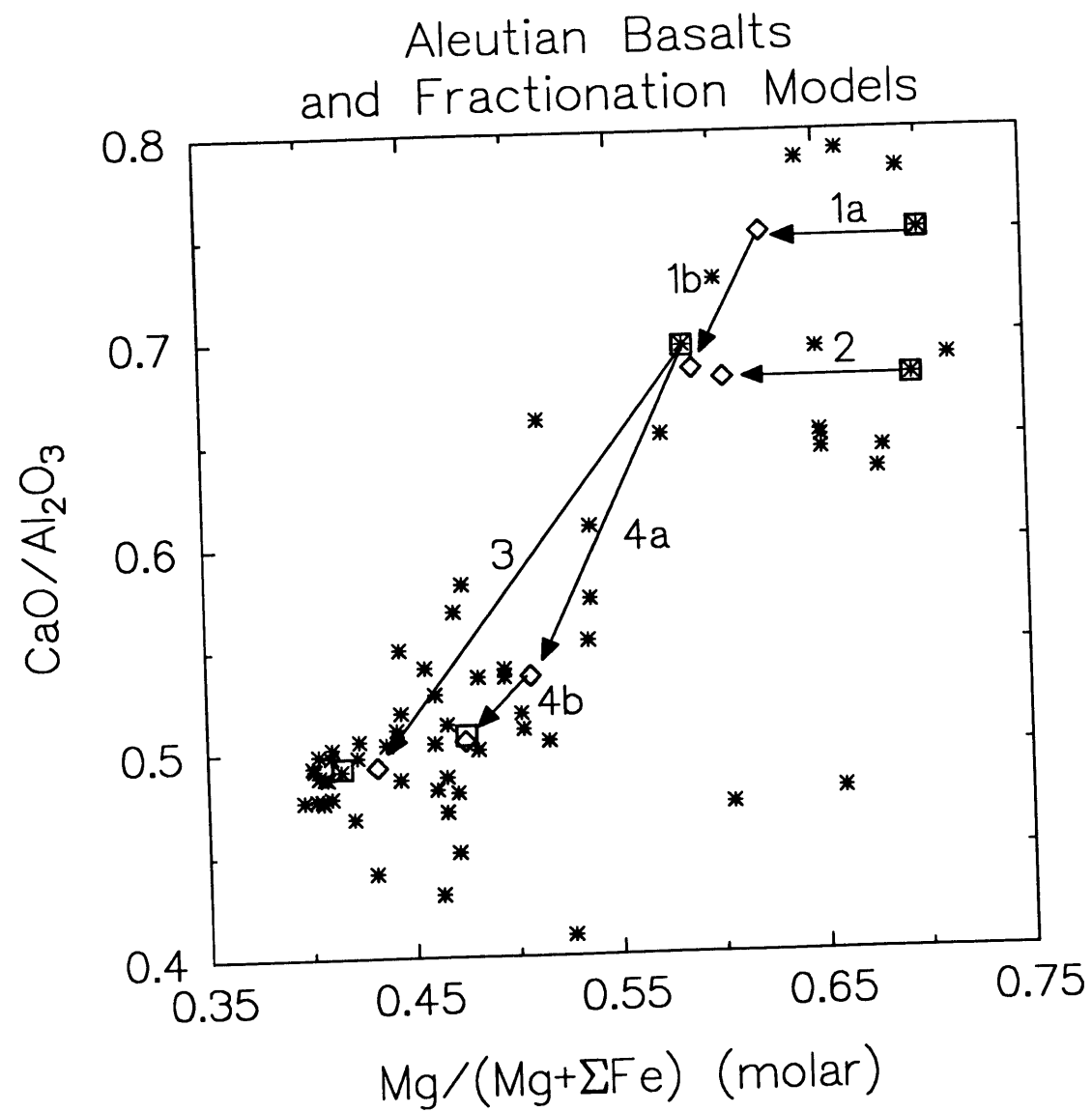


Figure 2-20. Eruptive materials from Fuego, Guatemala (crosses, CENTAM data base, Carr and Rose, 1987) compared with experimental multiple saturation boundaries at moderate to high water contents. Ferric iron calculated assuming that rocks represent liquids on the Ni-NiO buffer using the formulation of Sack et al. (1980). Fuego compositions range from HAB to minor corundum normative aluminous andesite. No compositions have $\text{Al}_2\text{O}_3 < 18$ wt.%. A. Subprojection from PLAG. B. Subprojection from QTZ. C. Subprojection from OLIV.

FUEGO, GUATEMALA
HAB, BA, A

- 2KB OL, HBL, PL, H₂O
- - - 2KB OL, CPX, PL, H₂O
- 2KB OL, CPX, PL,
pH₂O = 0.7 p_{total}

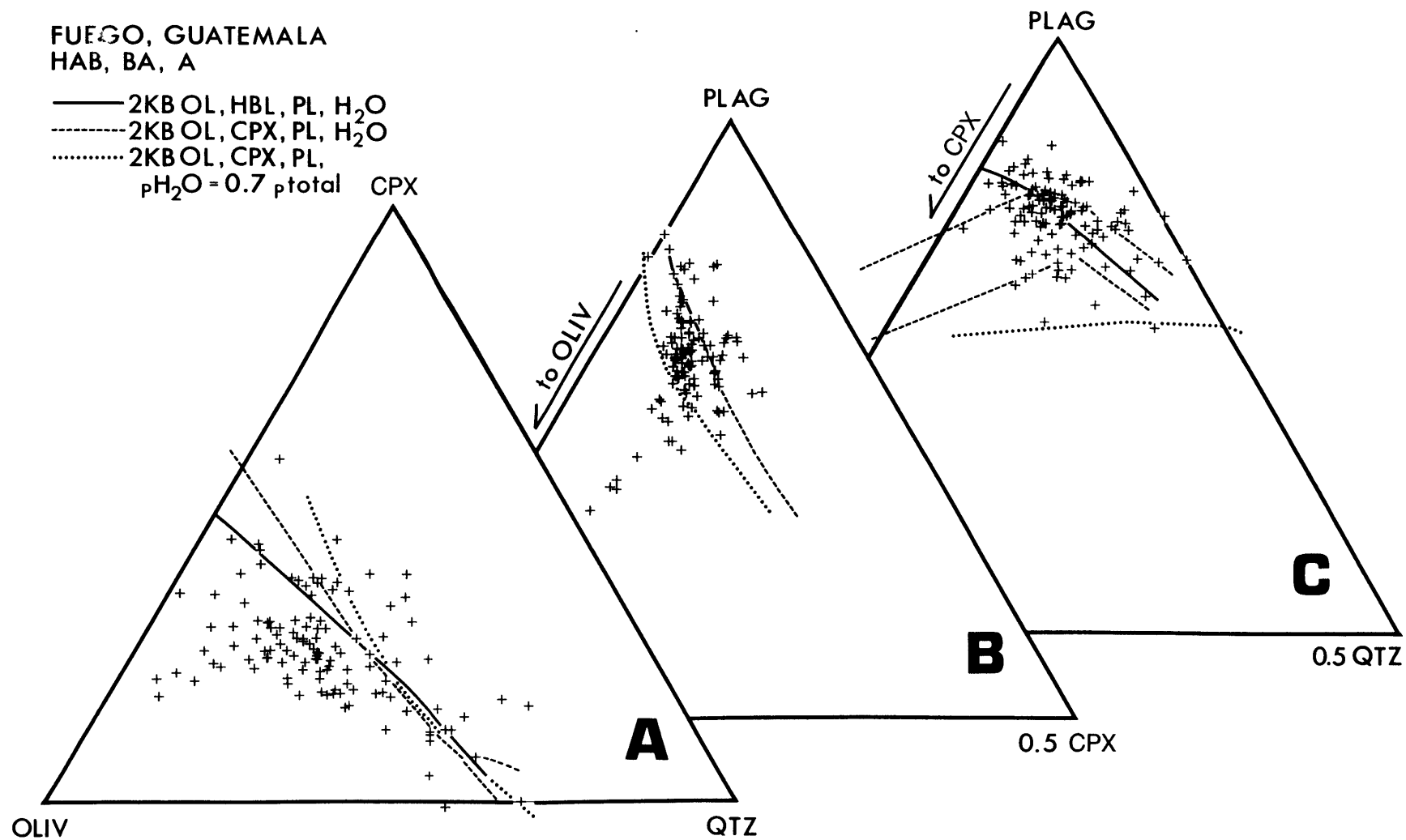


Figure 2-21. Mafic sills (hornblende gabbro and diorite) from the sheeted sill complex at Onion Valley, southeastern Sierra Nevada batholith (Sisson and Grove 1991), compared with the experimentally determined oliv + hbl + plag + liquid (+/- magnetite) reaction boundary. A. Subprojection from PLAG. B. Subprojection from QTZ. C. Subprojection from OLIV. Moderate-pH₂O water-saturated oliv + high-Ca pyx + plag (+/- spinel) multiple saturation boundaries provided for reference.

SIERRA NEVADA BATHOLITH
MAFIC SILLS, ONION VALLEY COMPLEX

- 2KB OL, HBL, PL, H₂O
- - - 2KB OL, CPX, PL, H₂O
- 2KB OL, CPX, PL,
pH₂O = 0.7 p_{total}

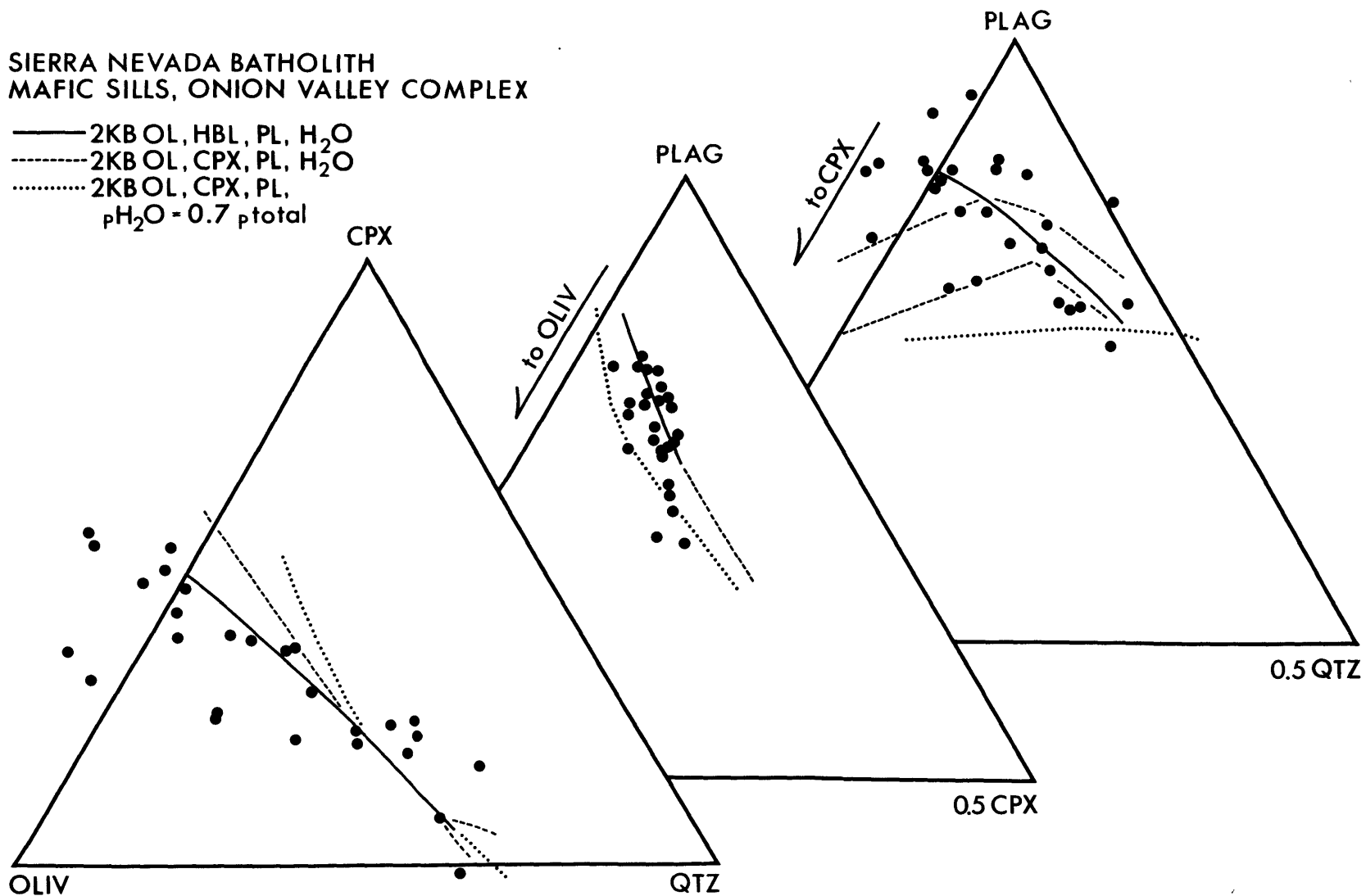


Figure 2-22 A. Estimated temperatures and water contents for representative HABs and BAs. Temperatures and water contents are calculated by simultaneous solution of olivine-liquid and multiply saturated liquid geothermometers, assuming that whole-rocks preserve liquid compositions. Uncertainties are calculated from the range of possible solutions assuming average errors in the olivine-liquid geothermometer of $\pm 15^{\circ}\text{C}$ at low water contents and $\pm 8.5^{\circ}\text{C}$ at high water contents (figure 13b) and an average error for the multiply saturated liquid geothermometer of $\pm 8^{\circ}\text{C}$ (figure 13a). Arrow shows the effect of subtracting 5 wt% An^{90} plag from the composition of a typical HAB from the Cold Bay volcanic center, Aleutians, and then calculating temperature and H_2O . Data from Brophy (1986), Myers et al. (1986), Kuno (1950, 1960), Rose et al. (1978), Gerlach and Grove (1982), and unpublished data of T.L. Grove and J. Donnelly-Nolan.

B. Estimated temperatures and water contents for HAB and BA (normalized $\text{SiO}_2 \leq 55$ wt.%, $\text{Al}_2\text{O}_3 > 17$ wt.%) glass occurring as inclusions in phenocrysts and as residual quenched liquid in cumulates erupted as xenoliths in the Lesser Antilles. Calculations and uncertainties as in A. Data from Anderson (1973, 1974a,b, 1979, 1982), Rose et al. (1978), Arculus and Wills (1980), Devine and Sigurdsson (1983), and Harris and Anderson (1984).

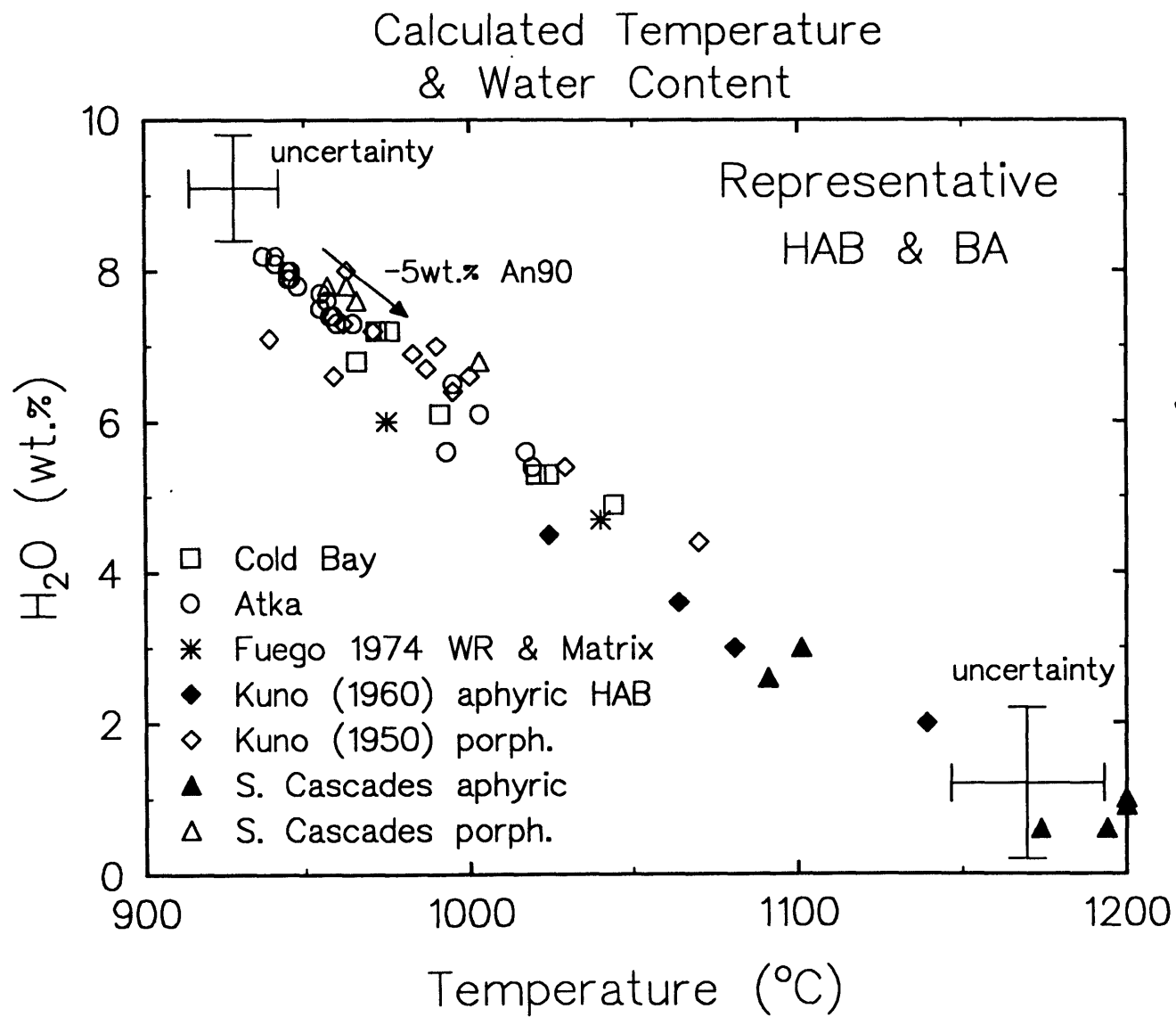


Figure 2-22a.

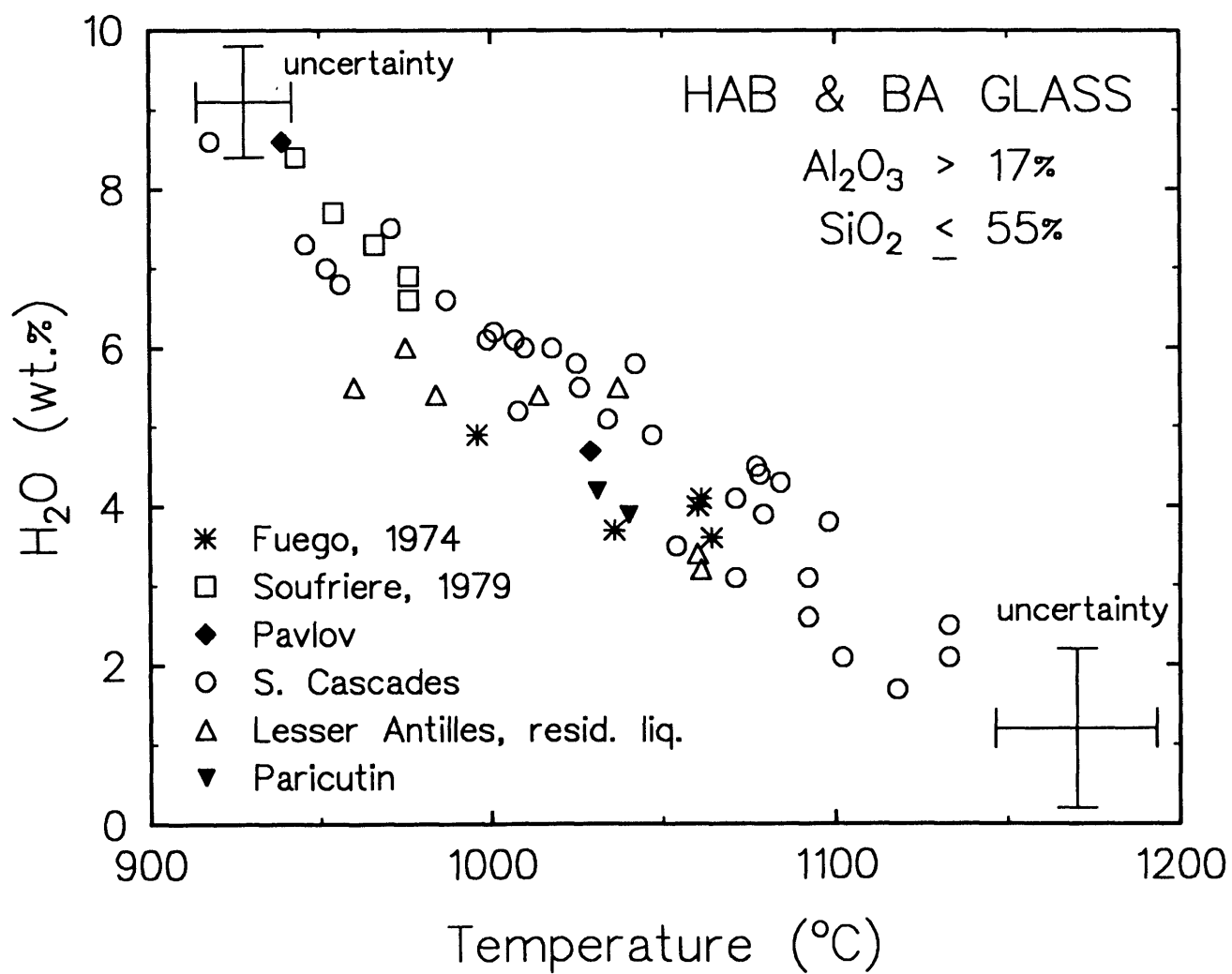


Figure 2-22b.

Table 2-1. High-alumina basalts and basaltic andesites with low MgO contents

	Rocks						Groundmass& Residual Liquids			Glass Inclusions		
	1	2	3	4	5	6	7	8	9	10	11	12
SiO ₂	52.1	50.6	51.4	52.5	51.3	53.7	53.0	51.3	53.3	51.9	50.1	53.0
Al ₂ O ₃	19.7	20.9	19.8	18.4	19.4	18.8	19.0	19.2	17.8	19.5	20.6	18.9
FeO*	8.75	9.26	9.47	10.6	8.81	8.52	9.18	10.1	10.5	10.1	8.98	6.68
MgO	4.46	3.69	5.10	3.9	4.38	4.36	3.44	4.46	4.21	4.8	3.70	5.72
CaO	10.0	10.3	9.18	8.2	8.98	7.84	9.48	9.58	9.04	9.4	11.3	11.0
Na ₂ O	2.80	3.27	3.47	3.8	4.29	3.99	3.92	3.23	3.13	2.72	3.53	3.31
K ₂ O	0.77	0.71	0.77	1.14	1.01	0.71	0.78	0.99	0.83	0.65	0.48	0.46
TiO ₂	0.96	0.91	0.90	1.30	1.29	1.61	1.18	0.86	0.89	0.90	1.08	0.85
MnO	0.17	0.18	--	--	0.17	--	0.14	0.23	0.25	--	0.24	--
P ₂ O ₅	0.30	0.16	--	0.25	0.38	0.29	--	--	--	--	--	--
Total: All analyses normalized to total 100%, volatile-free, with all Fe as FeO.												
Mg#	0.48	0.42	0.49	0.40	0.47	0.48	0.40	0.44	0.42	0.46	0.42	0.60
CaO/Al ₂ O ₃	0.51	0.49	0.46	0.45	0.46	0.42	0.50	0.50	0.51	0.48	0.55	0.58

1. Average Cold Bay HAB, Aleutians (n=7, Brophy, 1986). 2. Average Atka HAB, Aleutians (n=18, Myers et al., 1986). 3. Average Fuego, Guatemala 1974 eruptive (Rose et al., 1978). 4. Hornblende HAB, Ayarza, Guatemala (Peterson and Rose, 1985). 5. Aphyric hornblende HAB sill, Onion Valley, Sierra Nevada batholith, California (Sisson and Grove, 1991). 6. Aphyric high-alumina basaltic andesite, Sidara basin, Japan (Kuno, 1960). 7. Average groundmass, Fuego, Guatemala 1974 eruption (Rose, et al., 1978). 8. Average residual liquid with SiO₂ < 52 wt.% and Al₂O₃ > 17 wt.% in hornblende-bearing cumulate xenoliths, Lesser Antilles (n=4, Arculus and Wills, 1980). 9. Average residual liquid with SiO₂ 52-55 wt.%, Al₂O₃ > 17 wt.% in hornblende-bearing cumulate xenoliths, Lesser Antilles (n=3, Arculus and Wills, 1980). 10. Average low K₂O glass inclusion in olivine, Fuego, Guatemala 1974 eruption (n=7, Harris and Anderson, 1984). 11. Average glass inclusion with SiO₂ < 54 wt.%, Soufriere, St. Vincent 1979 eruption (Devine and Sigurdsson, 1983). 12. Average glass inclusion with SiO₂ ≤ 55 wt.%, Al₂O₃ > 17 wt.%, Mt. Shasta, California (n=19, Anderson, 1973, 1974, 1979, 1982).

Table 2-2. Compositions of Starting Materials

Medicine Lake Highlands Basalts^a

Sample	SiO ₂	Al ₂ O ₃	FeO*	MgO	CaO	Na ₂ O	K ₂ O	TiO ₂	P ₂ O ₅	MnO	Total
79-35g	48.2	18.2	8.39	9.86	12.01	2.29	0.09	0.66	0.05	0.16	99.91
82-62	49.3	17.7	9.02	8.61	11.27	2.58	0.30	0.95	0.11	0.17	100.01
82-66	51.2	17.3	8.66	7.47	10.21	3.11	0.70	1.01	0.16	0.16	99.98

Sierra Nevada Batholith Mafic Dikes^b

Sample	SiO ₂	Al ₂ O ₃	FeO	Fe ₂ O ₃	MgO	CaO	Na ₂ O	K ₂ O	TiO ₂	P ₂ O ₅	MnO	H ₂ O+	H ₂ O-	Total
87S35A	50.6	19.1	5.33	3.74	4.32	8.85	4.23	1.00	1.27	0.37	0.17	1.13	0.15	100.26
85S52B	53.3	17.5	5.95	2.56	4.78	7.27	3.68	2.02	1.12	0.33	0.18	1.07	0.16	99.92

Feldspars^c

Name	SiO ₂	Al ₂ O ₃	FeO	MgO	CaO	Na ₂ O	K ₂ O	Total
Stillwater	48.1	32.8	0.48	0.04	16.0	2.17	0.08	99.67
Bytownite ^d								
Amelia Albite ^e	68.6	19.4	0.0	0.0	0.02	11.8	0.16	99.98

Forsterite-Diopside-Anorthite Mix^f

SiO ₂	Al ₂ O ₃	MgO	CaO	Total
46.4	21.9	12.8	18.9	100

a. Analyses by XRF, U. Mass., Amherst. M.B. Baker-analyst.

b. Na₂O by flame photometry, H₂O+/- & FeO by gravimetry and titration, rest by XRF. Staff of U.S. Geological Survey, Branch of Analytical Chemistry Menlo Park, CA and Lakewood, CO - analysts.

c. Averages of >10 replicate analyses by electron microprobe - MIT.

d. Used in 85S52B + plagioclase mix in weight proportions 0.85 rock:0.15 plagioclase.

e. Used in 82-66 + albite mix in weight proportions 0.84 rock:0.16 plagioclase.

f. Calculated composition of oxide mix.

Table 2-3. Experimental conditions and products.
 See Table 4 for phase compositions.
 All experiments at 2kb pressure, $p_{H_2O}=p_{total}$,
 fO_2 buffered at Ni-NiO.

Run #	T°C	Time (hours)	Phases (+vapor)	Proportions ^a	+/-FeO ^b
<u>79-35g-</u>					
#6	1050	36	gl, ol, sp	92.4: 7.5: 0.1	+3.4
#4	1050	24	gl, ol, sp, pl, cpx	85.0: 8.1: 0.8: 3.8: 2.4	+1.5
#11	1035	41	gl, ol, sp, pl, cpx	80.8: 8.7: <0.3: 5.5: 5.0	+1.3
#10	1025	45	gl, ol, sp, pl, cpx	80.0: 9.2: <0.3: 6.6: 4.3	+2.9
#12	1000	62	gl, ol, sp, pl, cpx	49.9: 12.6: 1.5: 23.1: 12.9	+0.8
<u>82-62-</u>					
#3	1012	20	gl, ol, pl, cpx	70.8: 9.1: 10.2: 9.8	-3.3
#4	1000	30	gl, ol, pl, cpx	64.6: 10.4: 13.6: 11.4	-4.9
<u>82-66-</u>					
#3	1012	32	gl, ol, pl, cpx	86.2: 5.6: 1.3: 6.8	-3.5
#5	1000	31	gl, ol, pl, cpx	87.9: 8.6: <0.5: 12.6	-4.0
#7	965	72	gl, ol, pl, cpx, sp, hbl	52.7: <0.5: 8.1: 9.7: 3.4: 26.1	+1.2
<u>87S35A-</u>					
#1	1025	8	gl	100	-6.1
#2	1000	10	gl	100	-5.2
#5	985	18	gl	100	-5.4
#3	970	8	gl, ol, hbl, pl	96: <0.1: 3.6: 0.5	-2.3
#11	965	63	gl, ol, hbl, pl, sp	87: 6.4: 4.7: 0.5: 1.6	+0.1
#10	950	71	gl, hbl, pl, sp, ap	65.8: 17.4: 13.7: 3.2: tr	+0.2
#13	925	66	gl, hbl, pl, sp, ap	49.5: 25.9: 21.4: 3.2: tr	0
<u>85S52B-</u>					
#11	1024	8	gl, ol	99: 1	-1.4
#12	998	8	gl, ol	98: 2	-2.2
#13	968	12	gl, ol, q	96: 4	-0.3
#14	940	20	gl, ol, hbl	85: 1.5: 13.5	+2.4
<u>85S52B(85%) + An80(15%) -</u>					
#2	980	20	gl	100	-4.6
#4	975	22	gl	100	-7.6
#6	965	24	gl, pl	96 : 4	-2.3
#1	965	25	gl, pl, ol, hbl ^c , q	98 : 0.5: 1: 0.5	-1.5
#14	960	46	gl, pl, ol, hbl	79.1: 14.3: 2.8: 3.8	-4.3
#9	943	72	gl, pl, ol, hbl	71.7: 13.2: <0.1: 15.1	-3.6
<u>82-66(83.7%) + Albite(16.3%) -</u>					
#1	965	44	gl, ol, pl, cpx, sp	85.8: 3.4: 0.2: 10: 0.6	+0.4
<u>82-66(98.1%) + NaOH(1.9%) -</u>					
#2	985	54	gl, cpx, hbl, sp, ol	66.2: 10.9: 20.7: 1.2: 1	0
#1	965	42	gl, cpx, hbl, sp	57.4: 6.8: 34.9: 0.9	+0.3
<u>82-66(99.1%) + NaOH(0.9%) -</u>					
#1	965	49	gl, ol, pl, cpx, hbl, sp	63.6: <0.1: 2: 9.4: 23.8: 1.3	+0.2
<u>Fo-Di-An Mix</u>					
#1	1132	9	gl, ol, pl	91: 3: 6	
#2	1120	8	gl, ol, pl, cpx	4: 12: 54: 29	

a. Proportions calculated by mass balance incorporating analytical errors (Juster et al. 1989) for phase compositions normalized to 100%, H_2O , MnO , P_2O_5 - free, with all Fe as FeO. b. Apparent gain or loss of FeO expressed as: $100 * (total\ FeO_{calc.} - total\ FeO_{st.\ material}) / total\ FeO_{st.\ material}$. c. Hbl too small for accurate analysis, mass balanced with hbl from 85S52B+An⁸⁰-#14.

Table 2-4. Electron microprobe analyses of experimental phases.
See table 2-3 for conditions.

Run# Phase	SiO ₂	Al ₂ O ₃	FeO	MgO	CaO	TiO ₂	MnO	Na ₂ O	K ₂ O	P ₂ O ₅	Cr ₂ O ₃	NiO	Fe ₂ O ₃ ^a	Total
79-35g-#6														
gl ^b (13)	48.2(4)	^d 19.4(2)	8.37(17)	6.96(18)	13.2(1)	0.65(2)	0.16(1)	2.89(13)	0.12(1)	0.09(1)				93.8
ol(7) ^c	40.1(3)	0.06(2)	12.9(3)	46.1(5)	0.34(5)	0.03(2)	0.17(5)				0.11(4)	0		100.2
sp(4)	0.30(3)	37.7(19)	12.5(4)	16.6(3)	0.25(5)	0.35(8)	0				24.6(12)	0	7.04	99.6
#4														
gl(12)	49.4(2)	19.2(2)	8.28(9)	6.58(7)	12.6(6)	0.72(1)	0.15	2.77(22)	0.12(1)	0.06(1)	0.06(1)			92.8
ol(10)	39.9(2)	0.04(1)	14.6(7)	45.5(6)	0.41(2)	0	0.26(1)				0.02(1)	0.08(3)		100.8
sp(8)	0	38.4(14)	13.6(10)	16.1(3)		0.45(3)	0.22(2)				24.4(9)	0.05(2)	7.09	100.3
cpx(7)	50.9(4)	4.37(18)	4.56(22)	15.4(3)	23.1(2)	0.38(7)	0	0.20(2)			0.71(18)			99.6
pl(11)	44.6(3)	35.3(2)	0.57(3)	0.12(3)	18.9(2)			0.75(10)	0					100.2
#11														
gl(15)	49.0(5)	19.7(2)	8.69(16)	6.37(13)	12.1(1)	0.72(3)	0.16(2)	3.08(14)	0.11(2)	0.09(1)				92.8
ol(7)	39.7(4)	0.14(10)	14.3(6)	45.1(4)	0.37(6)	0	0.24(7)				0.06(5)	0.11(6)		100.0
sp(4)	0.24(5)	12.4(8)	22.4(7)	7.91(30)	0.21(3)	1.91(12)	0.27(5)				0.42(17)	0.19(9)	53.9	99.8
cpx(10)	51.0(8)	4.40(50)	4.70(24)	15.7(4)	22.3(2)	0.47(4)	0.07(5)	0.21(3)			0.67(10)			99.5
alpx(9)	49.3(5)	5.95(25)	5.93(41)	14.8(2)	22.2(2)	0.54(5)	0.08(6)	0.24(3)			0.53(20)			99.6
pl(7)	45.2(3)	34.9(2)	0.54(8)	0.07(2)	18.1(3)			0.77(11)	0.03(2)					99.6
#10														
gl(15)	49.1(5)	19.5(2)	8.77(11)	6.37(19)	12.2(2)	0.73(3)	0.17(1)	2.99(9)	0.11(2)	0.09(1)				93.1
ol(7)	39.6(4)	0.05(4)	15.5(2)	44.2(5)	0.33(7)	0	0.27(4)				0.04(3)	0.11(4)		100.1
sp(4)	0.16(18)	14.9(8)	21.4(17)	8.64(40)	0.09(9)	1.73(14)	0.20(9)				4.07(68)	0.27(5)	47.9	99.4
cpx(7)	51.0(5)	4.69(52)	5.14(44)	15.5(3)	22.1(2)	0.50(7)	0.10(2)	0.21(2)			0.51(12)			99.8
pl(9)	45.3(3)	34.5(4)	0.53(7)	0.06(2)	18.4(4)			0.88(17)	0					99.7
#12														
gl(15)	52.5(3)	19.2(2)	8.04(14)	4.99(12)	9.64(15)	0.98(4)	0.20(2)	4.15(9)	0.21(1)	0.14(1)				93.7
ol(10)	38.4(2)	0	19.1(8)	41.3(6)	0.40(4)	0	0.33(1)			0.14(2)	0.11(4)			99.8
sp(8)	0.17(14)	8.54(13)	26.4(3)	6.14(5)	0.16(10)	3.92(11)	0.33(3)				0	0.09(5)	54.4	100.2
cpx(9)	51.1(7)	4.41(58)	5.66(46)	15.6(4)	22.6(2)	0.63(12)	0.13(4)	0.23(4)			0.27(23)			100.6
pl(16)	45.7(4)	34.1(5)	0.62(12)	0.12(5)	18.2(3)			1.13(16)	0					99.9

82-62-#3

gl(10)	51.5(1)	19.2(1)	8.70(10)	4.98(7)	10.0(1)	1.19(5)	0.19(2)	3.72(9)	0.42(2)	0.14(2)		93.6
ol(11)	38.7(3)	0	20.5(3)	39.8(5)	0.46(13)	0.06(3)	0.30(2)		0	0		99.9
cpx(13)	50.3(3)	4.12(25)	5.83(13)	15.0(2)	22.7(1)	0.73(4)	0	0.24(2)		0.28(3)		99.2
pl(9)	46.0(4)	33.8(5)	0.66(3)	0.10(2)	17.5(3)			1.36(19)	0			99.4

#4

gl(12)	51.8(2)	19.4(1)	8.62(11)	4.56(6)	9.59(7)	1.28(3)	0.17(2)	3.96(11)	0.45(1)	0.18(1)		92.7
ol(9)	38.2(2)	0.07(1)	21.3(2)	39.7(5)	0.42(3)	0.04(2)	0.34(4)		0.02(1)	0.08(3)		100.2
cpx(11)	50.5(5)	4.50(46)	6.11(20)	15.0(4)	22.8(1)	0.93(8)	0.13(2)	0.27(3)		0.23(4)		100.5
pl(7)	46.5(4)	33.4(3)	0.42(8)	0.15(7)	17.6(3)			1.45(14)	0.02(1)			99.5

82-66-#3

gl(8)	52.9(2)	19.1(2)	7.90(10)	4.80(14)	9.66(13)	1.08(2)	0.17(2)	3.41(8)	0.82(4)	0.13(2)		93.0
ol(8)	38.9(2)	0.04(2)	20.1(3)	40.4(3)	0.36(3)	0.05(3)	0.31(3)		0.06(2)	0.13(2)		100.4
cpx(7)	51.4(6)	3.56(3)	5.43(8)	15.7(3)	22.6(2)	0.63(3)	0.06(4)	0.19(2)		0.34(3)		99.9
pl(5)	45.7(3)	33.8(3)	0.58(8)	0.06(1)	17.7(1)			1.29(9)	0			99.1

#5

gl(8)	52.7(2)	19.3(1)	7.75(8)	4.83(7)	9.80(6)	1.06(2)	0.14(2)	3.44(8)	0.80(5)	0.16(0)		93.3
ol(8)	38.7(5)	0.04(1)	20.2(3)	40.8(4)	0.37(4)	0.06(1)	0.33(4)		0.03(1)	0.04(3)		100.6
cpx(9)	51.4(5)	3.67(56)	5.27(22)	15.7(3)	22.7(3)	0.63(7)	0.10(4)	0.21(9)		0.28(5)		100.0
pl(6)	45.2(2)	35.1(1)	0.45(2)	0.08(1)	18.4(2)			0.98(6)	0.03(0)			100.2

#7

gl(5)	59.1(5)	19.1(2)	5.22(16)	3.25(12)	7.45(31)	0.54(3)	0.19(5)	4.00(16)	0.88(7)	0.31(3)		92.5
ol(6)	38.6(2)	0.04(2)	21.5(5)	40.0(4)	0.37(2)	0.03(0)	0.37(2)		0.01(0)	0		100.9
sp(11)	0.28(2)	5.74(18)	26.1(6)	5.55(10)	0.09(3)	3.05(62)	0.36(2)		0.06(4)	0.15(2)	58.6	100.0
cpx(6)	47.3(5)	7.85(94)	6.51(12)	13.1(6)	22.5(1)	1.75(22)	0.14(4)	0.25(3)		0.22(12)		99.6
pl(9)	46.6(5)	33.4(2)	0.46(14)	0.07(1)	17.2(3)			1.70(17)	0.04(2)			99.7
hbl(11)	42.4(5)	12.2(3)	9.54(27)	16.4(2)	11.7(1)	1.39(1)	0.14(5)	2.50(6)	0.36(2)			96.6

87S35A-#1

gl(7)	51.7(4)	19.3(2)	8.27(7)	4.38(5)	8.90(7)	1.26(4)	0.18(2)	4.46(16)	1.09(4)	0.42(2)		93.1
-------	---------	---------	---------	---------	---------	---------	---------	----------	---------	---------	--	------

#2

gl(7)	52.0(2)	19.2(1)	8.35(17)	4.41(6)	8.67(11)	1.30(2)	0.16(2)	4.41(16)	1.07(3)	0.42(3)		93.8
-------	---------	---------	----------	---------	----------	---------	---------	----------	---------	---------	--	------

#5

gl(7)	51.9(2)	19.1(1)	8.33(11)	4.36(6)	8.80(11)	1.30(2)	0.16(3)	4.51(24)	1.05(4)	0.44(3)		93.9
-------	---------	---------	----------	---------	----------	---------	---------	----------	---------	---------	--	------

#3
gl(7) 52.1(1) 19.3(1) 8.35(13) 4.14(4) 8.77(14) 1.27(3) 0.15(3) 4.49(12) 0.99(13) 0.42(3) 93.7
ol(5) 38.7(3) 0.01(1) 21.9(2) 39.3(4) 0.24(1) 0.04(1) 0.31(2) 0 0.04(1) 100.5
hbl(11) 40.7(4) 14.0(4) 10.6(9) 14.7(3) 11.9(3) 3.04(41) 0.13(3) 2.74(6) 0.46(2) 98.3
pl(10) 46.8(3) 34.2(3) 0.77(7) 0.08(2) 17.1(2) 1.61(13) 0.05(2) 100.6

#11
gl(10) 53.2(2) 19.2(1) 7.63(8) 3.66(4) 8.58(6) 1.10(3) 0.16(2) 4.54(9) 1.23(3) 0.64(2) 94.2
ol(6) 37.7(3) 0.02(1) 24.4(3) 37.4(2) 0.24(3) 0.02(1) 0.44(1) 0.02(1) 0 100.3
sp(10) 0.11(2) 6.92(13) 31.0(6) 4.86(18) 0.09(4) 6.95(25) 0.32(3) 0.08(5) 0.02(1) 49.9 100.3
hbl(16) 39.8(8) 13.6(4) 11.4(3) 14.2(3) 12.0(1) 2.72(11) 0.14(1) 2.67(4) 0.49(3) 97.0
pl(15) 47.4(6) 33.0(4) 0.79(12) 0.09(3) 16.6(5) 2.04(27) 0.07(2) 100.0

#10
gl(16) 56.9(4) 18.6(2) 6.29(10) 2.68(8) 7.23(7) 0.82(2) 0.18(5) 5.07(25) 1.48(4) 0.77(3) 94.4
sp(5) 0.09(1) 5.31(31) 33.1(4) 2.85(12) 0.13(3) 6.15(45) 0.38(3) 0.10(2) 0 52.6 100.7
hbl(16) 41.3(3) 13.4(3) 11.2(6) 13.7(4) 11.8(1) 3.17(29) 0.16(2) 2.77(5) 0.49(3) 98.0
pl(20) 48.2(4) 32.3(4) 0.58(10) 0.04(1) 16.0(4) 2.18(24) 0.06(2) 99.3
ap(3) 0 0.06(4) 0.41(2) 0.26(2) 54.2(4) 37.5(3) 92.4

#13
gl(10) 60.0(2) 18.9(3) 5.27(10) 1.76(3) 5.66(14) 0.58(4) 0.19(3) 5.44(17) 1.78(4) 0.37(4) 93.9
sp(10) 0.03(2) 3.92(12) 33.9(5) 2.61(6) 0.17(2) 7.53(37) 0.62(2) 0.24(0) 0.11(1) 51.3 100.4
hbl(8) 41.1(4) 13.4(2) 13.0(9) 13.4(4) 11.6(2) 2.71(18) 0.19(4) 2.76(5) 0.46(6) 98.6
pl(9) 50.9(3) 31.0(4) 0.59(6) 0.07(4) 14.2(3) 3.38(14) 0.07(2) 100.2
ap(4) 0 0.03(1) 0.45(8) 0.17(2) 54.4(9) 38.1(6) 93.2

85S52B-#11
gl(6) 54.9(2) 17.9(1) 7.83(11) 4.56(11) 7.12(24) 1.09(3) 0.16(3) 4.03(11) 2.07(10) 0.35(4) 93.2
ol(6) 38.9(5) 0.08(1) 19.8(5) 40.3(2) 0.21(1) 0.08(1) 0.41(3) 0.10(3) 0 99.9

#12
gl(12) 55.0(1) 18.0(1) 7.70(9) 4.42(6) 7.06(19) 1.13(2) 0.18(2) 4.04(14) 2.18(5) 0.18(2) 93.6
ol(5) 39.4(2) 0.03(2) 21.8(1) 39.4(2) 0.20(2) 0.04(2) 0.35(1) 0.02(0) 0 99.7

#13
gl(5) 55.4(1) 18.3(1) 7.64(10) 3.70(2) 7.42(8) 1.15(4) 0.13(2) 3.99(10) 1.94(6) 0.32(3) 93.2
ol(6) 38.5(4) 0.02(2) 22.1(9) 39.0(9) 0.18(1) 0.02(1) 0.39(2) 0 0.05(1) 100.2

#14
gl(6) 56.3(1) 18.6(1) 7.25(14) 3.09(11) 7.22(13) 1.09(3) 0.13(4) 4.09(13) 1.94(7) 0.30(1) 93.4
ol(5) 38.1(2) 0.03(0) 25.1(2) 37.0(2) 0.17(0) 0.03(0) 0.46(0) 0 0.02(1) 100.9
hbl(8) 41.4(7) 13.2(6) 12.(1) 13.9(8) 11.2(4) 2.58(38) 0.18(3) 2.31(10) 0.83(11) 97.6

85S52B+An⁸⁰-#2
gl(9) 53.8(3) 20.1(1) 6.90(10) 4.29(4) 8.42(16) 0.98(3) 0.18(4) 3.62(10) 1.60(15) 0.21(2) 93.9

#4
gl(5) 54.4(2) 19.9(1) 6.65(11) 4.22(4) 8.15(18) 0.90(4) 0.18(1) 3.62(13) 1.73(5) 0.25(3) 94.0

#6
gl(7) 54.3(2) 19.6(1) 7.05(13) 4.33(5) 8.25(21) 0.91(2) 0.15(3) 3.60(9) 1.62(7) 0.29(4) 94.3
pl(8) 45.5(6) 34.1(4) 0.55(9) 0.07(2) 17.7(6) 1.31(26) 0.06(1) 99.3

#1
gl(12) 53.7(2) 20.0(1) 6.84(20) 3.75(27) 8.77(22) 0.93(1) 0.16(1) 3.98(8) 1.57(14) 0.33(1) 86.7^e
ol(5) 38.3(4) 0.02(1) 19.9(2) 40.7(3) 0.25(1) 0.04(1) 0.34(0) 0 0.02(1) 99.6
pl(4) 46.8(1) 34.2(3) 0.62(9) 0.09(1) 17.5(1) 1.42(6) 0.09(1) 100.7

#14
gl(10) 56.5(2) 18.8(1) 6.82(13) 3.27(8) 7.42(7) 1.04(2) 0.17(2) 3.68(12) 2.04(4) 0.36(1) 94.0
ol(8) 37.7(2) 0.07(5) 23.9(5) 37.1(5) 0.27(3) 0.05(2) 0.47(4) 0 0.03(1) 99.6
pl(10) 46.9(7) 32.9(7) 0.70(7) 0.10(4) 17.1(6) 1.66(28) 0.11(2) 99.5
hbl(12) 42.4(6) 12.7(6) 10.0(5) 15.1(3) 11.8(4) 2.75(23) 0.15(2) 2.39(10) 0.82(3) 98.1

#9^f
gl1(10) 57.1(2) 19.1(1) 6.90(9) 2.80(3) 6.59(7) 0.70(2) 0.16(2) 4.17(21) 2.13(4) 0.39(1) 93.4
gl2(7) 56.4(4) 19.3(2) 6.97(9) 2.84(2) 6.59(8) 0.78(6) 0.23(3) 4.33(11) 2.20(5) 0.38(3) 92.9
ol(9) 37.1(2) 0 25.1(6) 36.6(6) 0.23(1) 0.04(2) 0.47(4) 0.02(1) 0.09(4) 99.7
pl(20) 47.8(7) 33.0(7) 0.63(11) 0.09(5) 16.4(6) 2.06(30) 0.12(3) 100.1
hbl(16) 42.0(6) 13.1(6) 10.8(6) 14.6(5) 11.7(3) 2.62(30) 0.20(4) 2.52(4) 0.73(6) 98.2

82-66+Albite-#1
gl(16) 55.9(3) 20.2(1) 6.37(7) 3.52(5) 7.35(5) 0.83(2) 0.14(1) 4.85(15) 0.76(3) 0.16(0) 93.6
ol(16) 38.5(2) 0 20.2(4) 40.5(3) 0.34(5) 0.02(1) 0.33(3) 0 0.05(4) 100.0
sp(6) 0.14(2) 7.33(14) 28.8(5) 5.08(9) 0.15(4) 4.90(14) 0.28(1) 0.4(2) 0.13(2) 53.3 100.5
cpx(5) 51.4(8) 2.86(57) 6.61(43) 15.5(4) 21.9(5) 0.59(9) 0.21(3) 0.22(5) 0.17(4) 99.5
alpx(10) 48.2(4) 6.62(4) 6.56(25) 13.6(3) 22.3(3) 1.40(17) 0.14(2) 0.32(2) 0.22(12) 99.4
pl(6) 48.7(2) 32.0(1) 0.51(1) 0.08(1) 15.4(2) 2.55(7) 0.04(0) 99.3

82-66(98.1%)+NaOH(1.9%)-#2

gl(6)	54.8(4)	20.1(1)	6.58(6)	3.32(3)	7.63(2)	0.62(3)	0.16(1)	5.56(15)	0.94(2)	0.28(2)		95.1
ol(10)	38.3(2)	0.06(4)	21.0(5)	40.0(4)	0.36(7)	0(0)	0.24(14)		0.09(4)	0.20(12)		100.3
sp(16)	0.14(2)	8.18(34)	29.1(9)	5.00(27)	0.08(4)	4.96(58)	0.21(7)		0.12(4)	0.3(3)	52.3	100.4
cpx(6)	49.4(6)	5.82(90)	6.35(10)	14.4(6)	23.0(2)	1.08(18)	0.13(2)	0.34(7)	0.08(4)			100.4
alpx(6)	47.3(5)	7.56(60)	6.61(26)	13.4(2)	22.7(2)	1.91(24)	0.12(0)	0.40(4)	0.15(6)			100.2
hbl(9)	40.6(3)	14.4(3)	11.0(3)	14.9(2)	11.8(2)	2.01(16)	0.14(2)	3.02(6)	0.32(2)			98.2

#1

gl(9)	56.2(2)	20.4(2)	5.88(0)	2.58(3)	7.18(6)	0.34(1)	0.20(2)	6.02(5)	1.02(3)	0.23(1)		94.2
sp(4)	0.11(1)	6.35(5)	28.9(7)	3.68(7)	0.13(5)	2.66(3)	0.38(2)		0.16(14)	0.08(2)	59	101.5
cpx(7)	51.0(4)	4.14(38)	7.33(31)	14.4(3)	22.4(2)	0.56(8)	0.20(4)	0.31(3)	0.09(3)			100.4
alpx(6)	48.4(4)	7.36(41)	7.34(12)	12.8(3)	22.5(3)	1.45(10)	0.18(2)	0.37(6)	0.15(5)			100.6
hbl(11)	42.1(4)	13.7(4)	11.1(6)	14.3(3)	11.6(2)	1.61(20)	0.14(2)	2.96(7)	0.33(2)			97.9

82-66(99.1%)+NaOH(0.9%)-#1

gl(12)	55.4(4)	19.9(2)	6.80(12)	3.64(9)	7.67(18)	0.60(4)	0.17(4)	4.64(23)	1.02(2)	0.25(1)		
93.6												
ol(7)	38.4(1)	0.05(3)	20.6(6)	40.2(5)	0.33(4)	0.02(3)	0.20(14)		0.09(4)	0		99.9
sp(9)	0.12(4)	7.61(58)	28.8(9)	5.06(27)	0.08(5)	4.83(44)	0.22(6)		0.14(4)	0	53.0	99.9
cpx(3)	49.3(8)	5.54(62)	7.14(28)	14.4(3)	22.3(4)	0.99(6)	0.25(9)	0.24(4)	0.09(4)			100.2
alpx(5)	48.2(2)	7.28(35)	6.92(11)	13.5(5)	22.5(2)	1.26(18)	0.25(7)	0.32(3)	0.09(4)			100.3
pl(7)	47.1(2)	32.6(4)	0.68(11)	0.07(0)	16.7(1)			2.00(11)	0.04(0)			99.2
hbl(11)	41.3(7)	13.7(6)	10.7(3)	15.4(3)	11.8(1)	1.75(9)	0.14(5)	2.70(3)	0.36(1)			97.9

Fo-Di-An Mix-#1

					Total
gl(7)	48.4(5)	21.4(1)		11.6(1)	18.7(1) 94.4

#2

gl(12)	48.0(6)	21.1(6)		10.7(8)	20.1(5) 93.5
ol(3)	42.4(3)	0.25(11)		56.8(1)	0.42(4) 99.9
cpx(3)	53.1(5)	4.6(10)		18.4(7)	24.7(2) 100.8
pl(4)	43.9(5)	36.1(5)		0.18(1)	20.0(3) 100.2

Notes for table 2-4.

Abbreviations: gl-glass, ol-olivine, sp-spinel, cpx-common high calcium pyroxene, alpx-alumina rich high calcium pyroxene grains or zones, pl-plagioclase, hbl-hornblende, ap-apatite. 0 indicates below detection limit, blank indicates not analyzed.

Notes: a. Fe_2O_3 calculated in spinels assuming a 3 cation-4 oxygen stoichiometry. b. Glass analyses normalized to total 100% anhydrous, with all Fe as FeO. Original unnormalized total is reported. c. Number of electron probe analyses. d. One standard deviation of replicate analyses in terms of least units cited. Thus, 50.0(2) should be read as 50.0 ± 0.2 . e. Exceptional analysis performed by rastering a 30micron beam over glass and quench crystals. f. Exceptional experiment with heterogeneous distribution of phases and minor variation in glass composition, gl1 - glass near hbl and pl and used in mass balance, gl2 - glass near oliv and hbl and away from plag.

Table 2-5. Experimental conditions and products. fO_2 >or< Ni-NiO.
 See table 4 for phase compositions.
 See table 3 for abbreviations and notes.

Run #	T(°C)	fO_2	Time (hrs.)	Phases (+ vapor)	Phase proportions	+/-FeO
79-35g-						
7	1000	>Ni-NiO	48	gl, ol, sp, cpx, pl	44.3:9.4:4.6:18.7:23.0	-1.0
82-66-						
6	975	<Ni-NiO	50	gl, ol, sp, cpx, pl	63.9:8.6:0.7:12.6:14.2	+0.8

Table 2-6. Electron microprobe analyses of experimental phases; fO_2 > or < Ni-NiO.
See table 5 for conditions.
See table 4 for abbreviations and notes.

Run#	Phase	SiO ₂	Al ₂ O ₃	FeO	MgO	CaO	TiO ₂	MnO	Na ₂ O	K ₂ O	P ₂ O ₅	Cr ₂ O ₃	NiO	Fe ₂ O ₃	Total
79-35g-#7															
gl(11)	55.6(6)	19.6(2)	4.99(9)	5.23	8.52(9)	0.90(2)	0.17(1)	4.63(15)	0.19(1)	0.12(2)					93.9
ol(11)	41.1(3)	0.08(7)	10.0(9)	48.4(7)	0.34(5)	0	0.34(3)					0	0.06(6)		100.3
sp(10)	0.28(2)	8.06(21)	17.9(5)	10.6(2)	0.07(2)	1.98(13)	0.43(3)					0.11(9)	0.15(3)	60.9	100.5
cpx(9)	47.4(6)	7.07(49)	7.60(48)	13.9(3)	22.1(1)	0.91(10)	0.16(3)	0.40(2)				0.12(2)			99.7
pl(8)	45.8(5)	34.0(4)	0.52(12)	0.08(3)	17.7(3)			1.26(19)	0.03(1)						99.4
82-66-#6															
gl(13)	54.9(2)	18.9(1)	7.91(12)	3.55(5)	7.87(5)	1.29(3)	0.15(2)	4.04(12)	1.11(3)	0.23(1)					93.0
ol(7)	37.7(2)	0.1(1)	24.5(5)	36.4(5)	0.35(8)	0.04(3)	0.39(5)					0	0.03(2)		99.5
sp(6)	0.18(1)	5.72(12)	34.9(6)	4.38(5)	0.10(3)	10.7(2)	0.33(2)					0.14(7)	0.05(1)	43.4	99.9
cpx(11)	51.2(4)	3.39(52)	7.32(13)	15.3(1)	21.5(2)	0.73(9)	0.05(4)	0.16(2)				0.18(5)			99.8
pl(7)	46.3(3)	33.6(3)	0.60(9)	0.07(1)	17.0(2)			1.73(10)	0.03(0)						99.3

Table 2-7.
Aleutian Fractionation Models

High-MgO Basalt to High-Alumina Basalt

Parent: Basaltic host for ultramafic xenoliths, Adak Island (Debari et al., 1987).

SiO ₂	TiO ₂	Al ₂ O ₃	FeO	MgO	CaO	Na ₂ O	K ₂ O	P ₂ O ₅ ^a
48.7	0.69	15.2	9.08	11.89	11.43	2.09	0.74	0.10 ^a

Crystallizing assemblage: 100% oliv^b to Mg#_{liq}=62.5, followed by 15% oliv + 85% Ca-pyx^b.

Target composition: HAB OK2, Okmok Volcano (Nye and Reid, 1986).

50.2	0.83	17.4	9.00	7.12	12.13	2.54	0.57	0.12
------	------	------	------	------	-------	------	------	------

Model after 15.7% crystallization:

49.6	0.79	17.8	8.96	7.22	12.17	2.47	0.88	0.12
------	------	------	------	------	-------	------	------	------

Parent: Magnesian basalt ID16, Okmok Volcano (Nye and Reid, 1986).

49.1	0.70	16.1	8.93	11.45	10.92	2.21	0.52	0.12
------	------	------	------	-------	-------	------	------	------

Crystallizing assemblage: 100% oliv.

Target composition: HAB OK2 (as above).

Model after 10.5% crystallization:

50.1	0.78	17.9	8.50	7.29	12.20	2.47	0.58	0.13
------	------	------	------	------	-------	------	------	------

High-Alumina Basalt to Low-MgO High-Alumina Basalt

Parent: HAB OK2 (as above).

Crystallizing assemblage: 15% oliv + 85% Ca-pyx.

Target composition: Average HAB, Atka Island (Myers et al., 1986).

50.7	0.91	20.9	9.28	3.70	10.31	3.28	0.71	0.16
------	------	------	------	------	-------	------	------	------

Model after 19% crystallization:

50.5	0.93	21.0	9.28	3.97	10.34	3.16	0.72	0.15
------	------	------	------	------	-------	------	------	------

Parent: HAB OK2 (as above).

Crystallizing assemblage: 8% oliv + 86% Ca-pyx + 6% magnetite^b to 20% Al₂O₃_{liq}, followed by 12% oliv + 26% Ca-pyx + 56% CA-plag^b + 6% magnetite (2kb cotectic assemblage, H₂O-saturated).

Target composition: Average HAB, Cold Bay volcanic center (Brophy, 1986).

52.1	0.96	19.7	8.75	4.46	10.01	2.80	0.77	0.17
------	------	------	------	------	-------	------	------	------

Model after 26.8% crystallization:

51.8	0.97	19.7	8.81	4.48	9.95	3.34	0.78	0.16
------	------	------	------	------	------	------	------	------

Total solidification High-MgO Basalt to Low-MgO HAB: 28-38%.

Notes: a. Assumed concentration for modeling purposes. b. Mineral compositions and exchange K_Ds from experiments on HAB 79-35g (table 3).

Appendix 1. Additional experimental results.

Results are reported for two experiments on a granodiorite, 83S296B, collected from the Cretaceous granodiorite of Mitchell Peak in the south central Sierra Nevada batholith (Moore and Sisson, 1987). Experiments were performed at 2kb pressure, 800(+/-5)°C, water-saturated, at the Ni-NiO oxygen buffer. Rock powders were held in unsealed Pt96-Fe4 capsules, surrounded by Ni+NiO buffer material, within sealed Au capsules. Experiments were run in standard cold seal hydrothermal pressure vessels and were quenched at pressure with compressed air. Analytical procedures were as reported previously except that glasses were analyzed with a 40 micron diameter electron beam with samples held at liquid N₂ temperature on a freezing stage to minimize Na migration.

Whole Rock		Experimental Phases (+op, ap, zr)							
83S296B ^a		Run #1-23 days				Run #10-18 days			
		gl(12) ^b	pl(4)	hbl(5)	bio(5)	gl(7)	pl(16)	hbl(5)	bio(6)
SiO ₂	61.1	73.1(5) ^c	55.3(4)	44.3(9)	37.2(4)	73.7(2)	57.1(7)	45.3(8)	37.4(9)
Al ₂ O ₃	16.4	15.0(3)	28.4(2)	8.92(90)	14.5(2)	14.7(3)	26.0(5)	8.11(98)	15.4(7)
FeO ^d	3.05	1.58(9)	0.36(4)	18.2(9)	18.8(3)	0.72(5)	0.22(4)	12.9(9)	13.0(9)
Fe ₂ O ₃	2.31								
MgO	2.55	0.19(4)	0	11.0(8)	13.5(4)	0.22(2)	0.02(2)	13.4(8)	15.3(6)
CaO	4.82	1.57(20)	10.7(3)	10.6(3)	0.05(3)	1.34(3)	8.56(49)	10.8(4)	0.11(3)
TiO ₂	0.76	0.19(2)		1.63(25)	2.66(22)	0.35(3)		1.76(55)	4.07(24)
MnO	0.10	0.08(2)		0.34(6)	0.16(4)	0.10(2)		0.43(9)	0.19(4)
Na ₂ O	3.48	3.74(27)	5.17(12)	1.59(17)	0.64(2)	4.09(8)	6.27(29)	1.49(27)	0.72(7)
K ₂ O	3.34	4.50(14)	0.36(4)	0.56(6)	8.42(9)	4.74(11)	0.48(4)	0.72(9)	8.48(23)
P ₂ O ₅	0.25	0.05(1)		0.04(2)					
H ₂ O ⁺	0.69								
H ₂ O ⁻	0.15								
CO ₂	0.05								
Total	99.05	91.33 ^e	100.3	97.14	95.93	91.98 ^e	98.65	94.9	94.7

Abbreviations. gl-glass, pl-plagioclase, hbl-hornblende, bio-biotite, op-opaque oxides, ap-apatite, zr-zircon.

Notes. Analysis by staff of the Branch of Analytical Chemistry, U.S. Geological Survey (T.W. Sisson, unpublished data). b. Number of replicate analyses. c. Standard deviation of replicate analyses in units of the least significant digit reported. d. FeO in whole rock measured by wet chemistry, all other analyses report all Fe as FeO. e. Glass analyses are normalized to total 100% volatile-free with all Fe as FeO. Total reports the original sum of the electron probe analysis.

Appendix 2. Coexisting natural hornblende rim and glass or matrix compositions.

Sample	IC-B	IC-B	AY-II-V	AY-II-V	81-T-116	81-T-116
	Material glass	hbl. ^a	matrix ^b	hbl.	matrix	hbl.
# analy.	9	7	13	5	13	6
SiO ₂	76.8(4) ^c	46.4(3)	62.9(2)	42.1(1)	55.8(1)	40.9(3)
Al ₂ O ₃	12.3(1)	6.94(13)	18.4(1)	11.7(2)	18.9(2)	13.1(2)
FeO*	0.79(4)	16.9(2)	4.25(10)	12.6(3)	8.03(10)	11.6(2)
MgO	0.033(6)	12.5(2)	1.78(2)	14.0(1)	3.73(4)	14.1(2)
CaO	0.54(3)	11.1(1)	4.71(6)	11.4(1)	7.53(2)	11.6(1)
Na ₂ O	3.69(11)	1.63(2)	4.95(16)	2.81(4)	4.04(18)	2.49(6)
K ₂ O	4.95(9)	0.75(2)	2.03(3)	0.47(3)	1.01(2)	0.38(1)
TiO ₂	0.06(1)	1.36(9)	0.72(3)	2.92(6)	0.72(1)	2.15(2)
MnO	0.03(1)	0.67(2)	0.15(1)	0.32(2)	0.14(1)	0.17(2)
P ₂ O ₅	<0.01		0.14(1)		0.18(1)	
Total	99.19	98.25	95.26 ^d	98.32	93.82 ^d	96.49

Sample origins: IC-B is porphyritic rhyodacite containing high-silica rhyolite glass, collected from Deer Mountain at the south end of the Inyo Volcanic Chain, eastern California. Sampson and Cameron (1987) describe the petrology of Inyo Volcanic Chain eruptives. Sample AY-II-V is hornblende HAB from Ayarza caldera, Guatemala, and was provided by W. Rose. A whole-rock analysis of Ayarza hornblende HAB is presented in table 1, after Peterson and Rose (1985). Sample 81-T-116 is hornblende high-alumina basaltic andesite from Santa Maria volcano, Guatemala, and was also provided by W. Rose. A whole rock analysis of 81-T-116 is presented in Rose (1987).

Notes. a. Hornblende analyses are exclusively within 15 microns of the rims of euhedral phenocrysts. b. Matrix was separated from phenocrysts by hand-picking under ethanol while viewing with a binocular microscope. Matrix separates are estimated to be better than 95% pure. Matrix was fused in Au capsules at 2kb with added doubly-distilled H₂O and was quenched to glass with the rapid technique. Quenched glasses were analyzed by electron probe using the same techniques employed for experiments. Analyses are normalized to total to 100% volatile-free with all Fe as FeO. c. Numbers in parentheses are one standard deviation of replicate analyses and are in units of the least significant digit reported. d. Original total of hydrous glass analysis.

APPENDIX A: TZM RUN ASSEMBLY

This appendix describes the construction of capsules for 2 kbar water-saturated experiments in the MIT design TZM pressure vessels. The MIT design vessel is ~12" long, with a 1/4" diameter axial bore sunk to within 1" of the base. The bore is rounded at the base and smooth with no burrs or irregularities. Vessels with flat-based or irregular bores failed on first or second uses. The vessel is run vertically in a Deltech DT31VT furnace. The pressure seal lies above the furnace and is cooled with recirculating chilled water. A mixture of Ar and CH₄ in proportions 2000:35 respectively is used as a pressure medium. The sample capsule rests vertically at the base of the bore during the experiment, with the sample positioned at the very bottom of the bore. The thermal gradient over the sample in this position is < 3 °C. The experiment is quenched by removing the vessel from the furnace and inverting it. The sample falls from the hot base of the bore to the water-cooled pressure seal and quenches. This quench technique is essential if hydrous basaltic liquids are to be preserved as glasses. The entire capsule assembly must therefore be sufficiently narrow to allow it to fall down the 1/4" bore without sticking. A number of assemblies have been tried, all modifications of the standard double capsule assemblies used in hydrothermal vessels. Two successful assemblies are described below.

AU-PLUG ASSEMBLY

The Au-plug assembly uses 0.12" outer diameter (OD) Au tubing with an 0.008" thick wall as an outer capsule. A 3/4" length of this tubing is cut, annealed, and closed at one end and welded (Au setting on MIT arc welder is ~20 units). Clipping the closed end of the tube with wire cutters helps to obtain a good weld. An ~1/16" long cylindrical Au plug, used to separate the sample from buffer capsules, is fabricated from clean scrap. The plug must fit snugly into the bore of the Au tube, and is best made by using drill bits or punches to drive annealed Au scrap through a series of successively-smaller holes drilled through a steel plate.

Pt buffer capsules also need to be constructed. These are made of available Pt tubing ~1/4" long and sufficiently narrow to fit into the Au tube. The Pt tubes are welded closed at one end and then filled with a buffer assemblage of powdered

Ni and NiO with Ni >> NiO. Preliminary results at 1 kbar suggest that Ni = NiO is more appropriate for pressures < 2 kbar. The open ends of the Pt capsules are cleaned of powder and welded shut. A complete weld is not necessary. If the capsules are welded completely shut, take a jeweler's file and cut a notch through the weld.

Clean the Au parts. If steel adheres to the plug, remove it by soaking the plug in a mixture of hot nitric acid and water in 1:1 proportions. Rinse and dry all parts. Load ~30-40 milligrams of powdered sample into the base of the Au capsule and tamp down with a metal punch. Clean the bore of the capsule with a damp paper tissue (kimwipe) and/or cotton-tipped applicator (Q-tip). Press the clean Au plug down the bore of the Au tube until it rests on or immediately above the sample. A very snug fit is important, but take care not to mangle the capsule. Load 15 microliters of millipore water onto the Au plug using a microsyringe. Drop by drop works best, letting successive drops soak down around the plug and into the sample. Place the Pt buffer capsules atop the Au plug, open end upward, and close the Au capsule with flat-ended pliers. Clip the end of the closed outer capsule with sharp wire cutters to firmly close the capsule and to raise the closed edges to a ridge (this raised edge easily draws an arc). Wrap the capsule in a wet tissue and weld shut, holding the end of the capsule in an appropriate vise. Welding is best performed as a series of smooth swipes separated by pauses of ~5 seconds to allow for heat dissipation (setting of ~20 on MIT arc welder). Troublesome spots can be closed with a very sharp carbon rod and a high current (setting ~10 on MIT arc welder). The finished weld should be smooth and cover the thickness of the capsule walls. Check that the capsule is sealed by weighing, heating in a drying oven > 10 min. and weighing again. Run the capsule with the sample on the bottom or the sample will leak around the plug and onto the Pt capsules. Au plugs and buffer capsules can be reused several times.

DOUBLE CAPSULE ASSEMBLY

The double capsule assembly uses a 1" length of annealed 0.186" OD by 0.01" wall Au tubing as an outer capsule, and a 1/4 - 5/16" length of annealed 0.12" OD by 0.008" wall Au tubing as an inner capsule. The clean inner capsule is welded closed at one end and shaped into an open cylinder with a flat

base using available tools. Thirty to 40 milligrams of sample are loaded into the capsule (ie. $\sim 2/3$ full) and the open end of the capsule is cleaned of powder. Three to 4 microliters of millipore water are loaded onto the sample drop by drop with a microsyringe, with sufficient time between drops for the water to soak into the sample. The sample capsule is closed with a triple crimp, the edges of the crimp are twisted around in a spiral, and the end of the resulting stub is clipped off with wire cutters.

The 1" annealed outer capsule is welded closed at one end. The OD of the outer capsule must be reduced to allow it to fall easily along the bore of the pressure vessel. The OD is reduced by placing a mandrel (shank of an 0.14" drill bit) down the length of the capsule along one side and shaping a flange along the length of the capsule by pinching the excess Au. This flange will subsequently be folded over, producing a narrow capsule (this step could be avoided if capsule material with the appropriate OD were available). Load 17-18 microliters of millipore water into the base of the outer capsule using a microsyringe. Slide the inner capsule down to the base of the outer capsule, unsealed end upward. Place buffer capsules (constructed as above) on top of the sample capsule, open end upward and resting on the side of the outer capsule opposite the flange. Close the outer capsule with flat-ended pliers and squeeze out extra air space with fingers (avoid squeezing water up to open end). Clip the end of the closed outer capsule with sharp wire cutters to firmly close the capsule and to raise the closed edges to a ridge (this raised edge easily draws an arc). Wrap the capsule in a wet tissue and weld shut, holding the end of the capsule in an appropriate vise. Welding is best performed as a series of smooth swipes separated by pauses of ~ 5 seconds to allow for heat dissipation (setting of ~ 20 on MIT arc welder). Troublesome spots can be closed with a very sharp carbon rod and a high current (setting ~ 10 on MIT arc welder). The finished weld should be smooth and cover the thickness of the capsule walls. Gently fold the flange back onto the filled part of the capsule using fingers or other tools that are soft and smooth (like wood). Continue folding the flange until the capsule has been reduced to a narrow cylinder that slides freely up and down the bore of the pressure vessel. Check to ensure that the capsule is sealed by weighing, heating in a

drying oven > 10 min., and reweighing. The capsule is run vertically, with the sample at the base of the vessel.

ADDITIONAL NOTES

Once a sample have been run and quenched, the capsule should fall easily from the vessel. If it does not fall easily or must be fished out with a wire, suspect that the quench was not successful. The capsules will have a thick carbon coat if mixed Ar and CH₄ were used as a pressure medium. Remove the carbon with hot water, soap, and a soft brush. Inspect the cleaned dry capsule for holes, cracks, or other significant markings. Weigh the capsule and compare with the original weight. Weight loss is typical, resulting from diffusive loss of hydrogen and perhaps oxygen out of the capsule. If the weight loss approaches the weight of the water added, suspect that the capsule has leaked or dried out. If the capsule has increased in weight and is clean, then hydrogen has been gained. If so, be sure to verify that NiO is still present in the buffer (if weight gain and loss of NiO are a persistent problem, reduce the proportion of CH₄ in the pressure medium).

Pierce the capsule with a teasing needle and watch for water bubbling or spraying out of the hole. Also note if a sulfurous odor is emitted from the capsule, further evidence that it has remained sealed. If water does not gush out, carefully tear the outer capsule open while viewing under low magnification and try to see if water is present. If water is observed in either instance, the run was likely water-saturated. Inspect the buffer capsules. The presence of Ni metal can be verified with a hand magnet without opening the buffer capsule. Nickle oxide has a distinct yellow-green color. It is good policy to open a buffer capsule to check for NiO; if done carefully, the capsule can be closed and reused. Buffer capsules should be retired after at most 4 uses since silicates are eventually transferred to the buffer through the vapor phase. Since the buffer and the sample are in contact with the same volatile (as evidenced by sulfur transported from inner to outer capsules), if both Ni and NiO are present, the run was likely buffered. This is confirmed by the observation that appropriately buffered experiments define coherent trends on variation diagrams whereas experiments that lost either Ni or NiO do not lie on the buffered trends. Oxide-saturated compositions show this

effect sensitively when the glass compositions are plotted on the AFM diagram because oxidation state changes the proportion of oxides in the crystallizing assemblage. Examination of the sample in reflected light and by backscatter electron imaging shows if the quench was successful. If the capsule contains water, the buffer contains Ni and NiO, the quench was successful, and the sample has not leaked out onto the buffer capsules, then the run most probably worked.